Generation and Characterization of Transgenic Mice for Noninvasive Cell Tracking with PET and for FRET-based cGMP Imaging

Dissertation

der Mathematisch-Naturwissenschaftlichen Fakultät

der Eberhard Karls Universität Tübingen

zur Erlangung des Grades eines

Doktors der Naturwissenschaften

(Dr. rer. nat.)

vorgelegt von

Martin Thunemann

aus Bonn

Tübingen

2012

Zusammenfassung

Moderne Bildgebungsmethoden werden im Rahmen der Grundlagenforschung und der angewandten biomedizinischen Forschung immer häufiger in Studien mit genetisch modifizierten Mäusen eingesetzt. Die nichtinvasive Bildgebung in transgenen Mäusen ermöglicht Studien, die mit konventionellen Methoden bisher nicht möglich waren. Diese Studien können dazu beitragen, qualitativ hochwertige Daten bei verringerten Tierzahlen zu erhalten. Insbesondere ermöglicht die nichtinvasive Bildgebung auch Einblicke in komplexe biologische Prozesse, die nur im lebenden Tier untersucht werden können. Das Ziel dieser Arbeit war es, transgene Mauslinien herzustellen und zu charakterisieren, die für die nicht-invasive Verfolgung von Zellen („Cell tracking") mittels Positronen-Emissions-Tomographie (PET) oder die Visualisierung des intrazellulären Signalmoleküls cyclisches Guanosinmonophosphat (cGMP) durch optische Biosensoren verwendet werden können.

Das nicht-invasive „Cell tracking" mittels PET kann dazu genutzt werden, Zellproliferation, -migration, oder -tod im Rahmen verschiedener physiologischer oder pathologischer Prozesse zu visualisieren. Zur genetischen Markierung ausgewählter Zellpopulationen wurde eine Mauslinie hergestellt, die ein konditionales *HSV1*-sr39tk PET-Reportertransgen im ubiquitär exprimierten ROSA26-Lokus trägt. *HSV1*-sr39tk stellt eine modifizierte Variante der Thymidinkinase aus dem *Herpes simplex*-Virus dar, die PET-Tracer wie z.B. 4-[^{18}F]-Fluoro-3-(hydroxymethyl)butyl]guanin ([^{18}F]FHBG) phosphorylieren kann. Die Anreicherung von phosphorylierten Tracer-Molekülen in *HSV1*-sr39tk-exprimierenden Zellen kann dann mittels PET nachgewiesen werden. In der neu hergestellten Mauslinie kann die Expression von *HSV1*-sr39tk mit Hilfe des Cre/loxP-Rekombinationssystems zelltypspezifisch aktiviert werden, sodass verschiedene Zelltypen durch Verpaarung mit geeigneten Cre-Mauslinien markiert werden können. Die Expression von *HSV1*-sr39tk und die Aufnahme von [^{18}F]FHBG in Abhängigkeit von Cre-Rekombination wurde in embryonalen Stammzellen gezeigt. Für PET-Studien wurden Mäuse hergestellt, die *HSV1*-sr39tk in den β-Zellen der Bauchspeicheldrüse herstellen. In einem ersten PET-Experiment konnte gezeigt werden, dass sich [^{18}F]FHBG tatsächlich in β-Zellen anreichert. Es sind nun weitere Studien notwendig, um die *in vivo*-Sensitivität und -Reproduzierbarkeit der neu hergestellten *HSV1*-sr39tk-Mauslinie zu testen.

Der sekundäre Botenstoff cGMP beeinflusst zahlreiche Körperfunktionen wie Glattmuskeltonus, Thrombozyten-Aggregation und neuronale Plastizität, wobei die zugrundeliegenden molekularen Wirkmechanismen oft nicht vollständig aufgeklärt sind. cGMP-spezifische Biosensoren, wie die auf Fluoreszenz-Resonanzenergietransfer (FRET) basierenden cGMP-Indikatoren (cGis), sind wichtige Werkzeuge zur Untersuchung des cGMP-Signalwegs. Um deren Nutzung im lebenden Tier zu ermöglichen, wurden transgene, cGi-exprimierende Mauslinien hergestellt. Zunächst wurden aus

diesen Mäusen neuronale Zellen und Glattmuskelzellen der Aorta, Blase und des Darms gewonnen, kultiviert und mittels FRET-Mikroskopie untersucht. Die Stimulation mit Stickstoffmonoxid (NO) führte in Körnerzellen des Kleinhirns und in allen Glattmuskelzelltypen zur cGMP-Bildung durch die lösliche Guanylatcyclase. Andererseits lösten natriuretische Peptide, die membranständige Guanylatcyclasen aktivieren, in Glattmuskelzellen verschiedener Herkunft unterschiedliche Reaktionen aus. Eine veränderte Reaktivität wurde darüber hinaus in Gegenwart von Phosphodiesterase-Inhibitoren beobachtet, die darauf hinweist, dass in kultivierten Glattmuskelzellen mindestens zwei verschiedene Phosphodiesterase-Familien für den Abbau von cGMP verantwortlich sind. Darüber hinaus konnte eine NO-induzierte cGMP-Synthese auch in den Gefäßen der Netzhaut beobachtet werden, die zuvor aus cGi-exprimierenden Mäusen isoliert wurde. Um zu zeigen, dass der cGi-Sensor auch für Experimente in lebenden Tieren genutzt werden kann, wurden Intravitalmikroskopie-Studien mit cGi-exprimierenden Tieren durchgeführt. Hierbei konnten NO-induzierte cGMP-Transienten in den Gefäßwänden des Cremaster-Muskels am anästhesierten Tier verfolgt werden. Diese Ergebnisse zeigen, dass die neu hergestellten Mauslinien wertvolle Quellen für cGi-exprimierende Primärzellen darstellen und vor allem dass sie für Studien am lebenden Tier genutzt werden können.

Abschließend lässt sich sagen, dass die im Rahmen dieser Arbeit hergestellten und charakterisierten Mauslinien der Untersuchung verschiedener Tiermodelle unter *in vivo*-Bedingungen dienen können, z.B. der Untersuchung von neurodegenerativen oder kardiovaskulären Erkrankungen sowie von Diabetes und Krebs.

Summary

In recent years, modern imaging techniques are being developed for highly sophisticated studies with genetically modified model organisms. Mice are the most commonly used mammalian model organisms in basic and applied biomedical research. Noninvasive imaging of transgenic mice allows for previously unfeasible experimental designs that can improve data quality with fewer animals needed in a particular study. In addition, and most importantly, novel imaging strategies provide new insights into biological processes that can only be studied in living animals. The aim of this work was to generate and characterize transgenic mice for 1) noninvasive cell tracking with positron emission tomography (PET) and 2) visualization of the intracellular signaling molecule cyclic guanosine monophosphate (cGMP) with biosensors based on fluorescence resonance energy transfer (FRET).

PET-based cell tracking can be used to follow cell proliferation, migration, or death associated with physiological or pathological processes. To label defined cell populations genetically for PET imaging, mice were generated carrying a conditional *HSV1*-sr39tk PET reporter transgene in the ubiquitously expressed ROSA26 locus. *HSV1*-sr39tk is an engineered variant of the *Herpes simplex virus* thymidine kinase, which phosphorylates PET tracers like 4-[^{18}F]-Fluoro-3-(hydroxymethyl)butyl]guanine ([^{18}F]FHBG) leading to their accumulation in *HSV1*-sr39tk-expressing cells. In the newly generated mouse line, Cre/loxP-mediated recombination activates *HSV1*-sr39tk expression driven by the C̲MV-enhancer/β-a̲ctin/β-g̲lobin (CAG) promoter. Thus, various tissues can be labeled by cross-breeding the conditional *HSV1*-sr39tk line to different tissue-specific Cre transgenic mouse lines. *HSV1*-sr39tk expression and [^{18}F]FHBG accumulation were detected in a Cre-dependent manner in embryonic stem cells carrying the conditional *HSV1*-sr39tk transgene. For PET experiments, mice were generated expressing *HSV1*-sr39tk in pancreatic β cells. Indeed, in a preliminary *in vivo* PET experiment it was shown that [^{18}F]FHBG accumulates in β cells. Further work is necessary to characterize the conditional *HSV1*-sr39tk mouse line for its sensitivity and reproducibility *in vivo*.

The second messenger cGMP modulates diverse physiological processes including smooth muscle relaxation, platelet aggregation, and neuronal plasticity, but the underlying molecular mechanisms are often poorly understood. Sensor proteins that detect cGMP, such as FRET-based 'cGMP indicators' (cGis), are valuable tools for the analysis of cGMP signaling. To enable studies with cGMP biosensors in living mice, cGi-transgenic animals were generated. Neural cells as well as smooth muscle cells (SMCs) from aorta, bladder, and colon were isolated from cGi-expressing mice and used for FRET imaging experiments. cGMP synthesis via nitric oxide (NO)-stimulated soluble guanylyl cyclase was observed in cerebellar granule neurons and all SMC types. Interestingly, different SMC types showed

different abilities to elevate cGMP in response to natriuretic peptides, which stimulate membrane-associated particulate guanylyl cyclases. Altered cGMP responses in the presence of phosphodiesterase inhibitors indicated that at least two phosphodiesterase families contribute to cGMP degradation in cultured SMCs. Furthermore, NO-induced cGMP elevations were observed in the vasculature of retinas isolated from cGi-expressing animals. Importantly, the feasibility of cGi-based imaging in living animals could be shown in intravital microscopy studies. NO treatment led to transient cGMP elevations in arterial walls of the cremaster muscle of anesthetized cGi-transgenic mice. Thus, the newly generated cGMP sensor mouse lines do not only represent valuable sources for cGi-expressing primary cells, but they can be used for intravital imaging studies in living animals.

In summary, the mouse lines that were generated and characterized in this work will find widespread applications, and in combination with other genetic mouse models, they will help to gain further insights into physiological or disease-associated processes like cardiovascular and neurodegenerative diseases, cancer and diabetes under *in vivo* conditions.

Table of Contents

List of Abbreviations

2-ME 2-Mercaptoethanol
4-OHT 4-Hydroxytamoxifen
aa .... Amino acids
ACh .... Acetylcholine
ACV .... Acyclovir
Ado .... Adenosine
ANP .... Atrial natriuretic peptide
APS .... Ammonium persulfate
Ara-C .... Cytosine-β-D-arabinofuranoside hydrochloride
BBSS .... Bicarbonate-buffered saline solution
bg .... Background
BLI .... Bioluminescence imaging
BNP .... Brain natriuretic peptide
bp .... Base pairs
BRET .... Bioluminescence energy transfer
BSA .... Bovine serum albumin
BSMCs .... Bladder smooth muscle cells
CAG.............. CMV immediate early enhancer, chicken β-actin and rabbit β-globin hybrid promoter
cAK............... cAMP-dependent protein kinase A
cAMP .... cyclic 3',5'-adenosine monophosphate
CAs............... Cortical astrocytes
cDNA .... Copy-DNA
CDS.............. Coding sequence
cGi .... cGMP indicator
cGK .... cGMP-dependent protein kinase
cGKII .... cGMP-dependent protein kinase II
cGKIα/β .... cGMP-dependent protein kinase Iα/Iβ
cGMP .... Cyclic 3',5'-guanosine monophosphate
cGMP-BD ..... cGMP-binding domain
CGNs............ Cerebellar granule neurons
CIP .... Calf intestine phosphatase
CMF-HBSS... Calcium/magnesium-free HBSS
CMV .... Cytomegalovirus
CNG .... Cyclic nucleotide-gated
CNP.............. C-type natriuretic peptide
cpEGFP........ Cyclic permutated EGFP
Cre................ Cyclisation/recombination SSR
CSMCs .... Colonic smooth muscle cells
CT................. X-ray computed tomography
DEA/NO........ 2-(N,N-diethylamino)-diazenolate-2-oxide diethylammonium salt
DEPC .... Diethylpyrocarbonat
DMEM .... Dulbecco's modified Eagle medium
DMSO.......... Dimethyl sulfoxide
DNA.............. Deoxyribonucleic acid
dNTP .... Deoxynucleotide triphosphate
dpc................ Days post coitum
dsDNA .... Double-stranded DNA
DTA .... Diphtheria toxin fragment A
DTT .... Dithiothreitol
ECFP........... Enhanced cyan FP
ECL .... Enhanced chemiluminescence
EDTA........... Ethylenediaminetetraacetic acid
EGFP........... Enhanced GFP
ELISA .... Enzyme-linked immunosorbent assay
EM-CCD .... Electron multiplying charge-coupled device
eNOS .... Endothelial NO synthase
ER .... Estrogen receptor

ESCs............ Embryonic stem cells
EYFP .... Enhanced yellow FP
FACV 8-Fluoroacyclovir
FEAU .... 2'-Deoxy-2'-fluoro-5-ethyl-1-β-D-arabinofuranosyluracil
FFAU .... 2'-Deoxy-2'-fluoro-5-fluoro-1-β-D-arabinofuranosyluracil
FGCV............ 8-Fluoroganciclovir
FHBG............ 9-[4-Fluoro-3-(hydroxymethyl)butyl]guanin
FHPG............ 9-[(3-Fluoro-1-hydroxy-2-propoxy)methyl]guanin
FIAU............. 2'-Deoxy-2'-fluoro-5-iodo-1-β-D-arabinofuranosyluracil
Flp................ Flippase
FMAU........... 2'-Deoxy-2'-fluoro-5-methyl-1-β-D-arabinofuranosyluracil
FMT .... Fluorescence-mediated molecular tomography
FOV .... Field of view
FP .... Fluorescent protein
FPCV 8-Fluoropenciclovir
FPLC............ Fast protein liquid chromatography
FRET .... Fluorescence resonance energy transfer
FRI .... Fluorescence reflectance imaging
FRT.............. Flp recombinase target sequence
G418 .... Geneticin
GAF .... GAF domains from cGMP-specific phosphodiesterases, Anabaena adenylyl cyclases, and E. coli FhlA
GCV .... Ganciclovir
GFP .... Green fluorescent protein
GIFM............ Genetic inducible fate mapping
GLT.............. Germ-line transmission
GSDB........... Goat serum dilution buffer
h................... Hill constant
HBSS .... Hank's balanced salt solution
HCN .... Hyperpolarization-activated cyclic nucleotide-gated
HNs............... Hippocampal neurons
HRP .... Horseradish peroxidase
HS................ Horse serum
Hsp .... Heat shock protein
HSV1 .... Herpes simplex virus 1
HSV1-tk .... Herpes simplex virus 1 thymidine kinase
IBMX 3-Isobutyl-1-methylxanthine
iNOS .... Inducible NO synthase
IP$_3$ .... Inositol triphosphate
lacZ .... β-Galactosidase-coding lacZ gene
LB .... Luria-Bertani
LIF................ Leukemia-inhibitory factor
loxP.............. Locus of X-over in P1
M.................. Molar, mol/L
MEM .... Minimum essential medium
MMLV-RT...... Moloney murine leukemia virus reverse transcriptase
MP .... Milk powder
MR .... Magnetic resonance
MRI .... Magnetic resonance imaging

mTagBFP .... Monomeric Tag blue fluorescent
protein
NANC .... Non-adrenergic, non-cholinergic
Neo^R .... Neomcyin resistance gene
Nes .... Nestin
NGS.............. Normal goat serum
NIR .... Near-infrared
NLS .... Nuclear localization signal
nNOS........... Neuronal NO synthase
NO .... Nitric oxide
NOS.............. Nitric oxide synthases
OD .... Optical density
ODQ .... 1H-[1,2,4]oxadiazolo[4,3-a]quinoxalin-
1-one
ORF.............. Open reading frame
PAGE .... Polyacrylamide gel electrophoresis
PBS .... Phosphate-buffered saline
PCR.............. Polymerase chain reaction
PDE .... Phosphodiesterase
Pen .... Penicillin
PET .... Positron emission tomography
PFA .... Paraformaldehyde
pGC .... Particulate guanylyl cyclase
PMSF .... Phenylmethylsulfonyl fluoride
PVDF........... Polyvinyliden fluoride
RFP .... Red fluorescent protein
RIA .... Radioimmunoassay
RIP .... Rat insulin promoter

RNA .... Ribonucleic acid
ROI .... Region of interest
ROSA........... Reverse orientation splice acceptor
RT .... Reverse transcriptase enzyme
SA .... Splice acceptor
SDS .... Sodium dodecyl sulfate
sGC .... Soluble guanylyl cyclase
SM22 .... SM22α (transgelin) gene
SM445 .... 445 bp promoter fragment of the
SM22α gene
SNP .... Sodium nitroprusside
SPECT......... Single-photon emission computed
tomography
sREACh .... Super resonance energy accepting
chromoprotein
SSR .... Site-specific recombinase
Strep .... Streptomycin
Tris............... Tris(hydroxymethyl)aminomethane
tRNA .... transfer-RNA
UTR .... Untranslated region
UV .... Ultraviolet
VSM .... Vascular smooth muscle
VSMCs......... Vascular smooth muscle cells
X-Gal............ 5-Bromo-4-chloro-3-indolyl-D-
galactoside
βgeo............. β-Galactosidase/neo^R fusion protein

1 Introduction

The mouse (*Mus musculus*) is the most abundant mammalian model organism in biomedical research. Mice show a high degree of homology with the human genome (1, 2). Large breeding colonies can be maintained with reasonable financial effort, well-characterized inbred strains are available, and most importantly, methods for genetic modification are outstandingly advanced (see 1.1). The use of murine embryonic stem cells (ESCs) for now more than 20 years is the major reason for the success of transgenic mice as model organisms. ESC-based methods are used to generate transgenic mice carrying gene deletions (*knock-outs*), mutations, insertions (*knock-ins*), or other mutations at well-defined loci in their genomes (3). The generation of *knock-out* mice became very popular to analyze roles and functions of particular genes in live animals (4). Mice carrying mutations in genes that are (or suspected to be) involved in disease pathogenesis can provide new insights into disease initiation and progression or new approaches for diagnosis and treatment (5-8). Large-scale efforts are ongoing to generate *knock-out* mice for every gene (9). Moreover, reporter gene-based methods help to understand complex physiological or pathological processes that can be associated with aberrant cell signaling, cell migration, proliferation, or death. Such reporters are used to label and follow cell populations during development or adulthood in cell fate mapping or cell tracking studies (10-12) (see 1.2). A special class of reporter genes are biosensors used to monitor spatiotemporal dynamics of second messengers like 3',5'-cyclic guanosine monophosphate (cGMP) or other metabolites and enzyme activities in intact cells or live animals (13) (see 1.3).

1.1 Generation of Transgenic Mice

1.1.1 Random Mutagenesis

Random mutagenesis is typically used to create transgenic mice that overexpress a particular protein. To generate transgenic mice, transgene DNA is microinjected into fertilized mouse oocytes, which are transferred into foster mothers. Resulting animals are tested for transgene integration after birth, and positively tested mice are called 'founder animals'. A transgenic line is established, when the transgene is inherited from the founder to the next generation. Every founder animal carries the transgene at a random site and in random copy number in the genome (14-16) (**Figure 1A**). Because of tissue-dependent epigenetic modifications and elements possibly surrounding the transgene at its integration site, transgene expression will vary between individual founder lines, although the same transgene DNA has been used for transgenesis (17-19). Every mouse line has therefore to be analyzed in order to detect transgene expression at all, and to characterize expression strength and specificity.

However, with the use of tissue-specific promoters and/or large transgenes carrying additional regulatory elements, expression can more or less reliably directed to a particular tissue (20).
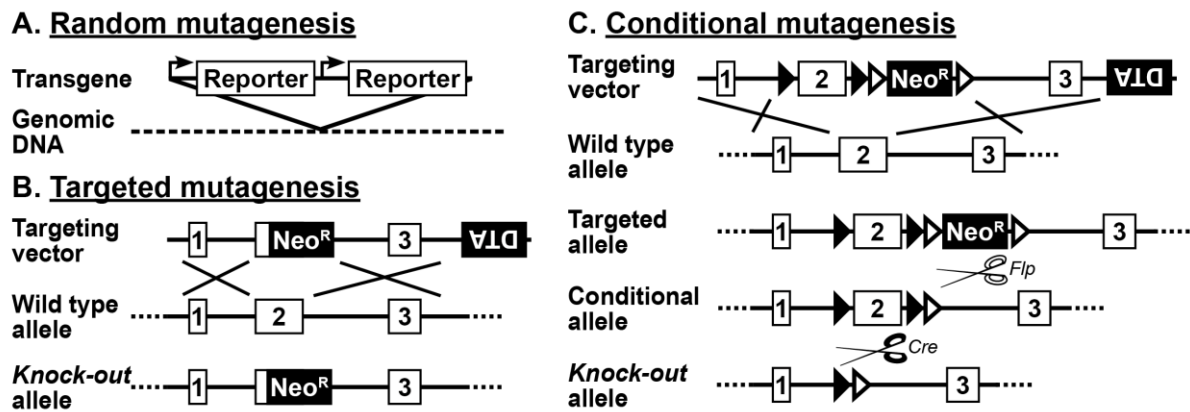

Figure 1. Strategies of random (A), targeted (B) and conditional mutagenesis (C).

A. Transgenes (e.g. a reporter gene) usually insert in multiple concatenate copies at a random integration site into the genome **B**. To generate a chronic *knock-out* by targeted mutagenesis, a transgene is inserted via homologous recombination that leads to deletion of a 'critical' exon and to premature termination of gene transcription. The transgene can represent a selection marker (here: Neo^R) necessary to select for targeted ESCs. **C.** For a conditional *knock-out*, a 'critical' exon is flanked with loxP sites (black triangles). The Neo^R cassette is flanked by FRT recognition sites (white triangles). Removal of the marker cassette by Flp leaves the conditional allele, which is converted to the *knock-out* allele by Cre recombination. Targeting vectors for targeted mutagenesis carry a DTA gene cassette that is not part of the transgene. It causes death of ESCs that integrated the complete targeting vector into their genome at random locations. Abbreviations: Cre, cyclisation recombination SSR; DTA, diphtheria toxin A; Flp, Flippase SSR; FRT, Flp recombinase target sequence; loxP, locus of X-over in P1 (Cre target sequence); Neo^R, Neomcycin resistance gene; SSR, site-specific recombinase.

1.1.2   Targeted Mutagenesis

To understand the role and function of genes *in vivo*, mice can be generated that carry defined genetic alterations. The generation of mice with defined genetic alterations relies on pluripotent embryonic stem cells (ESCs) isolated from blastocyst-stage embryos (**Figure 2**) (21). During *in vitro* culture, ESCs remain pluripotent, genetic modifications can be introduced into their genome, and selection procedures are used to enrich for modified ESCs (22-24). They are injected into blastocysts leading to chimeric animals, where modified ESCs eventually contribute to the germ-line thereby passing the mutation to their offspring (25), for methodical aspects see also chapter 2.3.4 on p. 43. Genetic modifications can be introduced into the ESC genome by gene trap mutagenesis (26-28) or via homologous recombination (24). Homologous recombination is used to generate mice carrying well-defined mutations like *knock-outs* or *knock-ins* within a preselected gene (22, 29). A linear targeting vector is used that carries the transgene flanked by two 2-10 kb-long homologous arms (30). Their sequence is identical to the region flanking the piece of DNA to be replaced by the transgene. After transfection, homologous recombination between ESC genomic DNA and the targeting vector leads to

a target-specific insertion of the transgene into the ESC genome. Because homologous recombination is markedly inefficient, selection strategies are needed to enrich for 'targeted' ESCs (23, 24) (see also chapter 2.3.4 and **Figure 9** on p. 45). If the transgene leads to disruption of a gene, a chronic *knock-out* allele is generated (**Figure 1B**). A targeted *knock-in* is used to express another gene (like a reporter gene) from the promoter of a gene that was replaced by homologous recombination (29). In contrast to transgenes introduced by random mutagenesis, the integration site of a *knock-in* transgene is well defined, and transgene expression usually follows the spatiotemporal expression pattern of the original gene (29). On the other hand, this strategy leads to a gene *knock-out* of the original gene. To circumvent this potentially deleterious situation, the transgene can be targeted to the 3'-untranslated region (3'-UTR) of the gene to generate bicistronic transcripts. For that purpose, viral internal ribosomal entry sites for cap-independent initiation of translation, or the viral 2A self-processing peptide for cotranslational cleavage can be used (31, 32).
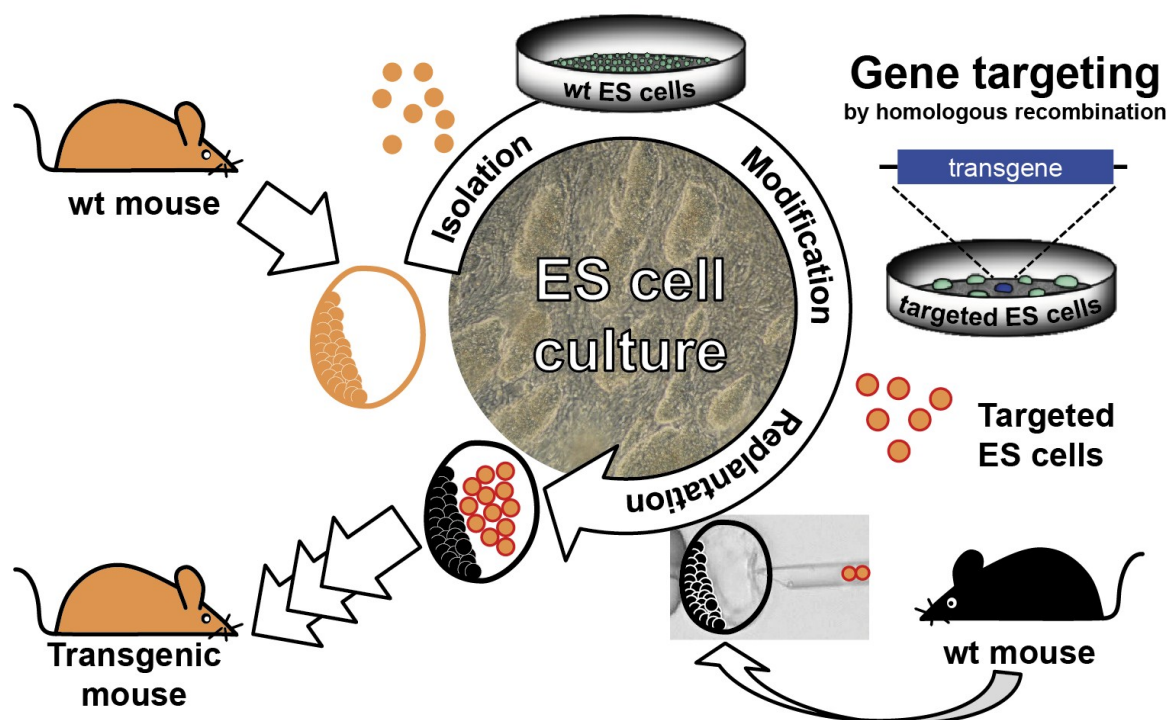
Figure 2. Fundamental role of ESCs for the generation of transgenic mice carrying targeted mutations.

Pluripotent embryonic stem cells (ES cells, ESCs) are derived from the inner cell mass of blastocyst-stage wild type (wt) embryos and can be kept in culture in their pluripotent state. During culture, ESCs are genetically modified, e.g. by homologous recombination in gene targeting experiments. Targeted ('transgenic') ESCs are injected into wt blastocyst-stage embryos to generate ESC-derived transgenic mice (for further details, see also **Figure 10** on p. 55).

1.1.3 Conditional Mutagenesis

In conventional *knock-out* mice, genes are deleted in every cell throughout the entire life of the animal. If the deleted gene is essential for development, *knock-out* animals eventually die *in utero*, during birth or shortly thereafter (33). If *knock-out* mice survive long enough to allow analyses in adult animals, results can be difficult to interpret because of complex phenotypes (34). The generation of time- and tissue-specific somatic *knock-outs* by conditional mutagenesis allows to circumvent these problems (35). Conditional mutagenesis combines homologous and site-specific recombination. Parts of a conditional (*knock-out* or *knock-in*) transgene are flanked by recognition sites for site-specific recombinases (SSRs). The most widely used SSR is the <u>c</u>yclization <u>re</u>combination (Cre) enzyme, found in the bacteriophage P1. Cre catalyzes the recombination between two 34 bp-long, semi-palindromic DNA sequences, called 'loxP' sites (from <u>lo</u>cus <u>of</u> <u>X</u>-over in <u>P</u>1) (36, 37). The Cre/loxP recombinase system works highly efficient in mammalian cells and was used for the first time in 1993 to generate a somatic *knock-out* of the DNA polymerase β gene (38). Nowadays, also other recombinase systems, like the <u>F</u>lippase enzyme/<u>F</u>lip <u>r</u>ecombinase <u>t</u>arget sequence (Flp/FRT) system, are used in transgenic mice (39). To generate a conditional (somatic) *knock-out*, two parallel loxP sites flanking an essential fragment of the gene of interest are introduced into the mouse genome by homologous recombination in ESCs. The selection marker cassette necessary to enrich for targeted ESCs can interfere with expression of the target gene, leading to hypomorphic alleles (40). For that reason, marker gene cassettes are typically flanked with loxP or FRT sites allowing their removal before ESC implantation or later in the germ-line of ESC-derived mice (**Figure 1C**). Mice carrying the loxP-flanked gene fragment even in homozygosity are usually indistinguishable from wild type animals (10). A tissue-specific gene *knock-out* is obtained with such conditional alleles by Cre recombination (**Figure 1C**). In animals carrying a tissue-specific Cre transgene and two conditional alleles, Cre-catalyzed excision of the loxP-flanked gene fragment generates a gene *knock-out* restricted to Cre-expressing cells and their descendants (41, 42).

Unspecific Cre expression causes recombination in tissues that are not expected to carry a gene *knock-out* possibly confounding analyses of the animals' phenotype. Especially when recombination occurs in the developing animal, inheritance of the recombined allele from cells to a large number of descendants might cause severe phenotypes that are not related to gene function in the tissue that was focused on (43). The problem of premature recombination can be circumvented by gaining temporal control over Cre activity. One strategy uses drug-inducible promoters that drive Cre expression, but promoter leakiness possibly leads to Cre expression also in absence of the activating drug (44-46). A more popular approach that allows controlling Cre activity is the use of ligand-inducible Cre fusion proteins, as for example fusions of Cre with hormone-binding domains of the estrogen receptor (ER) (47). Efforts by Feil, Metzger, Chambon and others led to CreER[T] and CreER[T2] fusion proteins

binding the synthetic drug 4-hydroxytamoxifen (4-OHT), but not the endogenous ER receptor ligand estrogen (48, 49). In the absence of 4-OHT, the ER-part of the fusion protein is most likely bound by heat-shock proteins such as Hsp90 causing the retention of the fusion protein in the cytosol. Upon4-OHT binding, Hsp90 dissociates and a nuclear localization signal (NLS) is exposed, which leads to the translocation of the fusion protein into the nucleus, where the Cre part of the fusion protein recombines its DNA substrate (35, 50) (**Figure 3A**). Spatiotemporal control over Cre activity is therefore obtained by tissue-specific CreER^{T2} expression and temporally restricted delivery of 4-OHT or its prodrug tamoxifen to the animal (51). 'Incomplete' *knock-outs* may occur when Cre or CreER^{T2} are not expressed in all cells of interest or if activating ligands do not reach those cells. This circumstance should be considered during phenotypic analyses of conditional *knock-out* animals (54).

Gene targeting experiments are nowadays typically performed to generate conditional *knock-out* alleles rather than chronic *knock-out* alleles, also for the reason that conditional *knock-out* alleles can be converted to chronic *knock-out* alleles by the use of germ-line or ubiquitously expressed Cre (52). For tissue-specific recombination, a huge variety of recombinase transgenes is available: 1716 Cre recombinase-encoding transgenes (and 24 transgenes with other SSRs) are listed in the Mouse Genome Informatics database; 510 Cre transgenes represent targeted mutations (*knock-ins*), 310 transgenes encode CreER or CreER^{T2} fusion proteins, while 22 transgenes carry ligand-inducible promoters (53). Currently, 481 Cre transgenic mouse lines are available through the International Mouse Strain Resource (54). These numbers emphasize the remarkable success of the Cre/loxP system and ligand-inducible Cre recombinases in the field of mouse genetics.

1.2   Cell Tracking with PET

'Cell tracking' describes the use of molecular imaging methods to label and detect cells in live animals (or humans) to monitor their presence, viability, and migration (55, 56). A major advantage of noninvasive cell tracking approaches is the opportunity to perform repeated experiments with the same group of animals. This reduces animal numbers in a particular study and errors resulting from inter-individual variability (57, 58). Furthermore, noninvasive cell tracking renders experimental designs feasible that are impracticable with conventional cell detection methods.

Cell tracking can be seen as an expansion of 'classical' genetic inducible fate mapping (GIFM) approaches, where reporter gene-expressing cells are typically detected in fixed and post-processed tissue samples. Cell fate mapping has become an important technique to study cells during development, in adulthood, and in disease models (10). Ligand-inducible SSRs, particularly tamoxifen-inducible CreER fusion proteins, as well as appropriate Cre reporter transgenes are used for highly sophisticated GIFM approaches. Moreover, as almost all conditional *knock-out* transgenes are

built on the Cre/loxP system, experiments can be performed with reporter-labeled cells that carry a gene *knock-out* at the same time. To detect reporter gene expression in typical GIFM experiments, animals have to be sacrificed. Here, longitudinal studies (weeks to months) with the same group of animals are impossible and representative sample collection within narrow time intervals requires large animal numbers and highly reproducible cell labeling techniques (11).

Alternatively, labeled cell populations can be followed in live animals with noninvasive molecular imaging techniques like fluorescence and bioluminescence imaging (FLI and BLI), magnetic resonance imaging (MRI), and positron emission tomography (PET). Among them, PET represents a powerful method, particularly with regard to sensitivity and quantification (59). The sr39tk variant of the *HSV1* thymidine kinase gene is a widely used PET reporter gene to label cells for noninvasive cell tracking studies in experimental animals and human patients (described in 1.2.3). Expression of *HSV1*-sr39tk leads to accumulation of radioactive PET tracer molecules that can noninvasively be detected in a PET scanner. The *HSV1*-sr39tk reporter and related PET reporter genes were used to label cells in transplantation experiments or tumor cells in cancer models, while until to date, only a small number of transgenic mice expressing *HSV1*-sr39tk or related reporters have been generated and used in cell tracking studies (see 1.2.3). In all of these mouse lines, reporter expression is driven by tissue-specific promoters, limiting their use to a particular cell type.

1.2.1   Genetic Cell Labeling

In cell tracking or fate mapping studies, the cell labeling technique is an important factor for experimental success. Direct cell labeling, for example with fluorescent dyes, suffers from several shortcomings: 1) cell division leads to label dilution and therefore to signal loss upon cell expansion, 2) label detection may not reflect cell viability, and 3) the label is not stable over extended periods (56). Genetic cell labeling approaches circumvent these complications. Cell expansion leads to signal increase when inheritable reporter genes are used. Only vital cells are detected, because reporter gene expression relies on intact transcription and translation machineries.

GIFM is the most advanced labeling approach and makes use of reporter transgenes activated by ligand-inducible Flp or Cre recombinases (10-12) (**Figure 3**). Hereinafter, CreER^{T2} and Cre reporter constructs are described, but similar experiments can also be performed with other ligand-inducible SSRs. A typical reporter construct carries a loxP-flanked 'STOP cassette' inhibiting transcription and translation of the reporter-coding sequence (CDS). Therefore, the STOP cassette resides between promoter and reporter CDS and contains stop codons and polyadenylation signals. Cre-mediated removal of the STOP cassette allows for expression of the previously 'silenced' reporter CDS in Cre-expressing cells and their descendants (**Figure 3A**).
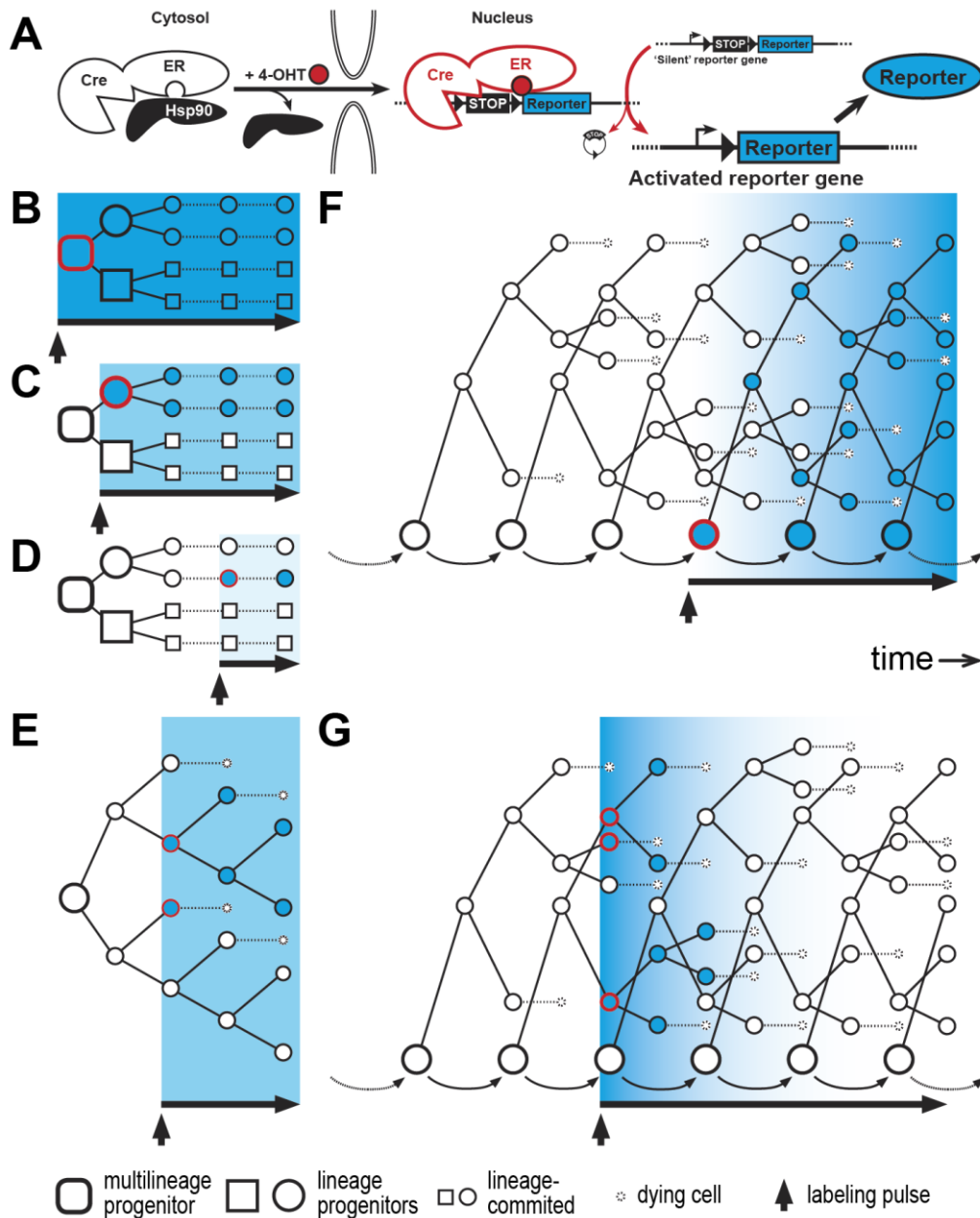
Figure 3. Genetic inducible fate mapping (GIFM).

A. Mechanism of 4-hydroxytamoxifen (4-OHT)-mediated CreER activation, and CreER-mediated activation of reporter gene expression. Without 4-OHT, CreER is bound to heat-shock protein (Hsp) chaperones which prevent its translocation into the nucleus. Chaperone binding is lost in presence of 4-OHT and allows CreER to translocate into the nucleus, where it recombines its DNA substrate (a conditional Cre reporter transgene). In conditional Cre reporters, a loxP-flanked STOP cassette prevents reporter expression. After Cre-mediated removal of the STOP cassette, the reporter can be expressed. **B-G.** Possible outcomes of GIFM studies depending on underlying biology, Cre expression, and labeling time. The labeling event (Cre-mediated reporter activation as shown in panel A) is indicated by red borders, labeled (=reporter-expressing) cells are indicated in blue and unlabeled cells in white. In B-D, tissue is shown which is labeled at different stages of cell differentiation. After final differentiation, cells are post-mitotic. **B.** The common progenitor of two distinct cell lineages is labeled; cells of both lineages express the reporter. **C.** One cell lineage-specific progenitor is labeled, only cells of that lineage express the reporter. **D.** Differentiated, post-mitotic cells of one lineage are labeled and express the reporter. In E-G, cells are labeled, which renew via mitosis (E) or from progenitor (stem) cells (F, G). **E.** Differentiated cells proliferate to maintain constant cell mass, the proportion of labeled cells is constant over time (found e.g. for pancreatic β cells). **F.** Progenitors are labeled that replace terminally differentiated cells; a constant increase of labeled cells is obtained over time (found e.g. in the small intestine). **G.** Cells are labeled that will be replaced by progenitor-derived cells; the number of labeled cells will decrease over time.

Two mouse lines are combined for a GIFM experiment: one carries the conditional Cre reporter transgene, while the other carries a CreER[T2] transgene. With the use of tissue-specific promoters for CreER[T2] expression, recombination is restricted to a particular tissue. Cre-mediated activation of the reporter gene takes place upon tamoxifen delivery to the animal, and the extent of cell labeling can be varied via ligand dose and/or application period (51). Once activated, reporter gene expression is independent from CreER[T2] presence and activity; inheritance of the activated reporter gene, also upon phenotypic changes of the cell after CreER[T2]-induced labeling is the underlying principle of GIFM studies (**Figure 3**).

CreER[T2] should be expressed only in a distinct tissue to allow for specific labeling. Compared to this, the Cre reporter transgene must allow for broad and tissue-independent reporter expression, once it has been activated by Cre recombination. Reliable expression in any given tissue is achieved with reporter *knock-ins* targeted to the ROSA26 locus. The ROSA26 locus was identified in an ESC-based gene trap screening for genes involved in embryonic development (26). Its name results from the underlying gene trap construct consisting of a splice acceptor (SA) site and the β-galactosidase/Neo[R] (βgeo) gene flanked by retroviral long tandem repeat integration sites in reverse orientation (ROSA = Reverse orientation splice acceptor). The gene trap integrated into the first intron of the ROSA26 gene located at 113,017,422-113,027,327 base pairs (bp) on the antisense strand of chromosome 6 (60, 61). A promoter region was identified that drives ubiquitous expression of the βgeo fusion protein in embryos, newborns, and adult mice carrying the gene trap construct (61). Endogenous ROSA26 transcripts do not encode proteins, but overlap with a protein-coding transcript of the neighboring Thumpd3 gene on the sense strand (61).

Some transgenic mouse lines were created by random mutagenesis using the ROSA26 promoter region (62, 63). The majority of ROSA26 transgenic mouse lines were generated by targeted mutagenesis. The first ROSA26 Cre reporter mouse line (ROSA26-lacZ) was generated by introducing a conditional, Cre-inducible lacZ transgene into the first intron of the ROSA26 gene in close vicinity to the original gene trap integration site (64). Further details on the ROSA26-lacZ transgene are found in 3.1.1.1 on p. 76. All subsequent ROSA26 *knock-ins* have been generated with similar homologous arms. In general, ROSA26 targeting vectors are designed in a way that transgene expression is driven by the endogenous ROSA26 promoter or by another promoter introduced with the transgene. Primarily the CAG promoter is used for that purpose, which is made from the cytomegalovirus immediate early enhancer and a hybrid promoter derived from chicken β-actin and rabbit β-globin genes (65). The CAG promoter leads to ubiquitous transgene expression at 10-times higher levels in comparison to expression from the endogenous ROSA26 promoter (66). Among eight promoters tested by Chen et al., the CAG promoter achieved highest expression levels (67).

Mice with two disrupted (transgene-containing) ROSA26 alleles usually do not show phenotypic alterations. However, for some ROSA26 *knock-ins*, phenotypes have been observed: altered growth of mammary tumors in ROSA26-lacZ transgenic mice (68) and defects in spermatogenesis and male infertility in ROSA26-EGFP transgenic mice (69). Ubiquitous Cre expression in ROSA26-CreER mice has been reported to lead to Cre-related toxicity (43, 70).

A wide variety of ROSA26 transgenic mouse lines is available: currently 360 ROSA26 *knock-in* alleles are listed in the MGI database (53). With SSR-based technologies, the generation of allelic series and ROSA26 transgenic mice was simplified, and studies on the effects of promoters, orientation, and other regulatory elements on transgene expression were performed (66, 67, 71-78). ROSA26 transgenic mouse lines were generated, where Cre recombination induces expression of β-galactosidase, alkaline phosphatase, luciferase, and various fluorescent proteins (FPs) (53). In other constructs, Cre induces the switch from one FP to another (e.g. 'ROSA-mT/mG', 79), or the stochastic activation of one out of four different FPs (*'Confetti'*, 80). An increasing number of ROSA26 transgenes contain the CAG promoter in order to achieve sufficient signal intensities for reliable detection of fluorescent proteins *in situ* or *in vivo* (79-81). Upon FP expression from the endogenous ROSA26 promoter, fluorescence can be detected in embryos or isolated cells (e.g. for cell sorting), but when tissues from adult mice are analyzed, FPs need to be detected via immunofluorescence or immunohistochemistry (82, 83).

GIFM studies with ROSA26 reporter transgenes were performed to study embryogenesis, and especially the developing nervous and cardiovascular system (84-90). Several studies were performed in adult mice, for example to analyze neurogenesis or tissue maintenance in colon and pancreas (91-95). Cells were also isolated from ROSA26-transgenic mice and transplanted into recipients to study, for example, the fates of neuronal or hematopoietic stem cells, or bone marrow cells (96-100). GIFM approaches have also been combined with conditional *knock-outs*, and cell fates were analyzed in disease models of diabetes, heart failure, and atherosclerosis (101-106). With conventional reporter genes, detection of reporter gene expression must be performed on fixed tissue samples (107). The need for *in vivo* molecular imaging methods in GIFM studies has been recognized (11, 108), and only very recently, GIFM studies were performed in live animals to study muscle stem cells, spermatogenesis, and tumor formation (109-111).

1.2.2 Molecular Imaging Methods

Noninvasive cell tracking methods (compared in **Table 1**) are commonly used to follow cell transplants for example in animal models of myocardial infarction and diabetes, or to study cancer biology and cell-based cancer treatment approaches. Within the scope of these applications, molecular

imaging has been shown to be extremely useful to track cells in experimental animals, but also in human patients (56, 112, 113).

Table 1. Overview of high-resolution small-animal imaging modalities (table taken from ref. 114).

Technique	Resolution	Depth	Time	Imaging agents	Target[*]	Cost[#]	Primary small-animal use	Clinical use
MR	10-100 µm	No limit	Minutes-hours	Gadolinium, dysprosium, Iron oxide particles	A, P, M	$$$	Versatile imaging modality with high soft-tissue contrast	Yes
CT	50 µm	No limit	Minutes	Iodine	A, P	$$	Lung and bone imaging	Yes
Ultrasound	50 µm	Millimeters	Minutes	Microbubbles	A, P	$$	Vascular and interventional imaging	Yes
PET	1-2 mm	No limit	Minutes	^{18}F, ^{11}C, ^{15}O	P, M	$$$	Versatile imaging modality with many different tracers	Yes
SPECT	1-2 mm	No limit	Minutes	^{99m}Tc, ^{111}In chelates	P, M	$$	Commonly used to image labeled antibodies peptides and so on	Yes
FRI	2-3 mm	< 1 cm	Seconds-minutes	Photoproteins (GFP), NIR fluorochromes	P, M	$	Rapid screening of molecular events in surface-based tumors	Development
FMT	1 mm	< 10 cm	Seconds-minutes	NIR fluorochromes	P, M	$$	Quantitative imaging of targeted 'smart' fluorochrome reporters in deep tumors	Development
BLI	Several millimeters	Centimeters	Minutes	Luciferins	M	$$	Gene expression, cell and bacterial tracking	No
Intravital microscopy (confocal, multiphoton)	1 µm	< 400 µm	Seconds-minutes	Photoproteins (GFP), Fluorochromes	P, M	$$$	All of the above at higher resolutions but at limited depths and coverage	Limited development (skin)

*Primary area that a given imaging modality interrogates: A, anatomical; M, molecular P, physiological. #Cost of system: $ <100,000; $$ 100–300,000; $$$ >300,000. BLI, bioluminescence imaging; CT, X-ray computed tomography; FMT, fluorescence-mediated molecular tomography; FRI, fluorescence reflectance imaging; GFP, green fluorescent protein; NIR; near-infrared; MR, magnetic resonance; PET, positron emission tomography; SPECT, single-photon emission computed tomography.

The noninvasive detection of reporter gene expression with fluorescence- and bioluminescence-based imaging methods uses light in the visible and near-infrared spectrum (115, 116). The use of green fluorescent protein (GFP)-derived FPs for imaging in live animals is limited. Tissue penetration of light to excite these FPs is low (<1 mm) (117). Fluorescence-based *in vivo* imaging is preferentially performed with red or near-infrared FPs or organic compounds, which allow for deeper light penetration (115, 118). The need for gene transfer and limited penetration depths makes the use of FPs unfeasible in humans, while fluorescent dyes can find clinical use in a limited number of situations (59, 117). For bioluminescence imaging (BLI), luciferase enzymes found in fireflies (*Photinus*) or sea

pansies (*Renilla*) are used as reporter genes. They catalyze light-generating reactions upon supply with their substrates (119). Bioluminescence imaging is one of the most sensitive molecular imaging methods, because of very low signal background (57, 117, 119). However, limited penetration depth and light absorption permit to obtain only semi-quantitative data (119).

Other imaging modalities were first used for clinical diagnosis and human research, but their use in biomedical research extended within the last 10 years (120). Among them are MRI and PET, which are more and more often used for imaging studies with genetically modified mice. Dedicated small animal PET and MR scanners are available and provide sufficient resolution and sensitivity for small animal studies (59, 121, 122). An important advantage of PET- and MR-based imaging approaches is the transferability of preclinical study protocols and results to human studies for research or clinical use (56, 57). In MRI, interactions of tissue protons with the magnetic fields of the MR scanner are spatially resolved. As these interactions depend on tissue type (water content, lipid composition), MRI yields anatomic images with high soft tissue contrast (123-125). Functional imaging studies can be performed as well (59). However, as MRI is reasonably insensitive, image acquisition periods might become exceptionally long (see e.g. 126). Although it has been shown that cells labeled with MR-compatible contrast agents or reporter genes can be detected at single cell resolution, currently available MR-based methods have to be improved in terms of sensitivity and specificity before they are used in research or clinical applications (127-129).

PET makes use of radioactive, positron-emitting isotopes incorporated into tracer molecules like organic compounds and peptides (130, 131). Among others, commonly used PET isotopes are ^{11}C or ^{18}F with half-lives of 20.3 min or 109.8 min, respectively. Radioactive decay of the tracer-bound PET isotope leads to emission of a positron, which recombines with an electron from surrounding tissue. This annihilation process generates two γ photons moving 180° apart. An event is recorded when two γ photons are coincidentally detected on opposite sides of the PET scanner (**Figure 4**). With many of these recorded events ($\sim10^6$-10^7), a three-dimensional dataset is reconstructed representing tracer distribution and concentration inside the subject (132, 133). A large number of tracers were developed to quantify physiological and pathophysiological processes in humans or animals (134). Tracers are intravenously injected into the subject and distribute according to their pharmacokinetic and -dynamic properties (130). Resulting spatial or spatiotemporal differences in tracer distribution are described with mathematical models (135-137) to quantify physiological processes like tissue perfusion, metabolic activity, and tracer binding potential (130, 138, 139), but reporter gene expression as well, as discussed hereinafter. The γ photons arising from the decay of PET radioisotopes show only low and predictable tissue absorption (140, 141). PET data is therefore fully quantifiable, in contrast to data obtained with fluorescence- or bioluminescence-based imaging methods. Furthermore, γ photons

are detected with very high sensitivities, minute amounts (femto- to picomoles) of tracer are sufficient to obtain appropriate signal-to-noise ratios (57). Typically, injected tracer does not interfere with the cellular process under investigation, and radiation doses are considerably low (142-144).

Commercially available dedicated small animal PET scanners generate PET datasets of 1-2 mm spatial resolution (145, 146), which is in range with optical methods, but lower than for MRI. PET datasets contain hardly any anatomical information. For that reason, PET acquisitions are usually preceded or followed by acquisition of anatomic images with MRI or X-ray computed tomography (CT). Here, MRI should be preferred over CT, as MRI has better soft tissue contrast and does not cause additional radiation doses (147, 148). Only recently, a system was described, where a newly developed PET scanner setup is placed inside a small animal MRI scanner allowing for simultaneous acquisition of PET and MR image datasets (149). Short half-lives of commonly used PET isotopes demand special procedures for tracer synthesis. The cyclotron used to generate PET isotopes, and laboratories for tracer production and imaging experiments are typically part of a single imaging facility (150, 151). These infrastructural needs make PET a reasonably expensive molecular imaging method.
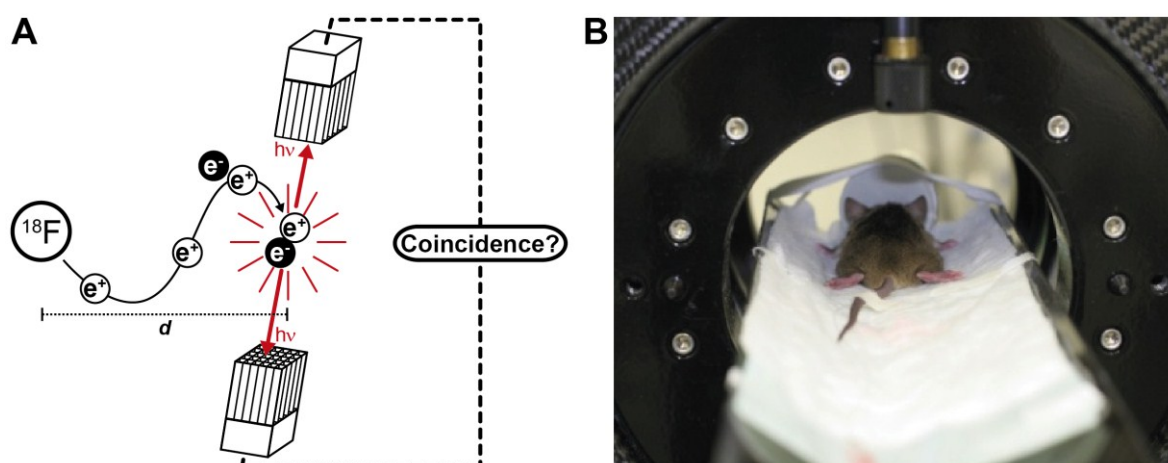
Figure 4. Working principle of positron emission tomography (PET).

A. Radioactive decay of a PET isotope (e.g. ^{18}F) leads to emission of a positron (e^+) that travels through the tissue while losing energy until it approximates an electron (e^-). Both recombine in an annihilation reaction, yielding two γ photons ($h\nu$) with energies of each 511 keV. Photons move away 180° apart and typically do not interact with tissue, so that they reach the PET scanner located around the subject (see panel B). The scanner records events when two photons are coincidentally registered by detectors on opposite sides. Note the free positron path d between actual radionuclide location and the registered annihilation event. d is within a range of 0.2-2 mm for typical PET isotopes and can become a limiting factor of PET image resolution. **B.** A mouse is anesthetized and placed on the bed of a dedicated small animal PET scanner, the radioactive tracer was intravenously injected into the tail vein. Detector modules (as shown in panel A) form several rings inside the scanner to generate a field of view that covers the whole animal.

1.2.3 The *HSV1*-tk PET Reporter Gene

Detection of reporter gene expression with PET is based on tracer retention or accumulation at or in reporter gene-expressing cells (152). All PET reporter genes used so far were selected according to the availability of highly selective tracers, causing tracer accumulation with acceptable specificities (153, 154). The use of the following tracer/reporter gene combinations has been reported: Dopamine D2 receptors with [^{18}F]FESP, somatostatin receptors with radiolabeled somatostatin analogues, and the Na/I symporter with iodine isotopes (155-157). However, expression of the aforementioned reporters occurs also naturally and causes tracer accumulation unrelated to the heterologous expression as reporter gene (153). The *Herpes simplex virus type 1* thymidine kinase (*HSV1*-tk) is not endogenously expressed and widely used as PET reporter gene in combination with pyrimidine- or acycloguanosine-derived tracers (158, 159). Until today, various radiolabeled *HSV1*-tk substrates were generated that represent either acycloguanosines (160-164) or pyrimidines (165-169), the most common tracers are shown in **Figure 5**.

Compound	R$_1$	R$_2$	R$_3$
FMAU	CH$_3$	F	H
FEAU	C$_2$H$_5$	F	H
FFAU	F	F	H
FIAU	I	F	H

Compound	R$_4$	R$_5$	R$_6$
GCV	O	OH	H
FGCV	O	OH	F
FHPG	O	F	H
PCV	CH$_2$	OH	H
FPCV	CH$_2$	OH	F
FHBG	CH$_2$	F	H

Pyrimidine-derived

Acycloguanosine-derived
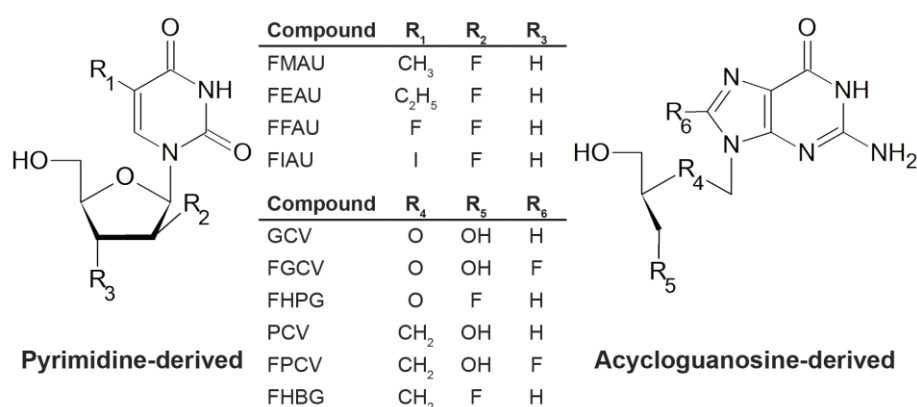
Figure 5. *HSV1*-tk substrates and *HSV1*-tk PET tracers.

Abbreviations: FMAU, 2'-Deoxy-2'-fluoro-5-methyl-1-β-D-arabinofuranosyluracil (170); FEAU, 2'-Deoxy-2'-fluoro-5-ethyl-1-β-D-arabinofuranosyluracil (171, 172); FFAU, 2'-Deoxy-2'-fluoro-5-fluoro-1-β-D-arabino-furanosyluracil (166); FIAU, 2'-deoxy-2'-fluoro-5-iodo-1-β-D-arabinofuranosyluracil (173); GCV, Ganciclovir (174); FGCV, 8-Fluoroganciclovir (175); FHPG, 9-[(3-Fluoro-1-hydroxy-2-propoxy)methyl]guanine (160); PCV, Penciclovir (162); FPCV: 8-Fluoropenciclovir (162); FHBG, 9-[4-Fluoro-3-(hydroxymethyl)butyl]-guanine (161).

The use of *HSV1*-tk as PET reporter gene results from the fact that *HSV1*-tk is the drug target for antiviral chemotherapy of *HSV1* infections (176). Mammalian thymidine kinases have more stringent substrate specificities in comparison to *HSV1*-tk. Acycloguanosine drugs like acyclovir (ACV) and ganciclovir (GCV) used to treat *HSV1* infections are phosphorylated by *HSV1*-tk but not by endogenous thymidine kinases in uninfected cells. Only subsequently, cellular enzymes convert acycloguanosine monophosphates to triphosphates. Their incorporation into a growing DNA strand

causes termination of DNA replication, which ultimately leads to the death of *HSV1*-infected, acycloguanosine-treated cells (174, 177-181). Several experiments show that *HSV1*-tk expression alone is sufficient to induce cell death upon ACV or GCV treatment (173, 182-184). Efforts were undertaken to establish *HSV1*-tk as suicide gene for gene therapy in animal models (185-187) and human patients (188-190). Here, the *HSV1*-tk gene needs to be delivered specifically to target cells. The safe and efficient delivery of therapeutic is a major challenge in the development of gene therapies (191, 192). The idea was to monitor *HSV1*-tk gene delivery with nuclear imaging methods. Initial studies were performed with [^{14}C]FIAU (for tracer names and structures see **Figure 5**) and autoradiography in rats carrying *HSV1*-tk-expressing glioblastoma (193). First noninvasive imaging experiments were performed with [^{131}I]FIAU, γ cameras and single photon emission computed tomography (SPECT) (194). First PET studies were performed by Tjuvajev et al. in glioblastoma-carrying rats with [^{124}I]FIAU (158) or by Gambhir et al. in mice infected with *HSV1*-tk-encoding adenoviruses and [^{18}F]FGCV (159). Then, TKGFP fusion proteins were generated for simplified detection and isolation of reporter gene-expressing cells before transplantation (195). *HSV1*-tk variants with favorable properties for PET imaging and cell ablation were generated by random sequence mutagenesis; they phosphorylate acycloguanosines more efficiently than wild type (wt) *HSV1*-tk (196-198). The most widely used mutant called '*HSV1*-sr39tk' was described by Gambhir et al. in 2000 (199) (**Figure 6**).
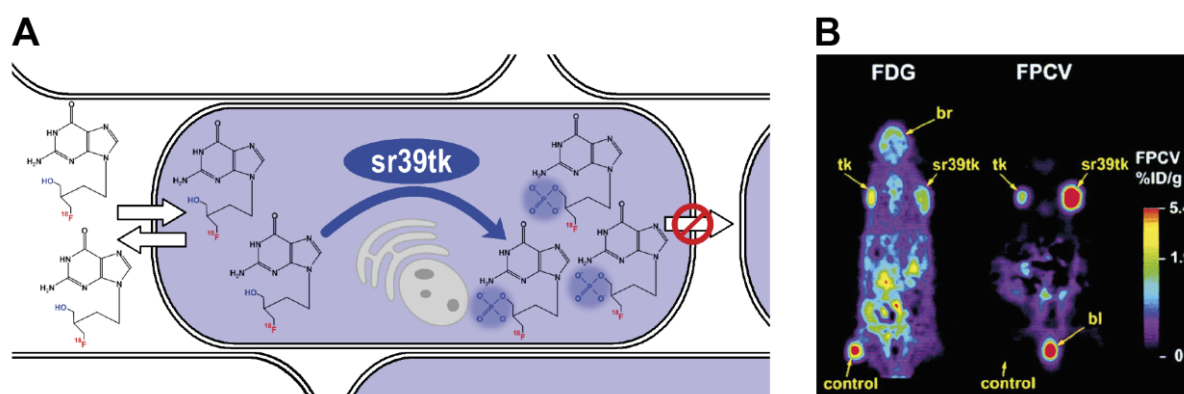
Figure 6. PET-based detection of *HSV1*-sr39tk-expressing cells.

A. Radioactively labeled *HSV1*-sr39tk substrate molecules are applied in sub-pharmacological doses to the animal (here, the PET tracer 9-[4-[^{18}F]-Fluoro-3-(hydroxymethyl)butyl]guanine ([^{18}F]FHBG) is shown). The tracer is taken up by all cells, but phosphorylated only by *HSV1*-sr39tk and not endogenous thymidine kinases. Phosphorylation leads to tracer retention in *HSV1*-sr39tk-expressing cells. After washout of non-phosphorylated tracer from *HSV1*-sr39tk-negative cells, radioactive decay of specifically accumulated tracer is noninvasively detected with the PET method, as shown in panel B. **B.** PET images of a mouse carrying xenografted C6 glioma cell tumors that express either no tk (control), wild type *HSV1*-tk (tk), or *HSV1*-sr39tk (sr39tk). The left PET image acquired with [^{18}F]Fluordeoxyglucose (FDG) shows tissue metabolic activity (br, brain). The right PET image was acquired 24 h later with the thymidine kinase substrate [^{18}F]Fluorpenciclovir (FPCV). FPCV accumulates specifically in *HSV1*-tk- or *HSV1*-sr39tk-expressing tumors, with a ~3-fold higher uptake into *HSV1*-sr39tk-expressing tumor cells. Bladder (bl) uptake is caused by tracer excretion through the kidneys. (Panel B taken from Fig. 5 in ref. 199).

Subsequently, a *HSV1*-sr39tk variant with altered subcellular localization was generated by disrupting the NLS with two amino acid exchanges (R25G, R26S); the resulting mNLS-sr39tk protein caused two-fold higher radiotracer accumulation into cultured cells in comparison to *HSV1*-sr39tk (200). In similar approaches, a truncated *HSV1*-sr39tk variant (*HSV1*-sr39Δtk) and TKGFP variants fused to nuclear export signals were generated (201, 202). So-called triple-fusion reporters were developed for multimodal imaging approaches. They represent fusion proteins of luciferase, GFP, and *HSV1*-tk, or of luciferase, monomeric red fluorescent protein, and *HSV1*-tk (202-204). The *HSV1*-tk protein was further engineered to limit substrate specificities to pyrimidine nucleotides or acycloguanosines (205-207). With these variants, it should be possible to visualize two distinct cell populations within the same subject by the expression of two thymidine kinase variants and subsequent use of two different, variant-specific tracers. Recently, thymidine kinase mutants of human origin that efficiently phosphorylate acycloguanosines were created, which should not cause immune reactions in human patients (208, 209).

Several studies were performed to follow viral gene delivery in animal models of gene therapy approaches (210-212). In other studies, *HSV1*-tk or *HSV1*-sr39tk was expressed in tumor cells by viral transduction. Cells were then injected into animals and tumor proliferation and metastasis was analyzed with PET, as well as tumor regression upon systemic GCV treatment (213-215). Other studies were performed to monitor cell or gene delivery into the heart, or to track transplanted hematopoietic stem cells, bone marrow cells, immune cells, or pancreatic islets (216-224). Activation of *HSV1*-sr39tk or *HSV1*-tk expression via Cre recombination was monitored with PET and [^{18}F]FHBG within liver and heart (225, 226). To induce *HSV1*-sr39tk expression in the liver, adenoviruses carrying a silenced, Cre-inducible *HSV1*-sr39tk transgene were intravenously injected together with Cre-encoding adenoviruses (225). To induce heart-specific *HSV1*-tk expression, adenoviruses carrying a silenced, Cre-inducible *HSV1*-tk transgene were injected into the heart of mice that express Cre under the control of a heart-specific promoter (226).

Beyond the scope of the aforementioned studies, people aimed to identify optimal combinations of *HSV1*-tk reporter gene and tracer. In summary, studies show that <u>sensitivities</u> of *HSV1*-tk with [^{124}I]FIAU or [^{124}I]FEAU and *HSV1*-sr39tk with [^{18}F]FHBG are about to be equivalent (167, 171, 227). The <u>selectivity</u> of *HSV1*-sr39tk and [^{18}F]FHBG is higher, as acycloguanosine-derived radiotracers are poorer substrates for endogenous thymidine kinases (167, 227). [^{18}F]FEAU shows the highest selectivity among pyrimidine-derived radiotracers, and is as well phosphorylated by *HSV1*-sr39tk (167, 171, 228). The longer half-life of [^{124}I]FIAU is advantageous, if tracer retention needs to be detected in tracer clearance routes, so that detection of specific signals is performed after an extended period for elimination of unbound tracer. On the other hand, repeated or sequential studies are complicated by the long half-life of ^{124}I (227, 229). [^{18}F]FHBG is eliminated to a considerable

extent via the hepatobiliary excretion pathway (230). In contrast, [^{18}F]FIAU and [^{18}F]FEAU are eliminated merely via the renal excretion pathway, leading to lower intestinal background and therefore simplified analyses of abdominal images (168, 231). As *HSV1*-sr39tk has a lower affinity for thymidine, changes in cellular thymidine content affect tracer accumulation not as much as *HSV1*-tk combined with pyrimidine derivatives (229). However, several authors claim that transport across the cell membrane might be a limiting factor for accumulation of acycloguanosine-derived radiotracers (167, 227, 229, 232-234). Also *in vivo* detection limits were determined, and vary within one order of magnitude between 1×10^5 and 1×10^6 cells/mL tissue (219, 235-238).

A number of *HSV1*-tk-based PET imaging studies were performed in humans. The first study was carried out with [^{124}I]FIAU to visualize vector-mediated *HSV1*-tk delivery into five patients with recurrent glioblastoma (239). Subsequent studies were performed with [^{18}F]FHBG to visualize delivery of *HSV1*-tk-carrying adenoviruses into hepatocarcinomas of 7 patients (240) or targeting of cytolytic T cells to a glioma in one patient (241). Besides, studies with [^{18}F]FHBG were performed with ten healthy volunteers to determine its pharmacokinetic properties (230), as well as with different animal species to perform a preclinical safety evaluation (242).

The use of transgenic mice for PET imaging was reported in 2000, where mice that express the *HSV1*-tk gene from the albumin promoter were used for PET imaging (154). Since then, pancreatic β cells were visualized with [^{18}F]FHBG and PET in a transgenic mouse line carrying a triple-fusion reporter gene (luciferase-egfp-sr39tk) under the control of the murine insulin promoter. In these mice, β cell masses were noninvasively quantified, and β cell ablation was followed upon treatment with GCV or streptotocozin (243). Another mouse line for noninvasive imaging of liver regeneration and tumor formation was recently created by the targeted insertion of a *HSV1*-tk/luciferase fusion reporter construct behind the α-fetoprotein promoter (244).

1.3 cGMP FRET Measurements with cGi Biosensors

Our current understanding of cyclic guanosine monophosphate (cGMP) signaling under physiological and pathological conditions results in large parts from the analysis of mice that carry mutations in cGMP generator and effector enzymes (245-248). The use of pharmaceutical compounds in animal studies, in studies with cultured cells or isolated proteins is helpful to dissect the function of components of the cGMP pathway. However, we just begin to understand the well-regulated interplay of pathway components among each other and their interactions with components of other signaling pathways in complex environments like whole organisms. It was proposed that subcellular compartmentalization and the formation of macromolecular complexes support the specificity of cGMP effects in particular tissues (**Figure 7**, p. 19) (249). Cyclic GMP-specific biosensors contribute to the understanding of the spatiotemporal dynamics of cGMP under 'native' conditions in live organisms. So far, studies with cGMP biosensors have been performed only in cultured cells or tissue explants (as described in 1.3.3); and in contrast to Ca^{2+} and cyclic adenosine monophosphate (cAMP) biosensors (see e.g. 250, 251), transgenic mice expressing cGMP biosensors for *in vivo* imaging studies have not been described yet.

Transgenic mice that express cGMP indicator (cGi) biosensor proteins (252) have been generated in this work; they were characterized and used as a source for primary cells and tissue samples for cGMP imaging studies. Most importantly, *proof-of-principle* experiments were performed with anesthetized mice to demonstrate that cGMP analyses with cGi-type biosensors is feasible *in vivo*. Hereinafter, the key components of the cGMP pathway will be introduced followed by a brief overview on conventional cGMP detection methods and details on protein-based biosensors in general and cGMP biosensors especially. Finally, the most prominent functions of the cGMP signaling pathway in health and disease will be explained with particular focus on studies performed with cGMP biosensors.

1.3.1 Components of the cGMP Pathway

Cyclic GMP can be synthetized by soluble guanylyl cyclases (sGC) upon stimulation by nitric oxide (NO) (253). NO synthesis from L-arginine and oxygen is catalyzed by tetrahydrobiopterin-dependent nitric oxide synthases (NOS), of which three isoforms have been identified (254). Neuronal NO synthase (nNOS) and endothelial NO synthase (eNOS) synthetize NO at low nanomolar concentrations after stimulation with Ca^{2+}-bound calmodulin (254). In contrast, inducible NO synthase (iNOS) in immune cells like macrophages and microglia is regulated on its expression level. iNOS is constitutively active and produces cytotoxic NO concentrations that act largely independent from the NO/sGC/cGMP pathway (255). Although it is generally accepted that sGCs are the only known class

of physiological NO receptors, NO might exert sGC/cGMP-independent effects, for example by protein S-nitrosylation or peroxonitrite formation, even when synthetized in low concentrations by nNOS or eNOS (256). The heterodimeric sGC protein binds NO to a prosthetic heme group that also binds carbon monoxide weakly, but not O_2, which is critical for sGC to function as NO receptor in an aerobic environment (257). Two catalytically active sGC heterodimers ($\alpha_1\beta_1$ and $\alpha_2\beta_1$) have been identified, which share the same β_1 subunit and possess identical biochemical properties (258). Another β subunit (called β_2) seems to represent a physiologically irrelevant isoform (258). Both relevant sGC heterodimers possess complex NO binding and activation mechanisms (259) and bind ATP as allosteric modulator (260), leading to an *in vivo* sensitivity for NO with an $EC_{50} \approx 10$ nM (261). Both sGC isoforms typically localize to the cytosol, but it has been shown that they might show altered subcellular localization in distinct tissues (262-264). The sGC α_2 isoform possesses an additional PDZ domain (from postsynaptic density protein PSD95, *Drosophila* disc large tumor suppressor Dlg1, and zonula occludens-1 protein zo-1) leading to its integration into localized protein complexes, for example in the presynaptic terminal (265). The sGC $\alpha_1\beta_1$ isozyme is expressed in most tissues, while the expression pattern of $\alpha_2\beta_1$ sGC is more restricted, showing highest expression in brain, and lower expression in lung, colon, heart, spleen, uterus, and placenta (258).

Another class of cGMP-synthetizing enzymes are particulate guanylyl cyclases (pGCs), of which seven isoforms (GC-A to GC-G) have been identified (246, 266, 267). pGCs span the plasma membrane, where they form catalytically active homodimers. For GC-A to GC-C, peptide ligands have been identified that activate cGMP synthesis (266), while ligands for the remaining isoforms remain unknown (246). GC-A is stimulated by atrial and brain natriuretic peptide (ANP, BNP), while GC-B synthesizes cGMP upon stimulation with C-type natriuretic peptide (CNP). GC-A and GC-B are expressed in vascular smooth muscle (VSM), endothelium, and heart; GC-A is also expressed in the central and peripheral nervous system, adrenals, spleen, and kidney, while GC-B is additionally expressed in the bone (246). Although all GC-A and -B ligands are called 'natriuretic' peptides (NPs), they modulate a variety of functions unrelated to natriuresis (266). GC-C is expressed in intestinal epithelium and kidney, and is stimulated by the intestinal peptides guanylin and uroguanylin, as well as by heat-stable bacterial enterotoxins (246). GC-E and GC-F are expressed in photoreceptor cells of the retina, GC-F is additionally expressed in pineal gland, olfactory bulb, and in auditory parts of the inner ear (246). Both GC-E and GC-F are activated ligand-independently by protein interactions at the inner side of the cell membrane; for example in the retina by the calcium-binding proteins GCAP-1 and GCAP-2 (246). GC-D and GC-G represent pseudogenes in humans, but they are functionally expressed in rodents, where GC-D contributes to olfactory sensation in a small cell population of the olfactory system, while GC-G seems to be involved in renal pathophysiology (246). The natriuretic peptide receptor C (NPR-C) carries no guanylyl cyclase activity, but acts as a clearance receptor for

NPs by mediating their cellular internalization and degradation. NPR-C is expressed in VSM, adrenals, brain, heart, kidney, and mesentery (268).
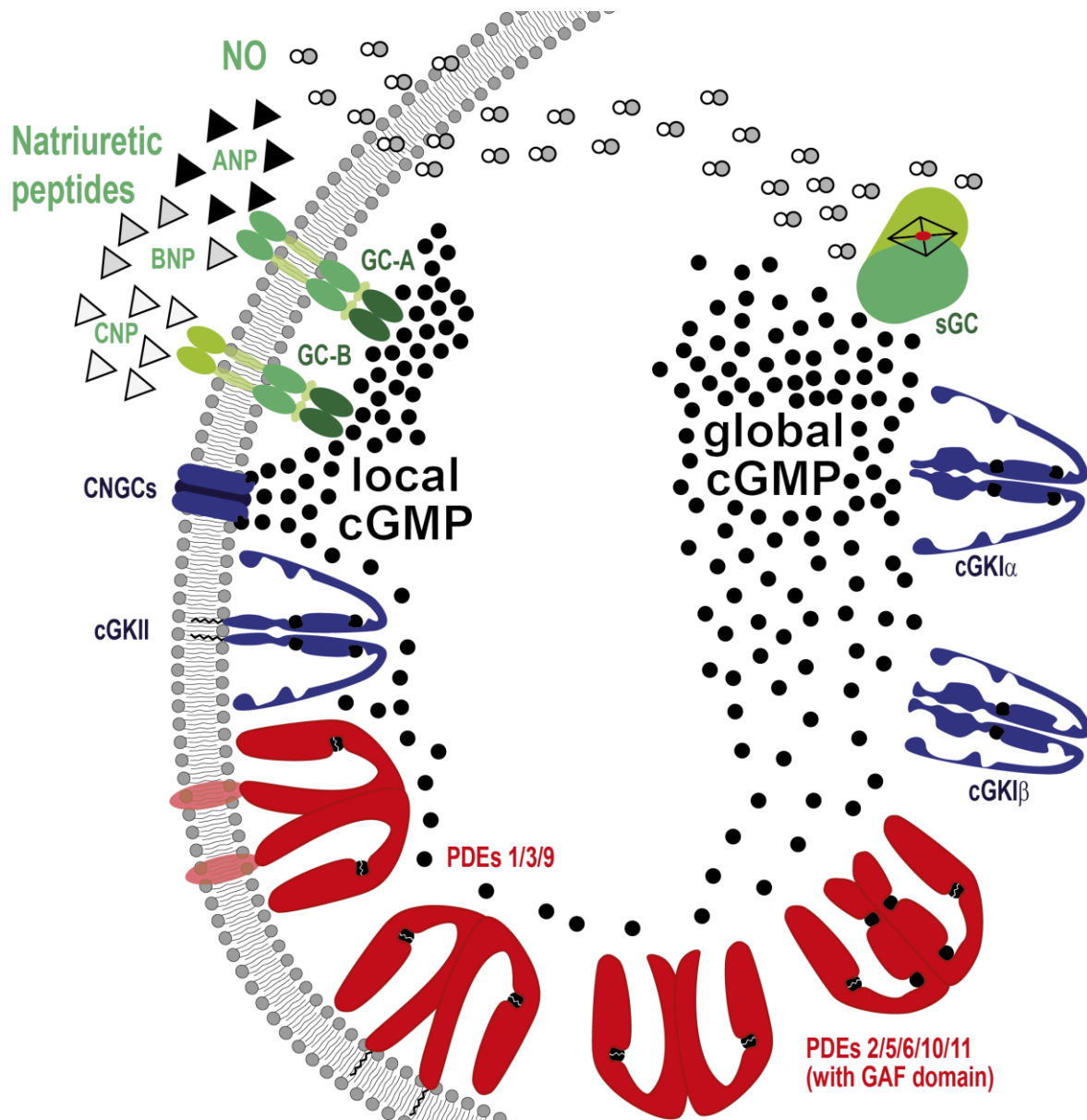
Figure 7. Subcellular localization of cGMP generators and effectors, and of cGMP-degrading phosphodiesterases.

Cyclic GMP generators are shown in green, cGMP effectors in blue and cGMP-degrading PDEs in red. According to their subcellular localization, it has been proposed that at least two different cGMP pools exist (249). The first pool represents cGMP in the cytosol (global cGMP), while the other pool represents cGMP at the plasma membrane (local cGMP). Abbreviations: sGC, NO-stimulated soluble guanylyl cyclase; GC-A, ANP/BNP-stimulated particulate guanylyl cyclase A; GC-B, CNP-stimulated particulate guanylyl cyclase B; ANP, atrial natriuretic peptide; BNP, brain natriuretic peptide; CNP, C-type natriuretic peptide; CNGC, cyclic nucleotide-gated channel; cGKIα/β, cGMP-dependent protein kinase type Iα or Iβ; cGKII, cGMP-dependent protein kinase type II; PDE, phosphodiesterase; GAF, regulatory domains identified in cGMP-specific phosphodiesterases, *Anabaena* adenylyl cyclases, and *E. coli* FhlA.

The biological effect of cGMP is transmitted by cyclic nucleotide-binding ion channels, cGMP-dependent protein kinases and cAMP- or cGMP-degrading phosphodiesterases. Cyclic nucleotide-binding ion channels span the plasma membrane and belong to the superfamily of pore-loop cation channels (269, 270). Three subfamilies have been identified: cyclic nucleotide-gated (CNG) channels that open upon intracellular binding of cyclic nucleotides and that are permeable for Na^+, K^+ and Ca^{2+}, and hyperpolarization-activated cyclic nucleotide-gated (HCN) channels that pass Na^+ and K^+ and whose voltage-dependent opening probabilities are shifted by cyclic nucleotide binding (269). The third family encompasses Eag-like K^+ channels, but the role and function of cyclic nucleotide binding at these channels remains elusive (269). The family of CNG channels encompasses six homologous members that are expressed in different combinations in photoreceptors and olfactory neurons with preferential cGMP or cAMP binding, respectively (270). In other tissues including brain, kidney, endocrine tissues, and sperm cells, CNG expression is detected on the RNA level, but a functional role in these tissues was not shown yet (269).

The cGMP-dependent protein kinases (cGKs) belong to the family of serine/threonine kinases. In vertebrates, the genes Prkg1 and Prkg2 encode three cGK isozymes, cGK type Iα or Iβ (cGKIα/β), and cGK type II (cGKII), respectively (271, 272). All cGK isozymes possess two cGMP binding sites and are activated by nanomolar to low micromolar cGMP concentrations (7). They undergo a remarkable structural change upon cGMP binding that releases an inhibitory pseudo-substrate domain on the N-terminus from the catalytic core and allows the phosphorylation of substrate proteins (7, 273, 274). Prkg1-encoded cGKIα and cGKIβ represent cytosolic enzymes that differ in their N-termini, resulting from the alternative use of 5' exons (275-277). The N-termini serve as anchors leading to subcellular targeting of the isoforms (277). Furthermore, they carry leucine zipper motifs that are necessary for the formation of catalytically active cGK homodimers. The N-termini also interact with isoform-specific substrate proteins, which might be essential for the integrity of distinct cGMP signaling pathways in the same cell (278). However, several cGKI substrates are phosphorylated by both isoforms and the analysis of isoform-specific 'cGKI rescue' mice raised the possibility that substrate specificity is less rigorous *in vivo* than *in vitro* (279, 280). cGKI is strongly expressed in smooth muscle (SM), platelets, cerebellum, hippocampus, dorsal root ganglia, neuromuscular junctions, and kidney, and at lower levels in cardiomyocytes, vascular endothelial cells, granulocytes, chondrocytes, osteoclasts, and in some brain nuclei (281, 282). The cGKIα isozyme is mainly found in lung, heart, dorsal root ganglia, and cerebellum, while the cGKIIβ isozyme predominates in platelets, hippocampal neurons, and neurons of the olfactory bulb. No such preference is observed for SM tissue (247, 281). Prkg2-encoded cGKII is located at the plasma membrane due to myristoylation of its `Gly2` residue and is expressed in several brain nuclei, intestinal mucosa, kidney, adrenal cortex, chondrocytes, and lung (277, 283). The cGKs I and II are typically not co-expressed within the same cell (277). Characteristic

substrates for cGKI or cGKII are ion channels, G proteins, and regulatory or cytoskeletal-associated proteins that modulate the function of other signaling pathways (278).

The superfamily of phosphodiesterase (PDE) enzymes includes eleven gene families that contain one or more family members (248, 284, 285). Members of some PDE families degrade only cGMP (PDEs 5, 6, 9) or cAMP (PDEs 4, 7, 8), while PDEs 1, 2, 3, 10, 11 degrade both cyclic nucleotide species with varying preference (248, 284). PDE activities are regulated by mutual competitive inhibition of cAMP or cGMP at the catalytic sites, while activities of PDEs 2, 5, 6, 10, and 11 are additionally regulated by cGMP or cAMP at allosteric binding sites in so-called GAF domains initially found in c<u>G</u>MP-specific phosphodiesterases, *Anabaena* <u>a</u>denylyl cyclases, and *Escherichia coli* (*E. coli*) <u>F</u>hlA (248). The 21 PDE genes further diversify on the transcript level by alternative initiation sites and alternative splicing, so that more than at least 50 different phosphodiesterase proteins are generated (248). All cells express a subset of certain PDEs that differ in specificity, kinetic properties, subcellular localization, regulation by distinct protein kinases, or in the capability to form macromolecular complexes with regulatory, anchoring, or scaffold proteins (286). Among cGMP-specific phosphodiesterases, PDE6 is exclusively expressed in photoreceptor cells (285), while PDE5 is of outstanding importance for the regulation of cGMP signaling in SM, heart, brain and other tissues (287, 288). cGMP binding to PDE5 GAF domains and phosphorylation by cGKI at $_{Ser92}$ increase its enzymatic activity as well as cGMP binding affinity, which generates a negative feedback loop that efficiently controls intracellular cGMP levels (289). Compartmentalization and other regulatory mechanisms enable crosstalk between cGMP and cAMP signaling pathways, mainly via PDEs 2, 3, and 10. cGMP binding to PDE2 GAF domains stimulates cAMP cleavage, while cGMP acts as a competitive inhibitor for cAMP at the catalytic site of PDE3, and therefore inhibits cAMP degradation (290). However, PDE3 will also degrade cGMP under physiological conditions (291). For PDE10, cAMP binding to GAF domains has been shown to inhibit cGMP degradation (292).

1.3.2   Detection of cGMP with Biosensors

The spectrum of *in vitro* methods for cGMP quantification was recently described in a comprehensive review by P. M. Schmidt (293). Biochemical methods vary in their need for preparative steps, for example to remove or inactivate interfering substances. cGMP antibodies are used to quantify cGMP in radioimmunoassays (RIA) and enzyme-linked immunosorbent assays (ELISA), among others. Antibody-based cGMP detection is very sensitive and selective, and cross-reactions with other nucleotides (especially cAMP) are virtually absent. Assays need to be performed with homogenous biological samples. Initial sample lysis does not permit detection of spatially distinct cGMP elevations, for example in cells at subcellular localization or in heterogeneous tissue samples. However, cGMP antibodies were also used to analyze spatially confined cGMP elevations *in situ* on

formaldehyde-fixed tissue samples (293, 294). Still, all aforementioned methods (methods like RIA and ELISA, and staining with cGMP antibodies) are end-point assays that require sample lysis or fixation rendering repeated cGMP measurements within the same sample impossible. As discussed below, the use of optical methods and fluorescence microscopy enables the spatiotemporal tracing of cGMP and other signaling molecules in living biological samples.

1.3.2.1 Analysis of Cell Signaling with Optical Imaging

Initially, optical imaging methods were used for Ca^{2+} quantification in live cells or tissues. Calcium-binding organic compounds were developed that alter their optical properties upon Ca^{2+} binding (295-297). A prominent member of this kind of indicators is fura-2, which has excitation maxima at 335 nm in the absence and 362 nm in the presence of Ca^{2+} and emits light at 510 nm (298). Other compounds have been developed being sensitive to pH, chloride, and metal ions (299-302). However, the design of compounds to detect molecules that are more complex failed. Alternative to compounds, many proteins bind (signaling) molecules with high affinity and specificity. Their use led to engineered, protein-based indicators (303-307). Actually, one of the first Ca^{2+} indicator proteins is the naturally occurring bioluminescent protein aequorin from the jellyfish *Aequorea victoria* (308). Later, a synthetic cAMP sensor was built by labeling purified catalytic and regulatory subunits of the cAMP-dependent protein kinase A (cAK) with fluorescent dyes. The reconstituted enzyme complex was microinjected into single cells to follow cAMP signals (309). Although this protein-based indicator was successfully used for studies in live cells (310-312), it requires high efforts that are not feasible for routine application, high-throughput screenings, or experiments in complex, multi-cellular organisms (306).

Many biosensors that are used today are derived from the green fluorescent protein (GFP). It was also isolated from *Aequorea victoria* (313) and is the natural resonance energy acceptor for aequorin (314). A fluorescent chromophore is created inside the β barrel of GFP by a cyclisation reaction between `Ser65`, `Tyr66`, and `Gly67` (315-317). After isolation of the gfp gene (315, 318), mutations were introduced to increase speed of folding and chromophore formation, quantum yield and photostability as well as its spectral properties leading to enhanced GFP (EGFP; 319-321). Furthermore, spectrally distinct EGFP variants were created by amino acid exchanges inside or around the chromophore, like enhanced cyan FP (ECFP) (322, 323) and enhanced yellow FP (EYFP) (323, 324).

ECFP and EYFP are included in many biosensors based on fluorescence resonance energy transfer (FRET). FRET is possible when emission wavelengths of the donor fluorophore (ECFP) overlap with the excitation wavelengths of the acceptor fluorophore (EYFP) (**Figure 8A**). Upon excitation of the donor, energy can be transferred to the acceptor, leading to light emission from the donor light at

higher wavelengths than the donor itself emits (**Figure 8B**) (325). FRET efficiencies depend on fluorophore distance and their relative orientation; at distances of more than 5-10 nm, FRET efficiencies drop dramatically, which leads to decreased light emission from the acceptor fluorophore and increased light emission from the donor fluorophore (325).
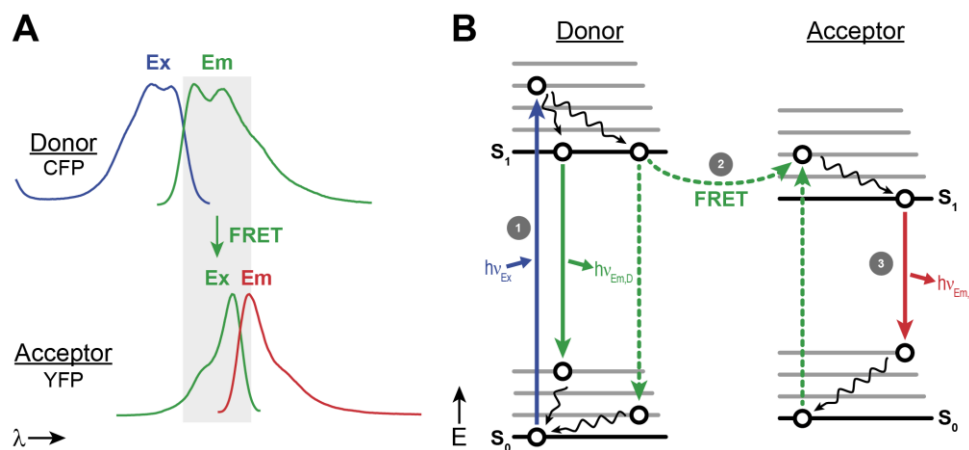

Figure 8. Fluorescence resonance energy transfer (FRET).

A. Excitation (Ex) and emission (Em) spectra of ECFP (donor fluorophore) and EYFP (acceptor fluorophore). Donor fluorophore emission and acceptor fluorophore excitation show significant overlap, which is necessary for two fluorophores to build an effective FRET pair. **B.** Jablonski diagram describing the FRET process. The donor fluorophore gets excited into its S_1 state by a photon with the energy $h\nu_{Ex}$ (**1**). After thermal equilibration (curved lines), the donor fluorophore will emit a photon with an energy of $h\nu_{Em,D}$, or it transfers its energy via FRET to the acceptor fluorophore (**2**). This results in radiation-free transitions between S_1 and S_0, or S_0 and S_1 of donor and acceptor fluorophore, respectively. The acceptor fluorophore now emits a photon with an energy of $h\nu_{Em,A}$ (**3**). Note that photon energies are in the order of $h\nu_{Ex} > h\nu_{Em,D} > h\nu_{Em,A}$.

The first CFP/YFP-FRET sensors were used to detect Ca^{2+} (326, 327) and cAMP (328). Since then, a vast number of biosensors based on ECFP and EYFP or their improved descendants were developed and used to follow dynamic changes of cGMP, cAMP, Ca^{2+}, and other messengers. Furthermore, sensors are used to monitor intracellular pH, chloride, glucose, activities of specific proteases or kinases, and interactions of FP-labeled proteins (13, 305, 329-333). All sensors share the common feature that analyte binding, phosphorylation, or proteolytic cleavage lead to a change in fluorophore distance and/or relative orientation. Sensors consist of two separate polypeptide chains, each carrying one fluorophore and a part of the sensor domain (intermolecular FRET), or they consist of a single polypeptide chain carrying sensor domain, ECFP, and EYFP (intramolecular FRET). Single-chain sensors simplify the analysis of FRET data, because fluorophores always exist in equimolar ratios (334). Optical sensors are also built from FRET pairs different from ECFP and EYFP (335). Moreover, biosensors built on other detection principles are created, for example bioluminescence energy transfer (BRET) and cyclic permutated EGFP (cpEGFP). Below, concrete examples for different sensor designs are given for cGMP biosensors.

1.3.2.2 cGMP-specific Biosensors

So far, CNG channels, FRET-based cGMP biosensors and other fluorescence-based cGMP biosensors are used to detect cGMP in live cells (**Table 2**) (336) .

Heterologous expression of CNGs allows for cGMP detection with electrophysiological recording methods or by measuring Ca^{2+} influx through CNG channels with fluorescent dyes or aequorin (337-340). As CNG channels are integrated into the plasma membrane, only plasma membrane-localized cGMP induces detectable signals. CNG channels have rather low cGMP selectivities in comparison to other biosensors and recognize cAMP at physiological concentrations (336).

Table 2. Properties of selected protein-based cGMP sensors.

Name	Fluorophores	Detection mode[1]	Signal change (%)[2]		EC_{50} cGMP [μM]	EC_{50} cAMP [μM]	Selectivity $\dfrac{EC_{50}(cAMP)}{EC_{50}(cGMP)}$	Ref.
			In vitro	Intracellular[3]				
CNGs								
wt CNG A2	-	Ion current↑	-	-	1.6	36	22.5	337, 338
cGKI cGMP-BD A & B								
CGY-Del1	ECFP/EYFP	FRET↑	n.d.	24[(Y/C)]	0.02	0.15	7.5	341
Cygnet-2	ECFP/EYFP	FRET↓	38[(C/Y)]	24[(C/Y)]	1.9	185	100	342
cGi-500	ECFP/EYFP	FRET↓	77[(C/Y)]	38[(C/Y)]	0.5	>100	>200	252
cGi-3000	ECFP/EYFP	FRET↓	72[(C/Y)]	37[(C/Y)]	3	>100	>30	252
cGi-6000	ECFP/EYFP	FRET↓	58[(C/Y)]	30[(C/Y)]	6	>1000	>166	252
δ-FlincG	cpEGFP	Fluorescence↑[4]	75	75	0.17	48	280	343
		Ratiometric↑[5]	250	n.d.	0.49	48	100	
cGKI cGMP-BD B								
cGES-GKIB	ECFP/EYFP	FRET↓	n.d.	30[(C/Y)]	5	485	100	344
PDE5 GAF A								
cGES-DE5	ECFP/EYFP	FRET↑	16[(Y/C)]	30[(Y/C)]	1.5	630	420	343
GFP2-GAFa-Rluc	RLuc/EGFP	BRET↑	30[(G/L)]	30[(G/L)]	0.03	>1	>33	345
Red cGES-DE5[6]	Sapphire/RFP	FRET↑	10[(R/S)]	15[(R/S)]	0.04	>100	>1000	346
Cygnus[7]	mTagBFP/sREACh	Fluorescence↓	10	20	1	400	400	347

1) Arrows indicate signal increase (↑) or decrease (↓) of the sensor upon cGMP binding; 2) In case of FRET-based sensors, signal changes were determined via emission ratios of the fluorophores as indicated in brackets; C, ECFP; Y, EYFP; G, EGFP; L, *Renilla* luciferase; R, RFP; S, sapphire; 3) Apparent intracellular FRET changes vary depending on the setup used for measurements (e.g. filter sets); 4) Determined using 480 nm excitation and 510 nm emission; 5) Determined using ratiometric measurement with excitation at 410 and 480 nm and emission at 510 nm (given as 480/410 nm ratio); 6) This is a 'red' FRET-based cGMP indicator; it can be used for ratiometric measurement with excitation of GFP-derived sapphire and emissions of sapphire and red fluorescent protein (RFP) dimer2; 7) This is a 'blue' cGMP sensor based on FRET between monomeric Tag blue fluorescent protein (mTagBFP) as FRET donor and super resonance energy accepting chromoprotein (sREACh) as FRET acceptor; sREACh is a so-called 'dark YFP quenching FRET acceptor' that does not emit light upon excitation; cGMP binding causes an increase of the FRET efficiency and, therefore, a decrease of mTagBFP emission; single-channel measurement of mTagBFP with 405 nm excitation and 440 nm emission is performed. Abbrevations: cGKI cGMP-BD, cGMP-binding domain of cGMP-dependent protein kinase type I; n.d., not determined; PDE5 GAF, cGMP-binding GAF domain of phosphodiesterase 5 (GAF: domain first identified in c<u>G</u>MP-specific phosphodiesterases, *Anabaena* <u>a</u>denylyl cyclases and *E. coli* <u>F</u>hlA).

A variety of FRET-based cGMP biosensors derived from cGKI or PDE2/PDE5 GAF domains exist. They differ in kinetic properties, sensitivity, and selectivity (**Table 2**) The first reported cGMP FRET sensor called CGY-Del1 was built by fusing ECFP and EYFP to full-length cGKIα lacking 47 amino acids of the N-terminus to prevent dimerization (341). In parallel, cygnet-2 was created, which is also derived from cGKIα, but the cGKI N-terminus was further truncated, and the cGKI kinase domain was inactivated by introducing a T516A point mutation that abolishes downstream effects caused by kinase activity of the sensor protein (342). Further truncation of cGKIα and deletion of the catalytic domain led to cGi-type biosensors: by screening different cGKIα truncations, 24 cGMP-responsive sensor constructs were obtained by Russwurm et al. (252). Three of them were chosen by the authors for further characterization and named cGi-500, cGi-3000, and cGi-6000 according to their respective cGMP affinities (=EC$_{50}$ values) of 500, 3000 and 6000 nM as determined with fluorescence spectroscopy with extracts of cGi-expressing cells (252). Fusion of ECFP and EYFP to single PDE2- or PDE5-derived GAF domains led to cGES-DE2 and cGES-DE5 sensors, respectively (344). A cGES-DE5 variant called red-cGES-DE5 made from the FRET pair sapphire/red fluorescent protein (RFP) is spectrally distinct from ECFP/EYFP, allowing for simultaneous measurements with two different biosensors in the same sample (346). The same group created another cGES-DE5 variant ('cygnus') that can also be used in parallel with ECFP/EYFP-based FRET sensors (347).

Another cGMP biosensor based on BRET was generated by fusing the PDE5 GAF A domain to *Renilla* luciferase and EGFP (345). Light energy is generated in a luciferase-catalyzed oxidation of luciferin, and is transferred via BRET to EGFP. In contrast to FRET-based biosensors, the sensor does not need to be excited with light, but sensor-expressing cells need to be supplied with luciferin. FlincG-type biosensors were generated by combining circular permutated EGFP (cpEGFP) with a truncated cGKIα protein that has approximately the same length as in cGi-type biosensors. Here, cGMP binding leads to conformational changes that increase cpEGFP fluorescence intensity (343, 348).

1.3.3   Functions of the cGMP Pathway

1.3.3.1 Vasculature

Cyclic GMP is generated in vascular smooth muscle cells (VSMCs) by sGC or pGC to induce vessel relaxation leading to a reduction of vascular tone and therefore systemic blood pressure (7). NO/sGC/cGMP signaling emanates in endothelial cells, where NO is synthetized by eNOS upon chemical and physical stimuli. NO diffuses into adjacent VSMCs and elevates cGMP by sGC activation (349). The increase in cGMP activates cGKIα- and cGKIβ-specific signaling pathways and results in reduced intracellular Ca^{2+} levels and Ca^{2+} sensitivity, and in activation of other,

Ca^{2+}-independent pathways causing SM relaxation. Individual contributions of each pathway may vary with type, function, and contractile status of the vessel (7, 247, 350, 351). Genetic ablation of eNOS, sGC β1, or cGKI leads to a loss of endothelium-induced relaxation (245, 352, 353). In sGC α_1 *knock-out* mice, remaining sGC $\alpha_2\beta_1$ activity restores normal NO/cGMP pathway function in large parts, albeit the sGC $\alpha_1\beta_1$ isoform is prevalent in VSMCs (354). Loss of sGC $\alpha_1\beta_1$ abolishes any detectable NO-induced cGMP elevations, but not NO-induced (and sGC inhibitor-sensitive) relaxation that is still present, but less efficient (245, 354). This finding can be explained by localized cGMP synthesis by remaining sGC $\alpha_1\beta_2$ to amounts sufficient for induction of SM relaxation (245). In fact, recent studies suggested that only very low amounts of cGMP are sufficient to cause a full biological response to sGC stimulators in the vasculature (354). However, other studies implied sGC, cGMP- and cGKI-independent relaxation via another 'endothelium-derived hyperpolarizing factor' released from endothelial cells upon stimulation with acetylcholine (355-357).

The ANP/GC-A/cGMP pathway plays as well a complex role in the vasculature, as it acts on both endothelial cells and VSMC function. VSMC-specific GC-A ablation abolishes vasodilation leading to acute hypertension, while GC-A ablation in endothelial cells does not affect vasodilation, but causes chronic hypervolemia and hypertension (358, 359). The ANP/GC-A/cGMP pathway probably modulates blood pressure via modulation of endothelial permeability in the microvasculature (360, 361). This shows that ANP/NO-induced and cGMP/cGKI-mediated vasorelaxation is not necessarily an essential regulator of chronic blood pressure, while it plays an important role in acute blood pressure regulation. Moreover, ANP and NO might act differently within the same (smooth muscle) cell. ANP-mediated vasodilation is insensitive to PDE5 inhibition by sildenafil *in vitro* and *in vivo*, except in the pulmonary vasculature (249, 362). Furthermore, failure of one cGMP pathway can be compensated by the up-regulation of the other pathway (245, 363). With the use of CNG channels expressed in cultured VSMCs, Piggott et al. showed that ANP induces membrane-localized cGMP elevations more readily than NO, while NO stimulation results in higher total cGMP levels (340). In similar experiments with FlincGs, it has been shown that ANP stimulation induces membrane-localized cGMP elevations, while NO stimulation leads to global cGMP increases. In contrast to findings mentioned above, sildenafil treatment has been shown here to cause a loss of spatially restricted cGMP elevations upon ANP stimulation (343). A possible reason for these contradictory results could be the fact that one finding was made *in vivo* (362), while the other was obtained in cultured VSMCs (343).

In addition to its role for vasodilation and blood pressure regulation, studies showed that cGMP pathways modulate angiogenesis and vasculogenesis, and play a role in disorders associated with pathological angiogenesis and vascular remodeling (364-367). Remarkably, it has been shown that the

NO/sGC/cGMP pathway can both promote and inhibit vascular remodeling (247, 368). The CNP/GC-B/cGMP pathway seems to affect angiogenesis as well as vascular regeneration, as vessel injury induces CNP expression in the vessel wall, which in turn stimulates endothelial cell proliferation, but attenuates proliferation of VSMCs (364, 369). BNP acts as an 'stress-responsive' hormone in a paracrine way to modulate endothelial proliferation and tissue remodeling in the heart, vasculature and other tissues (370). Other studies implicated a role of cGKI in the modulation of gene expression (7, 371-373). In GIFM experiments with hyperlipidemic mice, cGKI ablation was induced in individual VSMCs, which contributed less to atherosclerotic plaques in comparison to cGKI-expressing VSMCs in the same animal (103). These and other results suggested that cGMP signaling plays an adverse role, at least under distinct conditions, by contributing to phenotypic modulation and proliferation of VSMCs (247, 368). However, how cGMP signaling induces both beneficial and detrimental effects is largely unknown. Possible reasons for this opposing behavior might be distinct spatiotemporal profiles of cGMP synthesis and downstream signaling events (368, 374).

1.3.3.2 Heart

NO and NPs act as autocrine or paracrine messengers in the heart and mediate contractility and ventricular relaxation via activation of the cGMP pathway. NO and CNP exert a negative or positive inotropic effect, respectively, which is mediated by cGKI in both cases (375, 376). Compartmentalization of cGMP (and cAMP) signaling serves as a possible explanation. Indeed, with FRET-based cAMP sensors and CNG channels as cGMP sensors, it has been shown that cGMP and cAMP levels are highly compartmentalized in cardiomyocytes (377). Generation of cGMP by pGCs and sGCs occurs in distinct subcellular compartments, while PDEs 2 and 5 limit cGMP spreading throughout the cell. PDE2 limits ANP/GC-A-generated cGMP at the plasma membrane, and PDE5 NO/sGC-generated cGMP in the cytosol. Cytosolic cGMP does not reach the plasma membrane, except upon PDE5 inhibition (264). cGMP signaling is additionally modulated via cGKI by phosphorylation of PDE5 and possibly GC-A, leading to a reduction of NO/sGC-derived cGMP, but an increase of ANP/GC-A-generated cGMP (378). Interaction of cGMP with PDEs 2 and 3 regulates cAMP levels and therefore cAK activity in distinct cellular compartments. Spatially confined cAMP elevations are necessary to control specific modulatory effects on cardiac function (377).

1.3.3.3 Kidney and Adrenal Gland

cGMP signaling modulates blood pressure regulation also in kidney and adrenal gland (7, 379). In the kidney, cGMP signaling affects glomerular filtration rate, ion absorption, and renin release via inhibition of cAMP-hydrolyzing PDE3 or via cGKs (380, 381). In the adrenal gland, the

ANP/GC-A/cGMP pathway inhibits ACTH-dependent aldosterone secretion either by stimulating cAMP-hydrolyzing PDE2 or via cGKII-mediated effects (382, 383).

1.3.3.4 Urogenital System

The NO/cGMP signaling pathway plays an important role for penile erection: NO synthetized by eNOS in the endothelium and nNOS in non-adrenergic, non-cholinergic (NANC) neurons induces smooth muscle relaxation in the corpus cavernosum that fills with blood leading to penile erection (384). Several PDE5 inhibitors (sildenafil, tardenafil, and vardenafil) are approved for the treatment of erectile dysfunction (385). The NO/sGC/cGMP/cGKI pathway also modulates micturition and contractility of the urinary bladder and voiding in the urinary duct, where crosstalk between cAMP and cGKI has been reported (386).

With the combined use of cAMP and cGi-type cGMP biosensors, a modulatory effect of cGMP on oocyte maturation was shown (387). cGMP produced in follicles enters the oocyte through gap junctions, where it inhibits cAMP degradation by PDE3. High cAMP levels arrest the oocyte in the meiotic prophase. Upon stimulation with luteinizing hormone, cGMP levels decrease in follicle and oocyte, releasing PDE3 for cAMP degradation. The drop of cAMP leads to progression of meiosis (387). PDE3A deletion leads to female infertility due to defects in oocyte maturation and fertilization (388).

1.3.3.5 Gastrointestinal Tract

Deletions of sGC β_1 or cGKI lead to severe gastrointestinal phenotypes that cause a dramatically reduced lifespan. This phenotype emphasizes the importance of NO/sGC/cGMP/cGKI signaling for the regulation of intestinal smooth muscle tone, which is necessary for food transport and peristalsis (352, 353). The (uro)guanylin/GC-C/cGMP/cGKII pathway is an important regulator of gastrointestinal secretion in small intestine, where it regulates secretion of bicarbonate, chloride and water (389). Additionally, it has been proposed that (uro)guanylin and GC-C form an enteric-renal axis to coordinate salt ingestion and natriuresis (266, 390). Another proposed function of guanylin and GC-C is the regulation of intestinal cell proliferation, therefore, a role in colon cancer formation was suggested (246).

1.3.3.6 Bone

Signaling via CNP/GC-B/cGKII represents a local regulatory system in the bone to activate chondrocyte proliferation and differentiation in the growth plate, but particular intracellular pathways remain elusive (389, 391, 392).

1.3.3.7 Blood

NO/sGC/cGKI signaling modulates the inhibition of blood platelet adhesion and aggregation (393). Activation of the cGMP pathway reduces intracellular calcium levels and calcium sensitivity (394, 395). Furthermore, cGMP diminishes cAMP degradation via PDE3 inhibition, which further augments its anti-aggregatory effect via cAK activation (396, 397). Despite their small size, it has been proposed that platelets contain microdomains of cGMP signaling that consist of protein complexes of cGKIβ, PDE5 and type I inositol triphosphate (IP$_3$) receptor (398). Furthermore, it has been shown that the cGMP/cGKI pathway modulates erythrocyte survival, and that cGKI ablation leads to increased erythrocyte death, resulting in anemia and splenomegaly (399).

1.3.3.8 Nervous System

Modulatory effects of cGMP signaling on neuronal function were observed on molecular, cellular, and behavioural levels (400-402). NP receptors exist in various regions of the nervous system, but their role for neuronal function is largely unknown, except for few cases (403). ANP might regulate water drinking behavior, salt appetite and neuronal blood pressure regulation (246). The CNP/GC-B/cGMP/cGKI pathway is necessary for bifurcation and guidance of sensory axons in the developing spinal cord. Interference with this process (in *knock-out* mice) leads to impaired nociceptive flexion reflexes (404). The importance of cGKI in pain perception was also demonstrated in adult mice (405, 406). Another study implicated a modulatory role of p53 on cGKI expression in the process of axon guidance (407). In an *in vitro* study, Shelly et al. showed with the use of cGMP and cAMP FRET sensors that spatiotemporally restricted cAMP and cGMP elevations modulate axon and dendrite formation from undifferentiated neurites in cultured hippocampal neurons (408). However, neither NO nor NPs were tested, but cell-permeable cGMP analogs were used to induce cGMP signaling (408).

NO-induced cGMP increases depend on NO synthesis by nNOS and eNOS (261), and both sGC isoforms exist in the brain in equal amounts (409). The NO/sGC/cGMP pathway mediates distinct types of long-term potentiation (LTP) on synapses of hippocampal CA1 neurons and in neurons of the lateral amygdala and the visual cortex (410-415). In synapses of striatal interneurons and Purkinje cells, it mediates long-term depression (LTD) (416-418). The components of the cGMP pathway are located on the presynapse and postsynapse in both cases (402, 419). LTP and LTD describe activity-dependent facilitation (LTP) or depression (LTD) of synapse activity as underlying mechanisms of synaptic plasticity and memory formation (400, 402). However, tissue-specific ablation of pathway components in the aforementioned brain regions lead to no or very distinct phenotypes (412, 413, 417). Additional long-term effects on synaptic activity, plasticity, and behavior are eventually caused via cGKI-mediated regulation of gene expression in these and other brain regions (400).

Spatiotemporal cGMP elevations were analyzed by Pietrobon *et al*. in cultured olfactory sensory neurons (420). With the Cygnet 2.1 cGMP FRET sensor, fura-2, and a genetically encoded Ca^{2+} sensor, they showed that odorant stimulation leads to cAMP-triggered elevations of intracellular Ca^{2+} levels, which cause NO-mediated cGMP synthesis within the whole neuron. Furthermore, they showed increased phosphorylation of cAMP-response element binding protein (CREB) after stimulation with odorants or membrane-permeable cGMP analogs *in vivo* (420). CREB has been shown to be a direct or indirect target of the cGMP pathway in cells of the nervous system and modulates expression of several target genes (400).

Other studies in mice showed that cGMP signaling modulates cognition and circadian rhythmicity, as well as the control of aggression, anxiety, and ethanol drinking behavior (247, 406, 421-424). Further findings from pharmacological and genetic studies suggested roles of cGMP signaling and of cGMP-regulated PDEs in the pathogenesis of psychiatric diseases like depression, schizophrenia, or of neurodegenerative diseases such as Alzheimer's disease, but also noise-induced hearing loss (425-430).

1.4 Aim of the Work

One aim of this work was the design and creation of a modular *HSV1*-sr39tk-based reporter system for noninvasive cell tracking studies in transgenic mice. The functionality of the *HSV1*-sr39tk/PET reporter system has been shown in studies with animals and human patients. In a limited number of these studies, transgenic mice with stably integrated reporter transgenes were used. These mice carry tissue-specific promoters to drive reporter gene expression, which limits their use to a particular tissue.

The combination of Cre/lox-assisted cell fate mapping strategies with the *HSV1*-sr39tk PET reporter system unifies two methods to a powerful new tool for the analysis of transgenic animals: PET allows sensitive and quantitative detection of cell populations in live animals, while the Cre/loxP system enables noninvasive activation of *HSV1*-sr39tk expression within a pre-selected cell type. The need for cell transplantation and possible side effects resulting from viral induction of *HSV1*-sr39tk expression is avoided. The modular structure of the Cre/lox-based *HSV1*-sr39tk reporter system will permit the labeling of any given cell population by selection of an appropriate tissue-specific Cre transgene, and avoids limitations of tissue-specific reporter transgenes.

The key element for this approach is a mouse line carrying a conditional (Cre-inducible) *HSV1*-sr39tk reporter transgene. *HSV1*-sr39tk expression should be possible in any given cell type, but expression must be activated by Cre in a particular cell type on demand. A major aim of this work was the generation and characterization of a reporter mouse line carrying a Cre-inducible *HSV1*-sr39tk reporter transgene. To characterize the newly generated mouse line, PET experiments should be performed with animals carrying the *HSV1*-sr39tk reporter gene and tissue-specific Cre transgenes. Experiments should show the principal functionality of the reporter system, as well as Cre-dependency of the *HSV1*-sr39tk reporter gene. The PET/sr39tk reporter system will allow for cell tracking experiments to study any given cell type in live animals under conditions of health and disease.

Another aim was the generation and characterization of mice that express FRET-based cGMP indicator (cGi) proteins. Conventional methods for cGMP detection (like RIA or ELISA) contributed a lot to our current understanding of cGMP signaling. However, they fail to resolve cGMP signals in complex tissues or at subcellular resolution, and they cannot repeatedly be used with the same living sample. Protein-based cGMP biosensors allow for repeated cGMP detection in living samples with high spatial and temporal resolution. In cultured cells, different cGMP biosensors were used to study cGMP signaling and its potential subcellular compartmentalization.

The use of cGis for sensitive and specific cGMP detection in transgenic mice should allow experiments that were hitherto impossible. Intravital imaging experiments will allow studies on cGMP signaling under *in vivo* conditions, where cells are examined that reside in their natural environment.

Experiments with mice expressing cAMP or Ca^{2+} biosensors demonstrated the advantages of intravital imaging. *In vivo* methods to follow cAMP or Ca^{2+} are most likely adaptable to studies with cGi-expressing mice, for example the visualization of cGMP in the brain of learning and behaving mice using two-photon microscopy (see also discussion).

In contrast to cAMP and Ca^{2+} biosensors, mice expressing cGis or other cGMP biosensors have not yet been reported. A major aim of this work was therefore to show the feasibility of cGi-based cGMP imaging in live animals. Another aim was the establishment of study protocols for cultured SMCs isolated from cGi-expressing mice. This includes protocols for cGMP quantification, repeated stimulation, or analysis of cGMP signaling at subcellular resolution. These protocols can then be applied to other cell types, including cells carrying mutations in components of the cGMP signaling pathway.

2 Materials and Methods

Relevant devices are specified within the respective protocols. Centrifugation parameters refer to Eppendorf 5417C/R centrifuges (Eppendorf AG, Hamburg, Germany) for 1.5 and 2 mL reaction tubes and an Eppendorf 5804R centrifuge with A-4-44 rotor for 15 and 50 mL tubes. Chemicals are obtained from Carl Roth (Karlsruhe, Germany), if not stated otherwise. Solutions are prepared with ultrapure water from a Milli-Q Integral Water Purification System (Merck Millipore, Billerica, MA, USA) and stored at room temperature, if not stated otherwise. Solutions are autoclaved for 20 min at 121°C (Ventilab 3000, MMM GmbH, München, Germany), when specified.

2.1 Common Reagents and Buffers

- 0.4% Trypan blue (GIBCO, Life Technologies GmbH, Darmstadt, Germany).
- 0.5 M EDTA pH 8.0: Dissolve 186.1 g/L disodium ethylenediaminetetraacetic acid dihydrate (Na$_2$EDTA×2 H$_2$O) in 800 mL H$_2$O, add NaOH pellets until the solution reaches pH 8.0 and EDTA is dissolved. Adjust volume to 1 L and autoclave.
- 1 M KCl: 74.55 g/L KCl, autoclave.
- 1 M MgCl$_2$: 203.3 g/L MgCl$_2$×6 H$_2$O, autoclave.
- 1 M Tris-Cl pH 6.8/7.4/8.0: 121.14 g/L tris(hydroxymethyl)aminomethane (Tris), adjust pH to 6.8/7.4/8.0 with concentrated HCl, autoclave.
- 1×Trypsin/EDTA: Mix 9 parts PBS with 1 part 10×trypsin/EDTA, store at 4°C for up to 1 month.
- 10×TE pH 8.0: 100 mM Tris-Cl (100 mL/L 1 M Tris-Cl pH 8.0), 10 mM EDTA (20 mL/L 0.5 M EDTA pH 8.0), autoclave.
- 10×Trypsin/EDTA: 0.1% trypsin/EDTA (GIBCO, Life Technologies), store in 5 mL aliquots at −20°C.
- 100% Ethanol (analytical grade), store at −20°C.
- 100×Pen/strep: 10,000 U/mL penicillin and 10,000 μg/mL streptomycin (GIBCO, Life Technologies), store in 5 mL aliquots at −20°C.
- 1000×Hoechst 33258: 1 mg/mL Hoechst 33258 (Sigma-Aldrich Chemie GmbH, München, Germany) in H$_2$O, store in 1 mL aliquots at −20°C.
- 20% SDS: Dissolve 200 g/L sodium dodecyl sulfate (SDS) at 60°C in a water bath.
- 2-Propanol.
- 3 M NaOAc pH 5.5: 40.83 g/100 mL CH$_3$COONa×3 H$_2$O, adjust pH to 5.5 with acetic acid.
- 37% Formaldehyde.
- 5 M NaCl: 292.2 g/L NaCl.
- 70% Ethanol: 70 mL ethanol (analytical grade) and 30 mL H$_2$O, store at −20°C.
- Chloroform.
- DMEM: Dulbecco's modified Eagle medium (DMEM; GIBCO, Life Technologies) with 'stable' glutamine (L-alanyl-L-glutamine, Glutamax^{TM}), 4.5 g/L D-glucose, Na pyruvate, store at 4°C.
- PBS (pH 7.4): Phosphate-buffered saline (PBS) with 135 mM NaCl (7.89 g/L), 3 mM KCl (0.22 g/L), 8 mM Na$_2$HPO$_4$ (1.42 g/L Na$_2$HPO$_4$×2 H$_2$O), 2 mM KH$_2$PO$_4$ (0.27 g/L), adjust pH to 7.4 with HCl or NaOH, autoclave.

2.2 Modification of Recombinant Plasmid DNA

Molecular cloning describes the *in vitro* assembly of recombinant DNA and its amplification in a host organism. For the work described within this thesis, molecular cloning techniques are employed to create transgene and targeting constructs for the generation of genetically modified mice. Typical vectors for molecular cloning experiments are plasmids that are circular double-stranded DNA

(dsDNA) molecules with sizes of 3-20 kb. Plasmids derive from *E. coli* bacteria, which serve as host for plasmid amplification. Due to their small size, plasmids can easily be isolated and modified *in vitro* and introduced back into *E. coli* for clonal replication. Experiments are performed according to standard procedures described by Sambrook and Russell (431).

2.2.1   Nucleic Acid Quantification by UV Spectroscopy

Quantification of purified nucleic acids in aqueous solution is performed with ultraviolet (UV) spectroscopy. The absorption maxima of nucleic acids at ~260 nm are used for quantification according to the law of Lambert-Bouguer-Beer. One unit of optical density (OD) represents 50 µg/mL double-stranded DNA, 40 µg/mL single-stranded RNA, or 33 µg/mL oligonucleotides. Nucleic acid sample concentrations are estimated with a NanoDrop device (NanoDrop 1000 Spectrophotometer, Thermo Fisher Scientific, Wilmington, DE, USA) with sample volumes of 2-5 µL.

1. Initialize the NanoDrop device with a water sample.
2. Perform a blank measurement with the buffer used to dissolve the nucleic acid sample.
3. Add 2-5 µL of the nucleic acid solution and perform measurement.
4. Note concentration (in ng/µL) and OD_{260}/OD_{280} ratio.

2.2.2   Agarose Gel Electrophoresis

- 5×TBE: 450 mM Tris-borate (54 g/L Tris, 27.5 g/L boric acid), 10 mM EDTA (20 mL/L 0.5 M EDTA pH 8.0).
- 6×DNA loading dye: 30% glycerol, 10% 10×TE, 0.05% bromophenol blue, 0.05% xylene cyanol.
- Agarose: Biozym LE agarose (Biozym Scientific GmbH, Hessisch Oldendorf, Germany).
- Ethidium bromide: 10 mg/mL in H_2O, store light protected at 4°C.
- Molecular size marker: Add 250 µL 1 kb ladder (Life Technologies) to 8.25 mL 1×DNA loading dye and store in 500 µL aliquots at 4°C.

Agarose gel electrophoresis is used for separation of digested plasmid DNA, either for fragment size determination (analytical gel), fragment purification (preparative gel), to analyze PCR or RT-PCR products, or to separate digested genomic DNA for Southern blot analysis. Fragment sizes of linear DNA fragments are determined by comparison with a co-migrated molecular size marker. DNA fragments are visualized in the gel by ethidium bromide that is detected through its fluorescence upon excitation with UV light. An image of the gel is acquired with a gel documentation system and either saved digitally or printed on a thermo-transfer printer.

1. Heat 0.8-2 g agarose per 100 mL 1×TBE (10-1 kb, 0.8% and 1-0.2 kb, 2%) in a microwave oven to dissolve the agarose. Allow the gel solution to cool down to ~50°C, add 5 µL 10 mg/mL ethidium bromide per 100 mL, and pour immediately.
2. Add 6×DNA loading dye to the sample (1 volume dye to 5 volumes sample).
3. Load 12 µL (500 ng) DNA size marker and samples (2-60 µL) onto the gel.
4. Perform electrophoresis at ≤150 V in 1×TBE buffer for 30-45 min.
5. Take a gel picture on a gel documentation system. If fragments are to be purified for subsequent cloning steps, use long-wavelength UV light (380 nm) to reduce UV-induced DNA damage.

2.2.3   Enzymatic Modification of Plasmid DNA

2.2.3.1   Plasmid Cleavage with Restriction Endonucleases

- 10×NEBuffer 1: 100 mM Tris-bis-propane-chloride, 100 mM MgCl$_2$, 10 mM dithiothreitol (DTT), pH 7.0 (NEB, New England Biolabs, Frankfurt am Main, Germany), store at −20°C.
- 10×NEBuffer 2: 500 mM NaCl, 100 mM Tris-Cl, 100 mM MgCl$_2$, 10 mM DTT, pH 7.9 (NEB), store at −20°C.
- 10×NEBuffer 3: 1000 mM NaCl, 500 mM Tris-Cl, 100 mM MgCl$_2$, 10 mM DTT, pH 7.9 (NEB), store at −20°C.
- 10×NEBuffer 4: 500 mM CH$_3$COOK, 200 mM Tris-acetate, 10 mM (CH$_3$COO)$_2$Mg, 10 mM DTT, pH 7.9 (NEB), store at −20°C.
- 100×BSA: 10 mg/mL bovine serum albumin (BSA; NEB), store at −20°C.
- Restriction enzymes (see **Table 18**, p. 140).

Double-stranded DNA is cleaved at defined sequences by type II restriction endonucleases (restriction enzymes), which recognize 4-8 bp-long palindromic dsDNA sequences and cut both strands within the recognition site (432). Cleavage generates blunt-ended digestion products or products with overhanging ends. The restriction digest reaction is controlled by agarose gel electrophoresis. The digested DNA is either used to identify plasmids by their restriction pattern (analytical digest), or to purify restriction fragments for later use in ligation reactions (preparative digest).

1. Prepare digestion reactions with 1/10 volume 10×NEBuffer, 1/100 volume 100×BSA, and 1-3 µL restriction enzyme (~5 Units). *Always prepare controls with respective DNA samples in a reaction mix without restriction enzymes.*

   - Perform analytical digest with 300-500 ng DNA in a reaction volume of 20 µL. Incubate for 1-3 h at appropriate temperature (typically at 37°C).
   - Perform preparative digest with 5-40 µg DNA in a reaction volume of 50-200 µL. Incubate for 6-12 h at appropriate temperature (typically at 37°C).

2. Analyze 8-12 µL of an analytical digest or a diluted aliquot of a preparative digest (100-250 ng DNA/lane) via agarose gel electrophoresis.
3. For purification of restriction fragments, load complete preparative digest on an agarose gel with large pockets (distribute to 1-4 pockets).

2.2.3.2   Isolation of DNA Fragments from Agarose Gels by Electroelution

- Dialysis tube: Cut dialysis tube (high-retention, cellulose, MWCO 12400; Sigma-Aldrich) to 6-12 cm pieces and autoclave them twice in fresh 1×TE. Store in 1×TE.

In order to isolate a DNA fragment from a fragment mixture (typically after restriction digest), fragments of different size are separated by agarose gel electrophoresis. The gel piece containing the desired DNA fragment is excised and placed inside a dialysis tube with 1×TBE buffer. Driven by the electric field, DNA is eluted from the gel piece and stays in the buffer inside the dialysis tube, from which it is purified by alcohol precipitation. Isolated DNA fragments are used for example for ligation reactions.

1. Excise DNA-containing gel piece under illumination with long-wavelength UV light (380 nm) and place it in a piece of dialysis tube of appropriate length. Add as few 1×TBE buffer as possible, and close both ends of the tube. *No air bubbles should remain inside the tube.*
2. Elute DNA by electrophoresis for 1 h at room temperature or 4°C. Invert electric field for 30 s at the end of the electroelution.
3. Harvest DNA-containing buffer from the dialysis tube. Wash dialysis tube with little 1×TBE and add washing buffer to DNA-containing buffer. Remove any remaining agarose by centrifugation for 5 min at 13,000 rpm, as agarose interferes with subsequent ligation reactions.
4. Add either 1/10 volume 3 M NaOAc pH 5.5 and 2.5 volumes ethanol, incubate for ≥1 h at −20°C, or add 1/10 volume 3 M NaOAc pH 5.5 and 0.9 volumes 2-propanol, and incubate for ≥1 h at 4°C.
5. Centrifuge for 30-60 min with 13,000 rpm at 4°C. Wash pellet twice with 70% ethanol, dry for 10 min under vacuum at 40°C (Eppendorf Concentrator 5301), add 20-40 µL H_2O for resuspension.

2.2.3.3 Phosphorylation of Synthetic Oligonucleotides

- 10×T4 polynucleotide kinase reaction buffer: 700 mM Tris-Cl, 100 mM $MgCl_2$, 50 mM DTT, pH 7.6 (NEB), store at −20°C.
- T4 polynucleotide kinase: 10,000 units/mL (NEB), store at −20°C.

20-80 bp-long synthetic oligonucleotides (see 2.2.6 and **Table 19**) are used to introduce new DNA sequences into plasmid vectors. Therefore, two complementary oligonucleotides, which represent sense and antisense strand of the dsDNA fragment, are phosphorylated at their 5' ends with T4 polynucleotide kinase. Then the reaction is heated to inactivate the kinase enzyme and to melt dsDNA adducts. Upon slow cooling, both oligonucleotides form dsDNA dimers with overhanging ends used as insert in ligation reactions with compatible recipient fragments (obtained by restriction digest).

1. Prepare a polynucleotide kinase reaction:

    o 1 µL (=100 pmol) of each oligonucleotide (**Table 19**, p.141)
    o 2 µL 10×T4 polynucleotide kinase reaction buffer
    o 15 µL H_2O
    o 1 µL T4 polynucleotide kinase

2. Incubate for 90 min at room temperature.
3. Place the reaction mix in a 2 L beaker glass filled with water warmed to 75°C.
4. Allow for slowly cool down (stir overnight in a cold room at 4°C).
5. Fill reaction mix with H_2O to 200 µL, and use 2 or 0.2 µL per ligation reaction.

2.2.3.4 Ligation

- 10×T4 DNA ligase reaction buffer: 500 mM Tris-Cl, 100 mM $MgCl_2$, 10 mM ATP, 100 mM DTT, pH 7.5 (NEB), store at −20°C.
- CIP: calf intestine phosphatase, 10,000 units/mL (NEB), store at −20°C.
- dNTPs: 100 mM dATP, 100 mM dCTP, 100 mM dGTP, 100 mM dTTP (PEQLAB Biotechnologie GmbH, Erlangen, Germany)
- T4 DNA ligase: 400,000 cohesive end units/mL (NEB), store at −20°C.
- T4 DNA polymerase: 3,000 units/mL (NEB) store at −20°C.
- tRNA: Dilute 1 mg/mL transfer-RNA (tRNA) from *S. cerevisiae* (Sigma-Aldrich) to a concentration of 1 µg/mL with H_2O, store at −20°C.

T4 DNA ligase catalyzes the ATP-dependent linkage of 5' phosphate groups and 3' hydroxyl groups of dsDNA fragments. When dsDNA strands have incompatible ends or when 5' phosphate groups were removed by alkaline phosphatase treatment, ligation to a circular product cannot take place. The

inability of T4 ligase to ligate dsDNA under these conditions reduces the amount of (unwanted) ligation products that do not contain the insert fragment. Circular DNA is generated only in presence of compatible insert fragments with intact 5' phosphate groups. If dsDNA fragments with incompatible 5' overhangs need to be ligated, (incompatible) overhangs are filled with T4 DNA polymerase to (compatible) blunt ends. T4 DNA ligase also catalyzes the ligation of blunt-ended dsDNA, but with lower efficiency.

1. Prepare the vector DNA fragment: if necessary, add 1-2 μL CIP to the restriction digest reaction, and incubate for 1 h at 37°C to dephosphorylate the vector DNA. Then purify the fragment by agarose gel electrophoresis and electroelution (2.2.3.2). As insert DNA, use a DNA fragment purified after digestion (*do not use CIP here*), or use synthetic oligonucleotide linkers. Estimate the concentration of purified vector and insert DNA fragments on an agarose gel or via UV spectroscopy.
2. Use appropriate amounts of vector and insert fragments (~1:4 molar ratio) in a ligase reaction with 2 μL 10×T4 ligase reaction buffer in a final volume of 20 μL. Prepare control reactions with vector fragment but without insert DNA.

   o If no fill-in (T4 DNA polymerase) reaction is performed, heat the reaction for 5 min to 50°C, cool down to room temperature, and add 1 μL T4 DNA ligase. Incubate for 2-4 h or overnight at 12°C.
   o If incompatible ends need to be filled up, add dNTPs to a concentration of 100 μM and 1 μL T4 DNA polymerase. Incubate for 15 min at 12°C, denature for 20 min at 75°C, then add T4 DNA ligase.
   (The reaction can also be performed after a first ligation reaction in the order: ligation of compatible ends, fill-in, and second ligation of blunt ends).

3. Check an aliquot (3-4 μL) of the ligation reaction by agarose gel electrophoresis.
4. Inactivate T4 ligase for 10 min at 65°C and add H_2O to a final volume of 50 μL.
5. Add 1 μL 1 μg/μL tRNA, 5 μL 3 M NaOAc pH 5.5, and 250 μL ethanol. Incubate for ≥1 h at −20°C. Centrifuge for 20 min at 13,000 rpm and 4°C, wash pellet twice with 70% ethanol. Dry pellet under vacuum (Eppendorf Concentrator 5301), and resuspend in 20 μL H_2O. Use a part or the whole solution for transformation of *E. coli* .

2.2.4 Plasmid Amplification and Isolation from *E. coli*

- 1000×Ampicillin (100 mg/mL): Dissolve 1 g ampicillin in 10 mL H_2O, filter through a sterile filter and store in 1 mL aliquots at −20°C.
- 1000×Kanamycin (50 mg/mL): Dissolve 0.5 g kanamycin in 10 mL H_2O, filter through a sterile filter and store in 1 mL aliquots at −20°C.
- LB agar plates: 35 g/L Luria-Bertani (LB) agar ('Lennox', with 10 g tryptone, 5 g yeast extract, 5 g NaCl, 15 g agar). Autoclave, add antibiotics right before pouring into 100 mm petri dishes at ~50°C.
- LB medium: 20 g/L Luria-Bertani (LB) powder ('Lennox', with 10 g tryptone, 5 g yeast extract, 5 g NaCl). Autoclave, add antibiotics short before inoculation of the bacteria.

For amplification of plasmid DNA, electro-competent *E. coli* XL1-blue (genotype: *endA1 supE44 thi-1 hsdR17 recA1 gyrA96 relA1 lac* [F' *proAB lacI*^{q}*ZΔM15* Tn*10* (Tet^r)]) are used. Bacteria grow on LB agar plates at 37°C or in LB medium shaken at 37°C. LB agar and LB medium contain antibiotics to select for *E. coli* that carry plasmids coding for the respective antibiotic resistance gene.

2.2.4.1 *E. coli* Transformation by Electroporation

- 10% Glycerol: 10 mL glycerol and 90 mL H_2O, autoclave and store at 4°C.
- 50% Glycerol: 50 mL glycerol and 50 mL H_2O, autoclave and store at 4°C.
- Electroporation cuvettes, d=2 mm (Biorad Laboratories GmbH, München, Germany).

Electroporation is an efficient method to introduce recombinant DNA into *E. coli* (433). Electro-competent *E. coli* mixed with desalted ligations or salt-free plasmid solutions are placed in an electroporation cuvette, which serves as capacitor with the cell suspension between two conductor plates. An electric field is applied by the Gene Pulser Xcell Electroporation System (Bio-Rad), which induces the formation of temporary pores in the bacterial plasma membrane that allows DNA to enter the bacterium. Medium is added after electroporation, *E. coli* are allowed to recover, and transformed bacteria will start to express resistance genes. The bacterial suspension is plated on LB agar containing the respective antibiotic; plating densities must be chosen in a way that single colonies are obtained, which are isolated (picked) and separately expanded.

A) Preparation of Electro-competent *E. coli*

In order to obtain electro-competent *E. coli* , liquid cultures are harvested in their logarithmic growth phase and washed several times to remove as much ions from the bacteria suspension as possible. Ions induce electric currents during electroporation causing reduced cell survival and low DNA uptake efficiencies. *Do not use antibiotics throughout the whole procedure, and always work under sterile conditions: use only autoclaved solutions and vessels, and handle bacteria under a sterile workbench*.

1. Prepare a dilution streak of untransformed *E. coli* on LB agar.
2. Isolate a single colony for inoculation of 5 mL LB medium for an overnight culture. On the next day, store culture at 4°C. In the evening, inoculate 50 mL LB medium with 0.5 mL of the 5 mL overnight culture.
3. On the next morning, inoculate 4×500 mL LB medium with each 10 mL of the 50 mL overnight culture. Incubate at optimal growth conditions.
4. After 2-6 h, harvest bacteria in their logarithmic growth phase (0.5-0.6 OD_{650}, blank measurement with LB medium, path length: 1 cm) by centrifugation for 10 min at 5,000 rpm and 4°C (J2-H2 centrifuge with JA-10 rotor, Beckman Coulter, Brea, CA, USA). *For the following steps, take care that bacteria and solutions are always kept on ice.*
5. Wash the bacteria twice with 500 mL ice-cold H_2O, and twice with 50 mL ice-cold 50% glycerol, pelletize the bacteria each time by centrifugation for 10 min at 5,000 rpm and 4°C.
6. After the last washing step, resuspend the bacteria pellet in 4 mL 10% glycerol (2 mL/L culture volume).
7. Use bacteria directly or freeze 200 µL aliquots in liquid nitrogen for storage at −80°C.
8. Test frozen stock quality; plate bacteria on agar plates with antibiotics (no bacteria should grow). Estimate electroporation efficiency (10^8-10^9 colonies/µg DNA) in a control electroporation with pUC19 plasmid DNA.

B) Electroporation

1. Thaw an aliquot of electro-competent *E. coli* on ice. Still on ice, add a part or the complete desalted ligation (15-20 µL), or 50 ng purified plasmid DNA to 100 µL bacteria suspension. Transfer the mixture into a chilled electroporation cuvette (d=2 mm).
2. Transform *E. coli* by electroporation with 2.5 kV, 25 µF and 200 Ω; the resulting time constant τ should be ~5 ms.
3. Add 1 mL pre-warmed, antibiotic-free LB medium to the cuvette as fast as possible, and transfer the suspension into a 15 mL tube. Incubate for 1 h at 37°C.
4. If bacteria were transformed with a ligation, plate 10, 100, and 300 µL of the suspension to agar plates. If plasmid DNA was retransformed, plate 100 µL of 10^2-10^6-fold dilutions of the suspension to agar plates. Grow bacteria overnight at 37°C.
5. Count colonies and estimate the electroporation efficiency. For ligations, check whether the control reaction (vector w/o insert) leads to fewer *E. coli* colonies than reactions with both vector and insert.

2.2.4.2 Plasmid Preparation

- 1 M Tris: 121.14 g/L Tris.
- N2 (Equilibration buffer): 100 mM Tris (100 mL/L 1 M Tris), 900 mM KCl (67.1 g/L), 15% ethanol (150 mL/L), 0.15 % Triton X-100 (1.5 mL/L), adjust pH to 6.3 with H_3PO_4.
- N3 (Wash buffer): 100 mM Tris (100 mL/L 1 M Tris), 1150 mM KCl (85.73 g/L), 15% ethanol (150 mL/L), adjust pH to 6.3 with H_3PO_4.
- N5 (Elution buffer): 100 mM Tris (100 mL/L 1 M Tris), 1000 mM KCl (74.55 g/L), 15% ethanol (150 mL/L), adjust pH to 8.5 with H_3PO_4.
- RNase: 10 mg/mL RNase H in 1×TE, store in 1 mL aliquots at −20°C.
- S1 (Resuspension buffer): 50 mM Tris-Cl pH 8.0 (50 mL/L 1 M Tris-Cl pH 8.0), 10 mM EDTA pH 8.0 (20 mL/L 0.5 M EDTA pH 8.0). Supplement with 100 µg/mL RNase (10 µL 10 mg/mL RNase to 1 mL S1) before use.
- S2 (Lysis buffer): 200 mM NaOH (8 g/L), 1% SDS (10 g/L).
- S3 (Neutralization buffer): 2.8 M KOAc (274.82 g/L CH_3COOK), adjust pH to 5.1 with acetic acid, store at 4°C.

Plasmids are isolated from *E. coli* cultures by alkaline lysis (434) and subsequent alcohol precipitation. Small-scale plasmid preparation from 1 mL *E. coli* cultures yields plasmid DNA in sufficient amounts and quality for restriction analysis, sequence analysis, and retransformation into electro-competent *E. coli*. The major purpose of this method is to screen several (usually 3-30) *E. coli* cultures in parallel for the presence of plasmids with desired properties (e.g. after a ligation). In order to obtain plasmid amounts sufficient for subsequent cloning steps or for transfection of eukaryotic cells, plasmids are isolated from 100-500 mL *E. coli* cultures by alkaline lysis and subsequent purification via anion exchange chromatography and alcohol precipitation.

A) Small-Scale Plasmid Preparation

1. Isolate single *E. coli* colonies from LB agar plates and grow them overnight in 5 mL LB medium with antibiotic.
2. Centrifuge 1 mL from the culture for 3 min at 5,000 rpm. Store the remaining culture at 4°C for later use.
3. Resuspend the bacteria pellet in 100 µL S1 buffer (with RNase).
4. Add 200 µL S2 and invert (do not vortex), incubate for 30 s.
5. Add 150 µL S3 (pre-chilled to 4°C), invert again, add 100 µL chloroform and centrifuge for 2 min at 13,000 rpm and 4°C.
6. Transfer the supernatant to a new tube and add 1 mL 100% ethanol (pre-chilled to −20°C).
7. Mix by inversion and centrifuge for 5 min at 13,000 rpm and 4°C.
8. Wash the DNA pellet twice with 70% ethanol and dry it for 10 min under vacuum at 40°C (Eppendorf Concentrator 5301).
9. Resuspend pellet in 20 µL H_2O and use 3-5 µL for an analytical restriction digest.

B) Large-Scale Plasmid Preparation

1. Centrifuge 4 mL of an overnight culture for 5 min at 5,000 rpm and resuspend pellet in 1 mL LB medium.
2. Inoculate 100 or 500 mL LB medium and grow culture overnight at 37°C.
3. Pelletize bacteria by centrifugation for 10 min at 5,000 rpm and 4°C (J2-H2 centrifuge with JA-10 rotor).
4. Perform plasmid DNA isolation from 100 mL cultures with the NucleoBond PC 100 kit (Macherey-Nagel, Düren, Germany) and from 500 mL cultures with the NucleoBond PC 500 kit (Macherey-Nagel), follow the kit instructions; buffers S1-S3 and N2, N3, N5 are prepared as stated above.
5. Resuspend the dried DNA pellet in 150 or 300 µL H_2O. Determine DNA concentration and adjust to 1 µg/µL.

2.2.5 TOPO Cloning

- Zero Blunt® TOPO® PCR Cloning Kit (Life Technologies).
- DeepVent DNA polymerase (2,000 U/mL, NEB).

TOPO cloning is used to introduce blunt-ended polymerase chain reaction (PCR) products into a DNA vector (pCR-Blunt-II-TOPO). The PCR reaction has to be performed with a thermostable DNA polymerase that generates blunt-ended PCR products (e.g. DeepVent DNA polymerase). An aliquot of the reaction is added to the pCR-Blunt-II-TOPO vector, which is supplied in a linearized form with *Vaccinia virus* DNA topoisomerase I bound to the 3' ends of both DNA strands. During the TOPO cloning reaction, the PCR product is integrated into the pCR-Blunt-II-TOPO vector in a transesterification reaction leading to dissociation of the DNA topoisomerase and formation of a circular DNA product. The reaction is then transformed into *E. coli* bacteria. TOPO cloning is performed with the Zero Blunt® TOPO® PCR Cloning Kit according to the manufacturer's instructions. The TOPO reaction was used to transform chemo-competent *E. coli* TOP10 bacteria (genotype: F- *mcrA* Δ(*mrr-hsd*RMS-*mcr*BC) Φ80*lacZ*ΔM15 ΔlacX74 *recA1 araD139* Δ(*ara-leu*)7697 *galU galK rpsL* (Str^R) *endA1 nupG*) included in the kit.

2.2.6 Generation of Synthetic Oligonucleotides

Oligonucleotides are obtained from Eurofins MWG Operon (Ebersbach, Germany), where they are synthetized with the phosphoramidite method (435). After synthesis, products are purified by liquid chromatography (purity: 'HPSF'). Shipped freeze-dried oligonucleotides are resuspended in H$_2$O to a concentration of 100 μM and stored at −20°C.

2.2.7 DNA Sequence Analysis

DNA sequence analysis is performed by Eurofins MWG Operon using a modification of the didesoxy chain termination method (436) with fluorescently labeled dideoxynucleotides and thermostable DNA polymerases ('cycle sequencing'). Products of the sequencing reaction are analyzed by capillary electrophoresis.

2.3 Generation of Transgenic Mice

Different mouse strains are used for the generation and breeding of transgenic mouse lines (for an overview see **Table 20** on p. 142). **Table 3** lists transgenic mouse lines that are either generated and/or used throughout this work. Further details on Cre transgenic mouse lines are given in chapter 3.1.5 on p. 90.

Table 3. Transgenic mouse lines, transgene systematic names and genotypes, and genotyping primers.

The genotype nomenclature of mice (and ESCs) with targeted mutations is used as follows. '−' refers to targeted alleles and '+' to the wild type allele. For conditional alleles, '−' refers to targeted alleles regardless of the status of Cre recombination, while 'L2' refers to the targeted (loxP-flanked) allele before Cre recombination (2 loxP sites present), and 'L1' refers to the targeted allele after Cre recombination (1 loxP site left). Genotyping primers for targeted mutations are used to distinguish between wild type (+/+), heterozygous (+/−), and homozygous (−/−) genotypes; the primers cannot be used to distinguish between conditional 'L1' and 'L2' alleles. Genotyping primers to detect random transgene (tg) insertions bind within the transgene, therefore no PCR product is obtained with wild type (+/+) genotypes; primers cannot be used to distinguish between heterozygous (tg/+) and homozygous (tg/tg) genotypes. Primer sequences in **Table 19**, p. 141.

Transgene	Systematic name of the transgene[*]	Alleles	Genotyping primers	Reference
	Targeted mutation			
ROSA26-lacZ	B6.129S4-Gt(ROSA)26Sor^{tm1Sor}	+; − (L2; L1)	ROSA10, ROSA11, RF127	(64)
ROSA26-sr39tk	B6;129-Gt(ROSA)26Sor$^{tm1(sr39tk)Feil}$	+; − (L2; L1)	ROSA10, ROSA11, RF127	**this work**
ROSA26-mT/sr39tk	B6;129-Gt(ROSA)26Sor$^{tm2(ACTB-tdTomato,-sr39tk)Feil}$	+; − (L2; L1)	ROSA10, ROSA11, ROSA4	**this work**
ROSA26-CAG-cGi-500	B6;129-Gt(ROSA)26Sor$^{tm3.1(ACTB-cGi-500)Feil}$	+; − (L2; L1)	ROSA10, ROSA11, ROSA4	Thunemann & Wen, in preparation
SMKI	B6.129-Tagln$^{tm1(cre/ERT2)Feil}$	+; −	RF67, SW16, SC135	(51)
SMIβ rescue	129-Tagln$^{tm2(PRKG1*)Hfm}$	+; −	RF67, SW8, SW12	(279)
MLC2a-Cre	B6.129-Myl7$^{tm1(cre)Krc}$	+; tg	Cre800, Cre1200	(375, 437)
	Transgene insertion			
CMV-Cre	B6-Tg(CMV-cre)1Ipc	+; tg	Cre800, Cre1200	(438)
Nes-Cre	B6-Tg(Nes-cre)1Kln	+; tg	Cre800, Cre1200	(439)
RIP-Cre	B6-Tg(Ins2-cre)23Herr	+; tg	Cre800, Cre1200	(440, 441)
SM445-cGi-500-1	B6;B6D2-Tg(SM445-cGi-500)1Feil	+; tg	MH5, MH12	**this work**
SM445-cGi-500-5	B6;B6D2-Tg(SM445-cGi-500)5Feil	+; tg	MH5, MH12	**this work**
CMV-cGi-6000-6	B6;B6D2-Tg(CMV-cGi-6000)6Feil	+; tg	MH5, MH7	**this work**
CMV-cGi-6000-10	B6;B6D2-Tg(CMV-cGi-6000)10Feil	+; tg	MH5, MH7	**this work**
CMV-cGi-6000-11	B6;B6D2-Tg(CMV-cGi-6000)11Feil	+; tg	MH5, MH7	**this work**

[*]For further details on nomenclature, see **Table 20** on p. 142 and ref. 442, 443.

2.3.1 Mouse Husbandry and Breeding

Mice are housed in the animal facility of the Interfaculty Institute for Biochemistry at 20-22°C and 50-55% relative humidity in a 12 h light/12 h dark cycle. Single animals or groups of 2-4 animals are kept in type II standard cages (360 cm^2), or groups of up to eight animals in type III standard cages (1010 cm^2). For bedding, autoclaved shredded wood chips (Sniff Spezialdiäten GmbH, Soest,

Germany) are used; animals have access to standard rodent chow (Altromin Spezialfutter GmbH & Co. KG, Lage, Germany and Sniff) and tap water *ad libitum*. For breeding, one stud male (age ≥6 weeks) is placed together with 1-3 females (age 6-32 weeks) in a type II cage; before delivery, females are separated into type III cages (1-2 pregnant females per cage) with nesting material ('Nestlets', Emsicon-Jung GmbH, Forstinning, Germany) and extruded breeding chow (Altromin, Sniff). Weaning and separation of males and females is performed 3-4 weeks after birth. Upon weaning, animals receive ear tags for identification according to the 'universal mouse numbering system' (444); tissue obtained during ear tagging is used for routine genotyping as described in 2.3.2.

2.3.2 PCR-based Mouse Genotyping

- 10×Reaction buffer S: 100 mM Tris-Cl pH 8.8, 500 mM KCl, 0.1% Tween-20, 15 mM $MgCl_2$ (PEQLAB), store at −20°C.
- 10×RT buffer: 100 mM Tris-Cl pH 8.0 (1 mL 1 M Tris-Cl pH 8.0), 500 mM KCl (5 mL 1 M KCl), 15 mM $MgCl_2$ (0.15 mL 1 M $MgCl_2$), 2 mM of each dNTP (4×0.2 mL 100 mM dATP/dGTP/dCTP/dTTP), 3.65 mL H_2O. Store in 0.5 mL aliquots at −20°C.
- dNTPs: 100 mM dATP, 100 mM dCTP, 100 mM dGTP, 100 mM dTTP (PEQLAB).
- Oligonucleotide primers (**Table 19**, p. 141) diluted to 25 µM, store at −20°C.
- PCR lysis buffer: 1×reaction buffer S (100 µL/mL 10×reaction buffer S), 1 mg/mL proteinase K (20 µL/mL 50 mg/mL proteinase K), prepare fresh before use.
- Proteinase K: 50 mg/mL proteinase K in 1×TE, store at −20°C.
- *Taq* polymerase: SAWADY *Taq* polymerase (PEQLAB), store at −20°C.

Polymerase chain reaction (PCR, 445) is used for mouse genotyping. The template DNA for genotyping PCRs is isolated from ear punches or tail tip biopsies.

2.3.2.1 DNA Extraction from Mouse Tissues for Genotyping PCRs

1. Incubate tissue samples overnight at 55°C in PCR lysis buffer (50 µL for ear punches, 100 µL for tail tips).
2. Vortex and centrifuge for 3 min at 13,000 rpm. Transfer the supernatant into a new 0.5 mL PCR tube.
3. Inactivate remaining proteinase K activity and denature DNA for 15 min at 95°C.
4. Centrifuge for 3 min at 9,000 rpm.
5. Use 1-2 µL of the supernatant for PCR and store the remaining DNA-containing solution at −20°C.

2.3.2.2 PCR

PCR conditions depend on annealing temperatures (T_a) and PCR product length (**Table 21** on p. 142).

1. Prepare a master mix that contains (per reaction) 2.5 µL 10×RT buffer, 0.2 µL *Taq* polymerase, primers according to **Table 21**, and H_2O to 23 µL.
2. Distribute each time 23 µL of the master mix to PCR reaction tubes prepared with 1-2 µL genomic DNA. Prepare also a positive control with DNA from a mouse of known genotype and a negative control with H_2O instead of template DNA.
3. Spin down, if necessary, place the samples in the thermocycler (PEQLAB Primus 96 Advanced), and run the respective PCR program.
4. After PCR, analyze products on a 2% agarose gel.

2.3.3 Generation of Transgenic Mice by Oocyte Injection (Random Mutagenesis)

- Dialysis tube: Cut dialysis tube (high-retention, cellulose, MWCO 12400; Sigma-Aldrich) to 6-12 cm pieces and autoclave them twice in fresh 1×TE. Store in 1×TE.
- Oocyte injection buffer: 10 mM Tris-Cl pH 7.5 (10 mL/L 1 M Tris-Cl pH 7.5); 0.1 mM EDTA (200 μL/L 0.5 M EDTA pH 8.0). Filter through a 0.2 μm sterile filter and store at −20°C.

Transgene DNA must be free of impurities that disturb injection (e.g. dust or other particles) or impair oocyte survival (e.g. bacterial endotoxins, phenol). Furthermore, all prokaryotic sequences (i.e. the plasmid backbone) should be removed from the transgene DNA before oocyte injection, as prokaryotic sequences surrounding the transgene eventually inhibit transgene expression (446). Transgene DNA is excised from the plasmid vector by restriction digest. The transgene DNA fragment is purified by agarose gel electrophoresis, electroelution, filtration, and ethanol precipitation according to the following protocol (M. Hillenbrand, 2007):

1. Digest 50 μg plasmid DNA for transgene isolation.
2. Add 6×loading dye and load the restriction digest reaction to a preparative gel (0.8-1% agarose in 1×TBE). Place the electrophoresis chamber on ice and run the gel with 6.7 V/cm.
3. Excise the transgene DNA fragment under UV illumination with long-wavelength UV light (380 nm). Place the excised gel fragment in a dialysis tube. Add 1×TBE buffer and close the tube. Perform electroelution at 5.6 V/cm on ice (see also 2.2.3.2).
4. Place the DNA-containing buffer into a 2 mL tube and centrifuge for 5 min at 13,000 rpm and 4°C.
5. Filter the supernatant through a 0.2 μm filter that was pre-wetted with 1×TBE. Wash the filter with 200 μL 1×TBE.
6. Precipitate overnight with 1/10 volume 3 M NaOAc pH 5.5 and 2.5 volumes 100% ethanol at −80°C.
7. Centrifuge for 30 min at 5,000 rpm and 4°C.
8. Wash pellet twice with 70% ethanol (pre-chilled to −20°C), centrifuge for 10 min at 5,000 rpm and 4°C.
9. Dry pellet under vacuum and resuspend in 50 μL oocyte injection buffer.
10. Estimate the DNA concentration with UV spectroscopy, adjust concentration to 2 ng/μL with oocyte injection buffer, and check fragment integrity on an agarose gel (load different DNA amounts in a dilution series).

Injection of purified transgene DNA into male pronuclei of fertilized oocytes was performed by members of the Transgenic Facility Tübingen (Leader: Dr. Thomas Ott) according to standard procedures (447).

2.3.4 Generation of Transgenic Mice by Targeted Mutagenesis in ESCs

- 100×G418 (40 mg/mL): Dissolve 1.6 g geneticine sulfate (G418; GIBCO, Life Technologies) in 40 mL PBS, sterilize by filtration, and store in 5 mL aliquots at −20°C.
- 10^4×GCV (20 mM): Dissolve 50 mg ganciclovir-Na (Cymeven®, Roche Diagnostics Deutschland GmbH, Mannheim, Germany) in 10 mL H_2O, sterilize by filtration, and store in 50 μL aliquots at −20°C.
- 2×Trypsin/EDTA: Mix 4 parts PBS with 1 part 10×trypsin/EDTA, store at 4°C for up to 1 month.
- 500×2-ME (50 mM): Add 70 μL 2-mercaptoethanol (2-ME) to 20 mL PBS, sterilize by filtration and store in 1 mL aliquots at −20°C.
- 500×LIF ($0.5×10^6$ U/mL): Dilute 1 mL ($1×10^7$ U) leukemia-inhibitory factor (LIF; Millipore GmbH, Schwalbach/Ts., Germany) with 19 mL feeder medium, store in 1 mL aliquots at 4°C.
- DMSO (dimethyl sulfoxide).
- ESC medium: 80% DMEM (400 mL), 20% ESC-FBS (100 mL), 1×10^3 U/mL LIF (1 mL 500×LIF), 0.1 mM 2-ME (1 mL 500×2-ME), store at 4°C.
- ESC/G418-medium: 400 μg/mL G418 (5 mL 100×G418/500 mL ESC medium).

- ESC/GCV-medium: 2 μM GCV (50 μL $10^4 \times$GCV/500 mL ESC medium).
- ESC-FBS: ESC-tested FBS (GIBCO, Life Technologies, order no. 10270-10, lot 40F2342K), heat-inactivated (30 min at 56°C), store in 50 mL aliquots at −80°C.
- Feeder medium: 90% DMEM (450 mL), 10% ESC-FBS (50 mL), store at 4°C.

In comparison to random mutagenesis, methods of targeted mutagenesis cannot be performed in the mouse embryo itself, but are performed in ESCs (see **Figure 2** on p. 3). Culture is performed in presence of feeder cells and leukemia-inhibitory factor (LIF) added to the medium (448). LIF and other factors secreted by the feeder cells, as well as feeder-to-ESC contacts prevent ESC differentiation and loss of pluripotency. For successful generation of transgenic mice from targeted ESCs, pluripotent ESCs must contribute to the germ-line of chimeric mice generated by injection of ESCs into wild type blastocysts. It is therefore critical that ESCs remain pluripotent during in *vitro* culture. The time in culture should therefore be kept as short as possible and appropriate culture conditions must be strictly maintained.

In this work, the R1 ESC line (449) is used, and frozen stocks in passage 15 (frozen in 02/1999) are thawed for gene targeting experiments. General requirements and procedures for the culture of R1 ESCs are specified hereinafter.

- ESCs are cultured on mitotically inactive feeder cells (see below) at 37°C and 6% CO_2 (Innova-150 CO_2 incubator, New Brunswick Scientific, Enfield, CT, USA) in ESC medium containing LIF and 20% FBS. Recommended medium volumes for various culture vessels are given in **Table 4**.
- Thaw and plate feeder cells in ESC or feeder medium 6-24 h before ESCs are seeded onto the feeder cell layer. If feeder cells are plated in feeder medium, change to ESC medium ~1 h before ESCs are seeded.
- Change ESC medium every day or every other day, depending on culture density.
- Passage ESCs at 60-80% confluence: wash the cells once with PBS and add 1×trypsin/EDTA (volumes in **Table 4**) to detach the cells. When cells begin to detach (after 3-5 min), resuspend to obtain a single cell suspension, and add 1-2 volumes ESC medium. Pelletize cells by centrifugation for 5 min at 1,000 rpm. Resuspend the cell pellet in ESC medium, and plate ESCs onto new feeder cells in splitting ratios of 1:5 to 1:15, if not stated otherwise. *Keep notes on the passage number!*
- To prepare frozen stocks, detach cells by trypsinisation, add 1-2 volumes ESC medium, centrifuge, and resuspend cells in freezing medium (90% ESC medium, 10% DMSO). Subdivide cells to several frozen stocks to have cells from 12.5 cm^2 per vial (e.g. cells from a T75 flask into six 1 mL aliquots). Freeze cells in a Styrofoam box placed at −80°C for at least 24 h, then transfer the frozen stocks into a cell bank with liquid nitrogen.
- Thaw frozen stocks in a water bath at 37°C; add the cell suspension to 4 mL ESC medium, centrifuge for 5 min at 1,000 rpm, and resuspend the pellet in ESC medium. Cells are plated onto a T25 flask, if not stated otherwise.

Table 4. Surface areas, medium volumes, and trypsin volumes for typical culture vessels.

Format	Area (per well)	Total area	Medium	Trypsin
T25 flask	25 cm²	25 cm²	5 mL	2 mL
T75 flask	75 cm²	75 cm²	15 mL	5 mL
T175 flask	175 cm²	175 cm²	20 mL	8 mL
100 mm culture dish	55 cm²	55 cm²	10-15 mL	5 mL
6-well multi-well plate	9.5 cm²/well	57 cm²	2-3 mL	1 mL
12-well multi-well plate	3.8 cm²/well	45.6 cm²	1-1.5 mL	0.5 mL
24-well multi-well plate	1.9 cm²/well	45.6 cm²	0.5-1 mL	0.3 mL
96-well multi-well plate	0.32 cm²/well	31 cm²	100-200 μL	50 μL

2.3.4.1 Gene Targeting in ESCs

The introduction of a transgene at a defined genomic locus of the ESC genome is performed in gene targeting experiments. These experiments rely on homologous recombination between a transgene-containing targeting vector and corresponding genomic ESC DNA (see 1.1.2 on p. 2). Homologous recombination is very inefficient compared to the random integration of the targeting vector into the ESC genome. With the use of selection methods, ESCs are enriched, which integrated the transgene by homologous recombination and not the targeting vector by random integration (**Figure 9A**).
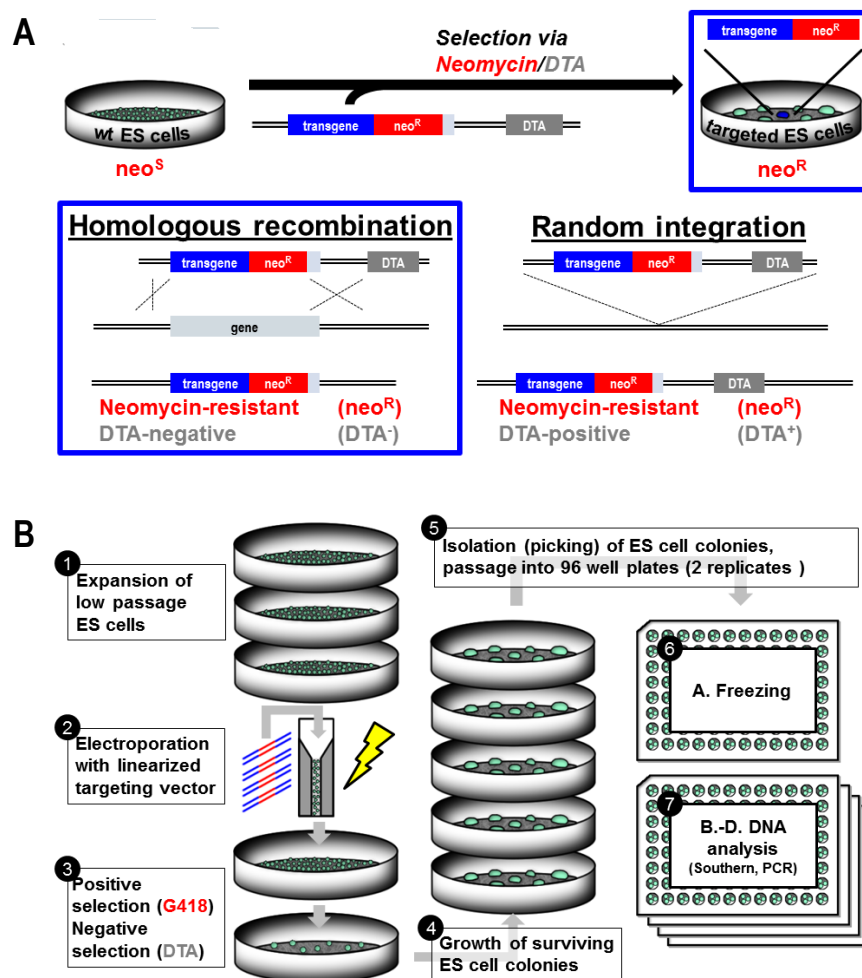
Figure 9. Gene targeting in ESCs.

A. Strategy for the enrichment of targeted ESCs by positive selection with neomycin-related G418 and negative selection by diphtheria toxin fragment A (DTA). G418 is added to the culture medium to select for Neo[R]-expressing ESCs by elimination of wild type (G418-sensitive) ESCs. Additionally, ESCs that carry random integrations of the targeting vector are eliminated by expression of the 'suicide gene' DTA, which lies outside of the homologous arms. During selection, neomycin-resistant, DTA-negative cells are enriched, which should have undergone correct homologous recombination. **B.** Low passage ESCs are thawed and expanded (1), transfected by electroporation with the linearized targeting vector (2). After electroporation, selection for targeted ESCs takes place (3, see panel A). After 7-9 days of selection, surviving ESCs form colonies large enough for manual isolation (4). Cells from individual colonies are isolated into 96-well plates and are passaged into two replicate cultures (5), of which one is frozen for later expansion and blastocyst injection (6); the other replicate is passaged to generate three replicates for DNA analysis by Southern blot or PCR (7).

Integration of the transgene leads to expression of the Neo^R gene, resulting in resistance against the neomycin-related aminoglycoside antibiotic geneticin (G418). Consequently, a positive selection for G418-resistant ESCs takes place that will kill all unmodified (wild type) ESCs. The targeting vector carries an additional negative selection marker that is not part of the transgene itself (**Figure 1B, C**). Its expression will lead to ablation of ESCs with random integrations of the targeting vector. A typical marker gene used for negative selection is diphtheria toxin fragment A (DTA), which is a genetically encoded inhibitor of protein synthesis leading to cell death (450). During a gene targeting experiment (overview in **Figure 9B**), ESCs are transfected with the linearized targeting vector by electroporation with the Gene Pulser Xcell Electroporation System (Bio-Rad). Then they are plated onto G418-resistant feeder cells to a density that allows for the growth of individual (clonal) ESC colonies. During selection, ~99% of the original ESC population dies, and the remaining G418-resistant, DTA-negative ESCs (**Figure 9A**) grow to colonies of a size that they can be manually isolated and passaged to duplicate 96-well plates (**Figure 9B**). One duplicate (plate A) is frozen for culture revitalization and blastocyst injection, while the other duplicate (plate B) is passaged to three replica plates (B-D), which are used to isolate ESC genomic DNA for analysis by Southern blot or PCR (**Figure 9B**).

Protocols follow standard procedures (as described in 447) and are adapted from S. Feil (451) with slight modifications for the use of an electronic multichannel pipette (Eppendorf Xplorer plus) for handling of ESC cultures in 96-well plates.

A) Generation and Irradiation of MEF Feeder Cells

Mitotically inhibited mouse embryonic fibroblasts (MEF cells) are used as feeder cells. To arrest their cell cycle, DNA damage is induced by γ irradiation. During gene targeting experiments, ESCs are treated with selection agents, usually with G418. Therefore, feeder cells must be G418-resistant, which means that they need to be derived from transgenic, Neo^R-expressing mice. During this work, MEF cells derived from embryos carrying the 'SMIβ rescue' transgene (279) are used.

1. Mate 2-4 males (homozygous for the Neo^R transgene) to each time two females (C57Bl/6, age ≥8 weeks). On the next morning (=0.5 dpc, days *post coitum*), check females for the presence of copulation plugs and separate plug-positive females.
2. On 14.5 dpc, sacrifice 1-3 pregnant females, sterilize the fur with 70% ethanol, and maintain sterility during the whole procedure. Open the abdomen and remove the uteri. Collect the embryos in a petri dish with PBS, remove the amniotic sac, and remove heads and all blood-filled (=red-colored) organs from the embryos.
3. Cut the carcasses into small pieces and transfer them into a 50 mL tube filled with 1×trypsin/EDTA (1 mL/embryo). Incubate for 10 min at 37°C.
4. Dissociate the tissue with pipettes (use in the order 25, 10, and 5 mL), incubate for another 5 min at 37°C, and homogenize the suspension with a 2 mL pipette. Add 2 mL feeder medium per embryo, resuspend, and allow debris to settle for 5 min. Add 20 mL feeder medium to T175 flasks (2 flasks/embryo), then add 1.5 mL of the cell suspension to each bottle. Grow cells to 90-100% confluence at 37°C and 6% CO_2 within 4-6 days.
5. Wash cells in each flask with 15 mL PBS, detach them with 5 mL 1×trypsin/EDTA (5-10 min at 37°C), then add 6 mL feeder medium and resuspend.

6. Remove 9 mL from every flask (collect into a 50 mL tube), add 18 mL feeder medium to the remaining 2 mL cell suspension, and let the cells grow again to 100% confluence.
7. Centrifuge the collected cell suspension for 5 min at 1,000 rpm and resuspend the cell pellet in feeder medium (4 mL/T175 flask). Allow the cells to settle and irradiate them with a dose of 5,000 Rad (50 Gray), either in the 'Verfügungsgebäude' or in the animal facility of the pediatric clinic (in both cases with a Gammacell 1000 device, Nordion, Ottawa, ON, Canada).
8. Centrifuge irradiated cells for 5 min at 1,000 rpm and resuspend the cell pellet in 3 mL freezing medium (90% feeder medium, 10% DMSO) per flask. Aliquot the cell suspension to frozen stocks with 1 mL/vial and freeze them at −80°C. Transfer the vials to a cell bank with liquid nitrogen.
9. Repeat the procedure up to the sixth passage.

B) Preparation of the Targeting Vector

1. Linearize 40-80 µg targeting vector by restriction digest.
2. Precipitate DNA with 3 M NaOAc pH 5.5 and 100% ethanol; wash twice with 70% ethanol and dry the pellet under sterile conditions.
3. Dissolve the DNA in sterile PBS and take an aliquot for concentration measurement and agarose gel electrophoresis, store DNA at −20°C.
4. Use 2-5 pmol (20-50 µg at 15 kb) linearized DNA for electroporation.

C) Preparation of ESCs

1. Thaw low-passage ESCs, plate them onto 25 cm², passage them to 75 cm², and let them grow to 60-80% confluence.
2. Wash the ESCs twice with PBS, detach them with 3 mL 1×trypsin/EDTA, resuspend, add 7 mL ESC medium, and centrifuge for 5 min at 1,000 rpm.
3. Resuspend the cell pellet in 10 mL PBS, add 5 µL trypan blue to a 45 µL aliquot of the cell suspension and count the cells in a Neubauer chamber (the viability should be ≥95%). Centrifuge again for 5 min at 1,000 rpm and resuspend the pellet in PBS to obtain a density of 0.5-1×10^7 ESCs/mL.

D) Electroporation and Selection

1. Mix 0.7 mL of the ESC suspension with linearized targeting vector and transfer the suspension into an electroporation cuvette (d=4 mm).
2. Perform the electroporation with 230 V and 500 µF, τ should be ~5 ms.
3. Leave the cells in the cuvette for 5 min at room temperature, then transfer them into 9 mL ESC medium, resuspend, and distribute the cells to 10 culture dishes (100 mm) with feeder cells.
4. Start G418 selection 24 h after electroporation. During selection, change medium every day or every other day, depending on culture density and the number of dead cells.
5. 4-6 days after electroporation, non-resistant ESCs will start to die, while colonies of G418-resistant ESCs will grow in size and are identified by their sharp borders.

E) Isolation of ESC Clones

1. ESC clones are isolated 7-9 days after electroporation. Isolation of clonal ESC colonies can be repeated up to three times every 1-2 days; 100-400 clones are isolated per day.
2. For the isolation of 96 ESC colonies, prepare two 96-well plates (replica plates A and B) with feeder cells in 100 µL ESC/G418 medium.
3. Prepare round-bottom 96-well plates with 50 µL PBS to accommodate the isolated ESC colonies.
4. Place a stereomicroscope (Stemi 2000C with transmitted-light unit S, Carl Zeiss Microscopy GmbH, Göttingen, Germany) inside a tissue culture hood. Detach undifferentiated ESC colonies with sharp borders from the culture dish using a 20 µL pipette set to 2 µL. Place every colony into a new well of the PBS-filled round-bottom 96-well plate, until 96 colonies are isolated (within ~60 min).
5. Add 50 µL 2×trypsin/EDTA, incubate for 10 min at 37°C, resuspend, add 100 µL ESC/G418 medium and resuspend again.
6. Plate each time 90 µL of the cell suspension to plates A and B; change the medium on the next day. Freeze plate A at 60-80% confluence, passage plate B at 90-100% confluence.

F) Freezing of ESC Clones in Plate A

1. Remove medium from plate A, wash cells with 150 μL PBS, and detach them with 50 μL 1×trypsin/EDTA for 10 min at 37°C.
2. Add 150 μL freezing medium (90% ESC/G418 medium with 10% DMSO) and resuspend.
3. Close the plate tightly with autoclave tape, and freeze cells slowly for 1-3 h at −20°C. Store the frozen plates at −80°C for up to 2 months.

G) Passage of ESC Clones in Plate B

1. Add 150 μL ESC/G418 medium to two new 96-well plates without feeder cells (Plate C and D).
2. Remove the medium from plate B, wash the cells with 150 μL PBS, detach them with 50 μL 1×trypsin/EDTA for 10 min at 37°C. Add 100 μL ESC/G418 medium and resuspend.
3. Transfer each time 50 μL of the cell suspension from plate B to the plates C and D, then add another 150 μL ESC/G418-medium to plate B. Grow cells to 100% confluence.
4. Remove the medium, wash the cells twice with 150 μL PBS and allow the cells to dry. Isolate the genomic ESC DNA, or store dried cells at −20°C.

2.3.4.2 Southern Blot Analysis

- 0.2 M HCl: Add 20 mL 37% HCl to 980 mL H_2O.
- 0.4×SSC, 0.1% SDS: 20 mL/L 20×SSC, 5 mL/L 20% SDS.
- 0.5 M NaOH/1.5 M NaCl: 20 g/L NaOH and 87.5 g/L NaCl.
- 0.5 M Tris/3 M NaCl pH 7.4: 60.58 g/L Tris, 175.3 g/L NaCl, adjust pH to 7.4 with HCl.
- 1 M Na_2HPO_4: 177.99 g/L Na_2HPO_4.
- 1 M NaH_2PO_4: 137.99 g/L NaH_2PO_4.
- 10% BSA: Dissolve 5 g BSA in 50 mL H_2O, heat in water bath at 65°C.
- 10×Labeling buffer with octadeoxyribonucleotides (NEB), store at −20°C.
- 2×SSC, 0.1% SDS: 100 mL/L 20×SSC, 5 mL/L 20% SDS.
- 20×SSC: 175.3 g/L NaCl, 88.2 g/L trisodium citrate dihydrate.
- 50×TAE: 400 mM Tris-acetate (242 g/L Tris, 57.1 mL/L acetic acid), 50 mM EDTA (100 mL/L 0.5 M EDTA pH 8.0).
- Chloroform/isoamyl alcohol.
- Church buffer: 1% BSA (50 mL 10% BSA), 0.5 M phosphate buffer pH 7.2 (193.5 mL 1 M Na_2HPO_4 and 56.3 mL 1 M NaH_2PO_4), 7% SDS (175 mL 20% SDS), 50 mM EDTA (1 mL 0.5 M EDTA), H_2O to 500 mL. Store in 50 mL aliquots at −20°C. Preheat and add ssDNA to a final concentration of 0.1 mg/mL (10 μL/mL 10 mg/mL ssDNA) before use.
- dCTP, $\alpha^{32}P$ (3000 Ci/mmol, 10 mCi/mL, EasyTide; Perkin-Elmer, Rodgau, Germany), store at 4°C.
- DNA lysis buffer variant 1 ('ESC'): 100 mM Tris-Cl pH 7.4 (10 mL/L 1 M Tris-Cl pH 7.4), 10 mM NaCl (2 mL/L 5 M NaCl), 10 mM EDTA (20 mL/L from 0.5 M EDTA pH 8.0), 0.5% sarcosyl (5 g/L N-lauroylsarcosine sodium salt; Sigma-Aldrich). Before use, add proteinase K to a final concentration of 0.25 mg/mL (5 μL/mL 50 mg/mL proteinase K).
- DNA lysis buffer variant 2 ('SF'): 50 mM Tris-Cl pH 7.4 (5 mL/L 1 M Tris-Cl pH 7.4), 5 mM EDTA (10 mL/L 0.5 M EDTA pH 8.0), 1% SDS (50 mL/L 20% SDS), 200 mM NaCl (40 mL/L 5 M NaCl), autoclave. Before use, add proteinase K to a final concentration of 0.5 mg/mL (10 μL/mL 50 mg/mL proteinase K).
- DNA lysis buffer variant 3 ('SNET'): 20 mM Tris-Cl pH 8.0 (2 mL/L 1 M Tris-Cl pH 8.0), 5 mM EDTA (10 mL/L 0.5 M EDTA pH 8.0), 1% SDS (50 mL/L 20% SDS), 400 mM NaCl (80 mL/L 5 M NaCl), autoclave. Before use, add proteinase K to 0.4 mg/mL (8 μL/mL 50 mg/mL proteinase K).
- dNTP mixture: Mix equal parts of 200-fold dilutions of 100 mM dATP, dGTP and dTTP (PEQLAB), store in 25 μL aliquots at −20°C.
- Ethanol/NaCl (for one 96-well plate): Add 150 μL 5 M NaCl to 10 mL ethanol (pre-chilled to −20°C).
- Filter paper: Whatman 3MM gel blotting paper, 0.34 mm×460 mm×570 mm.
- Klenow Fragment: 3′→5′ exo⁻ Klenow fragment (5,000 Units/mL; NEB), store at −20°C.
- LSC: Liquid scintillator cocktail UltimaGold (Perkin-Elmer, Rodgau, Germany).
- Membrane: Hybond N⁺, 20 cm×3 m (GE Healthcare, Freiburg, Germany).
- NICK columns: illustra NICK™ columns with sephadex G-50 (GE Healthcare).
- Phenol/chloroform/isoamyl alcohol, store at 4°C.
- Proteinase K: 50 mg/mL proteinase K in 1×TE, store at −20°C.
- RNase: 10 mg/mL RNase H in 1×TE, store in 1 mL aliquots at −20°C.
- ssDNA: 10 mg/mL salmon sperm DNA (Roche), store in 1 mL aliquots at −20°C. Denature for 5 min at 99°C to obtain single-stranded DNA (ssDNA) before use.

To identify targeted ESCs among cells that escaped positive and negative selection, Southern blot analysis is performed with genomic DNA isolated from ESC colonies. This analysis method is based on the detection of an altered restriction pattern upon integration of the transgene at the target locus. After isolation, genomic DNA is digested with an appropriate restriction enzyme, and separated by agarose gel electrophoresis. To visualize the restriction fragment specifically belonging to the targeted locus, DNA is blotted from the agarose gel to a membrane by capillary transfer (452). Then, the membrane is incubated with a radioactively labeled DNA probe binding only to the restriction fragment of interest. Probe labeling is performed with $\alpha[^{32}P]dCTP$ by random primed labeling (453, 454). Probe binding is detected by exposure of a storage phosphor screen (Fuji Imaging Plate, Fujifilm Medical Systems, Stamford, CT, USA) to the membrane. Further details on the choice of restriction enzymes compatible with the underlying screening protocol, on the choice of an appropriate probe, or on the use of PCR to screen for targeted ESCs can be found in ref. 447. Additionally, Southern blot analysis is used to analyze DNA of conditional transgenes after Cre-recombination in ESCs or tissue isolated from transgenic mice (according to protocol 2.3.4.2B), and to verify ESC genotypes after blastocyst injection.

A) Isolation and Digestion of ESC DNA in 96-Well Plates

1. Add 50 µL DNA lysis buffer (variant 1, 'ESC') with proteinase K to a 96-well plate with dried ESCs and wrap the plate tightly with saran wrap. Incubate the plate overnight at 55°C.
2. Allow the plate to cool down to room temperature, and then add 100 µL ethanol/NaCl, and precipitate the DNA for ≥1 h at room temperature (the DNA will stick to the plastic surface of the 96-well plate).
3. Decant ethanol carefully, wash the precipitated DNA 2-3 times with 100 µL 70% ethanol (pre-chilled to −20°C), dry the DNA for 1 h at room temperature. Dried DNA can be stored at −20°C.
4. For Southern blot analysis, add the restriction enzyme mixture directly to the dried genomic DNA in the 96-well plate (50 µL/well), wrap the plate tightly with saran wrap, and incubate overnight at 37°C. Restriction enzyme mix composition for 1 well:

   o Restriction enzyme buffer (NEB1/2/3/4): 5 µL
   o 100×BSA: 0.5 µL
   o Restriction enzyme: 1 µL (20 U)
   o H_2O: 43.5 µL

5. Prepare agarose gels with four rows á 26 lanes (0.8% agarose in 500 mL 1×TAE without ethidium bromide). Load 30-40 µL of the DNA size marker into the first and last lane of each row. Add 10 µL 6×loading dye to each well of the 96-well plate, and load 50-55 µL of the digested genomic DNA onto the agarose gel (row-wise: A, B / C, D / E, F / G, H).

B) DNA Isolation from ESC Pellets and Tissue Samples

If necessary, cut tissue samples into smaller pieces and make sure that samples are agitated during proteinase K digestion. Use 700 µL/ESC pellet or 700 µL/50-100 mg tissue of DNA lysis buffer variant 2 ('SF') or 1 mL/55 cm² cells or 4 mL/100 mg tissue of DNA lysis buffer variant 3 ('SNET'). Do not vortex the samples during DNA preparation.

1. Incubate samples overnight at 55°C under agitation in a water bath.
2. After overnight incubation, add RNase (10 μL/mL) and incubate for 1 h at room temperature.
3. Add the same volume of phenol/chloroform/isoamyl alcohol; shake for 30 min on a shaker.
4. Centrifuge 10 min at 5,000 rpm, transfer the supernatant (aqueous phase) to a new tube and add the same volume of chloroform/isoamyl alcohol, shake for 15 min on a shaker.
5. Centrifuge 10 min at 5,000 rpm, transfer the supernatant (aqueous phase) to a new tube and add the same volume of 2-propanol, mix by inversion and shake for 30 min on a shaker.
6. Centrifuge for 10 min at 10,000 rpm and 4°C; wash the pellet twice with 70% ethanol.
7. Dry the DNA pellet under vacuum (Eppendorf Concentrator 5301) for 10 min at 40°C. *Take care not to over-dry the pellet.*
8. Add 50-100 μL 1×TE buffer; shake overnight at 4°C, then for 0.5-1 h at 40°C.
9. Estimate DNA concentration and purity by UV spectroscopy. Use 5-15 μg DNA per restriction digest (in 50 μL final volume); load the complete digest onto the agarose gel.

C) Southern Blot

1. Run gel at 80-100 V. Check for the progress by the running fronts of bromophenol blue and xylene cyanol dyes.
2. Stain the gel for 30 min with ethidium bromide (0.01 mg/mL in 1×TAE). Destain the gel for 10-20 min in H_2O.
3. Take a photograph of the gel with lineal or size marker (take picture with a digital camera).
4. Perform depurination for 10 min with 0.2 M HCl (color change of bromophenol blue from blue to yellow). Wash with H_2O.
5. Perform denaturation for 45 min with 0.5 M NaOH/1.5 M NaCl. Wash with H_2O.
6. Neutralize the gel in 0.5 M Tris/3 M NaCl pH 7.4 for 30 min. Wash with H_2O.
7. Perform Southern blot; build the following setup (from the bottom to the top):

   o Buffer reservoir (2 L 10×SSC) in black tank with gel tray (tray is upside down)
   o Filter paper on top of the gel tray, filter paper dips into the buffer reservoir
   o Agarose gel (upside down)
   o Hybond N$^+$ membrane (pre-wetted with 10×SSC)
   o Parafilm around the membrane (no contact between filter papers above and below the membrane)
   o Filter paper (six sheets)
   o Two stacks of paper towels
   o Gel chamber lid with ~1 kg weight on top

8. After Southern blot, label pockets and the membrane, cut the membrane to the correct size (remove lanes with DNA size markers to reduce background during hybridization).
9. Dry the membrane for 3 h at 80°C. Store the membrane in saran wrap at 4°C.

D) Radioactive Labeling of DNA Probes by Random Primed Labeling

If more than two membranes are incubated with the probe, the labeling reaction needs to be upscaled, as well as the number of NICK columns used for purification. The ROSA26-5' probe is isolated with EcoRI from 'pCR-II-Rosa5' probe' (obtained from R. Kühn), the Neo-probe with PstI from pPGKneoA+LS1 (provided by R. Feil).

1. Dilute 100 ng of the probe template DNA in 33 μL H_2O. Denature the probe for 5 min at 99°C, chill on ice (2-5 min), and spin down. Perform the labeling reaction; therefore add to the denatured probe (33 μL):

   o 5 μL 10×labeling buffer with octadeoxyribonucleotides
   o 6 μL dNTP mixture
   o 5 μL α[^{32}P]dCTP
   o 1 μL (5 U) Klenow fragment

2. Incubate for ≥60 min at 37°C.

3. Remove storage buffer from NICK columns, wash once with 3 mL 1×TE, and equilibrate by addition of 3 mL 1×TE.
4. Remove a 1 μL aliquot from the labeling reaction, add the aliquot to 10 mL LSC. Add 30 μL 1×TE to the remaining labeling reaction (~50 μL), load the dilution on the NICK column and collect fractions upon buffer addition:

   o Fraction 1: 320 μL 1×TE (death volume, no radioactivity)
   o Fraction 2: 500 μL 1×TE (labeled probe)
   o Fraction 3: 800 μL 1×TE (free α[^{32}P]dCTP)

5. After mixing and centrifugation of the fractions, measure the radioactivity of 1 μL aliquots in 10 mL LSC of each fraction and the labeling reaction in a liquid scintillation analyzer (2500 TR, Packard, Frankfurt, Germany).
6. Denature the probe (fraction 2) for 5 min at 99°C. Chill for 2-5 min on ice.

E) Membrane Blocking, Hybridization and Washing

1. Build stack of membranes with nylon spacer mesh (Biometra GmbH, Göttingen, Germany) in between the membranes. Wrap to fit the stack into the hybridization tube. Put the membrane stack into the hybridization tube; add 10×SSC, close the tube, and roll it until the membrane stack is unwrapped. Remove 10×SSC, start pre-hybridization in the hybridization oven (OV1, Biometra) for ≥60 min at 60°C in pre-warmed Church buffer with denatured ssDNA (10 μL ssDNA/mL).
2. Remove the pre-hybridization buffer, add new pre-warmed Church buffer with the labeled, denatured probe.
3. Incubate overnight in the hybridization oven at 60°C.
4. Wash twice with pre-warmed 2×SSC, 0.1% SDS (60°C, 10 min).
5. Wash twice with pre-warmed 0.4×SSC, 0.1% SDS (60°C, 10 min).
6. Wash with pre-warmed 0.4×SSC, 0.1% SDS (70°C, 10 min), if necessary.
7. After two or three washing steps, remove the membrane stack from the hybridization tube and continue washing in plastic boxes (remove the spacer meshes).
8. Wash, until activities of 40-80 Bq are detected with a scintillation counter above the unwrapped membrane. Enwrap membranes in saran foil (on the left side: no space between membrane and foil), place the membrane inside an exposition cassette. Put a cleared phosphor screen that must not become wet on the wrapped membrane and expose the screen for 3-7 days.
9. Read the phosphor screen on the Bioimaging Analyzer System (Fujifilm) with 200 μm resolution in IP mode. Convert the image into the TIFF format and perform evaluation with ImageJ (NIH, Bethesda, MD, USA).

2.3.4.3 Thawing of ESCs from 96-Well Plates

1. Wrap the 96-well plate that contains the desired ESC clones with plastic foil. Place the wrapped 96-well plate in a 37°C water bath to thaw the cells.
2. Transfer the cell suspension from every well that contains a targeted ESC clone into a well of a 24-well plate with feeder cells and ESC medium. Perform a medium change after 1-2 days.
3. At 60-80% confluence, passage the ESCs to a 6-well plate. Upon the next passage, freeze a part of the cells (3-4.5 cm²/vial) and plate the remaining cells again to a 6-well plate. Expand the cells for a secondary targeting or use them for blastocyst injection.

2.3.4.4 ESC Secondary (Cre-) Targeting

Cre recombination of conditional transgenes is performed in cultured ESCs, either to verify transgene integrity or to obtain ESCs carrying a Cre-recombined transgene for blastocyst injection. Throughout this work, Cre recombination is performed in ESCs to test if reporter gene expression of targeted *knock-ins* can successfully be activated. To perform Cre recombination, ESCs (carrying a targeted, conditional transgene) are transfected with a Cre expression plasmid by electroporation. Then cells are

plated at low densities without selection agents that single ESCs can grow to individual colonies. These colonies are isolated as described for the primary targeting experiment in 2.3.4.1E).

1. Prepare the Cre expression plasmid: precipitate 50 µg plasmid DNA, wash the pellet twice with 70% ethanol and dry it under sterile conditions. Resuspend the pellet in PBS, use an aliquot for concentration determination, and adjust the concentration to 1 µg/µL.
2. Expand ESCs from a targeted ESC clone to a T75 flask.
3. At 60-80% confluence, perform steps similar to the electroporation of the targeting vector using 1×10^7 cells and 50 µg plasmid DNA. After electroporation, prepare 1:100 and 1:1000 dilutions of the cell suspension in PBS.
4. Add 1 mL of each dilution to 10 mm culture dishes with feeder cells and 9 mL ESC medium.
5. Change the medium on the next day after electroporation and grow cells for 5-7 days, until ESC colonies are isolated.
6. Perform isolation of ESC colonies as described for the initial gene targeting (2.3.4.1E), p.47).
7. From the two replicate plates, freeze plate A and passage plate B into 96-well plates without feeders for DNA analysis and into 96-well plates with feeder cells for selection assays.

2.3.4.5 Selection Assays

Selection assays are performed to test whether Cre-recombined transgenic ESCs express a functionally active *HSV1*-sr39tk reporter. For that purpose, ESCs are treated with GCV, which is phosphorylated by *HSV1*-sr39tk ultimately leading to cell death (see chapter 1.2.3 for further details).

1. For selection assays in 96-well plates:

   o Seed cells at 1:3-1:6 ratios to 96-well plates with feeder cells. Add 50 µL of the ESC suspension to 150 µL ESC medium in the well.
   o On the next day, replace medium with 100 µL ESC/G418 medium (400 µg/mL G418), ESC/GCV medium (2 µM GCV), or ESC medium without selection agent.
   o Change medium every other day, and then every day and check for cell growth or death with a phase contrast microscope (Axiovert 40, Carl Zeiss).
   o When cells are confluent, medium color is used as indicator for cell growth (if cells are confluent, color changes from red to yellow within 1 day).

2. For selection assays in 6-well plates:

   o Seed cells at 1:8-1:12 ratios into 6-wells with feeder cells.
   o On the next day, start selection with 2 mL ESC/G418 medium (400 µg/mL G418), ESC/GCV medium (2 µM GCV), or ESC medium without selection agent.
   o Change medium every other day, later every day. Check for cell growth or death with a phase contrast microscope (Axiovert 40) and take photographs for documentation.

2.3.4.6 Blastocyst Injection and Establishment of Transgenic Mouse Lines

- Holding pipette: VacuTip holding capillary (Eppendorf).
- Injection pipette: TransferTip ES (Eppendorf).
- M2 medium (Sigma-Aldrich).
- Mineral oil: light oil (neat), suitable for mouse embryo cell culture (Sigma-Aldrich).
- Narcosis antidote: naloxon (1.2 mg/kg), flumazenil (0.5 mg/kg), atipamezol (2.5 mg/kg).
- Narcosis: fentanyl (0.05 mg/kg), midazolam (5.00 mg/kg), medetomidin (0.50 mg/kg).
- Analgesia: carprofen (4 mg/kg).
- Surgical suture: Ethicon Vicryl P-3/5-0 (Johnson & Johnson Medical GmbH, Norderstedt, Germany).
- Transfer pipette: Self-made from glass capillaries with 1.5 mm O.D.×1.17 mm I.D. (Clark Electromedical Instruments, Warner Apparatus, Holliston, MA, USA)
- Vaseline

In order to obtain transgenic mice from genetically modified ESCs, they are injected into wild type recipient blastocyst-stage embryos to generate chimeric animals. If the transgene is transmitted through the chimera's germ-line, a transgenic mouse line can be established carrying the transgene previously introduced into the ESC genome (**Figure 10**). Chimeric blastocysts are transferred into the uterus of pseudo-pregnant foster mothers, where they settle and develop, until foster mothers give birth to chimeric mice. Foster mothers of the CD1 outbred strain are used as recipients for modified blastocysts. 6-8 'plug-positive' C57Bl/6 female mice (3.5 dpc) are needed for blastocyst isolation on one injection day, and 3-4 'plug-positive' CD1 foster mothers (2.5 dpc), into which 10-15 blastocysts per foster mother are implanted. If blastocyst injection and replantation are successful, foster mothers give birth to chimeric mice, which derive from (black) host C57Bl/6 blastocyst and injected ESCs from agouti-colored 129/Sv mice (**Figure 10**). The extent of ESC contribution to chimeric animals is estimated from the proportion of agouti-colored fur, at best 7-14 days after birth. ESCs possess a XY karyotype, while host embryos have either a male (XY) or female (XX) karyotype. Due to the incompatibility of 'female' host blastocysts and 'male' ESCs, female chimeras usually are infertile, or ESCs do not contribute to the germ-line of female chimeras. In contrast, ESCs can contribute to the germ-line of male chimeras; therefore, the transgene can be inherited to progeny of male chimeras that were mated to female C57Bl/6 mice. Only agouti-colored chimera progeny can carry the transgene, these animals are tested by PCR for presence of the transgene (**Figure 10**). Germ-line transmission occurs usually with male chimeras that show high proportions (60-90%) of agouti-colored fur. When chimeras are mated to C57Bl/6 mice, transgenic progeny will have a mixed genetic background (C57Bl/6 and 129/Sv), and to achieve uniform genetic background (usually C57Bl/6), transgenic mice need to be backcrossed to C57Bl/6 mice for ≥10 generations (N1-5: mixed, N6-9: incipient congenic, ≥N10: congenic background). Alternatively, chimeras are mated to 129/Sv mice, here all chimera progeny will be agouti-colored and needs to be tested for transgene presence by PCR, but transgenic mice have a 'uniform' 129/Sv background.

Vasectomy of FVB/N mice (according to standard surgery procedures described in ref. 447), ESC injection, and blastocyst replantation were performed by Dr. Susanne Feil.

A) Blastocyst Donor Mice and Foster Mothers

1. Targeted ESCs are injected into blastocyst-stage embryos (3.5 dpc) derived from C57Bl/6 mice: Mate 30 C57Bl/6 stud males (age ≥8 weeks) with each two female C57Bl/6 mice (age ≥8 weeks) on the evening four days before injection. On the next morning (0.5 dpc), check female mice for the presence of a copulation plug, and separate 'plug-positive' females.
2. To induce pseudo-pregnancy, mate CD1 females (age ≥8-12 weeks) to vasectomized FVB/N male mice (≥10 weeks). Mate 30 vasectomized FVB/N males with each two female CD1 mice on the evening three days before injection. Separate 'plug-positive' females on the next morning (0.5 dpc), so that blastocysts are implanted on day 2.5 dpc.

B) Blastocyst Isolation

1. Prepare two 35 mm dishes with 2-3 mL feeder medium per donor female, and equilibrate them for 30 min at 10% CO_2 and 37°C. Prepare two 35 mm dishes with 2-3 mL ESC medium.
2. Sacrifice donor females and disinfect the abdomen with 70% ethanol. Remove the ovaries and uterine horns. Cut the uterine horn at the cervical junction and then at the junction of uterus and oviduct.
3. Place uteri in a dish with feeder medium and wash the blastocysts out of the uteri using a syringe with bended 22G injection needle.
4. After blastocysts have settled, collect ~5 blastocysts/donor animal under a stereomicroscope (Stemi 2000C) at 10× magnification with a transfer pipette, transfer them into ESC medium, and incubate them for 1-3 h at 10% CO_2 and 37°C.

C) Preparation of ESCs for Injection

1. Start to culture ESCs 7-9 days before scheduled injection. Prepare ESCs in 6-well plates with different densities (1:3 to 1:10 splitting ratios upon passage) to ensure that ESCs with appropriate confluence are available on injection day. Prepare frozen stocks from remaining ESCs (3-4.5 cm²/cryovial).
2. On injection day, detach undifferentiated ESCs at 60% confluence from one 6-well and resuspend cells in 3-5 mL ESC medium. Use 1-1.5 mL for injection and harvest the remaining cells for DNA isolation and subsequent analysis by Southern blot.
3. Transfer the ESCs designated for the injection into a 1.5 mL tube and centrifuge for 2 min at 1,000 rpm. Discard the supernatant except 50 µL, and resuspend ESCs in the remaining medium. Use the cells immediately for injection, or store them for ≤2 h at 4°C, if necessary.

D) ESC Injection into Blastocysts

1. Fix a 24 mm×60 mm glass coverslip with vaseline on an 80 mm×25 mm aluminum frame to prepare the injection chamber with the glass coverslip as chamber bottom. Add two drops of M2 medium to the chamber and overlay them with mineral oil. One drop is used to clean the injection needles. Add 30-40 blastocysts and the ESCs to the other, larger drop of M2 medium.
2. Attach the holding and injection needles to the needle holders and fill the needles with oil, until no air remains inside the needles.
3. Place the injection chamber on the microscope stage that is cooled to 10°C, focus to the ESCs on the chamber bottom, and align the needles at 50× magnification.
4. Add medium into the holding pipette from the smaller medium drop and put both needles into the medium drop containing blastocysts and ESCs. Aspirate few medium into the injection needle; the medium/oil phase border should still be visible.
5. At 100× magnification, collect healthy ESCs, but not the larger feeder cells with the injection pipette and inject 10-15 ESCs into a blastocyst, which is fixed with the holding pipette in an appropriate position for injection. By using the holding and the injection pipette, the blastocyst can be rotated in a position that allows for ESCs injection into the inner cavity without hurting the inner cell mass of the blastocyst. The blastocyst is penetrated at the border between two trophoblasts. Upon injection, as few medium as possible should be injected together with the ESCs.
6. Collect injected blastocysts at an appropriate place in the medium drop. The injection procedure should not exceed 2 h.
7. After finishing the injection, transfer injected blastocysts to a dish with ESC medium and incubate them for 1-6 h until replantation at 10% CO_2 and 37°C.

E) Blastocyst Implantation into Foster Mothers

1. Anesthetize a pseudo-pregnant CD1 female mouse (weight: ~30 g).
2. Collect 8-12 blastocysts with a transfer pipette; collect also non-injected blastocysts, if necessary.
3. Place the anesthetized animal under a stereomicroscope (Stemi 2000C). Disinfect the skin with 70% ethanol and open the abdomen with a small incision between the upper leg and the lowest rib. Grasp the ovarian fat pad and pull ovary, oviduct, and upper part of the uterus out of the body cavity. With a 22G needle, cut a small hole into the top of the uterus.
4. Transfer the blastocysts with the transfer pipette into the uterine lumen and place uterus, ovary, and oviduct back into the body cavity. Close the wound, inject antidote and analgesia, and allow the animal to recover under warming infrared light.
5. Chimeras are born 20 days after blastocyst transfer.
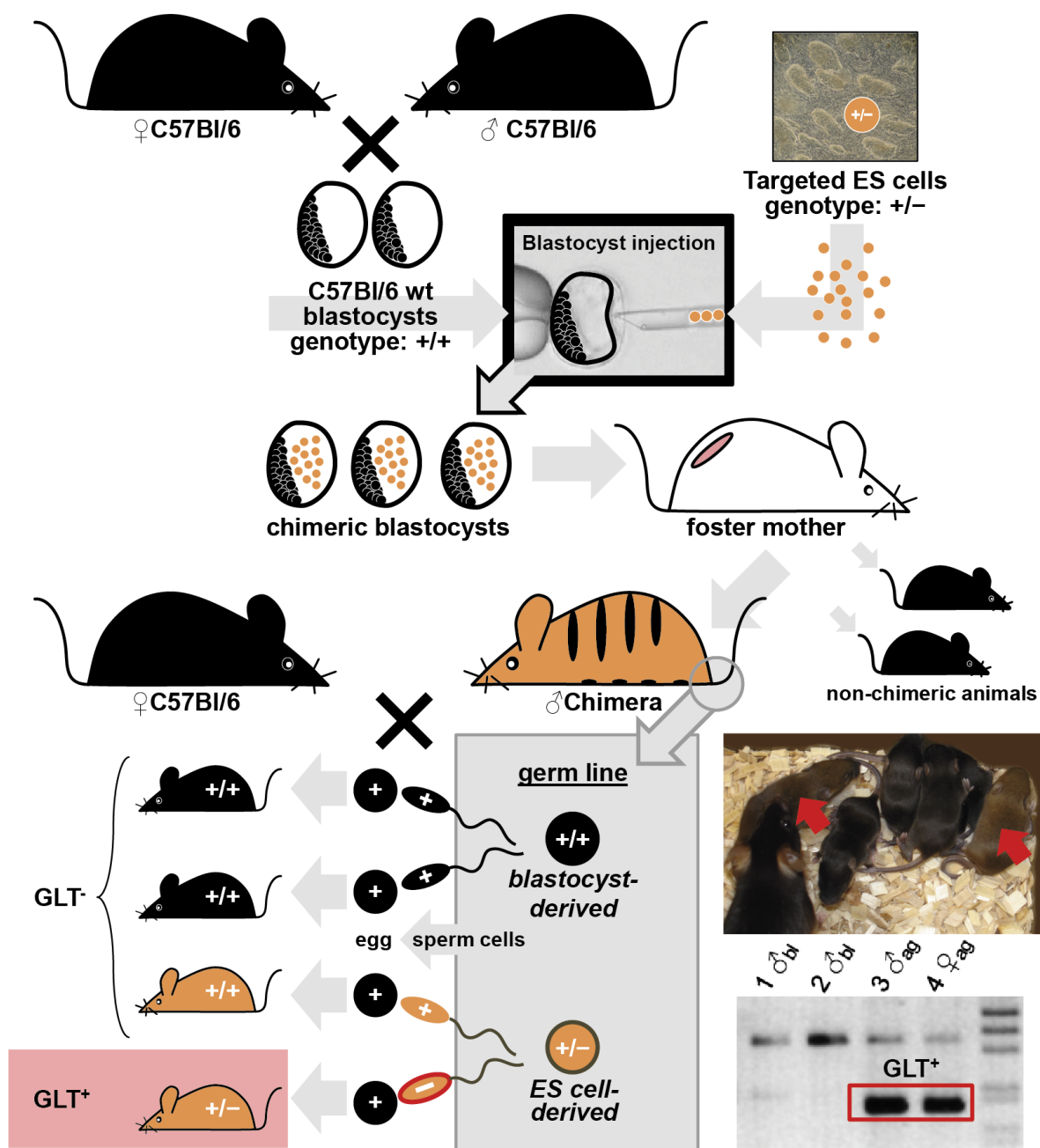
Figure 10. Generation of transgenic mice from targeted ESCs.

15-25 targeted ('transgenic') ESCs are injected into the blastocoel of blastocyst-stage host embryos from C57Bl/6 (wild type) mice. 'Chimeric' blastocysts are transferred into uteri of pseudo-pregnant foster mothers, which deliver chimeric mice. R1 ESCs are derived from 129/Sv mouse strains with agouti-colored fur (A^w/A^w genotype), while C57Bl/6 mice have black fur (a/a genotype); see also **Table 20** (p. 142) for nomenclature. Chimeric mice are recognized by black and agouti-colored fur (agouti: ESC-derived, black: host embryo-derived). Cells of the germ-line are host embryo-derived (wild type) and/or ESC-derived (transgenic). Male chimeras are mated to wild type C57Bl/6 females, and host embryo- or ESC-derived sperm cells fertilize a wild type C57Bl/6 egg cell. If the fertilizing sperm cell is derived from C57Bl/6 cells, offspring will have black fur (genotype: a/a) and cannot carry the transgene (GLT^-). If the fertilizing sperm cell is derived from transgenic ESCs, offspring will be agouti-colored (genotype: A^w/a), as the agouti (A^w) allele is dominant over non-agouti (a). In 'transgenic' ESCs one allele is genetically modified, and around 50% of agouti-colored offspring carries the transgene (GLT^+) that is detected in a PCR reaction (lower right). This GLT^+-offspring is used to establish a new transgenic mouse line.

2.4 Analysis of Transgenic Mice

Analysis of transgenic mice is performed on the DNA level to detect presence (and recombination) of the transgene, and on RNA and protein levels to characterize extent and/or spatial distribution of transgene expression, either in tissue lysates or *in situ* on formaldehyde-fixed tissue samples. To perform functional analyses, cells are isolated from transgenic mice, or transgenic mice are used for *in vivo* experiments.

2.4.1 DNA Analysis

The presence of a transgene is typically verified by genotyping PCRs (see 2.3.2). For targeted mutations, Southern blot or a PCR-based analysis is performed to detect Cre-mediated transgene recombination on the DNA level (see 2.3.4.2).

2.4.2 Transcript Analysis

- 10×DNase buffer: 10 mM Tris-Cl, 2.5 mM $MgCl_2$, 0.5 mM $CaCl_2$, pH 7.6 (NEB), store at −20°C.
- 10×RT buffer: 100 mM Tris-Cl pH 8.0 (1 mL 1 M Tris-Cl pH 8.0), 500 mM KCl (5 mL 1 M KCl), 15 mM $MgCl_2$ (0.15 mL 1 M $MgCl_2$), 2 mM of each dNTP (4×0.2 mL 100 mM dATP/dGTP/dCTP/dTTP), 3.65 mL H_2O. Store in 0.5 mL aliquots at −20°C.
- 70% Ethanol/DEPC: 70 mL ethanol, 30 mL DEPC-treated H_2O.
- DEPC-treated H_2O: 1 mL/L diethylpyrocarbonat (DEPC), shake or stir for ≥1 h, autoclave.
- DNase I: 2000 U/µL DNase I (RNase-free; NEB), store at −20°C.
- Lysis cups and lysing matrix A (MP Biomedicals, Illkirch, France).
- MMLV-RT: 200,000 U/mL Moloney murine leukemia virus reverse transcriptase (MMLV-RT; NEB), store at −20°C.
- peqGOLD RNAPure (PEQLAB), store light-protected at 4°C.

RNA is isolated from tissue samples according to the method of Chomczynski and Sacchi (455). Tissue samples are homogenized in a FastPrep-24 instrument (MP Biomedicals) that agitates 2 mL-tubes filled with lysing matrix, lysis buffer and the tissue sample (50-120 mg). The lysing matrix is composed of a single ceramic sphere and garnet matrix, which destroys the tissue sample during homogenization in the FastPrep instrument. Isolated RNA is used to detect transgene mRNA via RT-PCR. Therefore, the mRNA is converted to copy-DNA (cDNA) by the reverse transcriptase (RT) enzyme; the cDNA serves as template in a PCR reaction. The following protocol describes RNA isolation from tissue samples and one-step RT-PCR reactions with transcript-specific primers.

1. Sacrifice animal, collect tissue samples (~100-150 mg) in 2 mL tubes, and freeze them in liquid nitrogen. Store at −80°C or continue with RNA isolation.
2. Prepare lysis cups (add lysis matrix and label cups on wall and lid). Add 1 mL peqGOLD RNAPure per 100 mg tissue (but ≥150 µL) to the cups and then the frozen tissue. Keep the tubes on ice until all samples are prepared. Place the cup-holder in the FastPrep device (FastPrep-24, MP Biomedicals), run once for 1 min with 6.5 M/s; centrifuge for 10 min at 9,000 rpm and 4°C, transfer the supernatant into a new 2 mL tube and incubate the sample for 5 min at room temperature.
3. Add 0.2 mL chloroform per mL peqGOLD RNAPure, shake for 15 s, and incubate for 5 min on ice.

4. Centrifuge for 15 min at 9,000 rpm and 4°C. Transfer the upper (aqueous) phase into a new tube and add an equal volume 2-propanol. Incubate for 15 min on ice.
5. Centrifuge for 15 min at 9,000 rpm and 4°C. Wash the pellet two times with 70% ethanol; dry the RNA pellet under vacuum (Eppendorf Concentrator 5301) for 5 min at 40°C.
6. Resuspend the pellet in 50 µL DEPC-treated H_2O and incubate for 10 min at 55-60°C. Estimate the RNA concentration by UV spectroscopy.
7. Perform DNase digest: Use 10 µg RNA, add 10 µL 10×DNase buffer and DEPC-treated water to a volume of 99 µL. Add 1 µL DNase, incubate for 20 min at 37°C, and then for 10 min at 80°C. Add 100 µL peqGOLD RNAPure, mix, incubate for 5 min at room temperature and perform RNA isolation as described above (with 20 µL chloroform and 100 µL 2-propanol).
8. Resuspend the RNA pellet in 30 µL DEPC-treated H_2O and incubate for 10 min at 55-60°C. Estimate the RNA concentration by UV spectroscopy. Store the RNA at −20°C.
9. Prepare the RT-PCR reaction (primers in **Table 19**, p. 141):

    o   500 ng RNA
    o   5 µL 10×RT buffer
    o   0.5 µL forward primer (25 µM)
    o   0.5 µL reverse primer (25 µM)
    o   DEPC-treated H_2O to 45 µL

10. Denature reaction mixture for 5 min at 94°C, cool slowly to 50°C (ramp rate 0.1°C/s).
11. Add 200 U MMLV-RT in 5 µL 1×RT buffer. Perform RT reaction for 20 min at 42°C.
12. Add 2.5 U *Taq* polymerase in 5 µL 1×RT buffer.
13. Continue with PCR reaction (initial denaturation for 5 min at 94°C and 35 amplification cycles).
14. Add 10 µL 6×DNA loading dye and load 15 µL on a 2% agarose gel.

2.4.3   Analysis of Protein Lysates

2.4.3.1   Cell and Tissue Lysis

-   Lysis cups and lysing matrix A (MP Biomedicals).
-   PMSF: 100 mM phenylmethylsulfonylfluorid (PMSF) in 100% ethanol, store in 1 mL aliquots at −20°C.
-   Protein lysis buffer: 2% SDS (100 mL/L 20% SDS), 50 mM Tris-Cl pH 8.0 (50 mL/L 1 M Tris-Cl pH 8.0), 5 mM EDTA (10 mL/L 0.5 M EDTA pH 8.0), 100 mM NaCl (20 mL/L 5 M NaCl). Add 25 µL 100 mM PMSF per mL lysis buffer before use.

For the preparation of protein lysates from cultured cells, SDS-containing protein lysis buffer is directly added to the cells. Tissue samples are homogenized with SDS-containing protein lysis buffer in a FastPrep-24 instrument (MP Biomedicals).

1. For cell lysis, remove the medium and wash cells twice with PBS. Add protein lysis buffer (800 µL/6-well). Pipette up and down, wipe the surface of the culture dish with the pipette tip (avoid foam formation). Denature cell lysates for 10 min at 95°C, centrifuge for 5 min at 13,000 rpm and transfer the supernatant to a new tube.
2. For tissue lysis, prepare lysis cups (add lysis matrix and label cups on wall and lid). Prepare tissue samples with weights of 50-120 mg. Shock-freeze tissue samples in liquid nitrogen. Add 7.5 µL protein lysis buffer/mg tissue (but ≥150 µL) to the lysis cups, and then the frozen tissue. Keep the tubes on ice until all samples are prepared. Place the cup-holder in the FastPrep device, run once or twice for 1 min with 6.5 M/s; chill on ice for 5 min between runs or centrifuge, if necessary. Denature samples for 10 min at 94°C and centrifuge for 10 min at 13,000 rpm. Transfer the supernatant to new tubes. Dilute an aliquot of the sample with protein lysis buffer (e.g. 1:2 for lung; 1:3 for bladder, heart, skeletal muscle; 1:4 for kidney, colon, spleen; 1:8 for brain, liver).
3. Perform protein quantification with the protein lysates.

2.4.3.2 Protein Quantification with the Lowry Assay

- BSA standard: 12.5, 25, 50, 100, and 200 μg/mL BSA in H_2O.
- Total protein kit, micro Lowry, Peterson's modification (Sigma-Aldrich).

Protein concentrations of cell or tissue lysates are determined in a colorimetric reaction with the Peterson's modification (456) of the Lowry method (457). Protein determinations are performed in a 96-well plate; all samples are analyzed at least in duplicate. Products of the colorimetric reaction are quantified in a multi-well plate reader (Multiskan EX, Thermo Fisher) at 620 nm and correlate in a range of ~2-40 μg with the protein content in the sample.

1. Prepare negative controls (100 μL H_2O or 90 μL H_2O with 10 μL protein lysis buffer).
2. Prepare 100 μL of the BSA standard (12.5, 25, 50, 100, and 200 μg/mL BSA).
3. Add 10 μL cell or tissue lysates to 90 μL H_2O.
4. Add 100 μL Lowry reagent solution to all samples. Resuspend and incubate for 20 min in the dark.
5. Add 50 μl Folin-Ciocalteu's phenol reagent working solution to all samples. Resuspend and incubate for 30-60 min in the dark.
6. Read absorption at 620 nm in a multi-well plate reader.
7. With absorptions of the BSA samples (corrected for H_2O absorption), estimate a calibration curve and use it to determine the protein concentrations of the cell or tissue lysates (corrected for absorption of protein lysis buffer).

2.4.3.3 SDS-PAGE and Western Blot

- 1% and 5% MP: 1 g/100 mL or 5 g/100 mL non-fat dry milk powder (MP) in TBS-T; prepare freshly before use.
- 10×SDS running buffer: 0.25 M Tris-glycine (30.2 g/L Tris, 144.0 g/L glycine), 0.1% SDS (10 g/L).
- 10×TBS: 100 mM Tris-Cl pH 8.0 (100 mL/L 1 M Tris-Cl pH 8.0), 1.5 M NaCl (87.66 g/L).
- 12% separating gel (2×0.75 mm gels): 2.7 mL Rotiphorese Roth (30% acrylamide/0.8% bisacrylamide), 2.5 mL 4×Tris-Cl/SDS (pH 8.8), 4.7 mL H_2O, 50 μL 20% APS, 10 μL TEMED.
- 20% APS: Dissolve 2 g ammonium persulfate (APS) in 10 mL H_2O, store in 1 mL aliquots at −20°C.
- 4% stacking gel (two 0.75 mm gels): 0.65 mL Rotiphorese Roth (30% acrylamide/0.8% bisacrylamide), 1.25 mL 4×Tris-Cl/SDS (pH 6.8), 3.05 mL H_2O, 25 μL 20% APS, 10 μL TEMED.
- 4×Tris-Cl/SDS (pH 6.8): 0.5 M Tris-Cl (60.04 g/L Tris), 0.4% SDS (4 g/L), adjust pH to 6.8 with HCl, store at 4°C.
- 4×Tris-Cl/SDS (pH 8.8): 1.5 M Tris-Cl (182 g/L Tris), 0.4% SDS (4 g/L), adjust pH to 8.8 with HCl, store at 4°C.
- 5×Laemmli buffer: 0.32 M Tris-Cl pH 6.8 (3.2 mL 1 M Tris-Cl pH 6.8), 40% glycerol (4 mL), 15% SDS (1.5 g), 3.6 M 2-mercaptoethanol (2.5 mL), 0.1% bromophenol blue (10 mg), H_2O to 10 mL, store in 1 mL aliquots at −20°C.
- 8% separating gel (two 0.75 mm gels): 2.7 mL Rotiphorese Roth (30% acrylamide/0.8% bisacrylamide), 2.5 mL 4×Tris-Cl/SDS (pH 8.8), 4.7 mL H_2O , 50 μL 20% APS, 10 μL TEMED.
- Anode buffer I (pH 10.4): 0.3 M Tris (36.3 g/L), 20% methanol (200 mL/L).
- Anode buffer II (pH 10.4): 0.025 M Tris (3.03 g/L), 20% methanol (200 mL/L).
- Blotting paper: Whatman 3MM gel blotting paper, 0.34 mm×460 mm×570 mm.
- Cathode buffer (pH 7.6): 0.04 M aminocaproic acid (5.2 g/L), 0.025 M Tris-Cl (3.03 g/L Tris), 20% methanol (200 mL/L), adjust pH with HCl.
- Coomassie destaining solution: 20% methanol, 20% acetic acid, 20% 2-propanol.
- Coomassie staining solution: 2.5 g Coomasie brilliant blue R250, 500 mL methanol, 400 mL H_2O, at last 100 mL acetic acid.
- Enhanced chemiluminescence (ECL) reagent: ECL advance western blot detection kit (GE Healthcare).
- Primary antibody diluent: TBS-T with 5% BSA and 0.05% NaN_3, store at 4°C.
- Protein Ladder: PageRuler™ prestained protein ladder (Fermentas, Thermo Fisher)
- PVDF membrane: Polyvinylidenfluoride (PVDF) membrane (Immobilon-P with 0.45 μm pore size, Millipore).
- TBS-T: 1×TBS (100 mL/L 10×TBS) with 0.1% Tween-20 (1 mL/L).

Proteins are separated by SDS polyacrylamide gel electrophoresis (SDS-PAGE) under denaturing conditions according to their molecular weight (458) in a Mini-PROTEAN Electrophoresis System (Bio-Rad). To control for equal loading and for the integrity of the protein extract, proteins are stained in the gel with Coomassie brilliant blue. To detect a specific protein, a western blot analysis is performed, where proteins are transferred after SDS-PAGE from the gel to a polyvinylidenfluoride (PVDF) membrane in a semi-dry blotting apparatus (Carl Roth). Binding of protein-specific primary antibodies to proteins immobilized on the membrane is detected by horseradish peroxidase (HRP)-linked secondary antibodies. Hydrogen peroxide and a commercially available ECL reagent (ECL = enhanced chemiluminescence) react in a HRP-catalyzed reaction under light emission, which is detected by a digital camera in the AlphaImager HP system (Biozym).

1. Prepare protein samples: add 1 volume 5×Laemmli buffer to 4 volumes of the sample and incubate them for 5 min at 95°C. Allow to cool down and centrifuge for 1 min at 13,000 rpm.
2. Prepare polyacrylamide gels; first the resolving gel, then the stacking gel. Mount the gels into the running chamber, and fill the chamber with 1×SDS running buffer. Remove the combs and clean the gel pockets.
3. Load the protein ladder (3 μL) and the samples. Fill empty pockets with 1×Laemmli buffer.
4. Run the gel for 5 min at 100 V, then ~1 h at 150 V until the loading dye runs out of the gel.
5. Disassemble the gel chamber, discard the stacking gel, and use the running gel for western blot analysis or Coomassie staining.
6. For Coomassie staining, transfer the gel to the Coomassie staining solution, shake for 45 min. Transfer the gel into Coomassie destaining solution (first use already used, then fresh solution) until protein bands become visible.
7. For western blot analysis, prepare filter papers and PVDF membranes in dimensions of the protein gel and stack the blot from top (anode) to bottom (cathode):

   o Weight (~0.5 kg)
   o Cathode
   o 8 Whatman 3 MM blotting papers (wetted in cathode buffer)
   o Protein gel
   o PVDF membrane (immersed in methanol and anode buffer II)
   o 4 Whatman 3 MM blotting papers (wetted in anode buffer II)
   o 4 Whatman 3 MM blotting papers (wetted in anode buffer I)
   o Anode

8. After every layer, remove air bubbles by rolling over the stack with a plastic pipette.
9. Blot 1 h with 50 mA per blotting stack. After the blot, cut the membrane, label the membrane with a pencil, and transfer the marker bands.
10. Block the membrane with 5% MP for ≥1 h at room temperature (or overnight at 4°C).
11. Wash twice 3 min with 1% MP. Wash 3 min with TBS-T.
12. Incubate the membrane with the primary antibody (**Table 22**, p. 143) in primary antibody diluent in a 50 mL falcon tube overnight at 4°C (or 2 h at room temperature).
13. Wash 3 times 3 min with 1% MP.
14. Incubate the membrane with HRP-coupled secondary antibody (**Table 22**, p. 143) for ≥1 h at room temperature.
15. Wash once 3 min with 1% MP and twice 3 min with TBS-T.
16. Wet the membrane with ECL reagent (undiluted or diluted 1:2 to 1:20 in TBS-T), place the membrane inside the AlphaImager, and acquire chemiluminescence images of appropriate acquisition times (5 s to 10 min), and a bright-field image for comparison with the size marker.

2.4.4 *In Situ* Analysis of Mouse Tissue

2.4.4.1 Immunofluorescence on Frozen Sections

- 2-Methyl butane.
- 30% Sucrose: Dissolve 30 g sucrose in 100 mL PBS, store at 4°C.
- 4% PFA: Stir 4 g paraformaldehyde (PFA) in 100 mL PBS, heat to 55-57°C until the PFA gets dissolved. Allow the solution to cool down and filtrate before use.
- Blocking solution: 5% NGS and 1% BSA in PBS-T, store at 4°C.
- Heparin-PBS: 25 mg heparin/100 mL PBS, store at 4°C.
- Mounting medium: Shandon ImmuMount (Fisher HealthCare, Houston, TX, USA).
- NGS: normal goat serum (NGS; Axxora, Enzo Life Sciences GmbH, Lörrach, Germany), store in 1 mL aliquots at 4°C.
- PBS-T: 0.4% Triton X-100 (4 mL/L Triton X-100) in PBS.
- SuperFrost Plus glass slides (Thermo Fisher).
- Tissue-Tek: Tissue-Tek O.C.T. compound (Sakura Finetek Germany GmbH, Staufen, Germany).

The antibody-based *in situ* analysis of protein expression patterns is performed on frozen sections prepared from PFA-fixed tissue samples (for antibodies, see **Table 22** on p.143). Antibody binding is detected with fluorescence-labeled secondary antibodies. To control for unspecific binding, controls are performed with tissue from non-transgenic (or *knock-out*) mice, or by omission of primary antibody.

1. Sacrifice animals and perform transcardial perfusion to remove blood and to achieve uniform fixation of the organs. Place the animal on top of a paper stack to collect liquid spill. Open the thoracic cavity and insert a 27G needle into the left ventricle of the heart directed towards the ascending aorta. Perfuse the animals at 2 mL/min with heparin-PBS for 5 min followed by perfusion with 4% PFA for 10 min.
2. Dissect organs and continue fixation with 4% PFA overnight at 4°C.
3. Wash organs with PBS, place them in 30% sucrose at 4°C until they sink down (1-2 days). Embed them in Tissue-Tek. Freeze the embedded samples in 2-methyl butane at −80°C, and store them at −20°C.
4. Prepare frozen sections with 10 μm thickness on a cryostat (Microm, Thermo Fisher). Mount the sections on SuperFrost Plus glass slides, dry them at room temperature, and use them immediately or store at −20°C.
5. Incubate slides for 5 min in PBS, then for 5 min in PBS-T at room temperature.
6. Block unspecific binding with blocking solution for 45 min at room temperature.
7. Incubate sections overnight with primary antibody (**Table 22**, p. 143) diluted in blocking solution at 4°C.
8. Wash 3×5 min with PBS-T, and incubate with secondary antibody (**Table 22**, p. 143) and 1 μg/mL Hoechst 33258 in PBS-T and 1% BSA for 2 h at room temperature.
9. Wash 3×5 min with PBS-T, dip slides briefly into H_2O, add a drop of mounting medium and cover the slides with a coverslip of appropriate size.

2.4.4.2 X-Gal staining of Tissue Samples

- 25% Glutaraldehyde.
- 40×X-Gal: Dissolve 0.4 g 5-bromo-4-chloro-3-indolyl-D-galactoside (X-Gal) in 10 mL DMSO, store in 1 mL aliquots at –20°C.
- Heparin-PBS: 25 mg heparin/100 mL PBS, store at 4°C.
- X-Gal fixative solution: 2% formaldehyde (54 mL/L 37% formaldehyde), 0.2% glutaraldehyde (8 mL/L 25% glutaraldehyde) in PBS, store at 4°C.
- X-Gal staining solution: 2.5 mM $K_3Fe(CN)_6$ (1.6 g/L), 2.5 mM $K_4Fe(CN)_6$ (2.14 g/L) and 2 mM $MgCl_2$ (2 mL/L 1 M $MgCl_2$) in PBS, store in the dark. Add 1/40 volume 40×X-Gal (final concentration: 1 mg/mL) freshly before use.

Tissue from ROSA26-lacZ Cre reporter mice (64) is used to analyze recombination patterns of Cre transgenic mouse lines. For analysis, fixed tissue samples isolated from $Cre^{tg/+}$; ROSA26-lacZ$^{+/−}$ mice

are incubated with the β-galactosidase substrate X-Gal. After β-galactosidase-catalyzed hydrolysis of X-Gal, it reacts to a blue, water-insoluble indigo dye. Cre recombinase-driven activation of β-galactosidase expression is therefore indicated by a blue staining of the tissue. The X-Gal staining solution will penetrate only outer layers of larger samples, so they should be cut into halves or several slices before X-Gal staining. To exclude false-positive results, for example due to tissue-intrinsic galactosidase activities, a control staining has to be performed with tissue isolated from $Cre^{+/+}$; ROSA26-lacZ$^{+/−}$ mice (459).

1. Sacrifice animals and perform transcardial perfusion to remove blood and to achieve uniform fixation of the organs. Place the animal on top of a paper stack to collect liquid spill. Open the thoracic cavity and insert a 27G needle into the left ventricle of the heart directed towards the ascending aorta. Perfuse the animals at ~2 mL/min with heparin-PBS for 5 min and then with X-Gal fixative solution for 10 min.
2. Collect organs from the mouse, pool them in a 50 mL tube with 25 mL of X-Gal fixative solution, and continue fixation for 30 min under agitation.
3. Wash the fixed tissues three times with PBS for 15 min under agitation.
4. Incubate the samples overnight under agitation in X-Gal staining solution (in the dark).
5. Wash the X-Gal-stained tissues three times for 15 min with 10 mL of PBS.
6. Analyze the samples in a Petri dish on a stereomicroscope (Stemi 2000C). Documentation is performed with a digital camera under different illumination conditions.
7. Store stained organs in PBS or 70% ethanol in the dark at 4°C.

2.4.5   Isolation of Primary Cells from Transgenic Mice

- 10 μg/mL or 100 μg/mL PDL: Dissolve 1 mg poly-D-lysine HBr (PDL, Sigma-Aldrich) in 1 mL H_2O by shaking at 37°C for 2 h and then at 4°C overnight. Dilute PDL to 10 or 100 mL with H_2O to final concentrations of 100 or 10 μg/mL, respectively. Store at 4°C for up to 2 months.
- 100 mM Ara-C: Dissolve 100 mg cytosine-β-D-arabinofuranoside hydrochloride (Ara-C; Sigma-Aldrich) in 3.58 mL H_2O, store in 500 μL aliquots at −20°C.
- 100×L-Glutamine (200 mM; GIBCO, Life Technologies), store in 1 mL aliquots at −20°C.
- 2.5% Trypsin: Dissolve 1 g trypsin (Sigma-Aldrich) in 40 mL H_2O, store in 5 mL aliquots at −80°C.
- 50×B27 supplement (GIBCO, Life Technologies), store in 2 mL aliquots at −20°C.
- Cell strainer: 24 mm Netwell insert with 74 μm mesh size (Corning B.V. Life Sciences, Amsterdam, Netherlands).
- FBS: heat-inactivated FBS (GIBCO, Life Technologies), store in 50 mL aliquots at −20°C.
- MEM: Minimum essential medium (MEM) without L-glutamine (GIBCO, Life Technologies).

For FRET-based cGMP imaging, cells are isolated from mice that express cGi-type biosensors. Hippocampal neurons (HNs), cortical astrocytes (CAs), and cerebellar granule neurons (CGNs) are isolated from brains of transgenic mice. To obtain viable cultures and sufficient cell yields, these cells need to be isolated from newborn mice (1-7 days after birth, depending on isolated cell type). To allow cell attachment to the glass coverslip in the culture vessel, the coverslip needs to be coated with poly-D-lysine. Furthermore, neural cells need to be supplied with growth factors that promote their survival, which are supplemented as B27 cocktail (460). Astrocytes will proliferate in culture, while neurons are post-mitotic and do not divide in culture. If cells are present, which proliferate rapidly (like fibroblasts from the meninges), they overgrow cultured neurons. In order to inhibit proliferation of these cells, Ara-C is added to the medium, which interferes with DNA synthesis and is therefore cytotoxic for dividing cells, but not for post-mitotic neurons. Cells were not starved (e.g. by

withdrawal of serum or supplement) prior to imaging, because neural cells are sensitive to changes in culture conditions, especially to a change of the whole culture medium (461). For the preparation of neural cells, newborn mice are needed; separate pregnant females and check for pup delivery (postnatal day 0) and use 5-7 pups on the same day for HN or CA isolation, or keep them for CGN isolation on postnatal day 7. To identify cGi-transgenic pups for the isolation of CGNs (here, 3-5 are needed), the pups are labeled on postnatal day 5 with a waterproof marker pen and tail tips are collected for genotyping. Newborn pups used for HN and CA isolation are not genotyped before preparation, so that mixed cultures derived from transgenic and wild type animals are obtained.

2.4.5.1 Hippocampal Neurons and Cortical Astrocytes

- 1 M HEPES pH 7.3: 23.8 g/100 mL HEPES, adjust pH with NaOH, sterilize by filtration, store at 4°C.
- 1% DNase: Dissolve 100 mg DNase (Roche) in 10 mL H_2O, store in 0.3 mL aliquots at −20°C.
- 10×HBSS (Hank's balanced salt solution; GIBCO, Life Technologies).
- 12% D-Glucose: Dissolve 3 g D-glucose in 25 mL MEM, sterilize by filtration, store at 4°C.
- 20 mM Na pyruvate: Dissolve 56 mg Na pyruvate in 25 mL MEM, sterilize by filtration, store at 4°C.
- CMF-HBSS: calcium/magnesium-free HBSS, 10 mL 10×HBSS, 1 mL 1 M HEPES pH 7.3, 89 mL H_2O.
- DMEM+10% HS: 27 mL DMEM + 3 mL HS.
- Glial Medium: 40.525 mL MEM, 2.475 mL 12% D-glucose, 0.50 mL Pen/Strep, 0.50 mL 100×L-glutamine, 5.00 mL HS, 1 mL 50×B27 supplement.
- HN medium: 26.1 mL MEM, 1.5 mL 20 mM Na pyruvate, 1.5 mL 12% D-glucose, 300 µL 100×L-glutamine, 600 µL 50×B27.
- HS: Horse serum (GIBCO, Life Technologies), heat-inactivated (30 min at 56°C), store in 50 mL aliquots at −20°C.
- Trypsin inhibitor (GIBCO, Life Technologies).

A) PDL-coating of Glass Coverslips

1. One day before cell isolation, add 1 mL 100 µg/mL PDL to 20 mm glass coverslips in 12-well plates and incubate overnight in the tissue culture hood.
2. On the next day, collect PDL for reuse (reuse twice) and wash the wells three times with H_2O.
3. Dry open 12-well plates ≥2 h in the tissue culture hood before plating the cells.

B) Preparation of the Brain

1. Prepare one 100 mm and several 35 mm culture dishes with CMF-HBSS and 50 mL tubes with PBS on ice.
2. Wash dissection instruments thoroughly. Keep them in ethanol and rinse in H_2O before use.
3. Use 3-5 mouse pups of postnatal day 1. Dip the pup's head for 1 s into a beaker with 70% ethanol and then cut the neck and place the head in a 50 mL tube with ice-cold PBS. Collect the tail tip for genotyping.
4. After 30-60 s, take the head with a forceps and place it in a 100 mm petri dish with CMF-HBSS under a stereomicroscope. Take the head with a forceps and remove the skin. To open the skull, hold it at the nose and cut the skull with fine scissors above the brain from caudal to rostral. Pull the skull apart to each side with a bend forceps. Disconnect the brain from the skull by cutting at the olfactory bulb. Transfer the brain into a 35 mm culture dish with CMF-HBSS. Store the brains on ice while dissecting the remaining brains.
5. After all brains have been dissected, remove meninges and blood vessels from the outer part of the cortex (under 40× magnification). Then separate the cerebral hemispheres, remove the inner part of the brain and the meninges from the inner part of the cortex and above the hippocampi. Separate the hippocampi from the cortex and collect them in a new dish. Pick the tissues into small pieces while removing any remaining meninges or blood vessels.

C) Isolation of Hippocampal Neurons (HNs)

1. Transfer the hippocampi into a 50 mL tube with 2 mL CMF-HBSS. Add 40 μL 2.5% trypsin and swirl the tube once. Incubate for 15 min in a 37°C water bath.
2. Add 50 μL 1% DNase and wait for 1 min. Add 10 mL pre-warmed DMEM+10% HS, and allow the tissue pieces to settle down and carefully aspirate the supernatant with a 10 mL pipette. Repeat this washing step once with 10 mL DMEM+10% HS. Then add 2 mL DMEM+10% HS.
3. Dissociate the tissue by slow pipetting through a regular Pasteur pipette for 10 passes. Continue with 10 passes through a flame-polished Pasteur pipette (*opening width is important for cell survival!*). Expel the suspension against the tube wall to minimize foam formation.
4. When the solution becomes turbid and all tissue pieces disappears, centrifuge for 5 min at 600 rpm. Remove the supernatant and resuspend the pellet in 1.0 mL pre-warmed HN medium.
5. Mix 18 μL of the cell suspension with 2 μL trypan blue and count viable and dead (trypan blue-positive) cells in a cytometer. Calculate the titer of viable cells. The viability should be $\geq 90\%$ with a yield of $0.75\text{-}1\times10^5$ cells per animal. Seed 3.5×10^4 cells in 1 mL HN medium per 12-well equipped with a PDL-coated coverslip (1×10^4 cells/cm²). Grow cells at 37°C and 6% CO_2 (Innova-170 CO_2 incubator, New Brunswick Scientific). Imaging experiments are performed starting from day 3 after plating.
6. Add Ara-C to a final concentration of 5 μM to the cells 24 hours after plating the cells. Perform medium changes every 5-7 days. Replace one third of the medium with fresh HN medium (equilibrate the medium in the incubator before use).

D) Isolation of Cortical Astrocytes (CAs)

1. Transfer tissue pieces into a 50 mL tube with 5 mL CMF-HBSS. Add 125 μL 2.5% trypsin and 50 μL 1% DNase. Incubate for 5 min at 37°C in a water bath, swirl the tube every 60 s.
2. Triturate ten times with a 10 mL pipette; incubate the tube for another 2-3 min at 37°C in the water bath until the majority of tissue pieces disappear. Transfer cell suspension into a tube with 10 mg trypsin inhibitor; resuspend 10 times with a 10 mL pipette. Add another 100 μL 1% DNase and incubate for 15 min under agitation at 37°C in the water bath.
3. Pass the cell suspension through a cell strainer to remove any un-dissociated tissue, collect the flow-through in a 50 mL tube containing 10 mL glial medium. Centrifuge for 10 min at 1,100 rpm.
4. Resuspend the cell pellet in 5 mL glial medium. Mix 18 μL of the cell suspension with 2 μL trypan blue and count viable and dead (trypan blue-positive) cells in a cytometer. Calculate the titer of viable cells. The viability should be $\geq 90\%$ and the yield should be 5×10^5 cells/animal. Seed 3.5×10^5 cells in 1.0 mL glial medium per 12-well equipped with a PDL-coated coverslip (1×10^5 cells/cm²). Grow cells at 37°C and 6% CO_2 (Innova-170 CO_2 incubator).
5. Change the medium every 2-3 days. Imaging experiments are performed starting from day 5-7 after plating. To remove microglia that grow on top of the astrocytes, tap the culture dish 5-10 times before medium is exchanged.

2.4.5.2 Cerebellar Granular Neurons (CGNs)

- 0.3% BSA solution (prepare always fresh on the day of use): Weigh 450 mg BSA into a beaker glass, add 132.84 mL H_2O, 15 mL 10×Krebs buffer, 2.16 mL 1 M D-glucose and 1.2 mL 3.82% $MgSO_4$. Adjust the pH to 7.4 with NaOH, sterilize by filtration, store at 4°C.
- 1 M D-glucose (198.17 g/L D-glucose×H_2O), sterilize by filtration, store at 4°C.
- 1.2% $CaCl_2$: Dissolve 1.2 g $CaCl_2$×2 H_2O in 100 mL H_2O, sterilize by filtration, store at 4°C.
- 10×Krebs buffer (pH 7.4) without D-glucose: 1.24 M NaCl (72.5 g/L), 54 mM KCl (4 g/L), 5 mM NaH_2PO_4 (0.7 g/L NaH_2PO_4×H_2O). Adjust pH to 7.4 with NaOH, autoclave, store at 4°C.
- 3.82% $MgSO_4$: Dissolve 3.82 g $MgSO_4$×7 H_2O in 100 mL H_2O, sterilize by filtration, store at 4°C.
- 50 mg/mL Gentamicin (GIBCO, Life Technologies).
- CGN medium: To 88 mL HK medium, add 9 mL FBS, 0.9 mL 100×L-glutamine, 2 mL 50×B27 supplement, store at 4°C for up to 1 month.
- High K^+ (HK) medium: Weigh 825 mg KCl into an autoclaved beaker glass, add 50 mL from a medium bottle with 500 mL MEM. After the KCl has dissolved, sterilize the solution by filtration and transfer it back into the original medium bottle. Add 1 mL of gentamicin (50 mg/mL), store at 4°C for up to 2 months.

CGNs are obtained from cGi transgenic mice at postnatal day 7. Since CGNs are the most abundant neuronal cell type in the cerebellum, this protocol yields a relatively high number of cells and a largely homogeneous culture.

A) PDL-coating of Glass Coverslips

1. Perform coating according to 2.4.5.1A) with 10 μg/mL PDL.

B) Preparation of Solutions

1. On the day of preparation (postnatal day 7), prepare 5×50 mL centrifuge tubes in the tissue culture hood:

   o Tube 1: Add 30 mL 0.3% BSA solution.
   o Tube 2: Add 30 mL 0.3% BSA solution and, shortly before use, 300 μL 2.5% trypsin.
   o Tube 3: Dissolve 7.8 mg trypsin inhibitor in 15 mL 0.3% BSA solution (thorough mixing and warming to 37°C facilitates its dissolution), add 150 μL 3.82% $MgSO_4$ and, shortly before use, 150 μL 1% DNase.
   o Tube 4: Add 17 mL 0.3% BSA solution and 8 mL from tube 3; discard 10 mL, so that 15 mL remain in the tube.
   o Tube 5: Add 12.5 mL 0.3% BSA solution, 100 μL 3.82% $MgSO_4$ and 15 μL 1.2% $CaCl_2$.

2. Distribute part of the remaining 0.3% BSA solution into 10×35 mm culture dishes (3 mL/dish); keep them on ice for preparation of the brains.

C) Preparation of the Cerebellum and CGN Isolation

1. Perform preparation of the brain from 3-5 mouse pups of postnatal day 7 according to 2.4.5.1B), but use 0.3% BSA solution instead of CMF-HBSS for all steps.
2. Remove cerebella from the brains after all brains have been dissected. Remove meninges and blood vessels from the cerebella under high magnification (40×). Transfer the cerebella into a new petri dish with 0.3% BSA solution on ice. Up to this point, the preparation should not take longer than 1 h.
3. In the tissue culture hood, mince the cerebella in a 35 mm petri dish with 0.3% BSA solution using a razorblade until the suspension becomes turbid (~5 min). *A thorough disintegration is critical for a high cell yield.* Transfer the minced tissue into tube 1 using a Pasteur pipette.
4. Centrifuge for 5 min at 1,100 rpm. Remove the supernatant and resuspend the pellet in 30 mL solution from tube 2 (with trypsin). Incubate for 15 min in a 37°C water bath. Invert tube after 5 and 10 min.
5. Using a 25 mL pipette, resuspend the cells and transfer the suspension into tube 4 (with diluted trypsin inhibitor and DNase). Centrifuge for 5 min at 1,100 rpm. Remove the supernatant and resuspend the cell pellet with a 25 mL pipette in 7 mL solution from tube 3 (with trypsin inhibitor and DNase). Resuspend 20 times with a 10 mL pipette and then 10 times with a Pasteur pipette. Add 12 mL solution from tube 5.
6. Pass the cell suspension through a netwell mesh into a new 50 mL tube. Centrifuge for 5 min at 1,100 rpm. Remove the supernatant and resuspend the cell pellet in 5 mL CGN medium. Mix 18 μL of the cell suspension with 2 μL trypan blue and count viable and dead (trypan blue-positive) cells in a cytometer. Calculate the titer of viable cells. The viability should be ≥ 90% and the yield should be ~$4×10^6$ cells per cerebellum. Plate $4×10^5$ cells in 1.0 mL CGN medium per 12-well equipped with a PDL-coated coverslip ($1.1×10^5$ cells/cm²). From 3-5 pups, ~30-50 wells with cells are obtained.
7. Grow the cells at 37°C and 6% CO_2 (Innova-170 CO_2 incubator, New Brunswick Scientific). Imaging experiments are performed starting from day 2 after plating. If cells shall be cultured for more than 4 days, add Ara-C to a final concentration of 5 μM to the medium 24 h after plating. Change medium every 2-3 days according to the efficiency of cell attachment, the amount of cell debris and microglia.

2.4.5.3 Smooth Muscle Cells (SMCs)

- 10 mg/mL Collagenase: Dissolve 100 mg collagenase (Sigma-Aldrich) in 10 mL Ca^{2+}-free medium, store in 0.5 mL aliquots at −20°C.
- 10 mg/mL Hyaluronidase: Dissolve 100 mg hyaluronidase (Sigma-Aldrich) in 10 mL Ca^{2+}-free medium, store in 0.5 mL aliquots at −20°C.
- 100 mg/mL BSA: Dissolve 0.5 g BSA in 5 mL Ca^{2+}-free medium, sterilize by filtration, store in 0.5 mL aliquots at −20°C.
- 100 mg/mL DTT: Dissolve 0.5 g dithiothreitol (DTT) in 5 mL Ca^{2+}-free medium, sterilize by filtration, store in 0.5 mL aliquots at −20°C.
- 7 mg/mL Papain: Dissolve 100 mg papain (Sigma-Aldrich) in 14.29 mL Ca^{2+}-free medium, store in 0.5 mL aliquots at −20°C.

- Ca^{2+}-free medium (pH 7.4): 85 mM Na L-glutamate (15.91 g/L Na L-glutamate×H_2O), 60 mM NaCl (3.51 g/L), 10 mM HEPES (2.38 g/L), 5.6 mM KCl (0.42 g/L), 1 mM $MgCl_2$ (0.20 g/L $MgCl_2$×6 H_2O), adjust pH to 7.4 with HCl, autoclave, store at 4°C.
- Serum-free culture medium: Add 5 mL Pen/Strep to 500 mL DMEM, store at 4°C.
- SMC culture medium: Add 50 mL FBS and 5 mL Pen/Strep to 500 mL DMEM, store at 4°C.
- SMC enzyme solution A (5 mL, *prepare shortly before use*): 4.4 mL Ca^{2+}-free medium, 500 µL papain (final concentration: 0.7 mg/mL), 50 µL DTT (final concentration: 1 mg/mL), 50 µL BSA (final concentration: 1 mg/mL).
- SMC enzyme solution B (5 mL, *prepare shortly before use*): 3.95 mL Ca^{2+}-free medium, 500 µL collagenase (final concentration: 1 mg/mL), 500 µL hyaluronidase (final concentration: 1 mg/mL), 50 µL BSA (final concentration: 1 mg/mL).

SMCs are isolated from aorta (vascular SMCs, VSMCs), bladder (bladder SMCs, BSMCs), and colon (colonic SMCs, CSMCs) of transgenic mice. They are isolated from adult animals, but cell yield and transgene expression can change with increasing age, therefore 3-5 cGi-transgenic mice with ages of 1-3 months are used for SMC isolation.

1. Prepare 3×35 mm and several 100 mm petri dishes with PBS.
2. Sacrifice animals by CO_2 or diethyl ether inhalation. Do not perform cervical dislocation, as the aorta can be disrupted, making its isolation more difficult. Collect tail tips for re-genotyping. Wet fur of the animals with 70% ethanol and open abdominal and thoracic cavity.
3. Collect bladder and colon in a 100 mm petri dish with PBS. In order to isolate the aorta, remove diaphragm, remaining intestines and esophagus as well as liver and spleen. Cut ascending vessels, trachea and esophagus below the pharynx, grab the heart with a forceps and lift it carefully to set the aorta under some tension. Cut along the spine towards the tail. Transfer the excised aorta (still attached to heart and lung) into a 100 mm petri dish with PBS.
4. Under a stereomicroscope (Stemi 2000C), isolate the SM tissue from bladder, colon, and aorta. Remove as much fat as possible, because it interferes with the subsequent isolation steps. To isolate BSMCs, remove surrounding fat and cut the bladder open. Grab the urothelium and peel it off the smooth muscle layer. To isolate CSMCs, remove remaining feces from the colon by washing with PBS using a syringe with bended needle, and transfer it into a new 100 mm petri dish with PBS. Remove remaining mesenteries, fat, and blood vessels. Make a cut at the proximal part of the colon. Starting at this cut, peel off the SM layer from the enteric tissue. Once a small piece of the SM layer has been separated from the enteric tissue, it can easily be peeled off the whole colon. To isolate VSMCs from aorta, carefully remove the heart, thymus, lung, and remainders of the airways and the esophagus. Clean the vessel carefully from blood, fat, and connective tissue by using two fine forceps.
5. Place the dissected SM tissues into 35 mm petri dishes with PBS. Up to this point, the preparation should not take longer than 45 min.
6. Transfer the petri dishes into a tissue culture hood and cut the tissues into ~5 mm pieces using scissors. Transfer the pieces into 15 mL tubes with enzyme solution A (1.5 mL for 3-5 aortae or bladders, 2 mL for 3-5 colons). Incubate for 45 min in a water bath at 37°C; invert every 15 min.
7. Centrifuge at 1,000 rpm for 2 min, discard the supernatant and suspend the tissue fragments in enzyme solution B by gentle shaking; use the same volume as for solution A (see previous step 6).
8. Incubate for 10-15 min in a water bath at 37°C. After ~7 min in enzyme solution B, resuspend the digestion mixture with a 1000 µL pipette. If the tissue pieces occlude the opening of the pipette tip, incubate for another ~3 min. Resuspend 10 times and continue the incubation. After 5 min, resuspend again with a 1000 µL pipette until the majority of tissue pieces disappears and the solution becomes turbid. Even if some tissue pieces remain, stop the digestion after max. 15 min by adding culture medium to a final volume of 10 mL, and resuspend. (Optional step: Pass cells through a Netwell mesh.)
9. Centrifuge at 1,000 rpm for 7 min; discard the supernatant and resuspend the cell pellet containing the SMCs (VSMCs, BSMCs, or CSMCs) in 1.0 mL SMC culture medium. Mix 18 µL of the cell suspension with 2 µL trypan blue and count viable and dead (trypan blue-positive) cells in a cytometer. Calculate the titer of viable cells; the viability should be ≥90% with a yield of ~2×10^5 cells per aorta, bladder, or colon.
10. Adjust the number of cells in SMC culture medium to 6×10^4 VSMCs/mL, 4×10^4 BSMCs/mL, 3×10^4 CSMCs/mL. Plate 1.0 mL of each cell suspension per well into 12-well plates equipped with 20 mm coverslips. This corresponds to a plating density of 1.8×10^4 VSMCs/cm^2, 1.1×10^4 BSMCs/cm^2 and 0.9×10^4 CSMCs/cm^2. From 3-5 mice, the yield is ~10 wells with VSMCs, ~20 wells with BSMCs and ~30 wells with CSMCs.
11. Grow the cells in SMC culture medium at 37°C and 6% CO_2 (Innova-170 CO_2 incubator). Change the medium 3 days after plating. Change the SMC culture medium to serum-free medium when the cells are ~70% confluent (after 4-7 days) and keep the cells for another 24 h in culture before cGMP FRET imaging.

Cultured SMCs attach to the uncoated glass surface and proliferate in presence of FBS. They undergo phenotypic changes, especially when the culture gets confluent or when they are passaged to subcultures (462-464). For that reason, cells cultured under well-defined conditions (sub-confluent primary SMC cultures serum-starved for 24 h) are used for cGMP FRET imaging.

2.4.6 Cell Fixation and Immunofluorescence

- 1% BSA-PBS: Dissolve 1 g BSA in 100 mL PBS.
- 1×GSDB (goat serum dilution buffer): 0.3% Triton X-100 (1.08 mL 10% Triton X-100), 20 mM PB (3.00 mL 240 mM PB pH 7.4), 450 mM NaCl (4.05 mL 4 M NaCl), 27.87 mL H_2O. Add BSA to the required concentrations.
- 10% Triton X-100: 10 mL Triton X-100, 90 mL H_2O.
- 240 mM Na_2HPO_4: 34.07 g/L Na_2HPO_4
- 240 mM NaH_2PO_4: 42.72 g/L NaH_2PO_4.
- 4 M NaCl: 233.8 g/L NaCl.
- Cell fixation solution: 4% sucrose (4 g sucrose/100 mL), 4% formaldehyde (10.8 mL 37% formaldehyde/100 mL), prepare freshly with PBS.
- HS buffer: 20 mM PB (8.32 mL PB pH 7.4), 500 mM NaCl (12.48 mL 4 M NaCl), 79.20 mL H_2O.
- LS buffer: 10 mM PB (4.16 mL pH 7.4), 150 mM NaCl (3.76 mL 4 M NaCl), 92.08 mL H_2O.
- Mounting medium: Shandon ImmuMount (Fisher HealthCare).
- NGS: normal goat serum (NGS; Axxora), store in 1 mL aliquots at 4°C.
- PB pH 7.4: phosphate buffer (PB): Add 240 mM NaH_2PO_4 to 240 mM Na_2HPO_4, until the pH reaches 7.4.

The following protocol is used to perform immunofluorescence antibody staining to detect a single protein or two proteins in a double staining. In case of a double staining, antibodies (two primary antibodies and two secondary antibodies) may not cross-react with each other. To test for cross-reactions possibly leading to artificial signals, a control staining is performed with tissue from non-transgenic or *knock-out* animals (when available), or by omitting one of the two primary antibodies.

1. Fix cells for 25 min in cell fixation solution at 37°C.
2. Wash cells 3×5 min with PBS. Store cells in 1% BSA-PBS at 4°C, or continue with staining.
3. Wash 3×5 min with LS buffer, then 3×5 min with HS buffer.
4. Permeabilize and block for 30 min in 1×GSDB supplemented with 10% BSA and 10% NGS.
5. Incubate with primary antibody (**Table 22**, p. 143) in 1×GSDB supplemented with 3% BSA overnight at 4°C or 2 h at room temperature. (*Keep moist!*)
6. Wash 3×10 min with HS buffer.
7. Incubate for 1 h with secondary antibody (**Table 22**, p. 143) and 1×Hoechst 33258 in 1×GSDB supplemented with 3% BSA at room temperature.
8. Wash 3×5 min with HS buffer. *For double staining continue here, otherwise continue with step 14.*
9. Block for 30 min in 1×GSDB supplemented with 10% BSA and 10% NGS.
10. Incubate with primary antibody (**Table 22**, p. 143) in 1×GSDB supplemented with 3% BSA overnight at 4°C or 2 h at room temperature. (*Keep moist!*)
11. Wash 3×10 min with HS buffer.
12. Incubate for 1 h with secondary antibody (**Table 22**, p. 143) and 1×Hoechst 33258 in 1×GSDB supplemented with 3% BSA at room temperature. (*Keep moist!*)
13. Wash 3×5 min with HS buffer.
14. Wash 3×5 min with LS buffer.
15. Dip the cover slip carefully in distilled water and place it upside down on a glass slide with a drop of mounting medium with the cells facing to the medium. Store in the dark at 4°C.

2.4.7 FRET-based cGMP Imaging

- 100 µM ANP: Dissolve 0.1 mg ANP (1-28, rat; Sigma-Aldrich) in 0.327 mL H_2O, store in 50 µL aliquots at −20°C.
- 100 µM CNP: Dissolve 0.5 mg CNP (Sigma-Aldrich) in 2.275 mL H_2O, store in 50 µL aliquots at −20°C.
- 100 mM cGMP: Dissolve 100 µmol cGMP (BIOLOG Life Science Institute, Bremen, Germany) in 1 mL H_2O, store in 100 µL aliquots at −20 °C.
- 100 mM DEA/NO: Dissolve 50 mg 2-(N,N-diethylamino)-diazenolate-2-oxide diethylammonium salt (DEA/NO, Axxora) in 2.42 mL ice-cold 10 mM NaOH, store in 50 µL aliquots at −20°C.
- 100 mM Glutamate: Dissolve 18.71 g/L L-glutamic acid monosodium salt monohydrate, store in 1 mL aliquots at −20°C.
- 10 mM Norepinephrine: Dissolve 3.4 mg (-)Arterenol (Sigma-Aldrich) and 352 mg ascorbic acid (final concentration: 250 mM) in 2 mL H_2O, store in 10 µL aliquots at −20°C.
- 20 mM ODQ: Dissolve 10 mg 1H-[1,2,4]oxadiazolo[4,3-a]quinoxalin-1-one (ODQ, Axxora) in 2.67 mL DMSO, store in 100 µL aliquots at −20°C.
- 30 mM Sildenafil: Dissolve 50 mg sildenafil citrate (Santa Cruz, Santa Cruz, CA, USA) in 25 mL H_2O, store in 1.5 mL aliquots at −20°C.
- 50 mM Escin: Dissolve 55 mg/mL β-escin (Sigma-Aldrich) in H_2O. Store at −20 °C and protect from light.
- 500 mM IBMX: Dissolve 1.0 g 3-isobutyl-1-methylxanthine (IBMX, Sigma-Aldrich) in 9.0 mL DMSO, store in 1.5 mL aliquots at −20°C.
- High-K^+ imaging buffer (pH 7.4): 115 mM NaCl (6.72 g/L), 30 mM KCl (2.24 g/L), 1.2 mM $MgCl_2$ (0.296 g/L $MgSO_4 \times 7$ H_2O), 2.0 mM $CaCl_2$ (0.222 g/L), 5 mM HEPES (1.19 g/L). Adjust to pH 7.4 with NaOH, autoclave, store at room temperature. Add 10 mL 1 M D-glucose to 1000 mL high-K^+ imaging buffer before use (final concentration ~10 mM D-glucose).
- ICM (pH 7.3): intracellular-like medium (ICM) with 125 mM KCl (9.32 g/L), 19 mM NaCl (1.11 g/L), 1 mM EGTA (0.38 g/L), 10 mM HEPES (2.38 g/L), 0.33 mM $CaCl_2$ (37 mg/L). Adjust the pH to 7.3 with KOH, autoclave, store at room temperature.
- Imaging buffer (pH 7.4): 140 mM NaCl (8.18 g/L), 5 mM KCl (0.373 g/L), 1.2 mM $MgCl_2$ (0.296 g/L $MgSO_4 \times 7$ H_2O), 2.0 mM $CaCl_2$ (0.222 g/L), 5 mM HEPES (1.19 g/L). Adjust to pH 7.4 with NaOH, autoclave, store at room temperature. Add 10 mL 1 M D-glucose to 1000 mL imaging buffer before use (final concentration ~10 mM D-glucose).

2.4.7.1 Imaging of Cells and Tissue Samples

FRET-based cGMP measurements of cGi-expressing cells or tissue samples is performed by ratiometric epifluorescence microscopy under continuous superfusion with imaging buffer (**Figure 11**). The imaging platform is based on an inverted Axiovert 200 microscope with 1.0/1.6× Optovar lens (Carl Zeiss) that is equipped with fluorescence-grade objectives (Plan NeoFluar 10×/0.30; EC Plan NeoFluar 40×/1.30 Oil, Carl Zeiss). A computer-controlled light source with electronic shutter (Oligochrome, TILL Photonics, Gräfeling, Germany) is equipped with a 445/20 nm CFP excitation filter (AHF, Tübingen, Germany) and combined with a 470 nm dichroic mirror (AHF) in the microscope. The beam splitter (Micro-Imager DUAL-View, Photometrics, Tucson, AZ, USA) with 05-EM insert (516 nm dichroic mirror, 480/50 nm and 535/40 nm emission filters) is used to separate CFP and YFP signals that are recorded with a cooled electron-multiplying charged-coupled device (EM-CCD) camera (Retiga 2000R, QImaging, Surrey, BC, Canada). Additionally, an YFP filter set with 497/16 nm excitation filter, 516 nm dichroic mirror and 535/22 nm emission filter (AHF) is used to examine cell and tissue samples by eye and to record EYFP fluorescence images without beam splitter.

To superfuse the cells with imaging buffer and to apply cGMP-elevating or other drugs, a custom-built superfusion system is used (**Figure 11A**). It consists of a FPLC pump (Pharmacia P-500, GE Healthcare), FPLC injection valves (Pharmacia V-7, GE Healthcare), a self-made superfusion chamber (**Figure 11B**), a vacuum pump with adjustable vacuum (Laboport N86, KNF Neuberger, Freiburg, Germany), and sample loops with different sizes (2, 7, 20 mL). This setup provides stable and precise superfusion of the cells with imaging buffer and test compounds.

1. Cyclic GMP imaging is performed in an air-conditioned dark room at ~21°C.
2. Check the beam splitter for alignment of F_{480} and F_{535} channels every time before starting a FRET imaging session.
3. Install sample loops of appropriate volumes at the injection valves, e.g. a 2 mL loop for 2 min superfusion and a 20 mL loop for 20 min superfusion at 1 mL/min. Connect the imaging buffer reservoir (1 L) to the FPLC pump and flush the superfusion system including the sample loops with imaging buffer for 10 min at 5 mL/min (**Figure 11A**).
4. Place a coverslip with cGi-expressing cells in a 35 mm culture dish filled with imaging buffer.
5. Assemble the superfusion chamber. Place silicon grease on the chamber frame and the chamber plate to seal it (**Figure 11B**). Mount the coverslip with the cells facing to the inside of the chamber. Place the chamber plate on top of the coverslip, add 200 μL imaging buffer to cover the cells, and finish the chamber assembly. *Take care that the chamber is not leaky!*
6. Clean the glass coverslip on the outside and fix the chamber on the microscope stage.
7. Place inlet and outlet needles into the superfusion chamber and start the superfusion with imaging buffer at 1 mL/min. Adjust the vacuum and the level of the outlet needle so that steady superfusion of the cells is obtained.
8. By using the YFP filter set, identify a field of view (FOV) with fluorescent cells of appropriate brightness. Dim cells with signal-to-background ratios ≤2.5 should not be used as well as extremely bright cells, in which strong sensor expression could interfere with cell functions. Check also for cell morphology and sensor localization; the sensor should be homogeneously distributed in the cytosol without localized depositions ('bright spots'). Re-adjust the inlet and outlet needles if their positions have changed during the setup of the system.
9. Acquire a still image of the fluorescent cells. Select regions of interests (ROIs) to be imaged as well as a background (bg) region without fluorescent cells.
10. Adjust the camera settings (pixel binning, gain), exposure time and acquisition cycle interval (the time from the beginning of one acquisition to the beginning of the next acquisition). Ensure that the hardware settings are correct (FRET filter cube with CFP excitation filter, 470 nm dichroic mirror, light path through the beam splitter to the camera) and start the experiment.
11. Record images during superfusion with imaging buffer at 1 mL/min until a stable baseline is obtained.
12. Dilute test compounds in imaging buffer to their final concentrations. Typical final concentrations are: DEA/NO; 20-500 nM; ANP and CNP, 10-250 nM; IBMX, 100-500 μM; sildenafil, 10-30 μM; ODQ, 1-10 μM. To account for dead volumes of the superfusion system (tubing, syringes), the volume of a drug solution should be ~25% larger than the volume of the sample loop. With syringes, load the compounds via the injection valves into the respective sample loops (**Figure 11A**).
13. Apply the test compounds at 1 mL/min via valve switching and note down the time when the drugs are applied. To terminate the superfusion of a compound before the sample loop has been completely flushed, switch the valve back to the loading position and note down the time. Flush the sample loops with imaging buffer before loading the next drug solution.
14. Upon drug application, follow F_{480}/F_{535} ratio changes as well as changes in the individual ECFP and EYFP channels to recognize potential artificial F_{480}/F_{535} ratio changes.
15. After the imaging session, flush the complete superfusion system including injection valves, sample loops and all connective tubing with H_2O and then with 20% ethanol. Store the system in 20% ethanol. If necessary, clean the outlet needle from aspirated silicon grease.
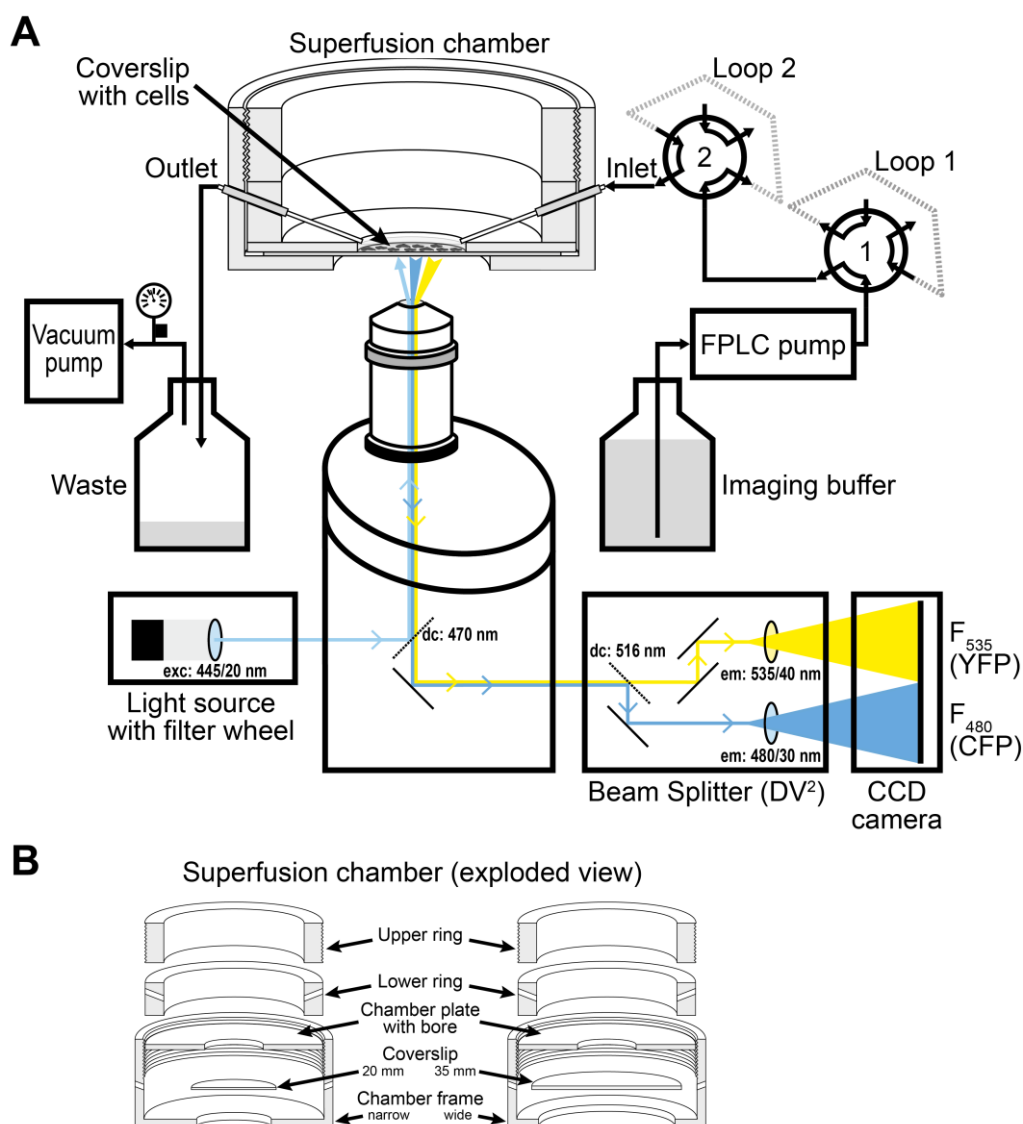
Figure 11. Imaging system for cGMP FRET measurements.

A. The sample is illuminated with light through an excitation (exc) filter and a dichroic mirror (dc). Emitted light reaches the camera through a beam splitter, where a dichroic mirror splits CFP and YFP signals. The same microscopic field of view illuminates the two halves of the camera chip, so that both emission intensities are recorded at the same time. Cells are continuously supplied with imaging buffer by a FPLC pump through two injection valves (1, 2). Cells are attached to a glass coverslip that serves as bottom of the superfusion chamber. The 'chamber plate' is placed on top of the coverslip and defines the geometry of the superfusion chamber (for details on chamber assembly, see panel B). The buffer is continuously removed from the chamber via suction by an adjustable vacuum pump. Drug solutions are loaded into sample loops (loop 1, loop 2) that are attached to the injection valves. By changing the valve position, the drug solution is delivered to the cells. Two valves connected in series are used to apply different drugs simultaneously (e.g. a PDE inhibitor from loop 1 followed by NO donors together with the same PDE inhibitor from loop 2). Valve settings shown in the figure would lead to drug application from loop 2, but not from loop 1. **B.** Exploded view on a cross-section of the superfusion chamber. Variants with a narrow (left) or wide (right) opening of the chamber frame are shown, which accommodate either 20 mm or 35 mm coverslips. The coverslips serve as bottom of the chamber. The 'chamber plate' with its central oval-shaped bore (5 mm×14 mm or 8 mm×20 mm) is placed on top of the coverslip. It defines the superfusion chamber and its maximal volume. Each type of chamber plate is used with both 20 mm and 35 mm coverslips. The upper ring is screwed into the metal frame and tightens the chamber assembly. The inlet and outlet needles are directed through bores in the lower ring and the chamber frame until they approach the borders of the chamber plate openings (see also panel A); fine-adjustment of the outlet needle is used to regulate the liquid level during superfusion.

2.4.7.2 Intravital Imaging of the Cremaster Muscle

- 1 mM ACh: Dissolve 1.2 mg acetylcholine chloride (ACh) in 10 mL H_2O.
- 1 mM Ado: Dissolve 2.67 mg adenosine (Ado) in 10 mL H_2O.
- 1 mM SNP: Dissolve 2.98 mg sodium nitroprusside dihydrate (SNP) in 10 mL H_2O, store in the dark.
- BBSS: bicarbonate-buffered saline solution pH 7.4 with (in mM): Na^+ 143, K^+ 6, Ca^{2+} 2.5, Mg^{2+} 1.2, Cl^- 128, HCO_3^- 25, SO_4^{2-} 1.2 and $H_2PO_4^-$ 1.2, gassed with 5% CO_2 and 95% N_2 (pCO_2 ~40 mm Hg, pO_2 ~30 mm Hg).

Preparation of the mice for cremaster muscle intravital microscopy was performed by Prof. C. de Wit and K. Schmidt (Universität Lübeck) as previously described (465). The imaging setup for intravital imaging experiments is composed of an upright Axioskop 2 FS microscope (Carl Zeiss) with water immersion objectives (Achroplan 10×/0.30w or 40×/1.75w, Carl Zeiss), a Polychrome V light source (TILL Photonics) set to 420 nm, an Andor iXon 885 EM-CCD camera (Andor Technology, Belfast, Northern Ireland), and a beam splitter (DualView, Photometrics). Dichroic mirrors and filters (except for the excitation filter) are similar to the setup described for *in vitro* experiments (2.4.7.1). The cremaster muscle is superfused with 8 mL/min BBSS at 34°C; flow is gravity-driven and regulated with valves. Drug solutions are applied into the BBSS superfusate with 80 µL/min, so that they get diluted 1:100 to their final concentration before they reach the tissue.

2.4.7.3 Fura-2-based Ca^{2+} imaging

- Fura-2/AM: 1 mM fura-2/AM (VWR International GmbH, Darmstadt, Germany) in DMSO, store in 10 µL aliquots at −20°C.

For fura-2-based Ca^{2+} imaging, cells are incubated for 30 min with 1 µM cell-permeable fura-2/AM in imaging buffer. Imaging setup and superfusion chamber are identical to the FRET imaging setup described before (2.4.7.1). To detect changes in intracellular Ca^{2+} concentrations, fura-2 is excited at 340 and 380 nm, and emission is recorded at 510 nm using alternating excitation with two excitation filters (340/26 nm and 387/11 nm), a 410 nm dichroic mirror, and a 440 nm long-pass emission filter. Image analysis is performed as described for FRET measurements (2.4.7.4) to obtain $\Delta R/R$ (F_{340}/F_{380}), $\Delta F_{340}/F_{340}$ and $\Delta F_{380}/F_{380}$ values.

2.4.7.4 Image Analysis and Quantification

For image acquisition and online analysis, Live acquisition (TILL Photonics) is used, and for offline image analysis either arivis Browser (arivis GmbH, Berlin, Germany) or ImageJ (NIH, Bethesda, MD, USA). Data analysis is performed with Microsoft Excel (Microsoft, Redmond, WA, USA) and Origin (OriginLab Corp., Northampton, MA, USA).

Table 5. Calculation of the background-corrected and baseline-normalized F_{480}/F_{535} (CFP/YFP) ratio $\Delta R/R$.

From time-lapse recordings of CFP and YFP emission intensities at 480 nm and 535 nm in a fluorescent ROI and a non-fluorescent background region (bg), the background-corrected F_{480}/F_{535} ratio 'R(t)' is calculated. The index '(t)' indicates the time dependency of parameters. For baseline normalization, n ratio values obtained from t_0 to t_1 during the baseline period (e.g. from the start of the experiment to the first drug application) are averaged, leading to R_0. With R_0, ratio changes are normalized to the baseline and denoted as $\Delta R/R$. Background correction and baseline-normalization is also directly applied to F_{480} and F_{535} emission intensities leading to $\Delta F/F$ values (not shown).

Measured parameters		
	F_{480} (CFP channel)	**F_{535} (YFP channel)**
ROI	$F_{480,ROI}(t)$	$F_{535,ROI}(t)$
Background	$F_{480,bg}(t)$	$F_{535,bg}(t)$
Calculated parameters		
	F_{480}/F_{535} ratio	
Background correction	$R(t) = \dfrac{F_{480,ROI}(t) - F_{480,bg}(t)}{F_{535,ROI}(t) - F_{535,bg}(t)}$	
Baseline normalization	$R_0 = \dfrac{1}{n}\sum\limits_{t_0}^{t_1} R(t)$	
Signal change relative to baseline	$\dfrac{\Delta R}{R} = \dfrac{R(t) - R_0}{R_0} x100\%$	

1. Recheck and correct (if necessary) ROIs selected at the beginning of the experiment for sample movement or focus drift.
2. Subtract F_{480} and F_{535} signals of a (non-fluorescent) background region (bg) from F_{480} and F_{535} signals of the (fluorescent) regions of interests, and calculate the (background-corrected) F_{480}/F_{535} ratio R using the 'Ratio (integrating)' algorithm of the arivis software. Average F_{480} and F_{535} emission intensities and F_{480}/F_{535} ratio values from the baseline period; use them for normalization according to **Table 5** to obtain baseline-corrected $\Delta F_{480}/F_{480}$, $\Delta F_{535}/F_{535}$, and $\Delta R/R$ values.
3. Examine single cell traces to exclude artifacts and check for the presence of antiparallel F_{480} and F_{535} changes upon stimulation of the cells with cGMP-elevating drugs. Exclude traces showing artifacts or insufficient signal-to-noise ratios from subsequent evaluation steps. For graphical presentation of mean±SEM traces, average single cells traces of $\Delta F_{480}/F_{480}$, $\Delta F_{535}/F_{535}$, or $\Delta R/R$ values.
4. To estimate peak areas from $\Delta R/R$ traces, use the Peak Analyzer Module of Origin 8.6: first, correct single cell traces for baseline drifts by subtracting a linear baseline. Define peaks and determine peak areas (keep peak borders constant for all cells in a single experiment). For data presentation, average peak areas (mean±SEM of n cells).
5. For the quantification of a dose-response relationship, use a dose-response function to describe the correlation between log(c[drug]) and the averaged peak area of the $\Delta R/R$ traces as shown in 6). Estimate the parameters A_{min}, A_{max}, $\log(EC_{50})$ and the Hill constant h. For normalization of the dose-response curve between experiments, divide the averaged peak area by A_{max}, and calculate error bars from [*err*(area)+*err*(A_{max})]/A_{max}. To compare dose-response relationships obtained in different experiments, a two-tailed student's t-test is performed. For studies with repeated stimulation of the same sample, a ranked ANOVA with repeated measurements is performed in SigmaPlot 11 (Systat Software, Inc., Chicago, IL, USA) with Tukey's post-hoc test to compare single stimulations. P values <0.05 are considered to be significant.

6. For the calibration of cGMP FRET sensors, draw a calibration curve with log[cGMP] vs. $\Delta R/R$ and perform a nonlinear regression analysis with a dose-response function:

$$\left(\frac{\Delta R}{R}\right) = \left(\frac{\Delta R}{R}\right)_{min} + \frac{\left(\frac{\Delta R}{R}\right)_{max} - \left(\frac{\Delta R}{R}\right)_{min}}{1 + 10^{(logEC_{50} - log[cGMP])h}}$$

to estimate $log(EC_{50})$, $(\Delta R/R)_{min}$, $(\Delta R/R)_{max}$ and the Hill constant h. To estimate unknown cGMP concentrations from $\Delta R/R$ values measured in native cells, the dose-response function is solved for [cGMP] using EC_{50}, $(\Delta R/R)_{min}$, $(\Delta R/R)_{max}$ and h obtained from the calibration:

$$[cGMP] = EC_{50} \left(\frac{\left(\frac{\Delta R}{R}\right)_{max} - \left(\frac{\Delta R}{R}\right)_{min}}{\left(\frac{\Delta R}{R}\right) \cdot \left(\frac{\Delta R}{R}\right)_{min}} - 1 \right)^{\frac{1}{h}}$$

cGMP concentrations are estimated from the 'linear' part of the calibration curve, for example between ~100 nM and ~3 μM cGMP for cGi-500.

2.4.8 PET Imaging of *HSV1*-sr39tk expression

[^{18}F]FHBG synthesis was performed by the chemists of the Department of Preclinical Imaging and Radiopharmacy according to standard procedures for radiotracer production as previously described (161).

2.4.8.1 PET and MRI

PET imaging with [^{18}F]FHBG was performed in the Laboratory for Preclinical Imaging and Imaging Technology according to ref. 224 with a dedicated small animal PET scanner (Inveon, Siemens Healthcare, Knoxville, TN, USA; performance evaluation in ref. 466) and a 7 Tesla MR scanner (ClinScan, Bruker BioSpin MRI, Ettlingen, Germany).

2.4.8.2 Tracer Uptake Studies with Cultured Cells

- Protein lysis buffer: 2% SDS (100 mL/L 20% SDS), 50 mM Tris-Cl pH 8.0 (50 mL/L 1 M Tris-Cl pH 8.0), 5 mM EDTA (10 mL/L 0.5 M EDTA pH 8.0), 100 mM NaCl (20 mL/L 5 M NaCl).

ESCs are incubated in 6-wells with 3 mL full culture medium containing 25 μCi/mL (925 kBq/mL) [^{18}F]FHBG. After 1, 2, 3 or 4 h (with 3 replicates per time point), supernatants are removed and cells are washed twice with 1 mL PBS (medium and wash PBS represent extracellular fraction). Cells are lysed with 1 mL protein lysis buffer, cell lysates are collected, and wells are washed twice with 2 mL PBS (lysates and wash PBS represent intracellular fraction). Radioactivity is measured in a γ counter (Wallac 1470 WIZARD, Perkin Elmer, Turku, Finland) and uptake is calculated as ratio of intracellular fraction to total radioactivity. Uptake of *HSV1*-sr39tk-expressing cells is normalized to the uptake of *HSV1*-sr39tk-negative cells. If cell cultures are compared that contain non-equal cell numbers, cell lysates are used for protein quantification to normalize [^{18}F]FHBG uptake to protein content.

3   Results

3.1   Cell Tracking with PET

One of the most commonly used reporter gene to label cells for their detection with PET is the sr39tk variant of the *HSV1* thymidine kinase enzyme. Although it was used in several studies, no conditional *HSV1*-sr39tk transgenic mouse line was generated yet, which allows for modular and inducible cell labeling. A strategy based on the Cre/loxP system was developed to generate such a mouse line, in which *HSV1*-sr39tk expression is induced by Cre recombination in a specific tissue (**Figure 12**).
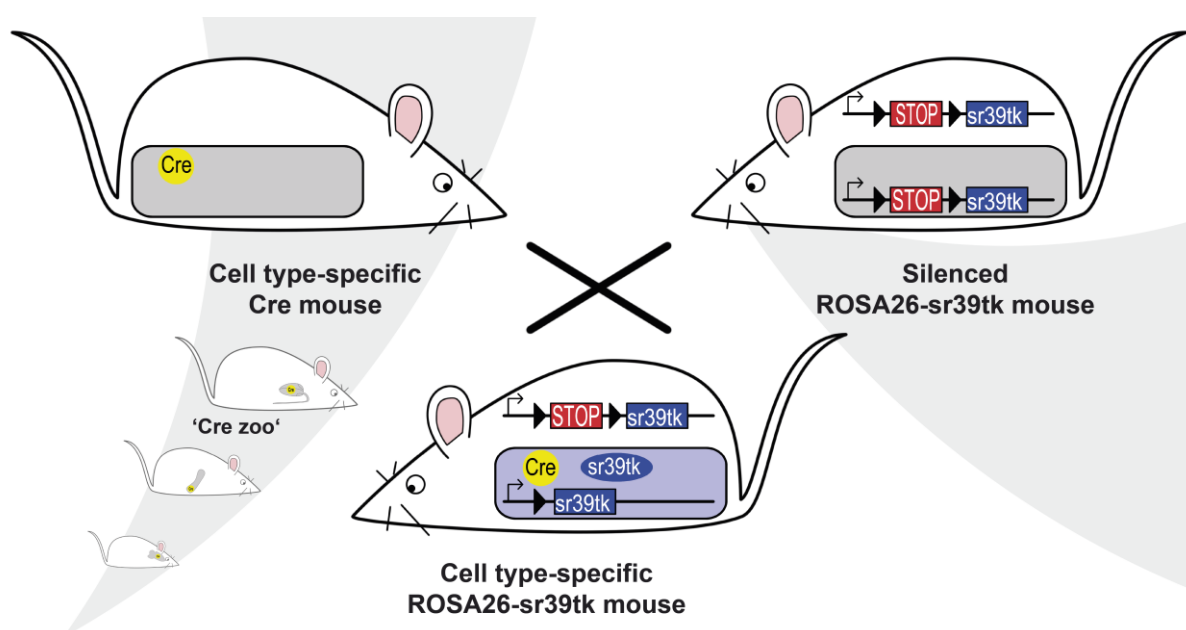

Figure 12. Strategy for the generation of tissue-specific *HSV1*-sr39tk reporter mice.

To generate mice that express the *HSV1*-sr39tk PET reporter gene in a tissue-specific manner, mice carrying a transgene for tissue-specific Cre expression are mated to mice carrying a silenced, Cre-inducible *HSV1*-sr39tk gene cassette in the ROSA26 locus (loxP sites are indicated by black triangles). The ROSA26 locus allows for ubiquitous *HSV1*-sr39tk expression, but its expression must be induced by tissue-specific activation of the transgene via Cre recombination. In animals that carry both transgenes, Cre recombines the ROSA26-sr39tk transgene leading to the removal of the loxP-flanked STOP cassette that inhibits *HSV1*-sr39tk expression.

Two different strategies were used to generate ROSA26-sr39tk mouse lines by introducing silenced *HSV1*-sr39tk transgenes into the ROSA26 locus via homologous recombination. The first transgene (ROSA26-sr39tk, **Figure 13A**) does not carry its own promoter. After Cre-mediated removal of the STOP cassette, *HSV1*-sr39tk expression is driven by the endogenous ROSA26 promoter. The STOP cassette is made of a loxP-flanked Neo^R gene cassette used to select for targeted ESCs.
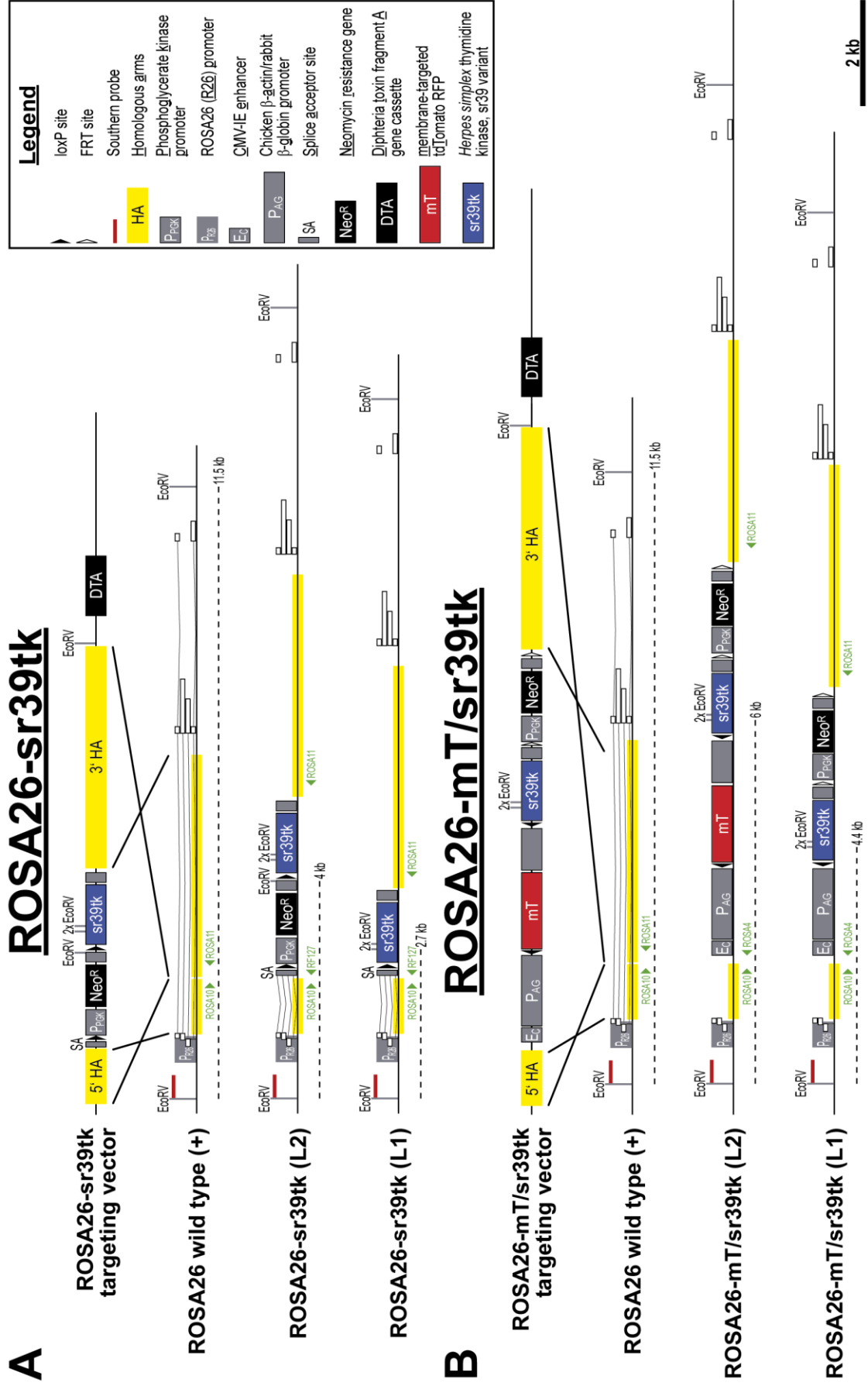
Figure 13 (left). ROSA26 gene targeting strategies to generate *HSV1-sr39tk* reporter mouse lines.

A. Targeting leads to integration of the ROSA26-sr39tk transgene into the first intron of the ROSA26 locus. Successfully targeted ESCs carry the silenced ROSA26-sr39tk transgene (L2 allele). Cre recombination leads to removal of the Neo^R gene cassette and activation of *HSV1*-sr39tk expression (L1 allele). *HSV1*-sr39tk expression is driven by the endogenous ROSA26 promoter. Therefore, a splice acceptor (SA) site in front of the transgene leads to splicing from exon 1 of the ROSA26 gene into the transgene (for details, see **Table 6**). **B.** Also the ROSA26-mT/sr39tk transgene is introduced into the first intron of the ROSA26 locus. From the L2 allele of the ROSA26-mT/sr39tk transgene, mT is expressed. Cre recombination leads to removal of the mT CDS, which leads to *HSV1*-sr39tk expression from the L1 allele. Expression of mT and *HSV1*-sr39tk is driven by the CAG promoter, which is part of the transgene; therefore, no SA site is necessary. EcoRV restriction fragments used for Southern blot analysis with a 5' probe are shown as dashed lines, binding sites for primers in genotyping PCRs are indicated in green. For further details on the wild type ROSA26 gene, see also **Figure 14A**.

In the second transgene (ROSA26-mT/sr39tk, **Figure 13B**), a CAG promoter drives *HSV1*-sr39tk expression after removal of the STOP cassette. Here, the STOP cassette carries the coding sequence (CDS) for the membrane-targeted RFP tandem-dimer tomato (mT), which is expressed until Cre recombination. The Neo^R gene cassette to select for targeted ESCs is placed at the 3' end of the transgene, and can be removed by Flp-mediated recombination, if desired.

3.1.1   Generation of *HSV1*-sr39tk Reporter ESC Lines

To produce *HSV1*-sr39tk reporter ESC lines, targeting vectors were generated to introduce the ROSA26-sr39tk or ROSA26-mT/sr39tk transgene into the wild type ROSA26 locus. In the promoter-less ROSA26-sr39tk transgene, the endogenous ROSA26 promoter drives *HSV1*-sr39tk expression after Cre-mediated removal of the STOP cassette. Thus, mRNA needs to start within the ROSA26 promoter and needs to be spliced into the transgene. This is achieved by placing a splice acceptor (SA) site at the 5' part of the transgene. Review of wild type ROSA26 transcript sequences and published ROSA26 reporter transgenes with a similar design as the ROSA26-sr39tk transgene raised some questions about the exact transcript sequence. Especially the location of the first start codon (AUG/ATG), which serves as translational start point, was uncertain. The first exon of the ROSA26 gene as well as the remaining loxP site, which resides between SA site and reporter gene CDS carry potential start and stop codons. To verify the transcript structure of a ROSA26 Cre reporter transgene with proven functionality, a RT-PCR-based analysis was performed with RNA isolated from mice carrying the ROSA26-lacZ transgene (64). Results from this analysis were included in the design of the ROSA26-sr39tk targeting vector. For the ROSA26-mT/sr39tk construct, the CAG promoter drives *HSV1*-sr39tk expression, and the transcript sequence is therefore predictable: the first start codon of the transcript is the start codon of the *HSV1*-sr39tk CDS, and serves as translational start point. Both targeting vectors carry diphtheria toxin A (DTA) gene cassettes to select against ESCs with random integrations of the targeting vectors.

3.1.1.1 Characterization of the Cre-recombined ROSA26-lacZ Transgene by RT-PCR

To acquire detailed insight into transcript sequences of a ROSA26 Cre reporter transgene, analysis of RNA isolated from mice expressing Cre and the ROSA26-lacZ reporter was performed. When the ROSA26 locus was analyzed upon its identification in the group of P. Soriano, a short open reading frame (ORF) of 15 amino acids (aa) was found in exon 1 of the ROSA26 gene (61). This short ORF probably precedes the lacZ CDS, as the ROSA26-lacZ transgene starts with a SA site that leads to splicing from ROSA26 exon 1 into the transgene. If so, the first start codon in the transcript, if it is derived from exon 1, should not be able to initiate lacZ translation. To analyze, if this or other transcripts can lead to lacZ expression in the ROSA26-lacZ reporter, RNA for RT-PCR analysis was isolated from urinary bladders of tamoxifen-treated SMKI-CreER$^{T2,+/-}$; ROSA26-lacZ$^{+/-}$, SMKI-CreER$^{T2,+/+}$; ROSA26-lacZ$^{+/-}$, and wild type mice (provided by Dr. S. Feil). The proposed gene and transcript structures are shown in **Figure 14**.
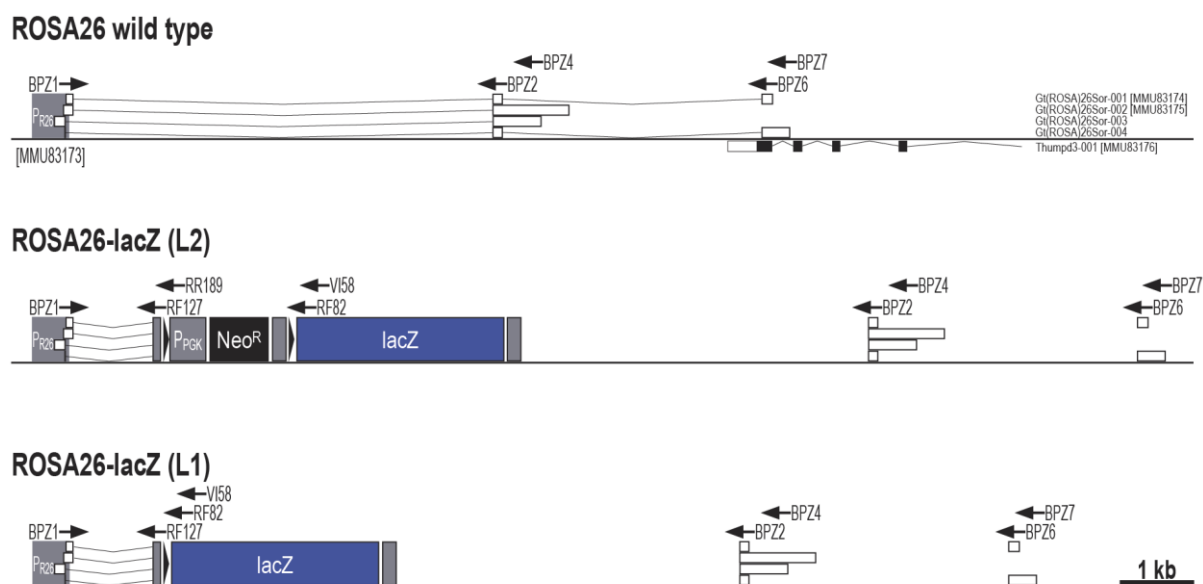
Figure 14. Schematic structures of the wild type ROSA26 gene, and the ROSA26-lacZ Cre reporter gene before (L2) and after (L1) Cre recombination.

From the wild type ROSA26 locus, four non-coding RNA species are transcribed (Gt(ROSA)26Sor-001 to -004); expression is driven by the ROSA26 promoter ('P$_{R26}$'; MMU83173, ref. 61). The transcripts MMU83174 and MMU83175 were described in ref. 61 together with MMU83176 from the protein-coding gene Thumpd3 that partially overlaps with the ROSA26 gene. In the ROSA26-lacZ reporter, RNA is spliced from the ROSA26 exon 1 to the SA site at the beginning of the reporter transgene. After Cre-mediated excision of the loxP-flanked Neo^R cassette, lacZ is expressed from the promoter-less transgene by the endogenous ROSA26 promoter. Protein-coding exons are indicated by closed rectangles, non-coding exons by open rectangles, and regulatory elements (SA site, promoter, polyadenylation signal) by gray rectangles. Primers for RT-PCR-based characterization of the ROSA26-lacZ reporter transgene and primers used during the initial characterization of the ROSA26 locus (BPZ1, 2, 4, 6; ref. 61) are indicated. For primer sequences, refer to **Table 19** on p. 141.

RT-PCR with RNA isolated from SMKI-CreER$^{T2,+/-}$; ROSA26-lacZ$^{+/-}$ mice yields products with BPZ1/RF127 (<200 bp), BPZ1/RF82 (~390 bp) and BPZ1/VI58 (~410 bp), which were not present in reactions with RNA from wild type or SMKI-CreER$^{T2,+/+}$; ROSA26-lacZ$^{+/-}$ mice (**Figure 15**). These results show that a transcript carrying the lacZ CDS was isolated from SMKI-CreER$^{T2,+/-}$; ROSA26-lacZ$^{+/-}$ mice, which is spliced from the endogenous ROSA26 exon 1 to the transgene's SA site as proposed in **Figure 14**. The 3' end of BPZ1 used as forward primer in the RT-PCR binds to the part of exon 1 carrying the start codon (see **Table 12**, p. 135). This indicates that exon 1 including its short ORF is a part of the transcript possibly leading to lacZ expression. But it cannot be excluded that other transcripts exist, which do not include the ORF-containing part of exon 1, for example when splicing similar to wild type Gt(ROSA)26Sor-003 and -004 transcripts occurs. These transcripts were not amplified in the RT-PCR reaction, as they do not bind the BPZ1 primer (see **Table 12**, p. 135).
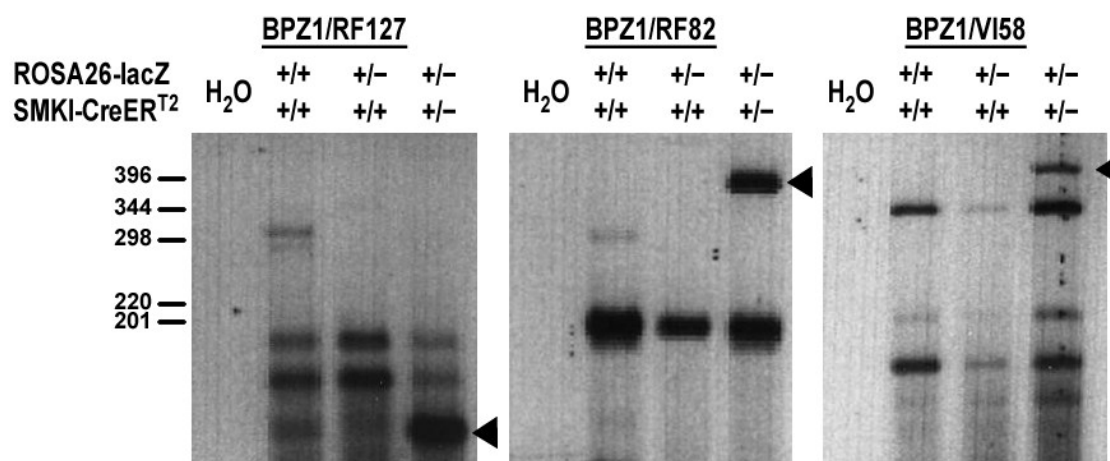
Figure 15. RT-PCR analysis of the Cre-recombined ROSA26-lacZ transgene.

Amplification was performed with primers as indicated in a RT-PCR reaction directly followed by the PCR reaction (35 cycles, T_a=58°C). Triangles point to PCR products purified for sequence analysis with BPZ1.

RT-PCR products obtained with RNA from SMKI-CreER$^{T2,+/-}$; ROSA26-lacZ$^{+/-}$ mice were purified via gel electrophoresis and electroelution, and then their sequence was determined. The proposed transcript structure was confirmed, and the sequence of the transgene's 5' part was determined (yellow highlight in **Table 12**, p. 135). Sequencing results show that additionally to the short ORF (16 aa) in exon 1 (partially covered by the sequence analysis) two other short ORFs (7 and 19 aa) precede the lacZ CDS, either in-frame or out-of-frame with the lacZ CDS. The analyzed transcript carries two start codons in exon 1 and inside loxP, which are in-frame with the lacZ CDS, but the ORFs are interrupted by three stop codons in exon 1, inside and behind the loxP site. Additionally, another out-of-frame ORF is present between the loxP site and the lacZ CDS (**Table 12**, p. 135).

3.1.1.2 Generation of the ROSA26-sr39tk Targeting Vector

With results of the ROSA26-lacZ transcript analysis at hand, the following requirements for the ROSA26-sr39tk targeting vector were defined (see also **Table 6**).

- The *HSV1*-sr39tk CDS is in-frame with the start codon in ROSA26 exon 1.
- Behind SA site and in front of the first loxP site, a start codon is placed in frame with the start codon in ROSA26 exon 1 and in context of a Kozak initiation sequence ('Kozak-ATG') leading to an uninterrupted ORF containing the *HSV1*-sr39tk CDS. The loxP site does not interrupt the ORF defined by ROSA26 exon 1 and Kozak-ATG.
- Inhibition of *HSV1*-sr39tk expression before Cre recombination is also caused by a stop codon inside the P_{PGK}-Neo^R cassette in-frame with the ORF defined by ROSA26 exon 1 and Kozak-ATG.
- The 42 additional N-terminal amino acids preceding the *HSV1*-sr39tk CDS upon expression from ROSA26-sr39tk do not interfere with *HSV1*-sr39tk protein stability or function.

In comparison to the ROSA26-lacZ transcript (see **Table 12**), only one start codon (Kozak-ATG) in-frame with the ROSA26 exon 1 start codon is present in the ROSA26-sr39tk transgene. No stop codons besides the stop codon in ROSA26 exon 1 should be able to interfere with *HSV1*-sr39tk translation (**Table 6**). Two out-of-frame ORFs (9 and 10 aa) are present in the transgene, but they follow the Kozak-ATG and should therefore not affect *HSV1*-sr39tk translation.

Table 6. Putative ROSA26-sr39tk reporter transcript after Cre recombination.

Transcript structure was assembled from published sequences of the ROSA26 gene (not the full-length ROSA26 exon 1 is shown), and from sequences used for cloning of the ROSA26-sr39tk reporter. '[' and ']' indicate exon borders, '*' and '#' start and stop codons, '<' and '>' primer 3' ends; the 5' part of the *HSV1*-sr39tk CDS is marked in red.

```
----BPZ1-- --- --- >
                *
tgcgtttgcg ggg ATG GGC GGC CGC GGC AGG CCC TCC GAG CGT GGT GGA


           001/002 E1] [ROSA26-sr39tk transgene
             #                                           001: Gt(ROSA26)Sor-001
GCC GTT CTG TGA gacagccgg ctcgcggttga ggacaaactc ttcgcggtct   002: Gt(ROSA26)Sor-002
                    <----- ---RF127-- ------
                               ••• ••• ••• loxP•*•
       M   E   L   E   G   G   R   S   S   I   T   S   Y
ttgccacc ATG GAG CTA GAA GGC GGC CGC TCT ATA ACT TCG TAT AAT    Kozak ATG

••* ••• ••• ••• ••• ••• •        #   #   #
 N   V   C   Y   T   K   L   S   R   V   V   D   R   D   L   R
GTA TGC TAT ACG AAG TTA TCC AGT CGG GTA GTA GAT AGA GAT CTG CGG

              #
 P   L   S   S   L   I   N   G   S   M   L   A   T   M   A   Y
CCG CTA AGC TCC TTA ATT AAC GGA TCC ATG CTA GCC ACC ATG GCT TCG    sr39tk


  S   P   G   H   Q   H   A   S   A
TAC CCC GGC CAT CAA CAC GCG TCT GCG
```

The steps summarized in **Table 7** led to the ROSA26-sr39tk targeting vector possessing the aforementioned features (a detailed description on the construction is given in 6.2 on p. 136). Cloning products were verified using analytical restriction digests and sequence analysis (with primers as indicated in **Table 7**).

Table 7. Generation of the ROSA26-sr39tk targeting vector.

Antibiotic resistance genes and other genetic elements not touched by the cloning procedure are not shown. Parental plasmid backbones are indicated on the right. Primers used for sequence analysis are marked in green. For further details on the cloning procedure, see 6.2 on p. 136.

1.	**SA site PCR**	
	Amplification of the SA site from pROSA26-ILD-P/F introducing XbaI and NheI restriction sites and a Kozak-ATG.	
2.	**pCR-Blunt-II-TOPO-SA**	
	TOPO cloning of the amplified SA site into pCR-Blunt-II-TOPO.	
3.	**pSA**	
	Transfer of the SA site from pCR-Blunt-II-TOPO-SA into pUC19 using XbaI.	
4.	**pSA-LNL**	
	Insertion of the loxP-flanked Neo^R gene cassette (LNL) excised with XbaI/HindIII from pCMV-LNL-lacZ into NheI/HindIII-digested pSA.	
5.	**pSA-LNL-ER-pA**	
	Transfer of SA-LNL into pCreER(GR)L using NdeI/HindIII.	
6.	**pSA-LNL-ER-pA-EcoRI^0**	
	Digestion of pSA-LNL-ER-pA with KpnI/NdeI, re-ligation after fill-in to remove EcoRI site 5' to the SA site.	
7.	**pSA-LNL-Linker-pA**	
	Exchange of the ER fragment in pSA-LNL-ER-pA-EcoRI^0 with an oligonucleotide linker carrying PacI and FseI restriction sites via HindIII/EcoRI.	
8.	**pLinker1**	
	Insertion of an oligonucleotide linker carrying PacI, BamHI, NheI, EcoRI, and FseI restriction sites into EcoRI/HindIII-digested pUC19.	
9.	**pPacI-sr39tk-FseI**	
	Transfer of *HSV1*-sr39tk from pCMV-sr39tk into pLinker1 using NheI/EcoRI.	
10.	**pSA-LNL-sr39tk-pA**	
	Transfer of *HSV1*-sr39tk from pPacI-sr39tk-FseI into pSA-LNL-Linker-pA using PacI/FseI.	
11.	**pROSA26-sr39tk (= pROSA-SA-LNL-sr39tk-pA)**	
	Transfer of SA-LNL-sr39tk-pA from pSA-LNL-sr39tk-pA into pROSA26.2 with XbaI.	

3.1.1.3 Generation of the ROSA26-mT/sr39tk targeting vector

The strategy for generation of the ROSA26-mT/sr39tk (and other reporter gene) targeting vectors based on the ROSA26-mT/mG construct (79) is summarized in **Table 8** (a detailed description can be found in 6.3 on p. 136). The preparation of pmT/sr39tk from pROSA-mT/mG was performed together with A. Vachaviolos during his diploma thesis (467). During targeting vector generation, cloning products were verified using analytical restriction digests and sequence analysis (primer as indicated in **Table 8**).

Table 8. Generation of the ROSA26-mT/sr39tk targeting vector.

Antibiotic resistance genes and other genetic elements not touched by the cloning procedure are not shown. Parental plasmid backbones are indicated on the right. Primers used for sequence analysis are marked in green. For further details on the cloning procedure, see 6.3 on p. 136.

1. pROSA-mT/mG

PacI · 5' HA · E₀ · P_AG · mT · mG · P_PGK · Neo^R · AscI · 3' HA · DTA

2. pLinker3

Insertion of an oligonucleotide linker carrying PacI and AscI restriction sites into EcoRI/HindIII-digested pUC19.

PacI · AscI · pQEfor · pUC19

3. pmT/mG

Transfer of mT/mG cassette into pLinker3 using PacI/AscI.

PacI · E₀ · P_AG · mT · HindIII · mG · EcoRI · P_PGK · Neo^R · AscI · pUC19

4. pLoxP-mG-pA

Isolation of loxP-mG-pA fragment from pmT/mG with HindIII/EcoR and insertion into EcoRI/HindIII-digested pUC19.

Kpn2I · HindIII · mG · XhoI · EcoRI · pUC19

5. pLoxP-MCS-pA

Replacement of mG by oligonucleotide linker carrying FseI, XmaI, MluI and AsiSI restriction sites via Kpn2I/XhoI.

FseI · AsiSI · Kpn2I · XhoI · HindIII · EcoRI · M13uni · pUC19

6. pmT/MCS

Retransfer of loxP-MCS-pA fragment from pLoxP-MCS-pA into HindIII/EcoRI-digested pmT/mG.

E₀ · P_AG · mT · FseI · AsiSI · HindIII · EcoRI · P_PGK · Neo^R · pUC19

7. pLinker5

Insertion of an oligonucleotide linker carrying FseI, NcoI, BamHI, and AsiSI restriction sites into EcoRI/HindIII-digested pUC19.

NcoI · BamHI · FseI · AsiSI · M13uni · pUC19

8. pFseI-sr39tk-AsiSI

Transfer of *HSV1*-sr39tk from pCMV-sr39tk into pLinker5 using NcoI/BamHI.

NcoI · FseI · sr39tk · BamHI · AsiSI · pUC19

9. pmT/sr39tk

Transfer of *HSV1*-sr39tk from pFseI-sr39tk-AsiSI into pmT/MCS using FseI/AsiSI.

PacI · E₀ · P_AG · mT · FseI · sr39tk · AsiSI · P_PGK · Neo^R · AscI · pUC19

10. pROSA-mT/sr39tk

Transfer of the mT/sr39tk cassette into PacI/AscI-digested pROSA26-mT/mG.

PacI · 5' HA · E₀ · P_AG · mT · sr39tk · P_PGK · Neo^R · AscI · 3' HA · DTA

3.1.1.4 Gene targeting in ESCs

Targeting vectors were linearized (pROSA26-sr39tk with I-SceI and pROSA-mT/sr39tk with AclI) and introduced into R1 ESCs by electroporation. After 7-9 days of G418 selection, surviving ESC colonies were isolated and passaged to establish replicate cultures. One culture replica was frozen for culture recovery and blastocyst injection, the other replica was expanded for DNA analysis by Southern blot. During this work, around 1000 ESC colonies were isolated and analyzed by Southern blot (**Table 9**).

Table 9. Gene targeting experimental conditions and results.

Targeting	Transgene	DNA (µg)	Cell number	G418 (µg/mL)	Analyzed clones		Targeted clones[*]
1	ROSA26-sr39tk	25 or 50	$2×4×10^6$	400	2×96=192	1 (0.5%)	1.1.F08[C,I]
2	ROSA26-sr39tk	112	$1.4×10^7$	400	3×96=288	0 (0.0%)	No targeted clones
3	ROSA26-sr39tk	43	$1.2×10^7$	300	3×96=288	1 (0.4%)	3.2.E07[I]
4	ROSA26-sr39Δtk	40	$5×10^6$	300	52	1 (1.9%)	4.1.E03
5	ROSA26-mT/sr39tk	60	$8×10^6$	320	2×96=192	15 (12.8%)	5.1.D04[C, I], 5.1.D01, 5.1.E05, 5.1.E11[C], 5.1.F07, 5.1.H01, 5.1.H04[C, I], 5.1.H06[C, I], 5.1.H09, 5.2.E04, 5.2.E07, 5.2.F03, 5.2.G06, 5.2.H04, 5.2.H09

[*]C, Cre-targeting performed; I, injection into blastocysts performed.

In three independent gene targeting experiments with the ROSA26-sr39tk targeting vector (targeting 1-3), two targeted ESC lines were identified (**Figure 16A**). In another gene targeting experiment (targeting 4) with pROSA26-sr39Δtk, one targeted ESC line was identified (**Figure 16B**). Here, a truncated *HSV1*-sr39tk variant, called 'sr39Δtk' (see also 1.2.3) was targeted into the ROSA26 locus; the transgene is otherwise similar to the ROSA26-sr39tk transgene. In one targeting experiment (targeting 5) with pROSA26-mT/sr39tk, 14 targeted ESC clones were identified (**Figure 16C**). Here, Southern analysis revealed one ESC clone with a different fragment size of the targeted allele (5.1.H01), and another clone seems to be contaminated with considerable amounts of wild type ESCs (5.1.H09), as judged from the band intensities in the Southern analysis.
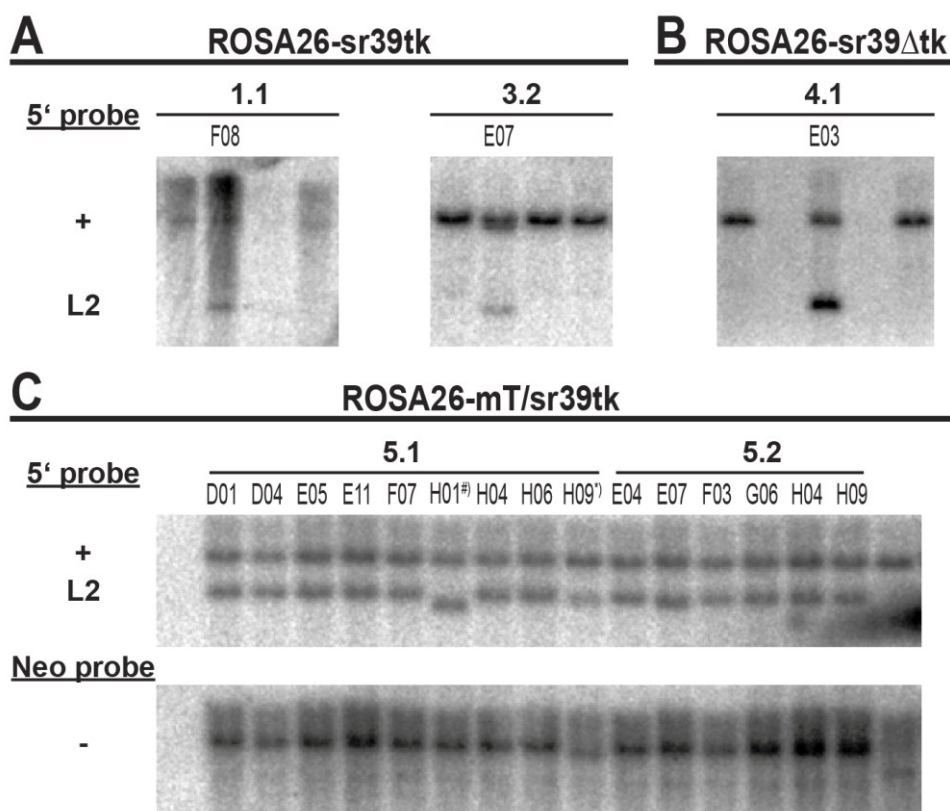
Figure 16. Identification of targeted ESC clones by Southern blot analysis.

A and B. Identification of targeted ESC clones in ROSA26-sr39tk (A) and ROSA26-sr39Δtk (B) gene targeting experiments. DNA isolated from G418-resistant ESC clones was digested in 96-well plates with EcoRV and blotted to a nylon membrane after electrophoresis, which was incubated with a ^{32}P-labeled probe binding 5' to the ROSA26 locus (see map in **Figure 13**). Targeted ESCs show 2 fragments; 1 wild type fragment ('+', 11.5 kb) and a shorter fragment ('L2', 4 kb) resulting from the transgene insertion into one allele of the ROSA26 locus (genotype: +/L2). **C.** Southern analysis of targeted clones identified in the ROSA26-mT/sr39tk gene targeting (5.1+5.2). DNA from ESC clones identified in the primary screen was digested with EcoRV in 96-well plates and hybridized with a ^{32}P-labeled 5' probe after Southern blot. Targeted clones are heterozygous (+/L2) and show the wild type fragment ('+', 11.5 kb) and a fragment from the targeted allele ('L2', 6 kb). After exposure, the membrane was stripped and hybridized with a ^{32}P-labeled probe binding within the Neo[R] gene; here targeted ESCs show a single fragment ('−', 12.2 kb). Note that clone 5.1.H01[#)] shows a shorter L2 fragment (<6 kb) upon hybridization with the 5' probe, while the signals of the L2 and '−' fragment from clone H09[*)] are weaker compared to the other clones.

3.1.2   Characterization of *HSV1*-sr39tk Reporter ESC Lines

Before mice were generated from targeted ESCs, transgene functionality was tested. For that purpose, targeted ESCs were transfected with Cre expression plasmids pIC-Cre (41) or pSG5-Cre (49) by electroporation, plated at low densities to obtain single ESC colonies, which were isolated and expanded for subsequent analyses. Southern blot analysis was performed to detect Cre recombination on the DNA level. Upon hybridization with a ROSA26 5' probe, targeted ROSA26-sr39tk ESCs show a 4 kb (L2) fragment, and after Cre recombination a 2.7 kb (L1) fragment (**Figure 17A**, map in **Figure 13A**). Targeted ROSA26-mT/sr39tk ESCs show a 6 kb (L2) fragment, and after Cre recombination a 4.4 kb (L1) fragment (**Figure 17B** and **C**, map in **Figure 13B**). Additionally, colonies were present,

which represent a mixture of cells that are either targeted or Cre-recombined; these colonies show both the L2 and L1 fragment (**Figure 17C**). In one case, colonies showing only the wild type (+) fragment were found (**Figure 17B**, clone G01). Here, the parental clone (5.1.E11) was probably contaminated with wild type ESCs and for that reason not used for blastocyst injection.
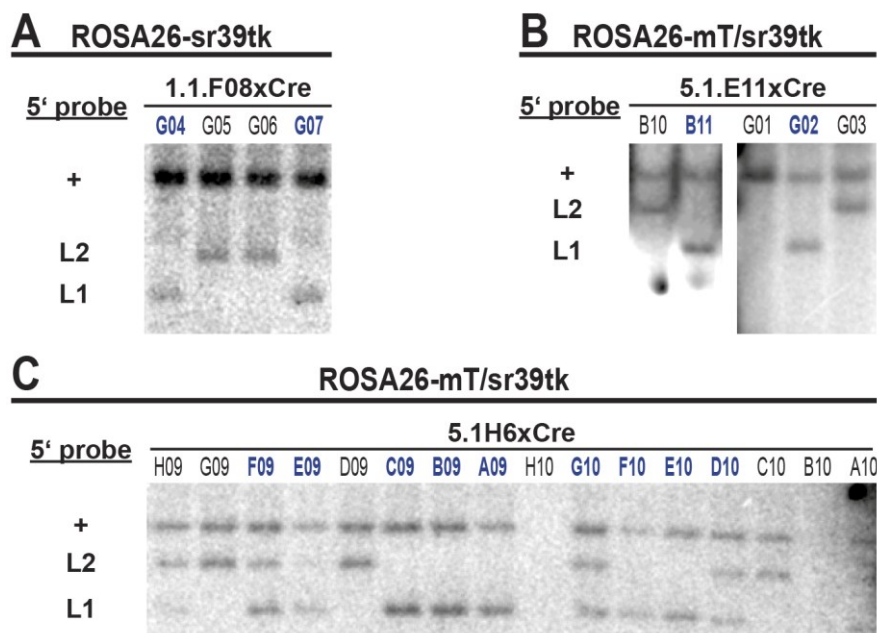

Figure 17. Southern blot analysis of ESC clones after transfection with a Cre expression plasmid.

DNA of targeted ESC clones isolated after electroporation with Cre expression plasmids was digested with EcoRV in 96-well plates and hybridized with the ROSA26 5' probe after Southern blot. **A.** Analysis of clones derived from the primary clone 1.1.F08 (ROSA26-sr39tk construct, see map in **Figure 13A**). Clones G05 and G06 show the same pattern as the primary clone ('L2', 4 kb) and have a +/L2 genotype, while clones G04 and G07 show the wild type fragment ('+', 11.5 kb) and a shorter fragment ('L1', 2.7 kb) resulting from the Cre-mediated excision of the Neo^R gene cassette (+/L1 genotype). **B.** Analysis of clones derived from the primary clone 5.1.E11 (ROSA26-mT/sr39tk construct, map in **Figure 13B**). Clones B10 and G03 show the same pattern as the primary clone ('+', 11.5 kb and L2, 6 kb) and have a +/L2 genotype, while clones B11 and G02 show beside the wild type fragment ('+', 11.5 kb) a shorter fragment ('L1', 4.4 kb), resulting from the Cre-mediated excision of the mT cassette (+/L1 genotype). Clone G01 shows only the wild type fragment ('+', 11 kb), probably due to a contamination of the primary clone 5.1.E11 with wild type (+/+) ESCs. Because of the possible contamination with wild type ESCs, this clone was not used for blastocyst injection. **C.** Analysis of clones derived from the blastocyst-injected, primary clone 5.1.H6. Either no DNA was isolated (H10, B10, A10), or ESCs show a +/L2 pattern (H09, G09, D09, C10), a +/L1 pattern (C09, B09, A09, F10, E10) or represent a mixture of Cre-recombined (+/L1) and non-recombined (+/L2) ESCs (F09, E09, G10, D10).

In parallel to recombination analysis by Southern blot, isolated ESC colonies were analyzed in selection assays with G418 and GCV. In ROSA26-sr39tk ESCs, Cre recombination removes the loxP-flanked Neo^R gene cassette, leading to *HSV1*-sr39tk expression (see map in **Figure 13A**). Targeted (+/L2) ESCs are resistant to G418 and not affected by GCV, while Cre-recombined ROSA26-sr39tk$^{+/L1}$ ESCs die in presence of G418 or GCV. In ROSA26-mT/sr39tk ESCs, Cre recombination removes the loxP-flanked mT cassette leading to *HSV1*-sr39tk expression, while the

FRT-flanked Neo^R gene cassette is unaffected (see map in **Figure 13B**). Consequently, targeted (+/L2) ESCs show mT fluorescence, and are neither affected by G418 nor by GCV. After Cre recombination, ROSA26-mT/sr39tk$^{+/L1}$ ESCs lose their fluorescence and die in presence of GCV, while still resistant to G418. Replicas of isolated ESC colonies were incubated with G418 or GCV, and visually examined for cell growth or death. Additionally, ESCs carrying the ROSA26-mT/sr39tk transgene were examined for the presence or absence of mT fluorescence. G418 or GCV sensitivity, as well as loss of red fluorescence (not shown) was in agreement with genotypes determined by Southern blot analysis.

For detailed analysis, selected targeted (+/L2) or Cre-recombined (+/L1) ESCs were thawed and expanded from frozen replica plates. Using a *HSV1*-tk antiserum, *HSV1*-sr39tk was detected in ESC protein extracts (**Figure 18A**). The *HSV1*-sr39tk protein is present in Cre-recombined (+/L1), but not in targeted (+/L2) ESCs carrying either transgene, showing Cre-dependency of *HSV1*-sr39tk expression. Furthermore, *HSV1*-sr39tk protein levels in ROSA26-sr39tk$^{+/L1}$ and ROSA26-mT/sr39tk$^{+/L1}$ ESCs are markedly different. The level is considerably higher in ROSA26-mT/sr39tk ESCs, where the CAG promoter drives *HSV1*-sr39tk expression. Additionally, the *HSV1*-sr39tk protein size is greater upon expression from the ROSA26-sr39tk transgene, where the original *HSV1*-sr39tk CDS is preceded by 42 additional amino acids (see **Table 6**), while translation starts at the original *HSV1*-sr39tk CDS (red letters in **Table 6**) upon expression from the ROSA26-mT/sr39tk transgene. To test for *HSV1*-sr39tk protein functionality in Cre-recombined ESCs, G418 and GCV selection assays were repeated. As observed when performed in 96-well plates, Cre-recombined ROSA26-sr39tk$^{+/L1}$ ESCs die in presence of G418 and GCV, while ROSA26-mT/sr39tk$^{+/L1}$ ESCs die only in presence of GCV (**Figure 18B**). Moreover, [^{18}F]FHBG uptake assays were performed. Targeted and Cre-recombined ESCs were incubated with [^{18}F]FHBG added to the culture medium, and after 1-4 h of incubation, amounts of extra- and intracellular radioactivity were measured to determine [^{18}F]FHBG uptake into Cre-recombined (+/L1) *versus* targeted (+/L2) ESCs. Targeted ESCs do not accumulate [^{18}F]FHBG over time, while *HSV1*-sr39tk-expressing (+/L1) ESCs show a time-dependent increase of intracellular [^{18}F]FHBG levels, leading to an overall L1/L2 [^{18}F]FHBG uptake ratio increase. ROSA26-sr39tk$^{+/L1}$ ESCs, which express *HSV1*-sr39tk from the endogenous ROSA26 promoter, show a L1/L2 ratio of 5 after 4 hours. Conversely, ROSA26-mT/sr39tk$^{+/L1}$ ESCs, which express *HSV1*-sr39tk from the CAG promoter, show higher [^{18}F]FHBG accumulation with L1/L2 ratios of 8 and 31 after 1 and 4 hours (**Figure 18C**), which correlates with higher *HSV1*-sr39tk protein levels found by western blot analysis (in **Figure 18A**). In case of ROSA26-mT/sr39tk ESCs, the L1/L2 uptake ratio might have been underestimated, as the γ-counter used for measurements was saturated by high radioactivity contents in ROSA26-sr39tk$^{+/L1}$ ESC lysates.
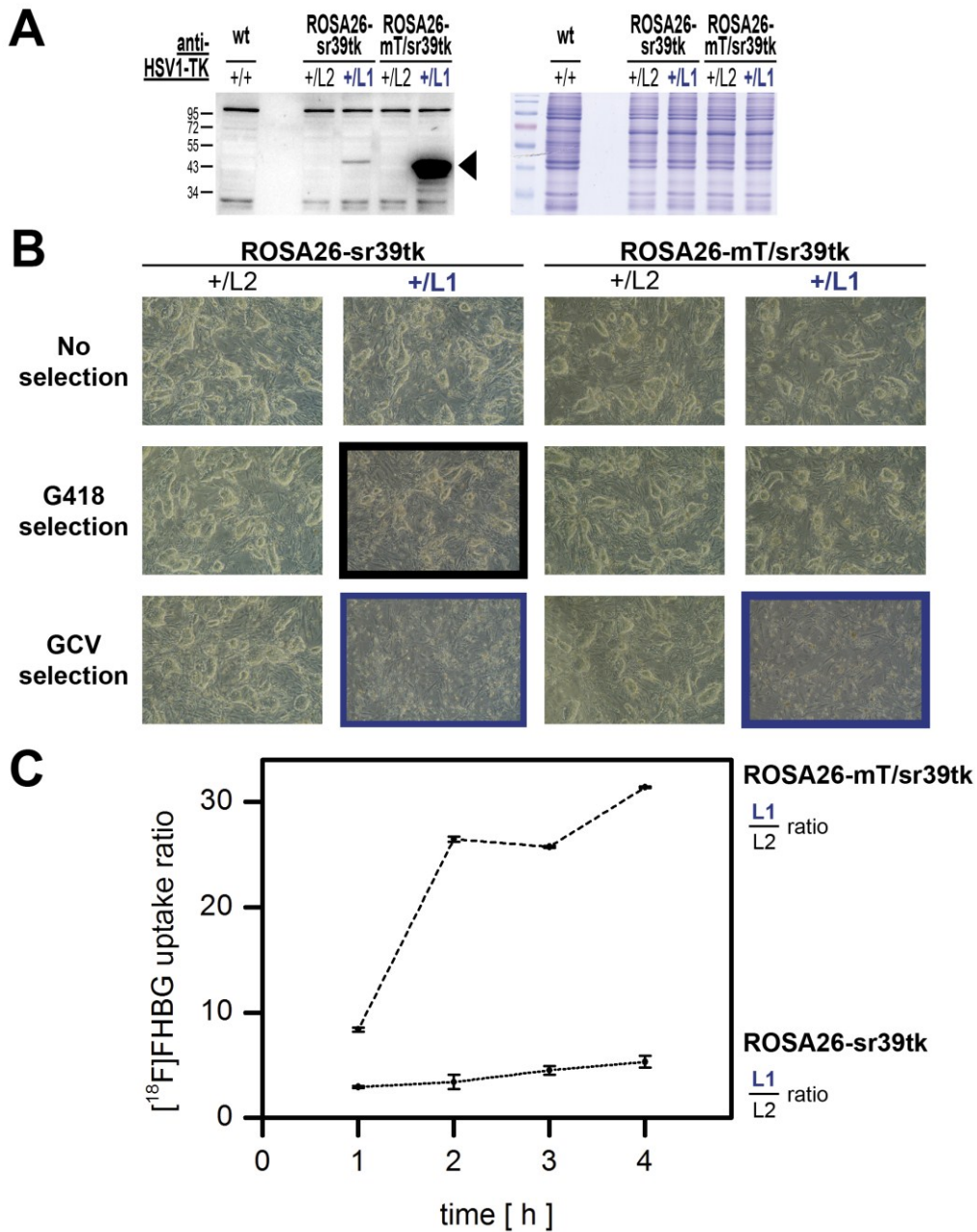
Figure 18. Test on *HSV1*-sr39tk expression (A) and functionality (B, C) in Cre-recombined ESCs carrying ROSA26-sr39tk or ROSA26-mT/sr39tk transgenes.

A. Western blot analysis reveals higher *HSV1*-sr39tk expression levels in Cre-recombined ROSA26-mT/sr39tk ESCs (+/L1) than in Cre-recombined ROSA26-sr39tk ESCs (+/L1). Here, the *HSV1*-sr39tk protein has a greater weight due to the transgene design. Non-recombined ESCs (+/L2 genotype) show no *HSV1*-sr39tk expression at all. Lysates (20 μg protein) from wild type (wt, +/+), targeted (+/L2) or Cre-recombined (+/L1) ESCs were separated by SDS-PAGE and stained with Coomassie Brilliant blue (right) or used for western blot analysis (left). Membrane was incubated with anti-*HSV1*-tk antiserum (1:2000); antibody binding was detected with HRP-coupled anti-rabbit antibodies (1:2000) in a chemiluminescence reaction. **B.** Upon incubation with G418 (black frame) and ganciclovir (GCV, blue frame), Cre-recombined ROSA26-sr39tk ESCs (+/L1) undergo cell death, as Cre recombination leads to *HSV1*-sr39tk activation by removal of the Neo[R] gene cassette. ESCs carrying the Cre-recombined ROSA26-mT/sr39tk construct (+/L1) die only in presence of GCV (blue frame), as Cre recombination leads to *HSV1*-sr39tk activation by mT cassette removal, but not removal of Neo[R]. Targeted ESCs (+/L2) of both constructs are neither affected by G418 nor by GCV. Phase contrast images were taken 4 days after seeding and 3 days after begin of the selection. Original magnification: 10×. **C.** Cre-recombined ROSA26-mT/sr39tk (+/L1) ESCs show higher intracellular [^{18}F]FHBG accumulation compared to ROSA26-sr39tk (+/L1) ESCs. [^{18}F]FHBG uptake is estimated as ratio of accumulation into recombined (+/L1) ESCs vs. non-recombined (+/L2) ESCs.

3.1.3 Generation of *HSV1*-sr39tk Reporter Mouse Lines

After successful test of ROSA26-sr39tk and ROSA26-mT/sr39tk transgenes in ESCs, targeted clones were injected by Dr. S. Feil into C57Bl/6 blastocyst-stage embryos in two sessions. In the first session, targeted ROSA26-sr39tk$^{+/L2}$ ESCs were injected into 116 blastocysts, and in the second session, targeted ROSA26-mT/sr39tk$^{+/L2}$ ESCs were injected into 76 blastocysts (**Table 10**).

Table 10. Overview on ESC blastocyst injection and chimeric progeny.

Session	Clone/Passage	Injected blastocysts	Implanted blastocysts	Progeny	Chimera gender (grade of chimerism and GLT)
1.1	1.1.F08/P28	23	14	no	No
1.2	1.1.F08/P28	24	12(+11†)	2(+1†)	♀1 (50%)
1.3	3.2.E07/P24	10	5+5	6	♂2 (80-90%), ♂**3 (80-90%, GLT)**
1.4	1.1.F08/P29	14	6+8	5	♂4 (80-90%), ♂5 (80-90%), ♂6 (20%)
1.5	3.2.E07/P24	16	8+8	7	♂7 (80-90%), ♂**8 (80-90%, GLT),** ♂9 (40%)
1.6	1.1.F08/P28	22	7+7+7	no	No
1.7	3.2.E07/P24	7	7	no	No
2.1	5.1.H06/P23	8	8	5	♂1 (80%), ♂2 (60-70%), ♀3 (60-70%)
2.2	5.1.D04/P23	26	9+9+8	6	♂4 (50%)
2.3	5.1.H04/P23	21	7+7+7	(4†)	No
2.4	5.1.H06/P24	21	7+7+7	5	♂**5 (70%, GLT),** ♀6 (60%), ♀7 (50%)

For implanted blastocysts, every number stands for transfer into one foster mother. Grading of chimerism was performed according to coat color (proportion of agouti-colored fur). GLT, germ-line transmission.

To establish transgenic mouse lines, male chimeras were mated to wild type C57Bl/6 females and agouti-colored progeny was tested for transgene presence by PCR. To detect the ROSA26-sr39tk transgene, the ROSA26-lacZ genotyping PCR was used, while for the detection of the ROSA26-mT/sr39tk transgene the ROSA26-mT/mG genotyping PCR was used (see also **Table 21** on p. 142). In both cases, three primers were used (see **Figure 13** for primer binding sites); the common forward primer ROSA10 and the wild type reverse primer ROSA11 amplify a 322 bp fragment from the wild type ROSA26 locus. ROSA10 and the '−' reverse primer RF127 amplify a 188 bp fragment from the ROSA26-sr39tk transgene; ROSA10 and the '−' reverse primer ROSA04 amplify a 249 bp fragment from the ROSA26-mT/sr39tk transgene. From the injection of ROSA26-sr39tk ESCs, eight male chimeras were derived, of which two show germ-line transmission (see **Table 10**, session 1 and **Figure 19A**). Both chimeras were derived from injections of the 3.2.E07 ESC clone, the ROSA26-sr39tk mouse line was established from progeny of chimera 8. In one of four male chimeras derived from the injection of ROSA26-mT/sr39tk ESCs, the transgene was transmitted through the germ-line (see **Table 10**, session 2 and **Figure 19B**); the chimera was derived from clone 5.1.H06.
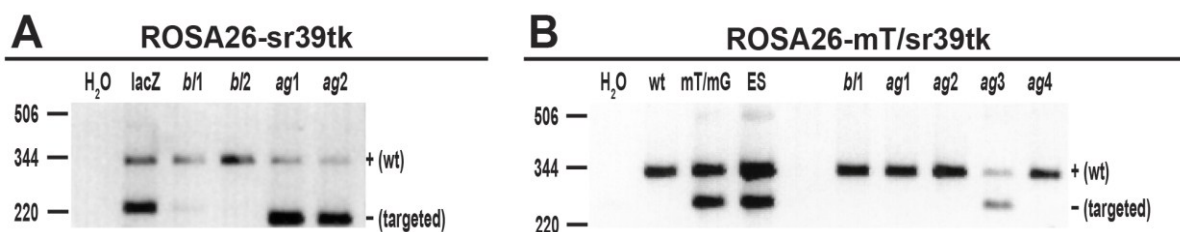
Figure 19. PCR analysis to detect germ-line transmission of ROSA26-sr39tk and ROSA26-mT/sr39tk transgenes.

A. DNA isolated from agouti-colored chimera progeny (*ag1*, *ag2*), from black-colored chimera progeny (*bl1* and *bl2*), and from ROSA26-lacZ mice (as positive control) was analyzed via PCR with primers ROSA10, RF127, and ROSA11. In 2/2 agouti-colored animals, the ROSA26-sr39tk transgene was detected by the presence of an additional PCR fragment ('−') of 188 bp (animals have +/− genotype). **B.** DNA isolated from agouti-colored chimera progeny (*ag1-ag4*), from black-colored chimera progeny (*bl1*), from wild type mice (wt), from ROSA26-mT/mG (mT/mG) mice (as positive control), and from the injected ESC clone (ES) was analyzed via PCR with primers ROSA10, ROSA04, and ROSA11. In 1/4 agouti-colored animals, the ROSA26-mT/sr39tk transgene was detected by the presence of a PCR fragment ('−') of 249 bp (animals have +/− genotype).

3.1.4 Characterization of *HSV1*-sr39tk Reporter Mouse Lines

Heterozygous animals of both mouse lines are fertile and display no overt phenotypes, while no reliable data is available for homozygous animals. DNA was isolated from tissue of transgenic mice and used in a Southern blot analysis to test for transgene presence and integrity, results obtained are similar to Southern blot analysis of ESC DNA (not shown).

First, it was tested whether *HSV1*-sr39tk is functionally expressed from the Cre-activated transgene in the ROSA26-sr39tk mouse line. Therefore, a western blot analysis of protein extracts from tissues of Cre$^{tg/+}$; ROSA26-sr39tk$^{+/-}$ mice was performed (**Figure 20A**; see 3.1.5 on p. 90 for further details on Cre transgenes). Additionally, colonic smooth muscle cells (CSMCs) isolated from CMV-Cre$^{tg/+}$; ROSA26-sr39tk$^{+/-}$ mice were analyzed using western blot (**Figure 20A**), and in a selection assay to test for *HSV1*-sr39tk functionality (**Figure 20B**). In the western blot with brain extracts of Nes-Cre$^{tg/+}$; ROSA26-sr39tk$^{+/-}$ mice, a slightly more intense signal is present at the expected height, but the result is not conclusive due to unspecific signals at the same height. Reliable *HSV1*-sr39tk detection was as well not possible in protein extracts from mice with the following genotypes: RIP-Cre$^{tg/+}$; ROSA26-sr39tk$^{+/-}$ (pancreas; **Figure 20A**); MLC2a-Cre$^{tg/+}$; ROSA26-sr39tk$^{+/-}$ (heart; not shown) and CMV-Cre$^{tg/+}$; ROSA26-sr39tk$^{+/-}$ (liver, colon; not shown). However, a signal was observed with protein extracts from cultured CSMCs isolated from CMV-Cre$^{tg/+}$; ROSA26-sr39tk$^{+/-}$ mice. In agreement with this result, these CSMCs show a clear reduction in cell number upon GCV treatment (**Figure 20B**), while the growth behavior of control CSMCs (from CMV-Cre$^{+/+}$; ROSA26-sr39tk$^{+/-}$ mice) is not affected. Some CSMCs seem to survive GCV selection, most likely because of non-recombined ROSA26-sr39tk transgene resulting from mosaic Cre expression.
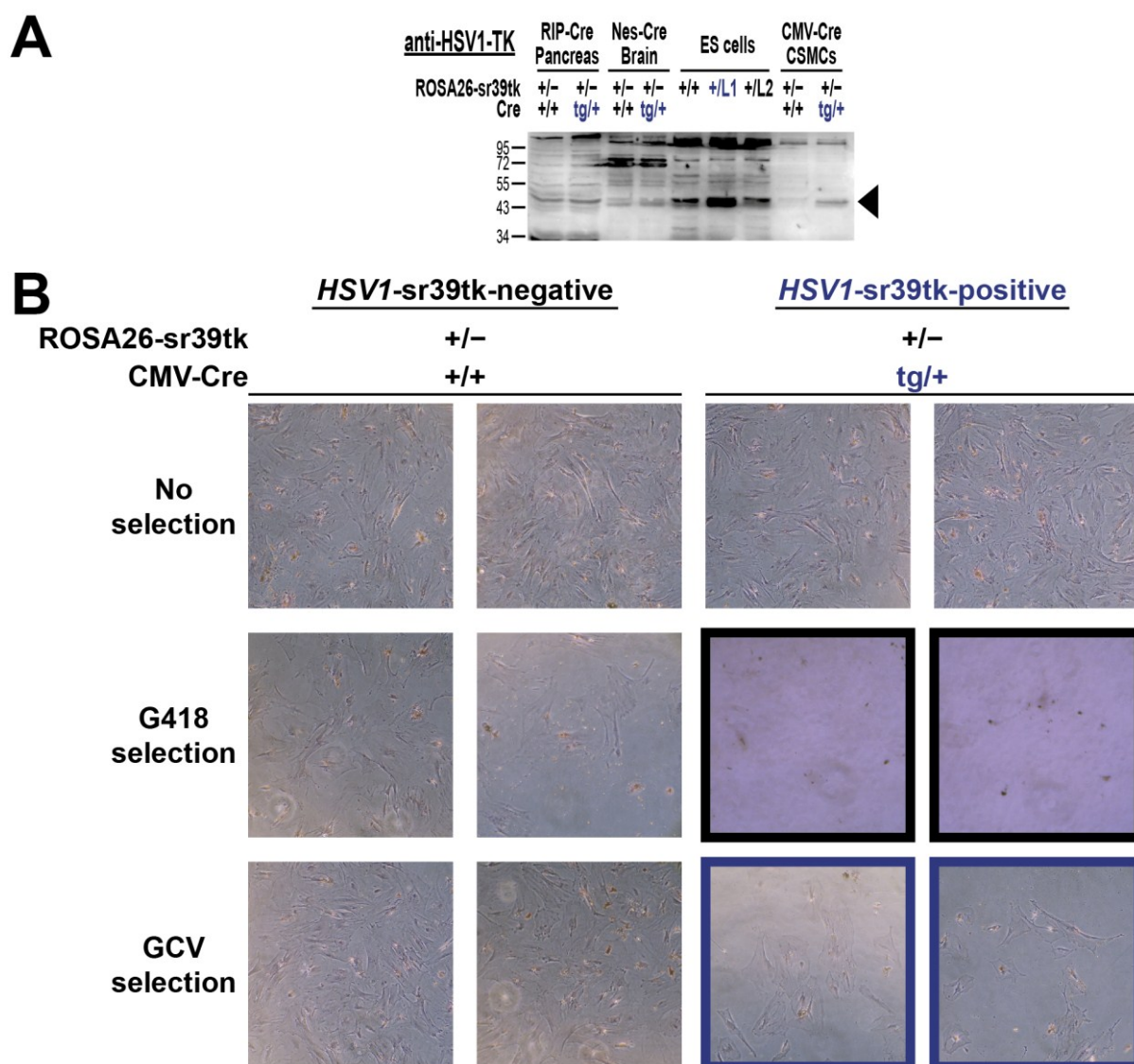
**Figure 20. Test on *HSV1*-sr39tk expression and functionality in tissues and cells carrying the Cre-activated ROSA26-sr39tk construct.**

A. Western blot analysis of protein extracts from ESCs (30 µg), and from tissue (30 µg) and colonic smooth muscle cells (CSMCs; 8 µg) isolated from Cre$^{tg/+}$; ROSA26-sr39tk$^{+/-}$ and Cre$^{+/+}$; ROSA26-sr39tk$^{+/-}$ control mice. Proteins were separated on a gel with 12% polyacrylamide, and blotted onto a PVDF membrane, which was incubated with *HSV1*-tk antiserum (1:2000); antibody binding was detected with HRP-coupled anti-rabbit antibodies (1:2000) in a chemiluminescence reaction. **B.** G418 and GCV selection assay with CSMCs. '*HSV1*-sr39tk-positive' CSMCs derived from CMV-Cre$^{tg/+}$; ROSA26-sr39tk$^{+/-}$ mice die in presence of G418 and GCV, as Cre recombination leads to excision of the Neo^{R} cassette and expression of *HSV1*-sr39tk, respectively. CSMCs from control mice (CMV-Cre$^{+/+}$; ROSA26-sr39tk$^{+/-}$) show slightly reduced growth in presence of G418, but grow normally with GCV. CSMCs were cultured and expanded in two passages. With the last passage, incubation with 400 µg/mL G418, and 2 µM GCV or normal media (no selection) was started. Phase contrast images of different FOVs were taken at 10× original magnification 14 days after the incubation with G418 or GCV was started.

These results show that Cre recombination of the ROSA26-sr39tk transgene results in ROSA26 promoter-driven expression of functionally active *HSV1*-sr39tk protein in ESCs and mice. The amount of *HSV1*-sr39tk protein expressed from the ROSA26-sr39tk$^{+/L1}$ transgene is appropriate for the

ablation of cultured cells isolated from ROSA26-sr39tk transgenic mice (or for the ablation of ROSA26-sr39tk[+/L1] ESCs). However, low *HSV1*-sr39tk expression levels render the usability of the ROSA26-sr39tk mouse line uncertain for PET experiments (see discussion). Therefore, the ROSA26-mT/sr39tk mouse line was used for a first *in vivo* PET experiment. For that purpose, a mouse with the genotype RIP-Cre[tg/+]; ROSA26-mT/sr39tk^{+/−} was analyzed in a PET experiment with [^{18}F]FHBG, and autoradiographs of frozen sections of the pancreas were prepared directly after the PET experiment. Specific tracer retention occurs in kidney and spleen, and unspecific [^{18}F]FHBG uptake in bladder, intestines, gall bladder and skeleton (**Figure 21A**; PET data of this experiment was compared with data of non-transgenic controls from ref. 224). Due to tracer accumulation in kidney and spleen, uptake into the pancreas could not be localized and quantified from the PET dataset. However, autoradiographs of the pancreas show a distinct intensity pattern (**Figure 21B**), which results from [^{18}F]FHBG uptake into cells located in the islets of Langerhans, but not in the exocrine pancreas, as judged from a comparison of autoradiographs with microphotographs of the same sections stained with hematoxylin and eosin after autoradiography (not shown). In summary, this first PET experiment with a ROSA26-mT/sr39tk transgenic mouse indicates that *HSV1*-sr39tk expression levels are sufficient for [^{18}F]FHBG accumulation into *HSV1*-sr39tk-expressing cells, which can therefore be visualized in a living animal by PET imaging (or *post mortem* via autoradiography).
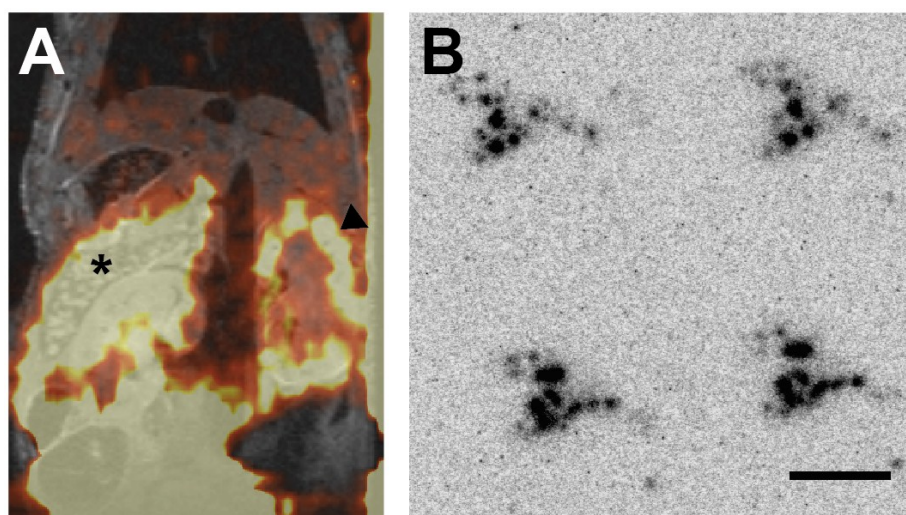

Figure 21. [^{18}F]FHBG PET/MR image (A) and autoradiography (B) of a RIP-Cre[tg/+]; ROSA26-mT/sr39tk^{+/−} mouse.

A. Coronal plane of a PET (heatmap) and MR (grayscale) image of the abdomen, with lungs on top and bladder (bright PET signal) at the bottom. Specific [^{18}F]FHBG uptake is found in spleen (asterisk) and the cortex of the kidney (arrowhead), while [^{18}F]FHBG uptake into intestines and bladder is unspecific. **B.** Autoradiographs of four frozen sections from the pancreas show localized sites of [^{18}F]FHBG accumulation. Sites of tracer uptake correlate with islets of Langerhans, according to hematoxylin/eosin staining performed after autoradiography (not shown). PET image was acquired 4 h after injection of ~300 µCi [^{18}F]FHBG, MR image was acquired thereafter. Images are manually registered using tracer-filled capillaries as fiducial landmarks. The pancreas was dissected after finishing PET/MR image acquisition. Frozen 10 µm sections were exposed to a phosphor screen ~7 h after tracer injection; scale bar for B: 10 mm.

3.1.5 ROSA26-lacZ-based Characterization of Cre Mouse Lines

Several Cre transgenic mice were used to induce *HSV1*-sr39tk expression from ROSA26-sr39tk or ROSA26-mT/sr39tk transgenes. In order to characterize recombination patterns caused by Cre expression, mice were bred to ROSA26-lacZ Cre reporter mice, and activation of β-galactosidase expression in Cre[tg/+]; ROSA26-lacZ^{+/-} was analyzed in aldehyde-fixed tissue samples by X-Gal staining (**Figure 22**). A summary on the observed recombination patters is given in **Table 11**. RIP-Cre transgenic mice were generated by using a 0.6 kb fragment with the rat insulin promoter (RIP) adjoined to the Cre CDS to drive Cre expression in pancreatic β cells (441). In these mice, recombination was observed in pancreatic islets, and in few cells of the brain, in single SMCs of various tissues, as well as in cells of the renal cortex (**Figure 22A, B**). In CMV-Cre transgenic mice, Cre expression is driven by the human cytomegalovirus promoter, and the transgene was reported to be active in nearly all tissues (438). Cre recombination of varying extent was detected in all tested tissues of CMV-Cre transgenic mice (**Table 11**; **Figure 22A**). To generate the MLC2a-Cre mouse line, exons 1-7 of Myl7 (synonym: MLC2a) were replaced with the CDS for Cre and Neo[R], leading to Cre expression driven by the endogenous Myl7 promoter (437). Recombination occurs most notably in heart, brain and SMCs in various tissues (**Figure 22A, B**). The Nestin-Cre transgene not tested here has been shown to cause widespread recombination in the central and peripheral nervous system (439).

Table 11. Cre recombination pattern in Cre[tg/+]; ROSA26-lacZ^{+/−} mice analyzed by X-Gal staining.

Tissue	RIP-Cre		CMV-Cre		MLC2a-Cre	
Aorta	-		+++		+	SMCs
Bladder	s	SMCs	+	SMCs	++	SMCs
Colon	s	SMCs	+		+	SMCs
Heart	-		h	weak	+++	
Small Intestine	s	SMCs	++		+	SMCs
					+	Others
Pancreas	++	Islets	+/++		+/++	
Brain	s	Brain	s	Brain	++	Cortex
			+	Meningeal vessels	++	Cerebellum
Skeletal muscle	-		s		+	
Kidney	+	Cortex	s		+	
Liver	-		+		+	
Spleen	-		+	Capsule	-	
Lung	s	Airway SMCs	+	Airways	+	Airways
	-		h	Parenchyma		

Abbreviations used for grading: -, negative; s, sparse mosaic; h, heterogeneous; +, some cells stained; ++, numerous cells stained; +++, virtually all cells stained.
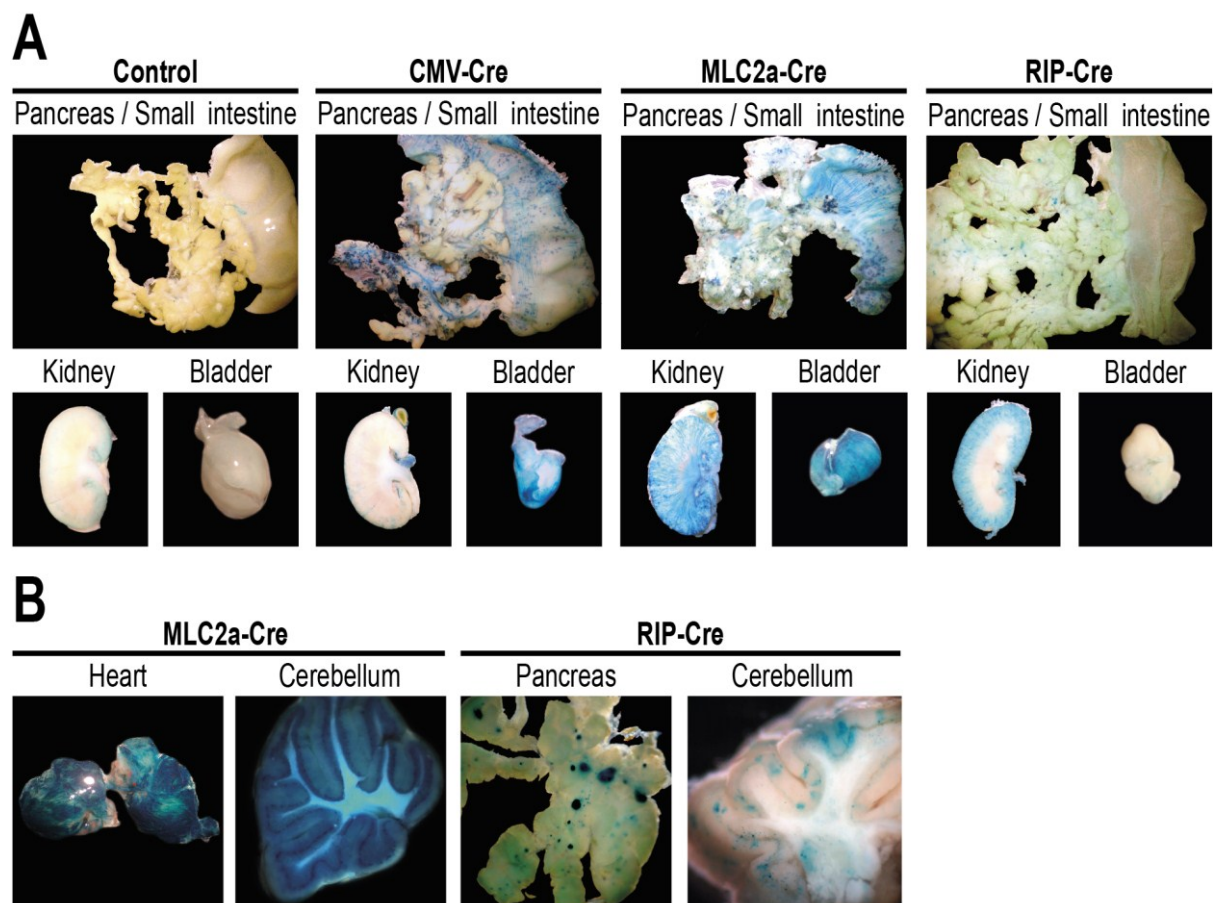
Figure 22. Cre recombination patterns of various Cre transgenes analyzed by X-Gal staining with ROSA26-lacZ Cre reporter mice.

Mice were sacrificed, blood was removed, and fixative was delivered by transcardial perfusion. Explanted tissues were post-fixed in fixative for one hour. X-Gal staining was performed overnight at room temperature. After staining, organs were stored in 70% ethanol at 4°C. Pictures were acquired with a digital camera on a stereomicroscope (Stemi 2000, Zeiss). Pictures in A were acquired at 6.5× original magnification, while pictures in B were acquired at magnifications of 6.5× (heart) or 25× (other organs). Experimental animals have the genotype $Cre^{tg/+}$; ROSA26-lacZ$^{+/-}$, the control animal the genotype $Cre^{+/+}$; ROSA26-lacZ$^{+/-}$.

Among the Cre transgenic mouse lines tested here, the RIP-Cre transgene causes recombination with highest specificity; but considerable recombination is present in cortical cells of the kidney. The MLC2a-Cre transgene causes robust recombination in heart and smooth muscle, but also in brain and other organs. The CMV-Cre transgene also leads to quite ubiquitous recombination, with a pattern that is different to the pattern observed with MLC2a-Cre mice (see e.g. small intestine and kidney in **Figure 22A**).

3.2 cGMP FRET Imaging with cGi Biosensors

## 3.2.1 Generation of cGi Transgenic Mouse Lines

Generation of cGi expression plasmids (see also 6.4 on p. 137) and transgene DNA purification for oocyte injection was performed by Matthias Hillenbrand. Oocyte injection was performed by members of the Transgenic Facility Tübingen. Transgene integration was tested by PCR with genomic DNA isolated from tail tips of possible founder animals. A common forward primer was used together with cGi-500-specific, cGi-3000-specific, or cGi-6000-specific reverse primers (**Table 21**, S. 142). Founder animals (generation N1) were mated to C57Bl/6 mice, and founder progeny (generation N2) was tested for transgene presence by PCR as described before. Adult mice (in N2 or N3 generation) were used to screen for cGi expression.

3.2.2 Screening of Transgenic Mice for cGi Expression

The central method to screen for cGi-expressing mice was the analysis of tissue samples by western blot with EGFP antibodies (mouse monoclonal, 1:1000 or rabbit polyclonal, 1:3000; see **Table 22**, p. 143) recognizing ECFP and EYFP of cGi-type sensors. Additionally, it was tried to detect cGi fluorescence in sacrificed animals *in situ* and to detect transcripts by RT-PCR in tissues or cultured cells isolated from cGi-transgenic animals (not shown). Out of 29 founder lines, 20 transmitted the transgene through the germ-line (see **Table 13** on p. 138). Out of these mouse lines, 18 were tested for cGi expression, and five mouse lines were identified that express cGi-500 (SM445-cGi-500-1 and -5) or cGi-6000 (CMV-cGi-6000-6, -10 and -11). Animals of these lines display no overt phenotypes, and show normal fertility and life expectancies. Mouse lines expressing cGi-500 or cGi-6000 were further characterized by western blot analysis, by antibody staining of frozen tissue sections, and by isolation, culture, and analysis of primary cells (derived from cGi-expressing mice). Most importantly, cGMP FRET imaging studies were performed with primary cells, tissue samples and living cGi-expressing mice.

3.2.3 Characterization of CMV-cGi-6000 Mice

Three of seven tested CMV-cGi-6000 mouse lines express cGi-6000 from a CMV-driven promoter (**Figure 23A**). Broadest expression was found in mice of the CMV-cGi-6000-10 line, where cGi-6000 was detected in brain, heart, kidney, and skeletal muscle by western blot analysis (**Figure 23B**). Mice of the CMV-cGi-6000-6 line show expression in brain and skeletal muscle, and mice of the CMV-cGi-6000-11 line in heart (**Figure 23B**).

A

B Western blot

Hippocampus

C EGFP Hoechst

D **E** Live YFP fluorescence

F βIII-Tubulin EGFP Hoechst

G GLAST EGFP Hoechst

Cortical astrocytes

L EGFP Hoechst

M Live YFP fluorescence

Cerebellar granule neurons

H EGFP Hoechst

I Live YFP fluorescence

J βIII-Tubulin EGFP Hoechst

K βIII-Tubulin EGFP Hoechst

Olfactory bulb

N EGFP Autofluorescence

Heart

O EGFP Hoechst
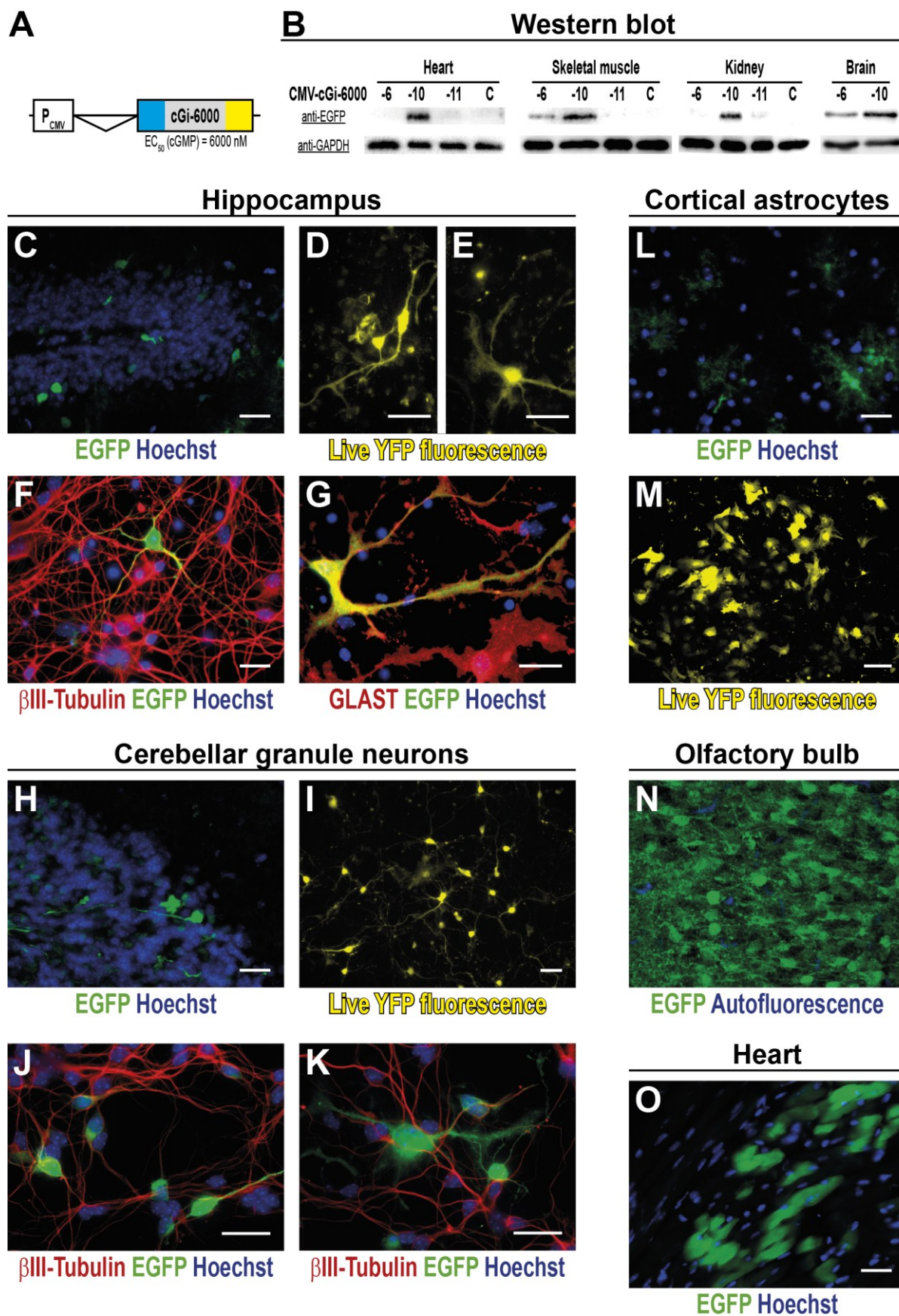
Due to comparably strong and broad cGi-6000 expression in CMV-cGi-6000-10 mice, this mouse line was chosen for further analysis. Therefore, an EGFP antibody was used to detect cGi-6000 expression on frozen sections of the brain (**Figure 23C**, **H**, **L** and **N**) and the heart (**Figure 23O**). In several brain regions, cells with different morphologies were found to express cGi-6000, but by their morphology, they could not easily be attributed to a certain cell type, and for (initial) FRET studies, cultured cells were needed. Therefore, cultures of primary neural cells were generated together with N. Fomin during her master thesis (468). Different types of cGi-6000-expressing cells were identified. cGi-6000 is not expressed in all cells in the culture, which correlates with the heterogeneous staining pattern of frozen brain sections. In hippocampal cultures from newborn mice, cGi-6000 expression was found in neurons and astrocytes, as seen from the morphology of cGi-6000-expressing cells (**Figure 23D**) and their co-staining with neuronal or glial cell markers (**Figure 23F**, **G**). Furthermore, CGNs isolated from 7-day-old mice show cGi-6000 expression (**Figure 23I-K**). Also small numbers of astrocyte-like cells present in the CGN culture were found to express cGi-6000 (**Figure 23K**). In cortical astrocytes isolated from newborn mice, broad cGi-6000 expression was found (**Figure 23M**). In all cell cultures, cGi-6000 expression was detected by its fluorescence in live cells and by staining with an EGFP antiserum, where co-staining with neuronal (βIII-Tubulin) or glial markers (GLAST) was used to confirm identities of cGi-6000-expressing cells. Additionally, expression was found in olfactory bulb (**Figure 23N**) and other brain regions of the midbrain and brain stem (not shown), which were not further analyzed. Cells isolated from mice of the CMV-cGi 6000-6 mouse line were also analyzed by N. Fomin, showing that cGi-6000 is predominantly expressed in cortical astrocytes (468).

Figure 23 (previous page). Analysis of cGi-6000 expression in CMV-cGi-6000 transgenic mice.

A. Structure of the CMV-cGi-6000 transgene. The CMV promoter drives expression of the cGi-6000 cGMP FRET sensor. **B.** Western blot analysis of tissue samples from CMV-cGi-6000 transgenic mice; 12 µg protein extract were blotted to a PVDF membrane after SDS-PAGE, membranes were incubated with rabbit EGFP antiserum (1:3000) and anti-GAPDH antibodies from rabbit (1:5000) to control for equal loading. Antibody binding was detected with HRP-coupled goat anti-rabbit antibodies (1:5000) in a chemiluminescence reaction. **C-O.** Analysis of cGi-6000 expression in hippocampus (C), in hippocampus-derived cell cultures (D-G), in cerebellum (H), in cultured cerebellar granule cells (I-K), in cortex (L), in cultures of cortical astrocytes (M), and in frozen sections of olfactory bulb (N) and heart (O) of CMV-cGi-6000-10 mice. **C, H, L, O**: cGi-6000 was detected on frozen tissue sections (thickness: 10 µm) with an EGFP antiserum and Alexa 488-conjugated secondary antibodies (green), nuclear DNA staining with Hoechst 33258 (blue). Scale bars: 25 µm. **N**: Staining and microscopy in the group of Prof. Garaschuk. cGi-6000 was detected on frozen brain sections (10 µm thickness) with EGFP antibodies (Rockland, Gilbertsville, PA, USA) and Alexa 594-conjugated secondary antibodies. Images of tissue autofluorescence (blue, 536/40 nm band pass filter) and antibody fluorescence (green, 568 nm long pass filter) were acquired with a 2-photon microscope (20× original magnification, 2× zoom). **D, E, I, M**: cGi-6000 was detected in live cells using an EYFP filterset (yellow). Scale bars: C, D, H, 25 µm; L: 100 µm. **F, G, J, K**: cGi-6000 was detected on fixed cells with an EGFP antiserum from rabbit (1:1000) and antibodies from mouse detecting the neuronal marker βIII-Tubulin (1:2000) or the glial marker GLAST (1:400). Antibody binding was detected with secondary anti-rabbit or anti-mouse antibodies conjugated with Alexa 488 (green) and Alexa 555 (red), nuclear DNA staining with Hoechst 33258 (blue). Scale bars: 25 µm. Panel I and J: Courtesy of Natalie Fomin.

3.2.4 Characterization of SM445-cGi-500 Mice

Two of nine SM445-cGi-500 transgenic mouse lines express cGi-500 from a SM445 promoter-driven transgene (**Figure 24A**) in smooth muscle. Expression was detected in protein lysates from both mouse lines in aorta, bladder, colon, lung, and heart, but not in skeletal muscle. SM445-cGi-500-1 mice show stronger signals in aorta, bladder, and colon, while SM445-cGi-500-5 mice show stronger expression in lung and heart (**Figure 24B**). SMC cultures from aorta, bladder, and colon were generated from animals of both mouse lines for further characterization and cGMP FRET imaging studies. Cells isolated from SM445-cGi-500-1 mice show a uniform distribution with relatively weak cGi-500 expression (**Figure 24B-D**), while cells isolated from SM445-cGi-500-5 mice show a heterogeneous distribution of cGi-500 expression, so that cells with variable fluorescence intensities were found (**Figure 24E-J**). It was tested, if SMCs from SM445-cGi-500-5 mice, which show no or only weak cGi-500 expression express the SMC marker protein SM22. Double staining of SMC cultures with EGFP and SM22 antisera confirmed the heterogeneous expression pattern and shows that cGi-500-'negative' cells express SM22 (**Figure 24K-M**).

For FRET studies, bright cells in cultures from SM445-cGi-500-5 mice show sufficient cGi-500 expression levels, while other SMCs in the same culture and all SMCs derived from SM445-cGi-500-1 mice were not bright enough for cGMP FRET imaging. Expression of cGi-500 was further analyzed in tissues of SM445-cGi-500-5 mice. Acute preparations of aorta, bladder, and colon were analyzed using a fluorescence stereo-microscope with EGFP filterset (**Figure 25A-C**). The fluorescence intensity of tissues from SM445-cGi-500-5 is higher in comparison to tissues from wild type mice. Especially the bladder shows a brighter signal (**Figure 25B**), while the signal difference of the aorta is not that prominent, probably due to strong background fluorescence of extracellular matrix components (**Figure 25A**). The colon from SM445-cGi-500-5 mice shows localized fluorescence corresponding to single SMCs with strong fluorescence among other, non-fluorescent or weakly fluorescent cells (**Figure 25C**).

Furthermore, tissue isolated from SM445-cGi-500-5 transgenic mice was analyzed, which should be used in FRET imaging experiments. The walls of vessels inside the retina show cGi-500 expression that is non-uniformly distributed between individual cells (**Figure 25D, E**), which correlates with the heterogeneous cGi-500 expression observed in cultured SMCs isolated from the same mouse line (**Figure 24E-M**). Expression of cGi-500 in vessels of the cremaster muscle, which is a thin (~50-100 μm) striated muscle that surrounds the testicle was found in very rare cases (**Figure 25F**). In summary, the expression of cGi-500 in cells from SM445-cGi-500-1 mice turned out to be insufficient for cGMP FRET experiments, while cGi-500 expression in cells and tissues from SM445-cGi-500-5 mice is strong enough for FRET imaging experiments.
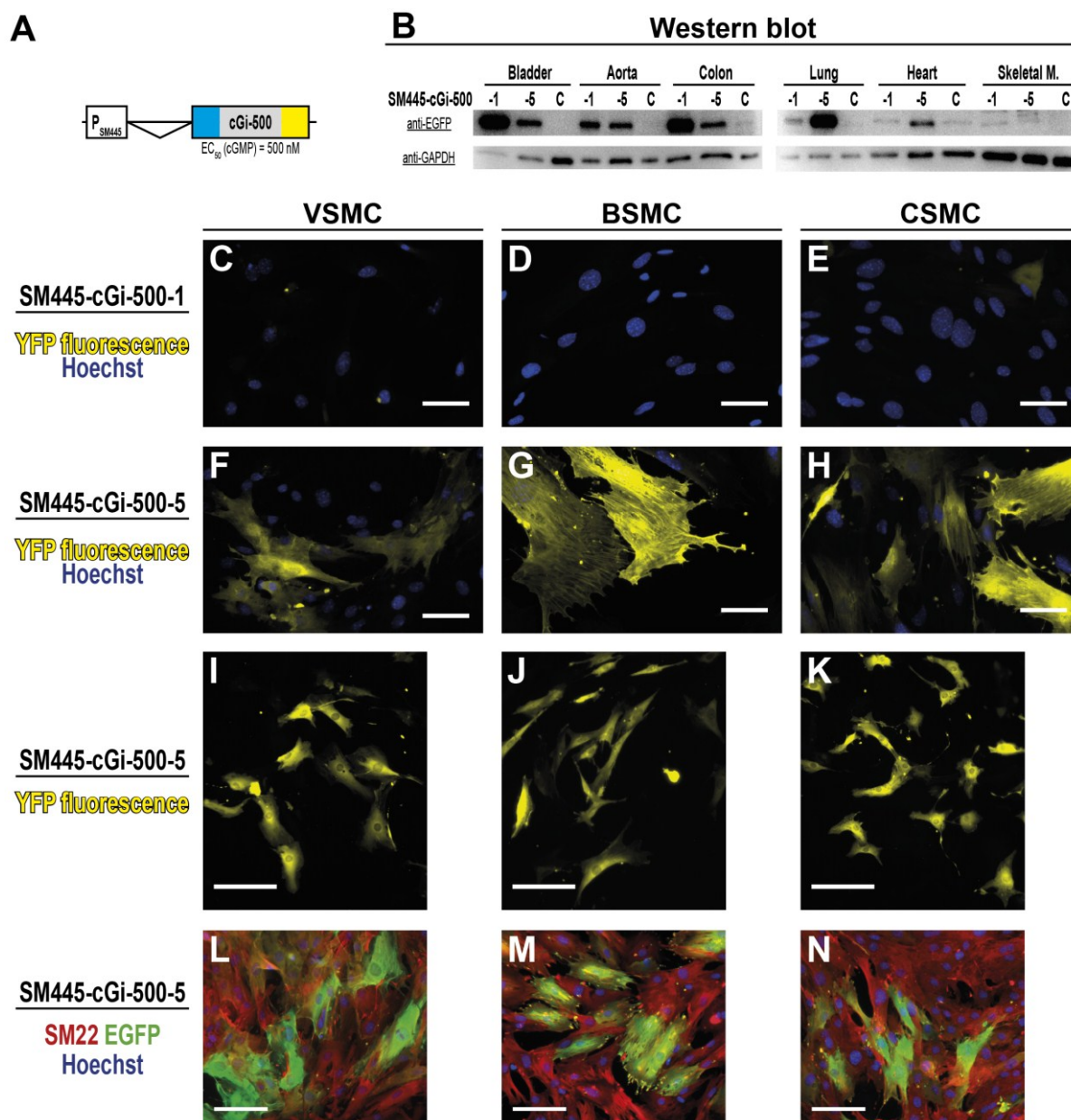
Figure 24. Analysis of cGi-500 expression in SM445-cGi-500 transgenic animals.

A. SM445-cGi-500 transgene structure. The SM445 promoter fragment (see ref. 469) from the gene of the smooth muscle-specific SM22 protein drives cGi-500 expression. **B.** Western blot analysis of tissue samples (10 µg protein) from SM445-cGi-500 transgenic mice. Membranes were incubated with a rabbit EGFP antiserum (1:3000) and anti-GAPDH antibodies from rabbit (1:5000) to control for equal loading. Antibody binding was detected with HRP-coupled goat anti-rabbit antibodies (1:5000) in a chemiluminescence reaction. **C-H.** Vascular SMCs from aorta (VSMCs), SMCs from bladder (BSMCs), and colonic SMCs (CSMCs) from SM445-cGi-500-1 mice show even cGi-500 expression, which is low compared to some SMCs in cultures derived from SM445-cGi-500-5 mice. Images of formaldehyde-fixed cells (passage 1 for VSMCs and CSMCs, passage 2 for BSMCs) were acquired using an EYFP filterset to detect cGi-500 fluorescence (yellow). The same imaging conditions (magnification, exposure time, brightness, contrast) were applied to SMCs isolated from the same organ; nuclear DNA staining with Hoechst 33258 (blue). Scale bars: 50 µm. **I-K.** Heterogeneous cGi-500 expression in primary SMCs derived from SM445-cGi-500-5 mice. Live fluorescence images were acquired with an EYFP filterset (yellow) after 5 days in culture. Scale bars: 100 µm. **L-N.** SMCs were fixed after 24 h incubation in serum-free medium and incubated with a rabbit antiserum detecting the smooth muscle marker protein SM22 (1:500) and with EGFP antibodies from mouse (1:1000). Antibody binding was detected with anti-rabbit and anti-mouse secondary antibodies conjugated with Alexa 488 (green) and Alexa 555 (red), nuclear DNA staining with Hoechst 33258 (blue). Scale bars: 100 µm.
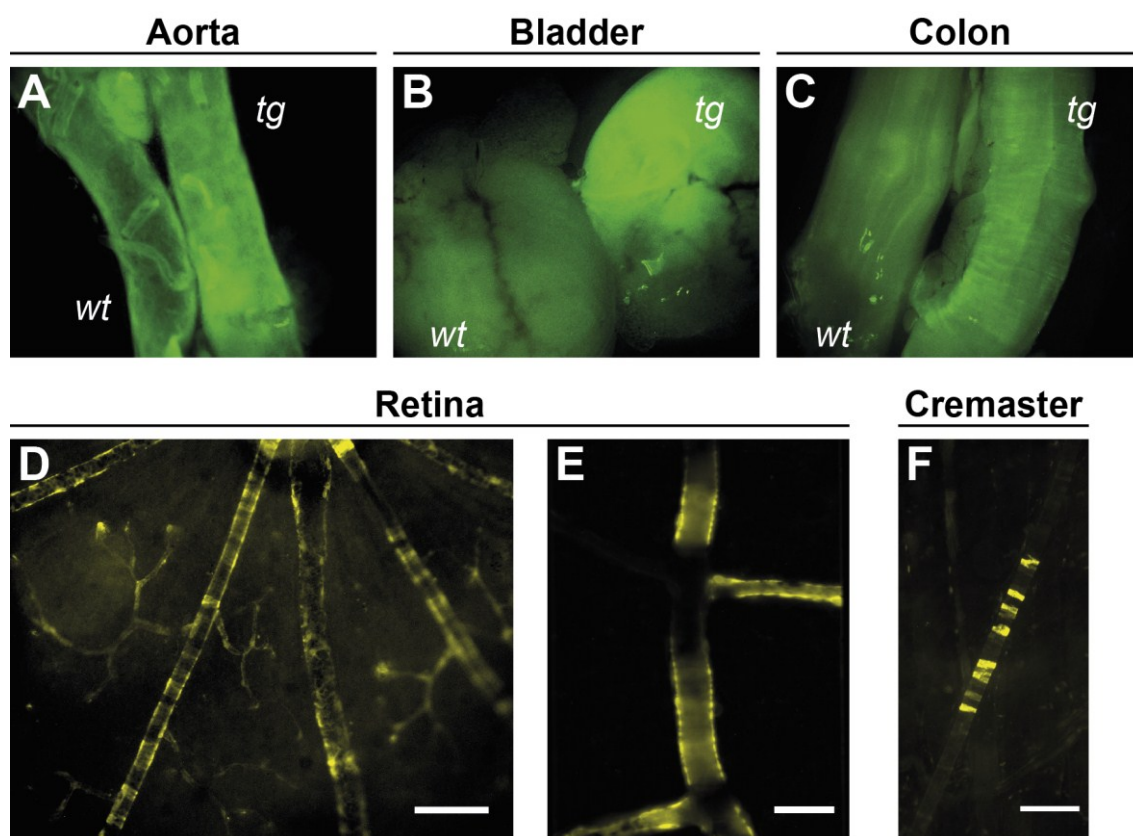
Figure 25. cGi-500 expression in organs and tissue of SM445-cGi-500-5 mice.

A-C. cGi-500 fluorescence (green) in isolated, smooth muscle-containing organs of SM445-cGi-500-5 transgenic (tg) mice. Images were acquired with a fluorescence stereomicroscope (in the Department for Anatomy and Experimental Embryology, University of Tübingen) upon illumination with an EGFP filterset. Organs of a wild type (wt) mouse serve as control. **D-F.** cGi-500 fluorescence (yellow) in vessel walls of tissue samples isolated from SM445-cGi-500-5 transgenic mice. Images were acquired with a fluorescence microscope using an EYFP filterset. Note that cGi-500-positive vessel walls in the cremaster muscle, as shown in panel F were observed only in very rare cases, while cGi-500-positive vessel walls were observed in all tested retinas. Scale bars for D, F: 100 µm, E: 25 µm.

3.2.5 FRET-based cGMP Imaging in Smooth Muscle Cells

FRET studies were performed with cGi-500-expressing SMCs from aorta, bladder, and colon. **Figure 26** shows typical cGMP FRET results obtained with VSMCs. Here, the experiment was performed at $40\times$ magnification, and three cells were in the field of view (FOV). Cells are stimulated with the cGMP-elevating drugs CNP and DEA/NO. cGMP binds to cGi-500 and induces a conformational change of the sensor protein that leads to a reduction in FRET efficiency. The reduced energy transfer from ECFP to EYFP leads to an increase of ECFP emission detected at 480 nm (F_{480}), and at the same time to decreased EYFP emission detected at 535 nm (F_{535}). Therefore, an increase in the F_{480}/F_{535} ratio is detected (**Figure 26**), which correlates with intracellular cGMP levels within a range of 100 nM to 3 µM cGMP.
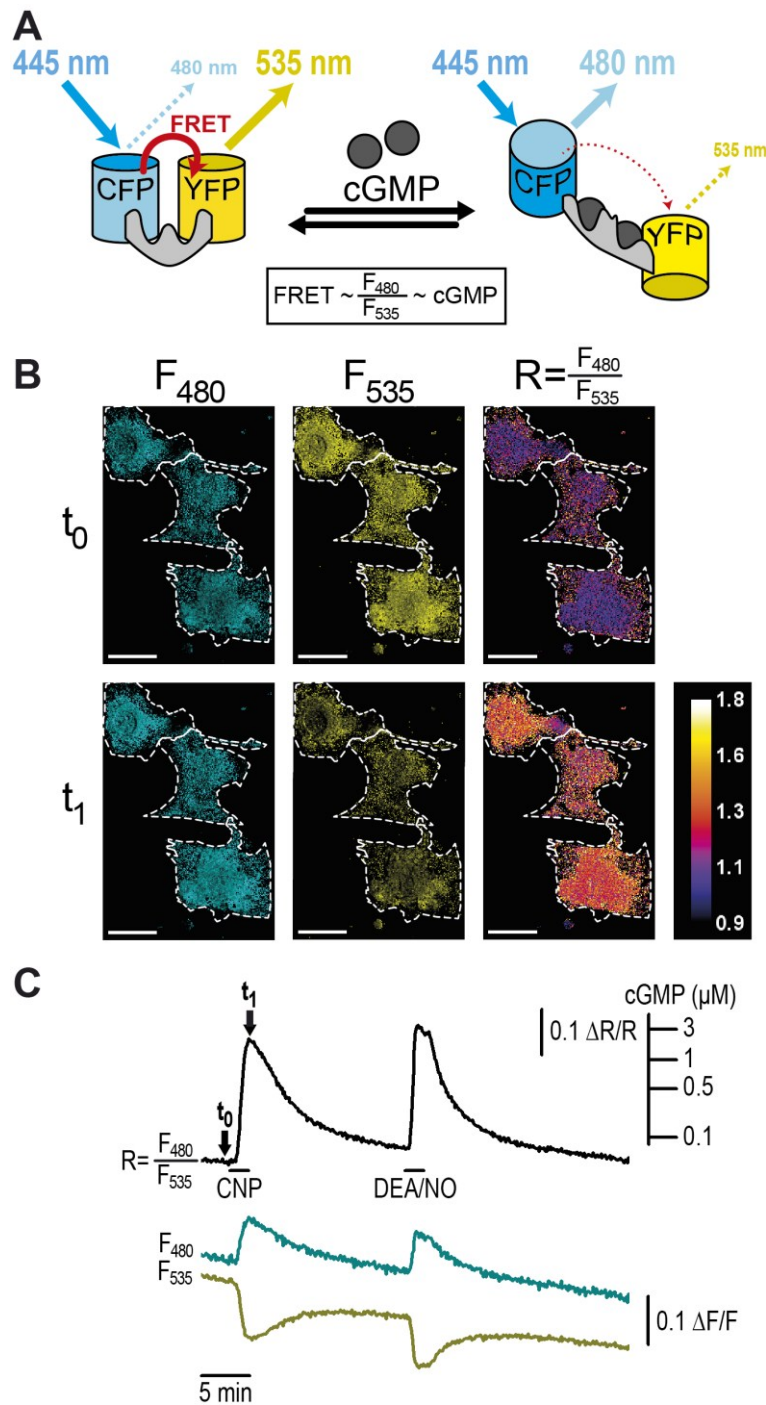
Figure 26. cGMP FRET in primary VSMCs from SM445-cGi-500-5 mice.

A. Working principle of FRET-based cGi-type cGMP biosensors. In cGi biosensors, the cGMP binding domain of bovine cGKI (grey) is flanked by ECFP and EYFP. In the absence of cGMP, FRET occurs from excited ECFP to EYFP leading to light emission from EYFP. Upon cGMP binding, the cGi biosensor undergoes a conformational change that causes a decrease in FRET efficiency. Thus, light emission from EYFP at 535 nm is reduced, while emission from ECFP at 480 nm is increased. The FRET efficiency of cGi-type biosensors is depicted as the F_{480}/F_{535} (=ECFP/EYFP) emission ratio, which rises upon cGMP binding to the biosensor. **B.** Compared to baseline (t_0), superfusion with 50 nM CNP leads to a F_{480}/F_{535} ratio increase (t_1), which is a measure for intracellular cGMP. Images are normalized to averaged baseline images from the beginning of the experiment. Cell borders as indicated, scale bars: 20 µm. **C.** Stimulations with 50 nM CNP and 100 nM DEA/NO lead to reversible cGMP elevations. Normalized traces show response of the upper left cell shown in panel B. Time points shown in B are indicated by t_0, t_1. cGMP calibration from **Figure 27**.

Normalized F_{480}/F_{535} ratio changes $\Delta R/R$ are correlated with intracellular cGMP concentrations (**Figure 26C**, calibration bar). At concentrations lower than 100 nM, cGMP concentration changes cannot be resolved, as the sensor does not bind enough cGMP to induce detectable changes in FRET efficiencies. At concentrations higher than 3-5 μM the cGi-500 sensor is saturated and increasing cGMP concentrations do not lead to further changes in FRET efficiency.

To establish the calibration of the cGi-500 sensor within its dynamic range, $\Delta R/R$ values need to be measured at defined cGMP concentrations. For that purpose, a protocol was established, where SMCs are permeabilized with β-escin and superfused with defined cGMP concentrations. After optimization of β-escin incubation, permeabilized cells retain the cGi-500 biosensor in their cytosol for 90 min of continuous superfusion with intracellular-like medium (ICM), while cGMP in the superfusate rapidly enters and leaves permeabilized cells (**Figure 27**). For the final calibration, ROSA26-CAG-cGi-500 VSMCs (see also 3.2.8) were imaged at 16× magnification and permeabilized with 50 μM β-escin for 80 s. Increasing cGMP concentrations (10 nM to 100 μM) were applied for 5 min followed by 5 min washes with ICM (**Figure 27A**). In order to obtain a calibration curve, baseline-corrected $\Delta R/R$ values from plateaus at respective cGMP concentrations were averaged from 88 cells in three experiments, and were used to fit a dose-response curve (**Figure 27B** and **Table 14** on p.139). To estimate cGMP concentrations from measured $\Delta R/R$ values, the parameters of the dose-response curve were used to calibrate baseline-subtracted $\Delta R/R$ traces (e.g. in **Figure 26C**).
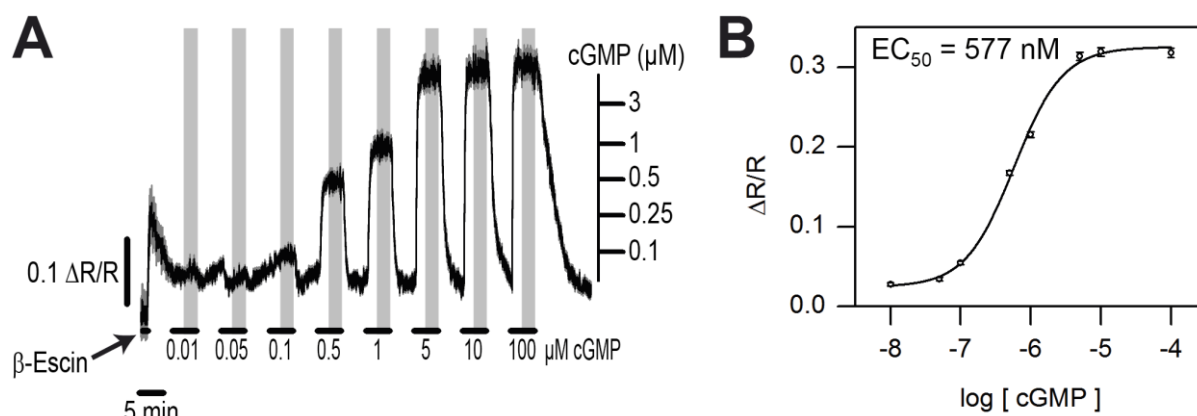

Figure 27. In-cell calibration of cGi-500 in β-escin-permeabilized VSMCs from ROSA26-CAG-cGi-500 mice.

A. After permeabilization with β-escin, cells were superfused with increasing cGMP concentrations (black bars) followed by a washout after each cGMP application. For every cell, $\Delta R/R$ values for each cGMP concentration were averaged during 160 s of the plateau (indicated by gray bars). These values were used for calibration; data shown are mean±SEM of 22 cells. The cGMP calibration bar at the right was generated using the calibration curve shown in panel B. **B.** To establish the cGMP calibration curve, $\Delta R/R$ values (mean±SEM) were pooled from 88 cells measured in three independent experiments (including the experiment shown in A). Data were used to fit a dose-response curve with an EC_{50} value of 577 nM (see also **Table 14** on p. 139).

By using cGMP FRET imaging, pharmacological experiments were performed with sub-confluent, primary SMCs isolated from SM445-cGi-500-5 mice, which were serum-starved for ≥24 h prior to imaging (**Figure 28**). Initially, SMC response was tested upon stimulation with DEA/NO. For that purpose, SMCs were stimulated with increasing DEA/NO concentrations. Areas of the resulting ΔR/R changes were used to determine EC_{50} values of dose-response curves. Representative results are shown in **Figure 28A** and **B**. Resulting EC_{50} values are 73±8 nM for BSMCs; 106±7 nM for VSMCs, and 147±1 nM for CSMCs; meaning that BSMCs show the highest and CSMCs the lowest DEA/NO sensitivity (see also **Table 15** and **Table 16** on p. 139). Although some variation exists between experiments with individual cell cultures, the sensitivity was typically found in the order BSMCs > VMSCs > CSMCs. Despite the fact that cells show different sensitivities when analyzed by ΔR/R peak areas, all cells show saturation of the FRET sensor at 100-150 nM DEA/NO; at these DEA/NO concentrations the intracellular cGMP concentration exceeds 3-5 µM.

In another set of experiments, SMC sensitivities against stimulation with natriuretic peptides were tested. In these experiments, VSMCs reacted to both ANP and CNP, whereas BSMCs react to CNP but not ANP, and CSMCs to neither ANP nor CNP (**Figure 28C**). Responses to ANP in VSMCs were weaker than responses to CNP, while VSMCs react stronger to CNP than BSMCs. DEA/NO and NP-elicited cGMP transients show a different kinetic behavior – time to reach the maximum and to return to the baseline are longer in ANP- and CNP-induced transients compared to DEA/NO-induced transients. Additionally, cGMP transients elicited by 500 nM CNP do not lead to cGMP concentrations higher than 3-5 µM, in comparison to DEA/NO concentrations of 100-150 nM, which lead to cGMP concentrations ≥3-5 µM that saturate cGi-500 (**Figure 28C**). To test whether cGMP generation upon ANP stimulation in BSMCs or ANP and CNP stimulation in CSMCs is camouflaged by PDE activities, BSMCs or CSMCs were stimulated with ANP and CNP in the presence of IBMX. Also in the presence of this unspecific PDE inhibitor, no FRET changes were detected (not shown). It must be noted that culture conditions affect responses to natriuretic peptides; in subcultures and primary cells that were not serum-starved, altered reactions to ANP and CNP were detected (not shown).

Figure 28 (right). cGMP pharmacology in different primary SMC types from SM445-cGi-500-5 mice.
A. DEA/NO-cGMP dose-response studies with n cells in the experiment. **B.** Estimation of ΔR/R peak areas upon stimulation with increasing DEA/NO doses (in nM). SMCs show different DEA/NO sensitivities (EC_{50} BSMCs: 73±8 nM; VSMCs: 106±7 nM; CSMCs: 147±1 nM; cell numbers as in A; statistics in **Table 15** and **Table 16** on p.139). Data is normalized to the dose-response curve maximum (**Table 15**). **C.** VSMCs increase cGMP upon ANP and CNP stimulation, while BSMCs respond to CNP, but not ANP. CSMCs do not respond to ANP or CNP (ANP and CNP concentrations in nM). DEA/NO (VSMCs: 500 nM; BSMCs: 100 nM; CSMCs: 100 nM) was applied to check for cell viability. **D and E.** Reversible phosphodiesterase inhibition leads to increased DEA/NO responses. Cells were stimulated with sub-saturating amounts of DEA/NO (VSMCs: 75 or 20 nM, BSMCs: 40 or 50 nM, CSMCs: 100 nM) before and after pre-incubation with 30 µM sildenafil (D) or 300 µM IBMX (E), and after inhibitor washout. Peak areas are normalized to the first peak; statistical analysis in **Table 17** on p. 140. ΔR/R changes in panel A, C, D are given as mean±SEM (of n cells in the experiment). Representative results from 3 experiments with independent cell cultures are shown.

A DEA/NO

VSMC
n=10

10 25 50 75   100   150   250   500

BSMC
n=10

|0.2 ΔR/R

10 20 40   80   100   250   500

CSMC
n=5

10 75 100 150 250   500   1000

5 min

B

norm. peak area

○ VSMC
□ BSMC
△ CSMC

log [DEA/NO]

C   ANP   CNP

VSMC
n=10

50   250   500   DEA/NO

n=15

50   250   500   DEA/NO

BSMC
n=9

10 100   500 DEA/NO

n=8

10 100   500   DEA/NO

CSMC
n=7

50 250 500 DEA/NO

n=8

50   250 500 DEA/NO

0.2 ΔR/R

5 min

D DEA/NO ± Sildenafil

BSMC
n=5

SIL

DEA/NO   DEA/NO   DEA/NO

0.2 ΔR/R

5 min

norm. peak area

n=12 VSMC
n=5 BSMC
n=22 CSMC

DEA/NO   DEA/NO   DEA/NO
         +SIL

E DEA/NO ± IBMX

BSMC
n=4

IBMX

DEA/NO   DEA/NO   DEA/NO

0.2 ΔR/R

5 min

norm. peak area

n=10 VSMC
n=4 BSMC
n=17 CSMC

DEA/NO   DEA/NO   DEA/NO
         +IBMX

To analyze effects of the PDE5-specific inhibitor sildenafil or the unspecific PDE inhibitor IBMX on DEA/NO-induced cGMP transients, SMCs were stimulated 3 times with sub-saturating amounts of DEA/NO (**Figure 28D, E**). After the first stimulus, cells were incubated with either 30 µM sildenafil or 300 µM IBMX, and were stimulated again with DEA/NO in presence of the inhibitor. Inhibitor concentrations were chosen to be appropriate for complete inhibition of the respective PDEs. After the inhibitor superfusion was finished, cells were washed for another 10 min with imaging buffer to remove inhibitors, and were stimulated a third time with DEA/NO. For analysis, peak areas of ΔR/R changes elicited by the three DEA/NO stimuli were compared; areas were normalized to the area of the first peak (statistical evaluation in **Table 17** on p. 140). In presence of sildenafil, the DEA/NO-elicited cGMP transient is 1.6-2.6 times larger compared to the stimulation without sildenafil (**Figure 28D)**, while incubation with IBMX leads to cGMP transients, which are nominally 8-8.6 times increased compared to the control stimulation (**Figure 28E**). The amount of cGMP generated in presence of IBMX might actually be higher than estimated from the comparison of peak areas, as cGi-500 becomes saturated, and a reduction of cGMP levels down into the sensors' dynamic range occurs only upon IBMX washout. In contrast, cGMP levels start to return to baseline when sildenafil is still present. In both cases, the third cGMP transient measured after inhibitor washout has the same or a smaller area than the first peak.

In addition to previously shown FRET measurements, efforts were undertaken to use another route of drug application, namely by local delivery of cGMP-elevating drugs via a fine glass pipette. In initial experiments, a glass pipette was filled with 10 µM CNP and 5 µg/mL fluorescein-coupled BSA, which was used to visualize the spread of the drug-containing solution. The glass pipette was positioned with a micromanipulator and drugs were applied via air pressure (Eppendorf FemtoJet, kindly provided by Prof. G. Dodt) from the pipette into the superfusate against the direction of superfusion. At 16× magnification, distinct cells within the FOV were subsequently stimulated (**Figure 29**).
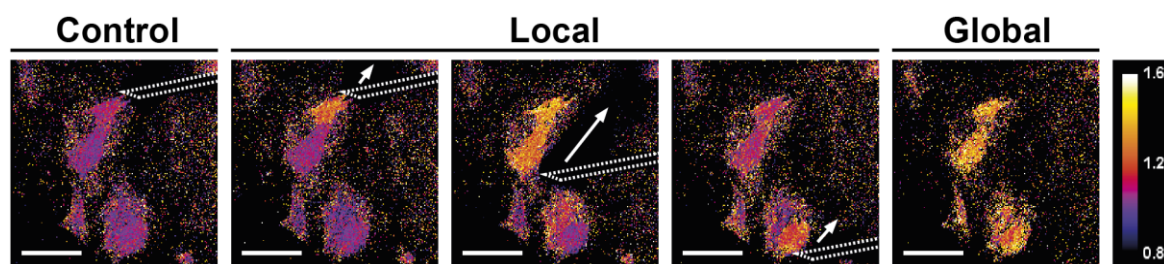

Figure 29. Local CNP stimulation with a micromanipulator-driven glass pipette.

BSMCs from SM445-cGi500-5 mice were used. In the control image, the glass pipette (dashed line) is located in the FOV, but no CNP is delivered. Local cGMP elevations restricted to single cells at different locations are achieved by CNP delivery through the glass pipette, the direction of CNP flow is indicated by arrows. At the end of the experiment, cells were stimulated by CNP in the superfusate (global). Images represent ΔR/R ratio changes normalized to baseline images from the beginning of the experiment, scale bars: 100 µm.

3.2.6 FRET-based cGMP Imaging in Cultured Neurons

After establishment of primary neural cell cultures and characterization of cultured neural cells for cGi-6000 expression, cGMP FRET imaging experiments were performed with cGi-6000-expressing cells. Expression in astrocytes isolated from the cortex of cGi-6000 transgenic animals was not sufficient for FRET experiments, as signal intensities were too low for FRET imaging (4×4 camera binning, exposure time 200-500 ms at $16 \times$ magnification). In cultures of hippocampus-derived cells, both astrocytes and neurons express cGi-6000, and were distinguished by their morphology (neurons: small soma, thin processes; astrocytes: larger somas, thicker processes, see also **Figure 23C**). cGi-6000 was not very strongly expressed in hippocampus-derived cells and only weak FRET responses were detected in neurons upon stimulation with DEA/NO (not shown). Expression of cGi-6000 was stronger in cultured CGNs, and FRET imaging experiments with repeated drug stimulations were performed. CGNs reacted to DEA/NO stimulation with cGMP elevations, also when repeated stimuli were applied (**Figure 30A**). Additionally, other drug stimuli were tested, but CGNs did not react with detectable cGMP elevations to natriuretic peptides, acetylcholine, noradrenaline, glutamate, or high K^+ concentrations (not shown). To test if these substances exert an effect on Ca^{2+} levels in CGNs, cells were loaded with fura-2 to detect changes in intracellular Ca^{2+} concentrations. CGNs react to K^+ and glutamate stimulations with reversible Ca^{2+} elevations, while DEA/NO and CNP did not lead to changes in intracellular Ca^{2+} concentration (**Figure 30B**). Noradrenaline did not lead to Ca^{2+} increase in CGNs, but in astrocyte-like cells present in the CGN culture (**Figure 30B**). Of interest is that glutamate-induced Ca^{2+} transients became smaller in amplitude, when CGNs were stimulated with DEA/NO before stimulation with glutamate. This suggests that cGMP signaling might affect glutamate-induced calcium transients. Although 252 individual CGNs were analyzed in this single experiment with fura-2, findings were not yet reproduced in other experiments and need further confirmation.
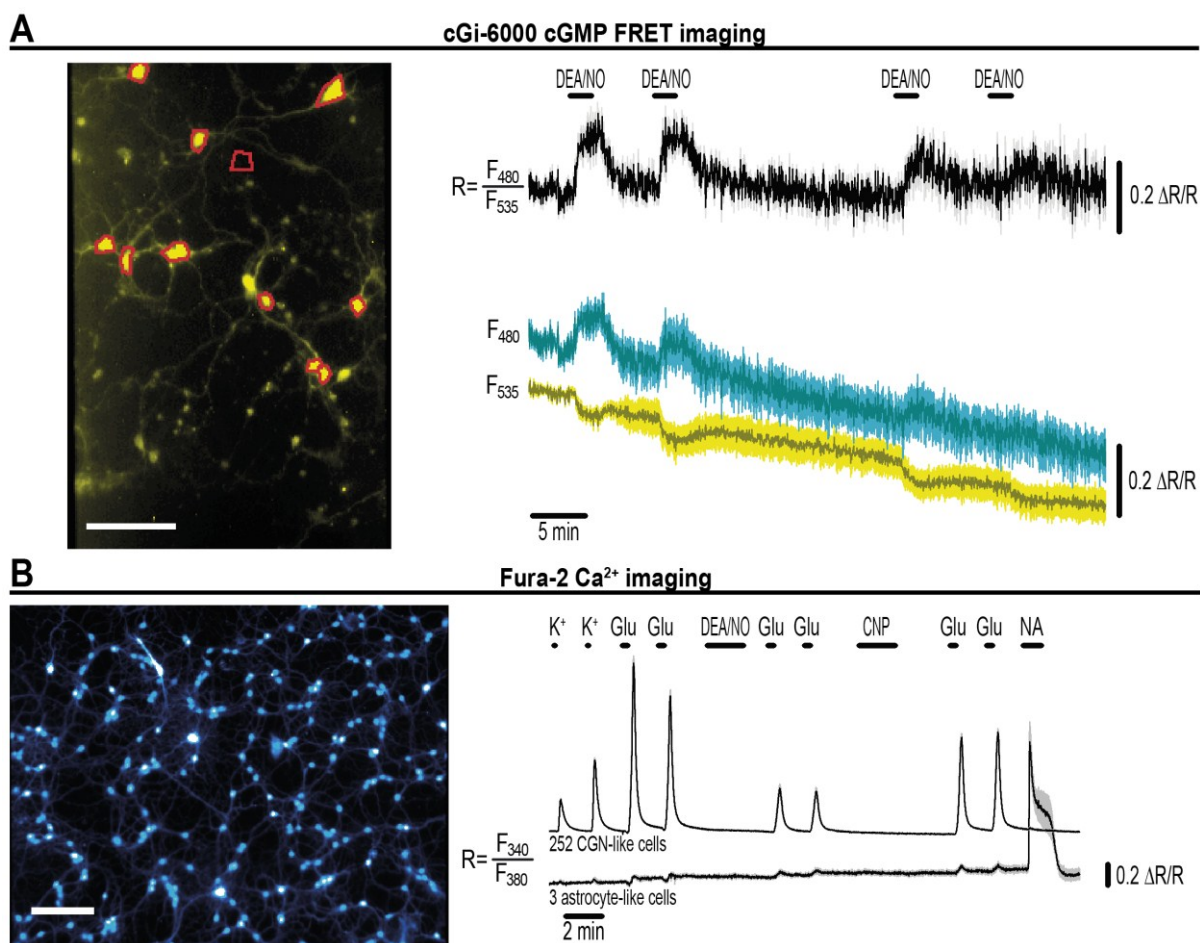
Figure 30. cGMP FRET (A) and fura-2 Ca^{2+} (B) imaging in CGNs isolated from CMV-cGi-6000-10 mice.
A. CGNs after 5 days in primary culture were used for imaging. Upon multiple stimulations with 100 nM DEA/NO, cells responded repeatedly with cGMP elevations. Regions of interest (ROIs) defining the cell bodies and a background region are indicated in red. Relative changes of F_{480} (ECFP) and F_{535} (EYFP) fluorescence ($\Delta F/F$) and of the F_{480}/F_{535} ratio ($\Delta R/R$) represent means±SEMs of the individual ROIs. **B.** Fura-2 Ca^{2+} measurements in CGNs after 7 days in culture. Field of view used for measurements is shown without ROIs, data is given as mean±SEM of individual cells (numbers as indicated). Stimulations were performed with 30 mM K$^+$, 50 µM glutamate (Glu), 200 nM DEA/NO, 200 nM CNP, or 2 µM norepinephrine (NA). Measurement shown in A was performed together with N. Fomin. Scale bars A: 100 µm, B: 50 µm.

3.2.7   FRET-based cGMP Imaging in Isolated Retinas

After successful establishment of cGMP FRET imaging in cultured cells, imaging of tissue samples was performed. Isolated retinas of SM445-cGi-500-5 mice turned out to be suitable for imaging studies. After isolation, the retina is immobilized on cellulose acetate/nitrate filter membranes fixed onto a glass coverslip in the superfusion chamber (**Figure 31A**). The filter paper carries a central hole of 2×2 mm, through which the retina is illuminated for FRET measurements (**Figure 31B**), while the retina is superfused with imaging buffer for drug application. The protocol for retina isolation and immobilization was kindly provided by Dr. T. Münch. As already shown in **Figure 25D** and **E**, distinct areas in the vessel walls show cGi-500 fluorescence, while adjacent tissue shows only background fluorescence; a representative FRET experiment is shown in **Figure 31C** and **D**. With

1 µM DEA/NO in the superfusate, no detectable cGMP elevations were observed, while repeated cGMP transients were elicited with 10 µM DEA/NO. No reaction was observed upon stimulation with natriuretic peptides or acetylcholine (not shown). In comparison to experiments with cultured smooth muscle cells, the DEA/NO concentrations necessary to elicit cGMP increases are about 10-fold higher, and changes in cGMP concentrations happen more slowly than in cultured cells (retina *vs.* SMCs time-to-peak maximum: 4 *vs.* 1 min, peak width: 15 min *vs.* 5 min).
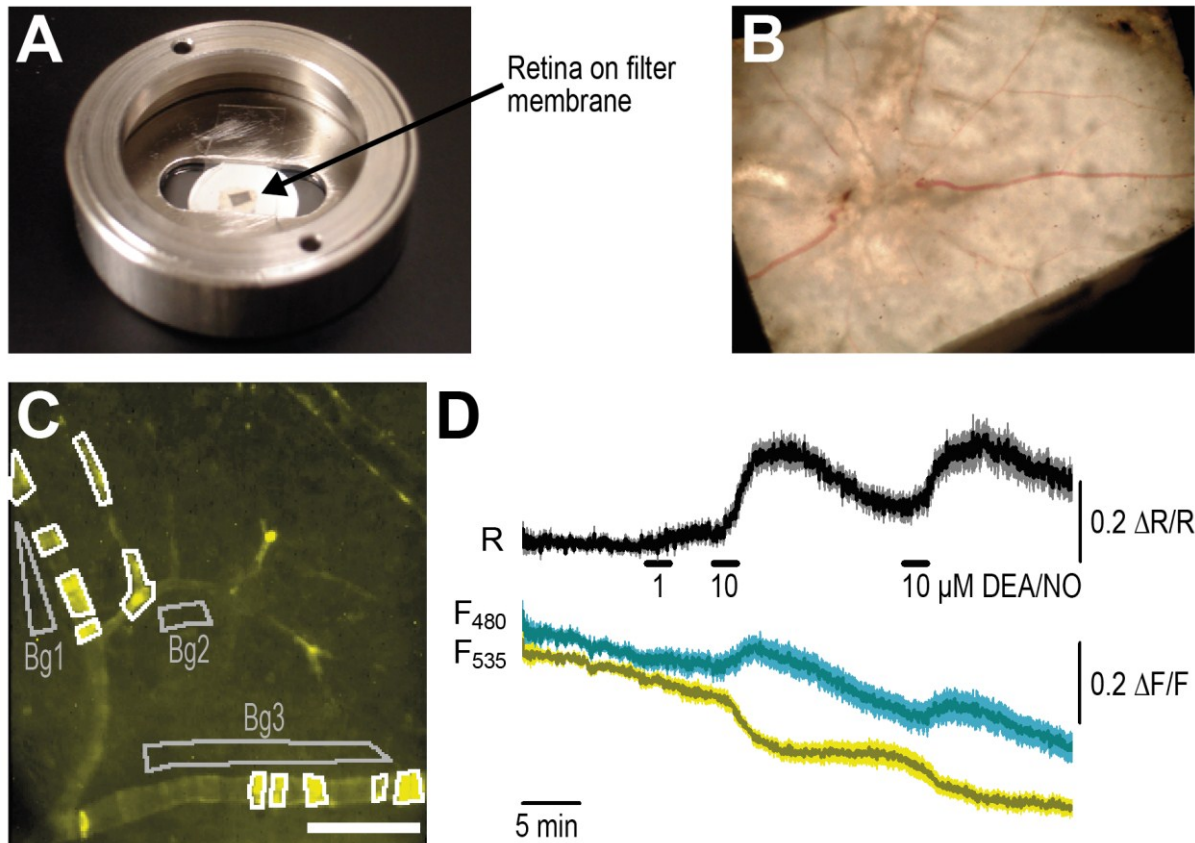

Figure 31. cGMP transients in retina vessel walls of a SM445-cGi-500-5 mouse.

A. Setup of the superfusion chamber for FRET imaging experiments with isolated retinas immobilized for superfusion. **B.** Localization of the retina on the filter membrane (black). Vessels leave the blind spot on the middle-left part of the image. **C.** Regions of interest (white) used for cGMP FRET measurements shown in D, scale bar: 100 µm. **D.** DEA/NO superfusion leads to cGMP elevations in retina vessels isolated from SM445-cGi-500-5 mice. Responses of n=11 fluorescent regions shown in A were averaged and shown as mean±SEM. ROIs were corrected with adjacent background regions (Bg1-3). A representative result of three experiments is shown.

3.2.8   Intravital FRET Imaging of the Cremaster Muscle

After it has been shown that cGMP FRET imaging is feasible in tissue preparations from SM445-cGi-500-5 mice, it was tested whether cGMP imaging can be performed in living animals using intravital microscopy of the cremaster muscle (**Figure 32A**). Because smooth muscle cells in vessel walls of the cremaster muscle in SM445-cGi-500-5 mice express cGi-500 only in very rare cases (no cGi-500-expressing cells are found at all, or single cells within the whole preparation), experiments were performed with mice of the ROSA26-CAG-cGi-500 mouse line. This mouse line was generated by Lai Wen via gene targeting with a construct (generated by the author of this work) similar to the ROSA26-mT/sr39tk targeting vector (see 3.1.1.3). For the generation of ROSA26-CAG-cGi-500 transgenic mice, ESCs that were targeted with the 'silenced' transgene were transfected with a Cre expression plasmid. Cre-recombined ESCs carrying the 'activated' transgene were used for blastocyst injection. In resulting ROSA26-CAG-cGi-500 transgenic mice, cGi-500 expression is driven by the CAG promoter from the ROSA26 locus, leading to ubiquitous cGi-500 expression (Thunemann & Wen, unpublished results).

Intravital imaging experiments were performed in the laboratory of Prof. C. de Wit (Universität Lübeck). The experimental animal is anesthetized, intubated with an intratracheal tubus for forced breathing and receives an intravenous catheter (*Vena jugularis*) for continuous supply with anesthetic drugs. Then, the mouse is placed on a specialized microscope stage, one cremaster muscle is prepared, and stretched above a coverslip with surgical suture (**Figure 32A**). For FRET imaging, water immersion objectives (10× or 40×) approximate the cremaster muscle from the top. The muscle is continuously superfused with pre-warmed BBSS at 34°C. In first attempts, it was tried to detect FRET signal changes in walls of small arteries, which are surrounded by cGi-500-expressing striated muscle (**Figure 32B**). Upon addition of sodium nitroprusside (SNP) or DEA/NO to the superfusate, vessels undergo relaxation, and after termination of SNP or DEA/NO superfusion, vessels contract again (**Figure 32B.1-B.3**). Additionally, acetylcholine (ACh) and adenosine (Ado) were used as control stimulants, and vessels were dilated with Cromakalim (K_{ATP} channel opener) and Verapamil (Ca^{2+} channel blocker) and then stimulated with SNP or DEA/NO. During evaluation of these experiments (similar to the experiment shown in **Figure 32B**), it was not possible to detect F_{480}/F_{535} ratio changes that are clearly attributed to FRET efficiency changes and not caused, for example, by movement artifacts or camouflaged by background fluorescence from striated muscle.

Then striated muscle was removed from a small artery (according to ref. 465) to reduce off-target fluorescence by surrounding muscle (**Figure 32C**). Upon stimulation of this prepared vessel, F_{480}/F_{535} ratio changes were detected, which clearly derive from FRET efficiency changes, because decreasing F_{535} signal intensities correlate with increasing F_{480} signal intensities (**Figure 32D**). Reversible cGMP

transients were detected upon repeated stimulation with 10 µM DEA/NO, but not upon stimulation with 10 µM Ado, which is a cGMP-independent vasoactive drug. Vessel relaxation was not observed upon any kind of stimulation after surrounding striated muscle has been removed. Overall, these results obtained in a well-known physiological model show that the cGi-500 FRET sensor is suitable for cGMP imaging in live animals.
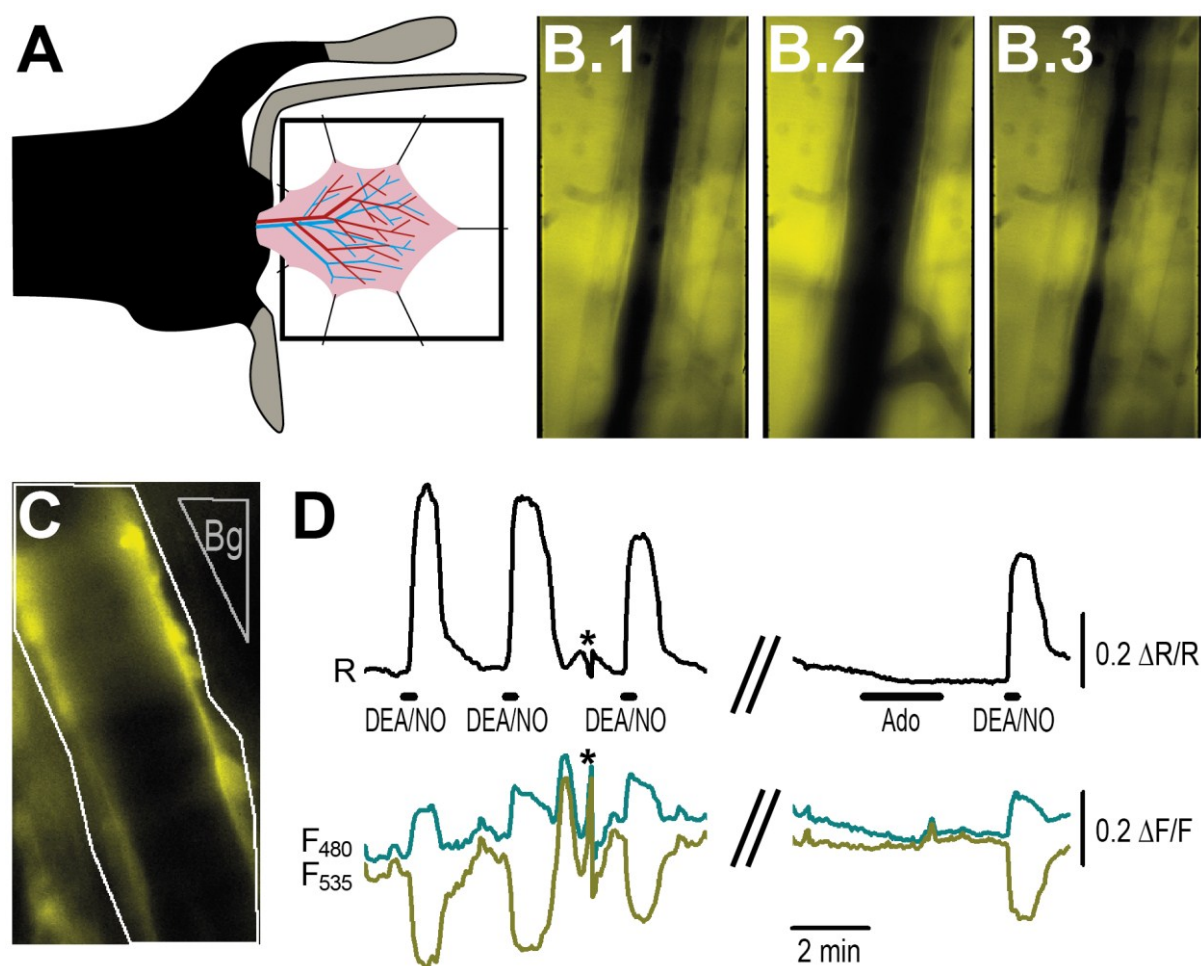

Figure 32. cGMP FRET imaging in small arteries of the cremaster muscle of a living ROSA26-cGi-500 sensor *knock-in* mouse.

A. Schematic drawing of the imaging setup. The anesthetized animal is placed in supine position on a stage where the cremaster muscle is stretched above a coverslip and superfused with BBSS; the objective (not shown) approximates the muscle from the top. **B.** Fluorescence images (EYFP channel) of a vessel (lumen appears in black) before (B.1), during (B.2), and after (B.3) superfusion with 10 µM sodium nitroprusside (SNP). Note the strong fluorescence of striated muscle surrounding the vessel. Images were acquired at 10× magnification with 120 ms exposure time at 2×2 camera binning with 2 acquisitions/s. **C.** Vessel in the cremaster used for FRET imaging shown in D. The surrounding striated muscle was manually removed before imaging. **D.** DEA/NO superfusion (10 µM) induces reversible cGMP elevations in a small artery of the cremaster muscle shown in C. Adenosine (Ado, 10 µM), which is known to induce relaxation via the cAMP pathway does not induce detectable ratio changes. * indicates artifacts induced by focus drift, which lead only to minor F_{480}/F_{535} ratio changes. Experiment was performed at 40× magnification with 150 ms exposure time at 2×2 camera binning with 2 acquisitions/s.

4 Discussion

4.1 Cell Tracking with PET

The major aim of this project is the establishment of a modular genetic system for noninvasive cell tracking with PET. For that purpose, mouse lines were generated that carry conditional *HSV1*-sr39tk reporter transgenes, which are activated in a Cre-catalyzed reaction by the excision of a 'STOP' cassette. The *HSV1*-sr39tk protein phosphorylates radiolabeled nucleoside analogues used as PET tracers, which are not phosphorylated by endogenous thymidine kinases. The retention of phosphorylated tracer molecules in *HSV1*-sr39tk-expressing cells is detected noninvasively with the PET method (199). By inserting the conditional *HSV1*-sr39tk reporter transgene into the ubiquitously expressed ROSA26 locus, *HSV1*-sr39tk expression can be induced in distinct tissues depending on Cre expression. This is achieved by breeding mice carrying the 'silenced' *HSV1*-sr39tk reporter transgene to mice with appropriate Cre transgenes.

Two strategies were used to generate conditional reporter *HSV1*-sr39tk transgenes. In both cases, the transgene was introduced into the ROSA26 locus of ESCs via homologous recombination. Although more elaborate, this approach avoids complicacies arising from the use of mice generated by random mutagenesis (20, 470). The first construct is called 'ROSA26-sr39tk', and designed in a way that *HSV1*-sr39tk expression is driven by the endogenous ROSA26 promoter after excision of the 'STOP' cassette. The second construct is called 'ROSA26-mT/sr39tk', and the CAG promoter drives *HSV1*-sr39tk expression after excision of the 'STOP' cassette. Both strategies have already been used to generate a variety of conditional reporter constructs, and comparative studies revealed that expression levels are ~10-fold higher when the CAG promoter is used (66). Comparably low expression levels from the ROSA26 promoter have been shown to be insufficient for a reliable detection of FP-based reporters, while detection of reporter gene expression is feasible with reporter genes coding for enzyme activities like β-galactosidase or alkaline phosphatase (60). The signal of these reporters is amplified, as they convert several substrate molecules over an extended period. The signal of FP-based reporters is not amplified, which is a likely explanation for the different performance of these two reporter classes when they are expressed at 'low' levels from the endogenous ROSA26 promoter.

The *HSV1*-sr39tk reporter belongs to the class of enzyme-based reporters, so it can be that comparably weak *HSV1*-sr39tk expression from the endogenous ROSA26 promoter might be sufficient to achieve detectable PET tracer accumulation *in vivo*. Therefore, also the ROSA26-sr39tk construct was used to create *HSV1*-sr39tk reporter mice.

Beforehand, the configuration of a conditional ROSA26 Cre reporter with proven functionality was analyzed. RNA from mice with a Cre-recombined ROSA26-lacZ transgene (64) was isolated and analyzed via RT-PCR. A transcript was amplified that spans from the endogenous ROSA26 exon 1 into the ROSA26-lacZ transgene. Although it was expected to find a transcript of this kind, sequence analysis revealed a remarkable transcript structure. In eukaryotes, the first start codon on a transcript usually serves as translational start point and defines the ORF, while subsequent 'start codons' are not used by the translational machinery (471, 472). In contrast, the amplified ROSA26-lacZ transcript carries several upstream ORFs in the endogenous exon 1 and in the 5' part of the ROSA26-lacZ transgene, which precede the lacZ-encoding ORF. Alternative splicing from exon 1 cannot serve as an explanation for successful lacZ expression, because splicing from any alternative ROSA26 exon 1 variant might lead to omission of the ORF in exon 1, but not to omission of the other short upstream ORFs within the transgene itself. Possible explanations for successful translation of β-galactosidase are alternative transcripts, alternative splicing with cryptic SA sites, translation independent from short upstream ORFs, or omission of start codons due to 'leaky scanning' (472-474). A transcript that unquestionably leads to lacZ expression was not identified, but functional β-galactosidase exists in tissue from Cre$^{tg/+}$; ROSA26-lacZ$^{+/-}$ mice (see 3.1.5).

If the ROSA26-sr39tk design meets the design of the ROSA26-lacZ transgene, it should be possible to build a transgene producing *HSV1*-sr39tk after Cre recombination. The ROSA26-sr39tk transgene was designed accordingly, but another start codon was introduced to reduce the number of 'unproductive' upstream ORFs preceding the *HSV1*-sr39tk-coding ORF. After construction of the ROSA26-sr39tk targeting vector, two targeted ESC clones were obtained in three targeting experiments. Cells from one clone were transfected with a Cre expression plasmid to remove the STOP cassette and to activate *HSV1*-sr39tk expression. Cre-mediated excision of the STOP cassette was detected on the DNA level by Southern blot analysis, and corresponding ESCs die upon GCV treatment and accumulate [^{18}F]FHBG *in vitro*. These findings indicate together with a western blot analysis of ESC protein lysates, that *HSV1*-sr39tk is functionally expressed from the Cre-recombined ROSA26-sr39tk transgene. From one targeted ROSA26-sr39tk ESC clone, transgenic mice were generated and bred to Cre transgenic mouse lines. *HSV1*-sr39tk could not reliably be detected by western blot analysis in protein lysates from tissue of these mice. Primary cells were isolated from double-transgenic mice to proof that Cre recombination leads to expression of functional *HSV1*-sr39tk. CSMCs isolated from CMV-Cre$^{tg/+}$; ROSA26-sr39tk$^{+/-}$ mice die in presence of GCV, and *HSV1*-sr39tk was detected in protein lysates from these cells. The results obtained with the ROSA26-sr39tk mouse line indicate that *HSV1*-sr39tk expression is induced by Cre recombination, but expression levels are eventually insufficient to cause detectable [^{18}F]FHBG retention *in vivo*. However, PET experiments should be

performed to test whether detectable [^{18}F]FHBG accumulation can be found in mice carrying the Cre-activated ROSA26-sr39tk transgene.

In parallel, the ROSA26-mT/sr39tk construct was generated, which contains the CAG promoter allowing for higher *HSV1*-sr39tk expression levels. In one gene targeting experiment, 14 targeted ROSA26-mT/sr39tk ESC clones were obtained, and Cre recombination was performed with ESCs *in vitro*. The 'STOP cassette' (= mT cassette) was removed in the resulting ESCs, and respective cells die upon GCV treatment, which indicates *HSV1*-sr39tk presence and functionality. Furthermore, *HSV1*-sr39tk expression levels and [^{18}F]FHBG accumulation are markedly higher in comparison to Cre-recombined ROSA26-sr39tk ESCs. These findings are in line with reports showing that transgene expression from the CAG promoter placed inside the ROSA26 locus is stronger than from the ROSA26 promoter itself (66). The ROSA26-mT/sr39tk mouse line was established, and mice were bred to the RIP-Cre mouse line to label insulin-producing β cells in the pancreas. In one preliminary PET experiment with a mouse of the genotype RIP-Cre$^{tg/+}$; ROSA26-mT/sr39tk$^{+/-}$, [^{18}F]FHBG accumulation was detected in the renal cortex and the spleen, which is known to be absent in mice that do not express *HSV1*-sr39tk (224, 243). Tracer uptake into the pancreas was not seen on PET images, primarily because of the strong signal from adjacent kidneys. However, in autoradiographs of frozen sections from the pancreas isolated after PET imaging, discrete sites of [^{18}F]FHBG accumulation were found, which correspond to the islets of Langerhans that are primarily composed of insulin-producing β cells. These results show that CAG-driven *HSV1*-sr39tk expression can lead to sufficient [^{18}F]FHBG retention for *in vivo* PET imaging. [^{18}F]FHBG accumulation in kidney and spleen was unexpected. Uptake into the kidney can be explained with (off-target) Cre recombination in cells of the renal cortex, which was also detected in an X-Gal staining with the ROSA26-lacZ Cre reporter in mice with RIP-Cre$^{tg/+}$; ROSA26-lacZ$^{+/-}$ genotype (see **Figure 22**). However, no X-Gal staining was observed in spleens of the same animals, so the reason for [^{18}F]FHBG accumulation into the spleen of the RIP-Cre$^{tg/+}$; ROSA26-mT/sr39tk$^{+/-}$ mouse remains elusive.

Although the *HSV1*-sr39tk protein can subsequently phosphorylate many tracer molecules, it can be expected that *HSV1*-sr39tk expression levels must be considerably high to achieve detectable tracer retention. In comparison to enzyme-based reporters like β-galactosidase and alkaline phosphatase, which are usually detected by incubating isolated tissue samples with an excess of reporter substrate for hours or days, *HSV1*-sr39tk needs to be detected *in vivo* by [^{18}F]FHBG retention that occurs within minutes. The PET tracer is injected as bolus into the bloodstream, distributes throughout the organism, and is eliminated soon via kidneys and hepatobiliary system (230, 242). The period, where sufficient tracer amounts are available at the site of interest is considerably shorter than the time between tracer injection and PET imaging. *HSV1*-sr39tk expression levels have therefore to be high enough to cause sufficient tracer retention directly after tracer injection, when [^{18}F]FHBG is present in sufficient

quantities. It still needs to be tested, if this can be achieved when *HSV1*-sr39tk expression is driven by the ROSA26 promoter, while the aforementioned PET experiment indicates that CAG promoter-driven *HSV1*-sr39tk expression levels are sufficient to cause [^{18}F]FHBG retention for *in vivo* detection with PET. However, further studies need to be performed to evaluate the ROSA26-mT/sr39tk mouse line in terms of sensitivity, selectivity, and reproducibility. One fundamental parameter that needs to be determined is the detection limit, i.e. how many *HSV1*-sr39tk-positive cells need to be present at a given location that they can reliably be detected by PET imaging. In previous studies, a detection limit of 1×10^5-1×10^6 cells/mL has been reported (219, 235-237), but the actual threshold is determined by *HSV1*-sr39tk expression levels, cell location, and background from surrounding tissue. This means that although noninvasive cell tracking methods will ultimately lead to a reduction of animal numbers needed for a particular study, initial experiments need be conducted to validate *in vivo* results with results obtained *post mortem* with 'conventional' methods like X-Gal-staining or immunohistochemistry.

With respect to the specificity of Cre recombination, the tracer's pharmacokinetic properties might affect the outcome of PET studies in another way. Assuming that off-target Cre recombination leads to *HSV1*-sr39tk expression in organs like kidney, bladder, and hepatobiliary system, where the tracer resides for longer periods. There, a small proportion of *HSV1*-sr39tk-expressing cells can be sufficient to accumulate comparably high amounts of [^{18}F]FHBG. A result of this kind is observed in the PET experiment with the RIP-Cre$^{tg/+}$; ROSA26-mT/sr39tk$^{+/-}$ mouse, where [^{18}F]FHBG accumulates due to 'off-target' recombination in the kidney, and in the spleen due to reasons that are unknown yet. In addition to this, uptake into kidney and spleen was stronger in comparison to uptake into pancreatic islets, thereby hindering the visualization of pancreatic β cells, which was the actual aim of the PET experiment. These results point to two important aspects, which have to be taken into regard when PET-based cell tracking studies are performed: 1.) Measured tracer retention at distinct locations must not necessary correlate with the number of *HSV1*-sr39tk-expressing cells. Uptake differences that result from varying tracer dwell times can be quantified by performing dynamic PET studies that are evaluated with appropriate mathematical models to describe [^{18}F]FHBG kinetics (e.g. 475). 2.) The pattern of Cre recombination must either be highly specific, or off-target recombination events must be well known and taken into regard during the evaluation of PET studies. A huge step to increase the specificity of Cre recombination is the use of ligand-inducible CreER proteins.

While the ROSA26-sr39tk and ROSA26-mT/sr39tk mouse lines were generated, Yong et al. published a study where β cells in the pancreas were visualized and quantified using a *HSV1*-tk-based reporter and [^{18}F]FHBG (243). For that purpose, a mouse line carrying a triple-fusion reporter under the control of the mouse insulin promoter was generated by random mutagenesis and shows exclusive reporter expression in the pancreas. The authors performed PET imaging studies to quantify β cell mass in the

healthy animal and to follow β cell ablation upon treatment with streptozotocin or therapeutic doses of GCV (243). Their results show that the noninvasive quantification of β cell mass in mouse models of type I or II diabetes is feasible allowing longitudinal studies with the same group of animals. However, as the reporter is constitutively expressed, the noninvasive analysis of β cell turnover is more difficult, as already existing β cells cannot be distinguished from newly formed β cells. The analysis of β cell turnover in animal models of diabetes will eventually provide further insight into the pathogenesis of diabetes or into compensatory and regenerative processes after β cell loss. With GIFM strategies, for example by combining the ROSA26-mT/sr39tk mouse line with a ligand-inducible RIP-CreER mouse line (94), the dynamics of β cell turnover might become accessible through noninvasive PET imaging studies.

The ROSA26-mT/sr39tk mouse line can be used for noninvasive cell tracking studies in various animal models, depending on the availability of appropriate Cre mouse lines. The system can be used to track immune cells (eventually after transplantation), to follow the pathogenesis and/or treatment of cardiovascular diseases like atherosclerosis and myocardial infarction, or to visualize tumor formation, spreading of tumor metastases, or reduction of tumor mass upon anti-cancer treatment. The use of *HSV1*-sr39tk in the brain (e.g. to track cells in animal models of neurodegenerative diseases) is limited to date, as currently available *HSV1*-sr39tk PET tracers do not cross the blood-brain barrier (230, 476). However, in situations where the integrity of the blood-brain barrier is compromised, cell tracking studies in the brain are feasible, for example to study glioma tropism of hematopoietic stem and progenitor cells (224).

The ROSA26-mT/sr39tk mouse line can also be combined with conditional *knock-out* mouse lines, leading at the same time to cell-specific and Cre-dependent activation of *HSV1*-sr39tk expression and deletion of a particular gene. In such a situation, the gene's role for cell proliferation, survival, or migration can be studied *in vivo*. Another possible use of the ROSA26-mT/sr39tk mouse line is the ablation of *HSV1*-sr39tk-expressing cells by delivery of therapeutic GCV doses to the animal, combined with PET imaging studies to follow cell loss and/or regeneration. An application that might find future use in human patients is the tracking of therapeutic cell transplants, which are derived, for example, from induced pluripotent stem cells (477). Although stem cell-based cell therapies represent a promising route towards the treatment of various diseases (478, 479), a major risk of stem cell-derived cell transplants is their uncontrolled growth possibly leading to tumor formation (480). Here, *HSV1*-sr39tk can be used to follow delivery, engraftment, survival, or proliferation of transplanted cells, or to ablate cells, which show adverse patterns of proliferation or migration in animal models or human patients. Valuable sources of donor cells are mice that carry a constitutively active ROSA26-mT/sr39tk reporter transgene, which can be generated by using Cre mouse lines with Cre

expression in the germ-line (481). Although transplantation of *HSV1*-sr39tk-expressing cell can be achieved without mice carrying the ROSA26-mT/sr39tk reporter, but its use circumvents cell transfection or viral transduction, which possibly affect cell physiology or survival.

4.2 cGMP FRET Imaging with cGi Biosensors

The cGMP signaling pathway is an essential regulator of several physiologic functions, and is involved in the pathogenesis of several diseases. Key components of the cGMP pathway reside either in the cytosol or at the plasma membrane, which implies that compartmentalization of cGMP signaling contributes to the regulation of cellular function (249, 377). Conventional cGMP quantification methods (e.g. RIA or ELISA) provide no spatial and only limited temporal resolution and cannot be performed repeatedly with the same sample, while the creation of protein-based cGMP sensors provides non-destructive methods to study spatiotemporal cGMP dynamics in living samples (336). Several FRET-based cGMP biosensors have been developed, and the class of cGis reported by Russwurm et al. possess desirable properties in terms of binding kinetics, cGMP selectivity, and detection sensitivity (252, 336). Several studies with cGMP indicators and other cGMP biosensors have been performed to identify spatially confined cGMP elevations in cultured cardiomyocytes, SMCs, and neurons (264, 343, 408). However, these studies were carried out in cultured cells that were transfected or virally infected with constructs coding for cGMP biosensors, while no cGMP biosensor-expressing transgenic mice have been described so far. For that reason, the major purpose of this project was to generate and characterize transgenic mice that express cGi-type biosensors. The final aim was to show the feasibility of cGMP FRET measurements in live cGi-expressing animals.

Initially, random mutagenesis was used to generate cGi-transgenic mice. Western blot analysis with EGFP antibodies was performed to identify cGi-expressing mice. Mouse lines were identified that express cGi-6000 in cells of brain and heart, and cGi-500 in aortic SMCs and vessel walls of the retina, as well as in bladder and colonic SMCs.

In primary cultures isolated from the brain of newborn cGi-6000-transgenic mice, cGi-6000 expression was detected in cortical and hippocampal astrocytes as well as in hippocampal neurons and CGNs. FRET measurements were performed primarily with CGNs, which increase cGMP levels upon DEA/NO stimulation, but not upon stimulation with other compounds including NPs, K^+ and glutamate. It has been reported that cultured CGNs synthetize cGMP upon stimulation with NO donors, glutamate, kainate, and N-methyl-D-aspartate (NMDA) (482). CNG channels have recently been identified as potential cGMP target in CGNs (483), and another study implicates an important role of Ca^{2+}/calmodulin-regulated PDE1 to control cGMP levels (484). In addition, compartmentalization of cGMP signaling has been proposed for CGNs, especially as nNOS and the

sGC α_2 subunit are targeted to NMDA receptor-associated protein complexes on the post-synapse (265, 485, 486). In experiments with cGi-6000-expressing CGNs discussed here, stimulation with glutamate did not induce (detectable) cGMP elevations, while Ca^{2+} imaging with fura-2 revealed that glutamate elicits Ca^{2+} elevations that have been shown to affect cGMP synthesis and breakdown (482, 487). The lack of detectable glutamate-induced cGMP elevations can be caused by different culture conditions (e.g. time in culture; see 486), stimulation protocol (effect of Mg^{2+} on NDMA receptors; see 482), or cGMP detection method (FRET *vs.* RIA). Furthermore, tested CGNs express the least sensitive cGi variant (cGi-6000), which might be too insensitive for the detection of cGMP elevations caused by stimuli different from DEA/NO. Further studies with CGNs should be performed to confirm reports showing that stimulation of glutamate receptors leads to cGMP synthesis, and to test whether cGMP elevations are confined to subcellular compartments. The availability of transgenic mice that express cGi-500 in CGNs and other cells of the brain (Thunemann & Wen, unpublished results) will facilitate analyses of CGNs and other neural cells in culture.

For studies with cultured SMCs, the cGi-500 sensor was calibrated by measuring FRET efficiency changes (given as $\Delta R/R$ values) at clamped cGMP concentrations with escin-permeabilized VSMCs. The resulting calibration curve shows that the cGi-500 sensor covers a dynamic range of approximately 100 nM to 3 µM cGMP with an EC_{50} value of 577 nM. These values are in good agreement with the calibration reported in ref. 252, where cytosolic extracts of sensor-expressing cells were used. However, the maximal $\Delta R/R$ change (40%) observed here is considerably lower than the one reported in ref. 252 (77%), but in line with other studies performed with intact cells, where maximal $\Delta R/R$ changes of 40% were observed (252, 387). A fluorimeter was used for the calibration in ref. 252, while studies with intact cells were performed via fluorescence microscopy; this dissimilarity can cause the observed differences. The cGi-500 calibration shows that $\Delta R/R$ measurements can be used to monitor cGMP dynamics at concentrations between 0.1 and 3 µM cGMP, which is in range with most cGMP binding constants to its effector proteins (488). The cGi-500 sensor should therefore perform well to monitor physiological cGMP concentrations. Another recently described cGMP sensor, δ-FlincG (343), has a fairly similar dynamic range of 20 nM to 2 µM cGMP, and has been reported to be sufficient for monitoring physiological cGMP levels (489).

From aorta, bladder and colon of adult cGi-500-expressing mice, VSMCs, BSMCs and CSMCs were isolated and analyzed by FRET imaging. To compare SMCs from different origin, cGMP elevations (given as $\Delta R/R$ curves) were quantified in response to increasing DEA/NO concentrations. All SMC types generate cGMP levels >3 µM (measured as $\Delta R/R$ peak height) upon superfusion with 100-150 nM DEA/NO, leading to saturation of the cGi-500 sensor. However, when peak areas (although truncated at cGMP levels ≥3 µM) are correlated with DEA/NO concentrations, cells show

different DEA/NO sensitivities; here BSMCs show the highest sensitivity, followed by VSMCs and CSMCs. The overall concentration range in which DEA/NO elicited rapid and transient cGMP elevations meets results obtained with cygnet2-based FRET measurements in rat VSMCs (490). In other studies in rat VSMCs analyzed with δ-FlincG biosensors, EC_{50} values of 0.28 nM NO and 4 nM DEA/NO were estimated, and saturation was observed at 10 nM DEA/NO (343, 489). In contrast to these results, 4-10 nM DEA/NO did not led to detectable cGMP elevations in measurements described here, and for saturating cGMP-levels, approximately 15-times higher DEA/NO concentrations were necessary in comparison to experiments described in ref. 343. A likely explanation for this discrepancy is the temperature at which experiments were performed: Measurements with δ-FlincG were performed at 37°C (343, 489), while our cGi-500 FRET measurements were performed at room temperature (20-22°C). This difference leads to an increased DEA/NO half-live from 2 to ~16 min, 10-fold lower NO release rates and therefore to a marked decrease in NO availability during superfusion.

Peak height and area of ΔR/R curves reflect an integrated cellular response governed by sGC activity (including time and intensity of NO stimulation), PDE activities, and possible cGMP buffers (491-493). Several studies were performed to establish quantitative models to describe kinetics of NO-induced cGMP generation and degradation measured with cGMP biosensors, wherein numerous experimental conditions are covered to estimate reliable kinetic constants (489, 490, 494). The use of cGi-500 transgenic mice, eventually carrying gene *knock-outs* (e.g. for sGC α_1 or α_2, or cGKI), combined with the use of specific PDE inhibitors (see below), and improved NO delivery systems (493, 495) might help to develop more detailed quantitative models to describe the interplay of cGMP pathway components in different primary cell cultures. Moreover, only with the use of cGMP biosensors, subcellular compartmentalization of cGMP signaling can be included into these models.

In another set of experiments, SMCs were superfused with ANP and CNP to elevate cGMP levels via stimulation of GC-A or GC-B, respectively. CSMCs reacted neither to CNP nor to ANP, while BSMCs reacted to CNP, and VSMCs to both NPs. These results implicate that cultured SMCs of different origin express GC-A and GC-B (VSMCs), GC-B (BSMCs), or neither GC-A nor GC-B (CSMCs). Elevation of cGMP levels upon stimulation with ANP and CNP is well documented for cultured primary VSMCs (340, 343, 496-498), while data on GC-A/B expression and ANP/CNP reactivity in cultured BSMCs and CSMCs is not available. In freshly isolated rat colon, ANP reduces SM tone, and in freshly isolated guinea pig CSMCs, CNP has been shown to increase cGMP levels ~2-fold (499, 500). ANP, but not CNP elevates cGMP levels in interstitial (but not smooth muscle) cells in freshly isolated bladder from mice and guinea pig (501, 502). However, reports on cGMP signaling in freshly isolated tissue are difficult to compare with results obtained in cultured SMCs, as

cells undergo phenotypic changes when brought into culture, which can be associated with altered expression levels of cGMP pathway components (462, 490). The results obtained via FRET imaging indicate that VSMCs express GC-A and GC-B, BSMCs only GC-B, and CSMCs neither GC-A nor GC-B should therefore be confirmed via immunofluorescence staining, western blot analysis or transcript analysis via RT-PCR, and eventually compared with tissue samples or freshly isolated cells. Another finding that needs further attention is the observation of comparatively weak cGMP elevations in response to ANP stimulation in VSMCs. Although it has been shown that ANP causes lower global cGMP elevations in contrast to NO (340), the responses observed here were weaker than those found by Nausch et al. using δ-FlincG sensors in rat VSMCs stimulated with 10 nM ANP, although the response kinetics seem to be comparable. However, Nausch et al. observed spatially confined cGMP elevations upon ANP stimulation (343). With the experimental conditions (16× magnification) used to obtain the results presented in **Figure 28C**, localized cGMP elevations cannot be detected. On the other hand, this can eventually explain the observation of weak cGMP elevations in response to ANP. If ANP leads to localized cGMP elevations, a 'whole-cell' cGMP FRET measurement (as performed here) would cover large amounts of cGi-500 sensor that cannot bind cGMP, while only a small proportion, namely cGi-500 that resides in the same compartment where ANP stimulation leads to cGMP generation, binds cGMP. To test this possibilty, high-resolution FRET experiments should be performed, for example using confocal microscopy (as done for δ-FlincG, see ref. 343), or with sensor variants targeted to distinct cellular compartments, e.g. to the cell membrane. Furthermore, results can be verified by stimulating cell cultures with ANP, CNP, or DEA/NO, while cGMP responses are measured via cGi-500 FRET, and in parallel in cell lysates with cGMP ELISA. Additionally, possible differences in the activation of the cGMP pathway caused by DEA/NO or natriuretic peptide stimulation could be analyzed via western blot to detect phosphorylation of cGKI substrate proteins like PDE5 or vasodilator-stimulated phosphoprotein (see e.g. 503). Furthermore, it would be interesting to see whether NP-induced cGMP elevations are augmented in the presence of PDE inhibitors, e.g. in experiments similar to those discussed hereinafter.

In further experiments, SMCs were stimulated with DEA/NO in presence of PDE inhibitors. Here, all SMCs behaved similarly, and show modest increase of cGMP elevations in presence of 30 μM sildenafil, while presence of 300 μM IBMX led to strongly increased and sustained cGMP elevations ($\geq$3 μM). With sildenafil, cGMP returned already to baseline when sildenafil was still present, but with IBMX, a return to baseline was not observed before IBMX washout. The concentrations of sildenafil and IBMX were chosen to cause complete PDE inhibition (sildenafil IC_{50} for PDE5=4 nM, IBMX IC_{50}=2-50 μM for different PDEs; 248, 504). Incomplete PDE5 inhibition is therefore an unlikely cause for the comparably small increase of cGMP elevation with sildenafil. A more likely explanation

for the difference between sildenafil and IBMX is the presence of sildenafil-insensitive, cGMP-degrading PDEs like PDEs 1, 2, and 3. cGMP-degrading PDEs 1, 3 and 5 have been detected in human, bovine and rat SM (505-508) and contribute to cGMP degradation in cultured VSMCs from rat and swine (509-511). In rat VSMCs, PDE1 has been shown to account for 63% of total cGMP-PDE activity (512), while in other experiments, in which rat VSMCs were stimulated with 400 nM DEA/NO, pre-treatment with 100 µM sildenafil led to complete inhibition of cGMP degradation (490). PDEs 1 and 5 have been identified in colonic SM of dog, rat, rabbit, and guinea pig (513-516), and PDEs 1-5 have been detected in rat bladder (517). However, PDE5 inhibition did not affect cGMP signaling in an acute bladder preparation (518). The expression levels of various PDE families in cultured BSMCs and CSMCs are not described, and should therefore be verified by RT-PCR. The definite contribution of different PDE families to cGMP degradation can be tested in FRET studies with family-specific PDE inhibitors (e.g. for PDEs 1, 2, 3, 5). Besides, chosen sildenafil concentration (30 µM) might cause inhibition of other PDEs, especially PDE1 (with an IC_{50} of 350 nM; 248). Therefore, it cannot be excluded that augmented cGMP elevations caused by 30 µM sildenafil result also from (partial) PDE1 inhibition. To analyze this question, experiments can be performed using two isoform-specific inhibitors at the same time, or by the quantification of cGMP elevations upon stimulation with constant DEA/NO doses and increasing PDE inhibitor concentrations (as performed in 264, 519). The results can be used to establish IC_{50} values in live cells, which encompass PDE binding, but also efficiency of inhibitor uptake and other factors that affect PDE and inhibitor interaction. To analyze the influence of Ca^{2+}/calmodulin-regulated PDE1 on cGMP levels, norepinephrine, or angiotensin II can be used to increase Ca^{2+} levels (see e.g. 520). It should be noted that also PDE expression could change during SMC culture, as it was shown for example for PDE1B, which is not expressed in the human aorta, but in cultured SMCs (521). With the use of cGi-500-based FRET sensors, subcellular compartmentalization of PDE activities can be studied, for instance by inducing cGMP synthesis with NPs at the membrane or NO in the cytosol, and to follow the spread of cGMP signals under the influence of different PDE inhibitors. For that purpose, spatially confined drug delivery during FRET measurements would be necessary. To show the feasibility of drug delivery different from global superfusion, micromanipulator-driven glass pipettes were used for FRET experiments with BSMCs. CNP delivery through the pipette led to cGMP elevations confined to single cells in the field of view. By using appropriate pipettes and superfusion chambers with optimized geometry, it should be possible to perform experiments at high magnification to induce cGMP elevations in a confined region of a cell, and to follow spatiotemporal dynamics of cGMP originating from the site of drug application.

Transgenic, cGi-expressing mice are a valuable source of primary cells for pharmacological studies similar to those presented here. In FRET-based studies, cGMP signals are resolved with spatial and

temporal resolutions that cannot be realized with conventional methods like RIA or ELISA. On the other hand, cells underdo notable phenotypic alterations when they are brought from their natural environment into culture (462-464), and experimental results obtained with cultured cells must not necessarily reflect the *in vivo* situation. To analyze 'more realistic' cGMP signals, studies with acute tissue preparations from cGi-500-expressing mice can be performed, or with intravital microscopy in living animals. These experiments will reflect the *in vivo* situation more correctly and form a better basis for our understanding of cGMP signaling.

To show the feasibility of cGMP FRET imaging in tissue samples, experiments were performed with retina preparations from SM445-cGi-500-5 transgenic mice, where cGi-500 is expressed in the SM of retinal vessel walls. DEA/NO concentrations necessary to elicit cGMP elevations were in an order of magnitude higher in comparison to cultured SMCs, and cGMP signal changes were markedly slower. A possible explanation for this observation is inappropriate NO delivery: due to the geometry of the imaging setup, the analyzed vessels were not in direct contact to the superfusate. NO applied via superfusion has to cross the retina from top to bottom (~200 µm) to reach the vessels. During this transit, NO interacts with various biomolecules, probably leading to a considerable reduction of available NO at the target. If molecules are present in the retina, which bind NO and release it later again (as it has been proposed for sGC; 493), an extended NO availability might cause a prolonged cGMP signal. Despite those ambiguities that are most likely caused by sub-optimal NO delivery, results show that cGi-500 fluorescence intensity is sufficient for FRET imaging in tissue samples.

For the analysis of cGMP signaling in living mice, the mouse line (SM445-cGi-500-5) used for the aforementioned studies was tested for cGi-500 expression in vessel walls in the cremaster muscle. The cremaster is a thin striated muscle which surrounds the testicle and that can be exposed for high-resolution imaging in anesthetized mice, while the muscle is still attached to the animal, and blood-perfusion is maintained (522). FRET imaging experiments can be performed under nearly physiological conditions. Intravital imaging of the cremaster is a well-established method to study vascular physiology, microcirculatory regulation, and myoendothelial coupling in living, anesthetized mice (356, 361, 465, 523). Although single SMCs in vessel walls of the cremaster muscle were found to express cGi-500 in SM445-cGi-500-5 mice, the overall number was insufficient for intravital imaging studies. For that reason, another recently generated mouse line (ROSA26-CAG-cGi-500; M. Thunemann & L. Wen, unpublished results) was used for pilot experiments performed with Prof. C. de Wit in Lübeck. In the cremaster muscle of these mice, cGi-500 is strongly expressed in striated muscle, which made FRET measurements in vessel walls impossible in the first instance. After removal of striated muscle surrounding a small artery, cGMP elevations were measured in the vessel wall upon repeated DEA/NO stimulations. The cGMP signals show rapid kinetics that rather reflects the behavior of cultured cells than the behavior of isolated retinas. A small number of experiments

were performed, which show that cGMP FRET imaging is feasible in living mice. However, pharmacological studies similar to the previously discussed studies with cultured SMCs were not yet performed. All that can be said is that DEA/NO at a concentration of 10 µM leads to a rapid rise in cGMP levels up to $\Delta R/R$ values of ~40% and therefore to cGMP concentrations that seem to saturate the cGi-500 sensor. Although these results are encouraging, conditions need to be optimized, especially in regards of cGi-500-expressing mice. The smooth muscle-specific SM445-cGi-500 mouse line cannot be used for studies in the cremaster muscle, as cGi-500 expression is virtually absent, while the ROSA26-CAG-cGi-500 mouse line shows very strong 'off-target' cGi-500 expression, especially from the striated muscle that surrounds the vasculature. The most promising solution is the generation of a Cre-inducible cGi-500 mouse line ('ROSA26-mT/cGi-500'; Lai Wen, personal communication), where cGi-500 expression can be induced in distinct cell types of the vessel wall by breeding with respective Cre mouse lines. With these mice at hand, animals with cGi-500 expression restricted to endothelial cells or smooth muscle cells are available for imaging studies of the cremaster muscle, or with cGi-500 expression in any other tissue of interest for different intravital imaging experiments.

Important aspects of cGi-based cGMP imaging are the analysis of subcellular compartmentalization and the analysis of cGMP signaling in living mice. For the former, imaging experiments can be performed with cultured cells that are isolated from cGi-expressing mice. Several technical and methodological improvements will facilitate the analysis of cGMP signaling with subcellular resolution. These are, among others, local drug delivery, for example with micromanipulator-driven pipettes or drug-coated micro-beads (see e.g. 408), the use of more sophisticated microscopic techniques like confocal microscopy, total internal reflection fluorescence microscopy, fluorescence lifetime imaging microscopy (524), and the generation of cGi-500 sensor variants that are targeted to the plasma membrane or other subcellular compartments. Furthermore, cGi-type biosensors can be combined with (spectrally compatible) biosensors or fluorescent dyes for the simultaneous analysis of cGMP and other signaling molecules like Ca^{2+} and cAMP (335). For imaging studies in living mice, animals should show strong cGi expression, which is restricted to a particular tissue, while protocols and methods established for cultured cells can probably be adapted for *in vivo* experiments. 2-photon microscopy is a frequently used intravital imaging method for *in vivo* studies, which allows for deeper light penetration and high-resolution imaging in complex samples (525, 526). For instance, 2-photon microscopy is a popular method to study neural activity by recording Ca^{2+} dynamics in anesthetized and conscious mice and rats with fluorescence-based biosensors (527-529). However, strong tissue light absorption will always make it necessary to expose the tissue of interest (as for the cremaster muscle) or to provide mice with 'imaging windows' to allow for repeated imaging sessions (as for the brain and tumor models; 530, 531). The use of cGi-expressing mice for *in vivo* imaging will open new

insights into the role and importance of cGMP signaling for numerous cellular and physiological functions, either under normal conditions, or in animal models of disease.

Altogether, two reporter-based techniques were established during this work. The basic functionality of the ROSA26-mT/sr39tk mouse line used for noninvasive cell tracking was shown in an initial PET experiment. Further experiments are necessary to characterize its sensitivity and reproducibility in noninvasive cell tracking studies. Thereinafter, the ROSA26-mT/sr39tk mouse line can be used to study physiological and pathological processes in the living animal, also in complicated genetic mouse models. For cGMP FRET imaging, several cGi-expressing transgenic mouse lines have been characterized. Mice were used as source for primary cells for a FRET-based characterization of cGMP pathway components in different types of isolated cells. In proof-of-principle studies, cGi-transgenic mice were used for intravital cGMP imaging experiments in living animals. Results obtained up to this point can form the basis for further studies on cGMP compartmentalization, and on cGMP signaling in live animals. Furthermore, altered cGMP signaling can be studied under 'native' conditions in animal models of neurodegenerative, cardiovascular or other disorders.

5   Literature

1.   Waterston, R.H., et al. Initial sequencing and comparative analysis of the mouse genome. *Nature* **420**, 520-562 (2002).
2.   Mural, R.J., et al. A comparison of whole-genome shotgun-derived mouse chromosome 16 and the human genome. *Science* **296**, 1661-1671 (2002).
3.   Kuhn, R. & Wurst, W. Overview on mouse mutagenesis. *Methods Mol Biol* **530**, 1-12 (2009).
4.   Capecchi, M.R. Gene targeting in mice: functional analysis of the mammalian genome for the twenty-first century. *Nat Rev Genet* **6**, 507-512 (2005).
5.   Smithies, O. & Maeda, N. Gene targeting approaches to complex genetic diseases: atherosclerosis and essential hypertension. *Proc Natl Acad Sci U S A* **92**, 5266-5272 (1995).
6.   Zambrowicz, B.P. & Sands, A.T. Knockouts model the 100 best-selling drugs--will they model the next 100? *Nat Rev Drug Discov* **2**, 38-51 (2003).
7.   Feil, R., et al. Cyclic GMP-dependent protein kinases and the cardiovascular system: insights from genetically modified mice. *Circ Res* **93**, 907-916 (2003).
8.   Jucker, M. The benefits and limitations of animal models for translational research in neurodegenerative diseases. *Nat Med* **16**, 1210-1214 (2010).
9.   Austin, C.P., et al. The knockout mouse project. *Nat Genet* **36**, 921-924 (2004).
10. Branda, C.S. & Dymecki, S.M. Talking about a revolution: The impact of site-specific recombinases on genetic analyses in mice. *Dev Cell* **6**, 7-28 (2004).
11. Joyner, A.L. & Zervas, M. Genetic inducible fate mapping in mouse: establishing genetic lineages and defining genetic neuroanatomy in the nervous system. *Dev Dyn* **235**, 2376-2385 (2006).
12. Buckingham, M.E. & Meilhac, S.M. Tracing cells for tracking cell lineage and clonal behavior. *Dev Cell* **21**, 394-409 (2011).
13. Mehta, S. & Zhang, J. Reporting from the field: genetically encoded fluorescent reporters uncover signaling dynamics in living biological systems. *Annu Rev Biochem* **80**, 375-401 (2011).
14. Brinster, R.L., et al. Somatic expression of herpes thymidine kinase in mice following injection of a fusion gene into eggs. *Cell* **27**, 223-231 (1981).
15. Palmiter, R.D., Chen, H.Y. & Brinster, R.L. Differential regulation of metallothionein-thymidine kinase fusion genes in transgenic mice and their offspring. *Cell* **29**, 701-710 (1982).
16. Palmiter, R.D. & Brinster, R.L. Germ-line transformation of mice. *Annu Rev Genet* **20**, 465-499 (1986).
17. MacGregor, G.R., et al. Histochemical staining of clonal mammalian cell lines expressing E. coli beta galactosidase indicates heterogeneous expression of the bacterial gene. *Somat Cell Mol Genet* **13**, 253-265 (1987).
18. Wilson, C., Bellen, H.J. & Gehring, W.J. Position effects on eukaryotic gene expression. *Annu Rev Cell Biol* **6**, 679-714 (1990).
19. Clark, A.J., et al. Chromosomal position effects and the modulation of transgene expression. *Reprod Fertil Dev* **6**, 589-598 (1994).
20. Giraldo, P. & Montoliu, L. Size matters: use of YACs, BACs and PACs in transgenic animals. *Transgenic Res* **10**, 83-103 (2001).
21. Evans, M.J. & Kaufman, M.H. Establishment in culture of pluripotential cells from mouse embryos. *Nature* **292**, 154-156 (1981).
22. Thomas, K.R. & Capecchi, M.R. Site-directed mutagenesis by gene targeting in mouse embryo-derived stem cells. *Cell* **51**, 503-512 (1987).
23. Mansour, S.L., Thomas, K.R. & Capecchi, M.R. Disruption of the proto-oncogene int-2 in mouse embryo-derived stem cells: a general strategy for targeting mutations to non-selectable genes. *Nature* **336**, 348-352 (1988).
24. Capecchi, M.R. Altering the genome by homologous recombination. *Science* **244**, 1288-1292 (1989).
25. Bradley, A., et al. Formation of germ-line chimaeras from embryo-derived teratocarcinoma cell lines. *Nature* **309**, 255-256 (1984).
26. Friedrich, G. & Soriano, P. Promoter traps in embryonic stem cells: a genetic screen to identify and mutate developmental genes in mice. *Genes Dev* **5**, 1513-1523 (1991).
27. Wurst, W., et al. A large-scale gene-trap screen for insertional mutations in developmentally regulated genes in mice. *Genetics* **139**, 889-899 (1995).
28. Stanford, W.L., Cohn, J.B. & Cordes, S.P. Gene-trap mutagenesis: past, present and beyond. *Nat Rev Genet* **2**, 756-768 (2001).
29. Mansour, S.L., et al. Introduction of a lacZ reporter gene into the mouse int-2 locus by homologous recombination. *Proc Natl Acad Sci U S A* **87**, 7688-7692 (1990).
30. Hasty, P., Rivera-Perez, J. & Bradley, A. The length of homology required for gene targeting in embryonic stem cells. *Mol Cell Biol* **11**, 5586-5591 (1991).
31. Vagner, S., Galy, B. & Pyronnet, S. Irresistible IRES. Attracting the translation machinery to internal ribosome entry sites. *EMBO Rep* **2**, 893-898 (2001).
32. Szymczak, A.L., et al. Correction of multi-gene deficiency in vivo using a single 'self-cleaving' 2A peptide–based retroviral vector. *Nat Biotechnol* **22**, 589-594 (2004).
33. Copp, A.J. Death before birth: clues from gene knockouts and mutations. *Trends Genet* **11**, 87-93 (1995).
34. Metzger, D. & Feil, R. Engineering the mouse genome by site-specific recombination. *Curr Opin Biotechnol* **10**, 470-476 (1999).
35. Feil, R. Conditional somatic mutagenesis in the mouse using site-specific recombinases. *Handb Exp Pharmacol* 3-28 (2007).
36. Sternberg, N. & Hamilton, D. Bacteriophage P1 site-specific recombination. I. Recombination between loxP sites. *J Mol Biol* **150**, 467-486 (1981).
37. Abremski, K., Hoess, R. & Sternberg, N. Studies on the properties of P1 site-specific recombination: evidence for topologically unlinked products following recombination. *Cell* **32**, 1301-1311 (1983).
38. Gu, H., et al. Deletion of a DNA polymerase beta gene segment in T cells using cell type-specific gene targeting. *Science* **265**, 103-106 (1994).

39. Buchholz, F., Angrand, P.O. & Stewart, A.F. Improved properties of FLP recombinase evolved by cycling mutagenesis. *Nat Biotechnol* **16**, 657-662 (1998).
40. Olson, E.N., et al. Know your neighbors: three phenotypes in null mutants of the myogenic bHLH gene MRF4. *Cell* **85**, 1-4 (1996).
41. Gu, H., Zou, Y.R. & Rajewsky, K. Independent control of immunoglobulin switch recombination at individual switch regions evidenced through Cre-loxP-mediated gene targeting. *Cell* **73**, 1155-1164 (1993).
42. Kuhn, R., et al. Inducible gene targeting in mice. *Science* **269**, 1427-1429 (1995).
43. Schmidt-Supprian, M. & Rajewsky, K. Vagaries of conditional gene targeting. *Nat Immunol* **8**, 665-668 (2007).
44. Utomo, A.R., Nikitin, A.Y. & Lee, W.H. Temporal, spatial, and cell type-specific control of Cre-mediated DNA recombination in transgenic mice. *Nat Biotechnol* **17**, 1091-1096 (1999).
45. Gossen, M. & Bujard, H. Studying gene function in eukaryotes by conditional gene inactivation. *Annu Rev Genet* **36**, 153-173 (2002).
46. Akagi, K., et al. Cre-mediated somatic site-specific recombination in mice. *Nucleic Acids Res* **25**, 1766-1773 (1997).
47. Metzger, D., et al. Conditional site-specific recombination in mammalian cells using a ligand-dependent chimeric Cre recombinase. *Proc Natl Acad Sci U S A* **92**, 6991-6995 (1995).
48. Feil, R., et al. Ligand-activated site-specific recombination in mice. *Proc Natl Acad Sci U S A* **93**, 10887-10890 (1996).
49. Feil, R., et al. Regulation of Cre recombinase activity by mutated estrogen receptor ligand-binding domains. *Biochem Biophys Res Commun* **237**, 752-757 (1997).
50. Brocard, J., et al. Spatio-temporally controlled site-specific somatic mutagenesis in the mouse. *Proc Natl Acad Sci U S A* **94**, 14559-14563 (1997).
51. Kuhbandner, S., et al. Temporally controlled somatic mutagenesis in smooth muscle. *Genesis* **28**, 15-22 (2000).
52. Friedel, R.H., et al. Generating conditional knockout mice. *Methods Mol Biol* **693**, 205-231 (2011).
53. Mouse Genome Informatics, The Jackson Laboratory. Gene expression database (GXD). 2012 [cited 2012/06/22]. Available from: http://www.informatics.jax.org.
54. Eppig, J.T. & Strivens, M. Finding a mouse: the International Mouse Strain Resource (IMSR). *Trends Genet* **15**, 81-82 (1999).
55. Grimm, J., Kircher, M.F. & Weissleder, R. Cell Tracking. Prinzipien und Anwendungen [Cell tracking. Principles and applications]. *Radiologe* **47**, 25-33 (2007).
56. Kircher, M.F., Gambhir, S.S. & Grimm, J. Noninvasive cell-tracking methods. *Nat Rev Clin Oncol* **8**, 677-688 (2011).
57. Massoud, T.F. & Gambhir, S.S. Molecular imaging in living subjects: seeing fundamental biological processes in a new light. *Genes Dev* **17**, 545-580 (2003).
58. Weissleder, R. & Mahmood, U. Molecular imaging. *Radiology* **219**, 316-333 (2001).
59. Pichler, B.J., Wehrl, H.F. & Judenhofer, M.S. Latest advances in molecular imaging instrumentation. *J Nucl Med* **49 Suppl 2**, 5S-23S (2008).
60. The Jackson Laboratory. Mouse genome database (MGD). 2012 [cited 2012-07-01]. Available from: http://www.informatics.jax.org.
61. Zambrowicz, B.P., et al. Disruption of overlapping transcripts in the ROSA beta geo 26 gene trap strain leads to widespread expression of beta-galactosidase in mouse embryos and hematopoietic cells. *Proc Natl Acad Sci U S A* **94**, 3789-3794 (1997).
62. Kisseberth, W.C., et al. Ubiquitous expression of marker transgenes in mice and rats. *Dev Biol* **214**, 128-138 (1999).
63. Giel-Moloney, M., et al. Ubiquitous and uniform in vivo fluorescence in ROSA26-EGFP BAC transgenic mice. *Genesis* **45**, 83-89 (2007).
64. Soriano, P. Generalized lacZ expression with the ROSA26 Cre reporter strain. *Nat Genet* **21**, 70-71 (1999).
65. Niwa, H., Yamamura, K. & Miyazaki, J. Efficient selection for high-expression transfectants with a novel eukaryotic vector. *Gene* **108**, 193-199 (1991).
66. Nyabi, O., et al. Efficient mouse transgenesis using Gateway-compatible ROSA26 locus targeting vectors and F1 hybrid ES cells. *Nucleic Acids Res* **37**, e55 (2009).
67. Chen, C.M., et al. A comparison of exogenous promoter activity at the ROSA26 locus using a PhiiC31 integrase mediated cassette exchange approach in mouse ES cells. *PLoS One* **6**, e23376 (2011).
68. Kohlhepp, R.L., Hegge, L.F. & Moser, A.R. The ROSA26 LacZ-neo(R) insertion confers resistance to mammary tumors in Apc(Min/+) mice. *Mamm Genome* **12**, 606-611 (2001).
69. Walters, E.M., et al. Mutational insertion of a ROSA26-EGFP transgene leads to defects in spermiogenesis and male infertility in mice. *Comp Med* **59**, 545-552 (2009).
70. Naiche, L.A. & Papaioannou, V.E. Cre activity causes widespread apoptosis and lethal anemia during embryonic development. *Genesis* **45**, 768-775 (2007).
71. Seibler, J., et al. Rapid generation of inducible mouse mutants. *Nucleic Acids Res* **31**, e12 (2003).
72. Hohenstein, P., et al. High-efficiency Rosa26 knock-in vector construction for Cre-regulated overexpression and RNAi. *PathoGenetics* **1**, 3 (2008).
73. Strathdee, D., Ibbotson, H. & Grant, S.G. Expression of transgenes targeted to the Gt(ROSA)26Sor locus is orientation dependent. *PLoS One* **1**, e4 (2006).
74. Madisen, L., et al. A robust and high-throughput Cre reporting and characterization system for the whole mouse brain. *Nat Neurosci* **13**, 133-140 (2010).
75. Ohtsuka, M., et al. Pronuclear injection-based mouse targeted transgenesis for reproducible and highly efficient transgene expression. *Nucleic Acids Res* **38**, e198 (2010).
76. Chen, S.X., et al. Quantification of factors influencing fluorescent protein expression using RMCE to generate an allelic series in the ROSA26 locus in mice. *Dis Model Mech* **4**, 537-547 (2011).
77. Sandhu, U., et al. Strict control of transgene expression in a mouse model for sensitive biological applications based on RMCE compatible ES cells. *Nucleic Acids Res* **39**, e1 (2011).
78. Tchorz, J.S., et al. A modified RMCE-compatible Rosa26 locus for the expression of transgenes from exogenous promoters. *PLoS One* **7**, e30011 (2012).

79. Muzumdar, M.D., et al. A global double-fluorescent Cre reporter mouse. *Genesis* **45**, 593-605 (2007).
80. Snippert, H.J., et al. Intestinal crypt homeostasis results from neutral competition between symmetrically dividing Lgr5 stem cells. *Cell* **143**, 134-144 (2010).
81. Abe, T., et al. Establishment of conditional reporter mouse lines at ROSA26 locus for live cell imaging. *Genesis* **49**, 579-590 (2011).
82. Mao, X., Fujiwara, Y. & Orkin, S.H. Improved reporter strain for monitoring Cre recombinase-mediated DNA excisions in mice. *Proc Natl Acad Sci U S A* **96**, 5037-5042 (1999).
83. Srinivas, S., et al. Cre reporter strains produced by targeted insertion of EYFP and ECFP into the ROSA26 locus. *BMC Dev Biol* **1**, 4 (2001).
84. Ueno, H. & Weissman, I.L. Clonal analysis of mouse development reveals a polyclonal origin for yolk sac blood islands. *Dev Cell* **11**, 519-533 (2006).
85. Zong, H., et al. Mosaic analysis with double markers in mice. *Cell* **121**, 479-492 (2005).
86. Laugwitz, K.L., et al. Postnatal isl1+ cardioblasts enter fully differentiated cardiomyocyte lineages. *Nature* **433**, 647-653 (2005).
87. Moretti, A., et al. Multipotent embryonic isl1+ progenitor cells lead to cardiac, smooth muscle, and endothelial cell diversification. *Cell* **127**, 1151-1165 (2006).
88. Zhou, B., et al. Epicardial progenitors contribute to the cardiomyocyte lineage in the developing heart. *Nature* **454**, 109-113 (2008).
89. Zovein, A.C., et al. Fate tracing reveals the endothelial origin of hematopoietic stem cells. *Cell stem cell* **3**, 625-636 (2008).
90. Sudarov, A., et al. Ascl1 genetics reveals insights into cerebellum local circuit assembly. *J Neurosci* **31**, 11055-11069 (2011).
91. Barker, N., et al. Identification of stem cells in small intestine and colon by marker gene Lgr5. *Nature* **449**, 1003-1007 (2007).
92. Sato, T., et al. Paneth cells constitute the niche for Lgr5 stem cells in intestinal crypts. *Nature* **469**, 415-418 (2011).
93. Imayoshi, I., et al. Roles of continuous neurogenesis in the structural and functional integrity of the adult forebrain. *Nat Neurosci* **11**, 1153-1161 (2008).
94. Dor, Y., et al. Adult pancreatic beta-cells are formed by self-duplication rather than stem-cell differentiation. *Nature* **429**, 41-46 (2004).
95. Zhou, Q., et al. In vivo reprogramming of adult pancreatic exocrine cells to beta-cells. *Nature* **455**, 627-632 (2008).
96. Bjornson, C.R., et al. Turning brain into blood: a hematopoietic fate adopted by adult neural stem cells in vivo. *Science* **283**, 534-537 (1999).
97. Clarke, D.L., et al. Generalized potential of adult neural stem cells. *Science* **288**, 1660-1663 (2000).
98. Castro, R.F., et al. Failure of bone marrow cells to transdifferentiate into neural cells in vivo. *Science* **297**, 1299 (2002).
99. Lagasse, E., et al. Purified hematopoietic stem cells can differentiate into hepatocytes in vivo. *Nat Med* **6**, 1229-1234 (2000).
100. Geoffroy, C.G. & Raineteau, O. A Cre-lox approach for transient transgene expression in neural precursor cells and long-term tracking of their progeny in vitro and in vivo. *BMC Dev Biol* **7**, 45 (2007).
101. Jackson, K.A., et al. Regeneration of ischemic cardiac muscle and vascular endothelium by adult stem cells. *J Clin Invest* **107**, 1395-1402 (2001).
102. Sata, M., et al. Hematopoietic stem cells differentiate into vascular cells that participate in the pathogenesis of atherosclerosis. *Nat Med* **8**, 403-409 (2002).
103. Wolfsgruber, W., et al. A proatherogenic role for cGMP-dependent protein kinase in vascular smooth muscle cells. *Proc Natl Acad Sci U S A* **100**, 13519-13524 (2003).
104. Nir, T., Melton, D.A. & Dor, Y. Recovery from diabetes in mice by beta cell regeneration. *J Clin Invest* **117**, 2553-2561 (2007).
105. Naik, V., et al. Sources of cells that contribute to atherosclerotic intimal calcification: an in vivo genetic fate mapping study. *Cardiovasc Res* **94**, 545-554 (2012).
106. Lao, Z., et al. MASTR: A Technique for Mosaic Mutant Analysis with Spatial and Temporal Control of Recombination Using Conditional Floxed Alleles in Mice. *Cell Rep* **2**, 386-396 (2012).
107. Saunders, T.L. Reporter molecules in genetically engineered mice. *Methods Mol Biol* **209**, 125-143 (2003).
108. Fuchs, E. & Horsley, V. Ferreting out stem cells from their niches. *Nat Cell Biol* **13**, 513-518 (2011).
109. Nishijo, K., et al. Biomarker system for studying muscle, stem cells, and cancer in vivo. *FASEB J* **23**, 2681-2690 (2009).
110. Nakagawa, T., et al. Functional hierarchy and reversibility within the murine spermatogenic stem cell compartment. *Science* **328**, 62-67 (2010).
111. Lei, L., et al. Glioblastoma models reveal the connection between adult glial progenitors and the proneural phenotype. *PLoS One* **6**, e20041 (2011).
112. Weissleder, R. & Pittet, M.J. Imaging in the era of molecular oncology. *Nature* **452**, 580-589 (2008).
113. Nguyen, P.K., et al. Imaging: guiding the clinical translation of cardiac stem cell therapy. *Circ Res* **109**, 962-979 (2011).
114. Rudin, M. & Weissleder, R. Molecular imaging in drug discovery and development. *Nat Rev Drug Discov* **2**, 123-131 (2003).
115. Ntziachristos, V. Fluorescence molecular imaging. *Annu Rev Biomed Eng* **8**, 1-33 (2006).
116. Sutton, E.J., et al. Cell tracking with optical imaging. *Eur Radiol* **18**, 2021-2032 (2008).
117. Weissleder, R. & Ntziachristos, V. Shedding light onto live molecular targets. *Nat Med* **9**, 123-128 (2003).
118. Lin, M.Z., et al. Autofluorescent proteins with excitation in the optical window for intravital imaging in mammals. *Chem Biol* **16**, 1169-1179 (2009).
119. de Almeida, P.E., van Rappard, J.R. & Wu, J.C. In vivo bioluminescence for tracking cell fate and function. *Am J Physiol Heart Circ Physiol* **301**, H663-671 (2011).
120. de Kemp, R.A., et al. Small-animal molecular imaging methods. *J Nucl Med* **51 Suppl 1**, 18S-32S (2010).
121. Budinger, T.F., Benaron, D.A. & Koretsky, A.P. Imaging transgenic animals. *Annu Rev Biomed Eng* **1**, 611-648 (1999).
122. Cherry, S.R. & Gambhir, S.S. Use of positron emission tomography in animal research. *ILAR J* **42**, 219-232 (2001).
123. Damadian, R. Tumor detection by nuclear magnetic resonance. *Science* **171**, 1151-1153 (1971).
124. Lauterbur, P.C. Image formation by induced local interactions: examples employing nuclear magnetic resonance. *Nature* **242**, 190-191 (1973).
125. Mansfield, P. Multi-planar image formation using NMR spin echoes. *J. Phys.: Condens. Matter* **10**, L55-L58 (1977).

126. Lee, S.P., et al. Visualization of beta-amyloid plaques in a transgenic mouse model of Alzheimer's disease using MR microscopy without contrast reagents. *Magn Reson Med* **52**, 538-544 (2004).
127. Louie, A.Y., et al. In vivo visualization of gene expression using magnetic resonance imaging. *Nat Biotech* **18**, 321-325 (2000).
128. Gilad, A.A., et al. MRI reporter genes. *J Nucl Med* **49**, 1905-1908 (2008).
129. Budde, M.D. & Frank, J.A. Magnetic tagging of therapeutic cells for MRI. *J Nucl Med* **50**, 171-174 (2009).
130. Phelps, M.E. Positron emission tomography provides molecular imaging of biological processes. *Proc Natl Acad Sci U S A* **97**, 9226-9233 (2000).
131. Antoni, G. & Langstrom, B. Radiopharmaceuticals: molecular imaging using positron emission tomography. *Handb Exp Pharmacol* **185/1**, 177-201 (2008).
132. Phelps, M.E., et al. Application of annihilation coincidence detection to transaxial reconstruction tomography. *J Nucl Med* **16**, 210-224 (1975).
133. Ter-Pogossian, M.M., et al. A positron-emission transaxial tomograph for nuclear imaging (PETT). *Radiology* **114**, 89-98 (1975).
134. National Center for Biotechnology Information (US). Molecular imaging and contrast agent database (MICAD). 2004-2011. Available from: http://www.ncbi.nlm.nih.gov/books/NBK5923/.
135. Logan, J. Graphical analysis of PET data applied to reversible and irreversible tracers. *Nucl Med Biol* **27**, 661-670 (2000).
136. Lammertsma, A.A. Radioligand studies: imaging and quantitative analysis. *Eur Neuropsychopharmacol* **12**, 513-516 (2002).
137. Gunn, R.N., Gunn, S.R. & Cunningham, V.J. Positron emission tomography compartmental models. *J Cereb Blood Flow Metab* **21**, 635-652 (2001).
138. Sossi, V. & Ruth, T.J. Micropet imaging: in vivo biochemistry in small animals. *J Neural Transm* **112**, 319-330 (2005).
139. Fischer, K., et al. Noninvasive nuclear imaging enables the in vivo quantification of striatal dopamine receptor expression and raclopride affinity in mice. *J Nucl Med* **52**, 1133-1141 (2011).
140. Patrick, L.C., Fernando, R.R. & Arion, F.C. Attenuation correction for small animal PET tomographs. *Phys Med Biol* **50**, 1837 (2005).
141. Mannheim, J.G., et al. Quantification accuracy and partial volume effect in dependence of the attenuation correction of a state-of-the-art small animal PET scanner. *Phys Med Biol* **57**, 3981-3993 (2012).
142. Raichle, M.E. Positron emission tomography. *Annu Rev Neurosci* **6**, 249-267 (1983).
143. Funk, T., Sun, M. & Hasegawa, B.H. Radiation dose estimate in small animal SPECT and PET. *Med Phys* **31**, 2680-2686 (2004).
144. Sandhu, G.S., et al. Whole animal imaging. *Wiley Interdiscip Rev Syst Biol Med* **2**, 398-421 (2010).
145. Chatziioannou, A.F. Molecular imaging of small animals with dedicated PET tomographs. *Eur J Nucl Med Mol Imaging* **29**, 98-114 (2002).
146. Schafers, K.P. Imaging small animals with positron emission tomography. *Nuklearmedizin* **42**, 86-89 (2003).
147. Cherry, S.R. Multimodality imaging: beyond PET/CT and SPECT/CT. *Semin Nucl Med* **39**, 348-353 (2009).
148. Wehrl, H.F., et al. Pre-clinical PET/MR: technological advances and new perspectives in biomedical research. *Eur J Nucl Med Mol Imaging* **36 Suppl 1**, S56-68 (2009).
149. Judenhofer, M.S., et al. Simultaneous PET-MRI: a new approach for functional and morphological imaging. *Nat Med* **14**, 459-465 (2008).
150. Klaunberg, B.A. & Davis, J.A. Considerations for laboratory animal imaging center design and setup. *ILAR J* **49**, 4-16 (2008).
151. Stout, D.B., et al. Small animal imaging center design: the facility at the UCLA Crump Institute for Molecular Imaging. *Mol Imaging Biol* **7**, 393-402 (2005).
152. Gambhir, S.S., et al. Imaging transgene expression with radionuclide imaging technologies. *Neoplasia* **2**, 118-138 (2000).
153. Gambhir, S.S., et al. Assays for noninvasive imaging of reporter gene expression. *Nucl Med Biol* **26**, 481-490 (1999).
154. Herschman, H.R., et al. Seeing is believing: non-invasive, quantitative and repetitive imaging of reporter gene expression in living animals, using positron emission tomography. *J Neurosci Res* **59**, 699-705 (2000).
155. MacLaren, D.C., et al. Repetitive, non-invasive imaging of the dopamine D2 receptor as a reporter gene in living animals. *Gene Ther* **6**, 785-791 (1999).
156. Zinn, K.R., et al. Noninvasive monitoring of gene transfer using a reporter receptor imaged with a high-affinity peptide radiolabeled with 99mTc or 188Re. *J Nucl Med* **41**, 887-895 (2000).
157. Haberkorn, U., et al. Transfer of the human NaI symporter gene enhances iodide uptake in hepatoma cells. *J Nucl Med* **42**, 317-325 (2001).
158. Tjuvajev, J.G., et al. Imaging herpes virus thymidine kinase gene transfer and expression by positron emission tomography. *Cancer Res* **58**, 4333-4341 (1998).
159. Gambhir, S.S., et al. Imaging of adenoviral-directed herpes simplex virus type 1 thymidine kinase reporter gene expression in mice with radiolabeled ganciclovir. *J Nucl Med* **39**, 2003-2011 (1998).
160. Alauddin, M.M., et al. 9-[(3-[18F]-fluoro-1-hydroxy-2-propoxy)methyl]guanine ([18F]-FHPG): a potential imaging agent of viral infection and gene therapy using PET. *Nucl Med Biol* **23**, 787-792 (1996).
161. Alauddin, M.M. & Conti, P.S. Synthesis and preliminary evaluation of 9-(4-[18F]-fluoro-3-hydroxymethylbutyl)guanine ([18F]FHBG): a new potential imaging agent for viral infection and gene therapy using PET. *Nucl Med Biol* **25**, 175-180 (1998).
162. Iyer, M., et al. 8-[18F]Fluoropenciclovir: an improved reporter probe for imaging HSV1-tk reporter gene expression in vivo using PET. *J Nucl Med* **42**, 96-105 (2001).
163. Cai, H., et al. Preparation and biological evaluation of 2-amino-6-[18F]fluoro-9-(4-hydroxy-3-hydroxy-methylbutyl)purine (6-[18F]FPCV) as a novel PET probe for imaging HSV1-tk reporter gene expression. *Nucl Med Biol* **34**, 717-725 (2007).
164. Sundaram, G.S., et al. A new nucleoside analogue with potent activity against mutant sr39 herpes simplex virus-1 (HSV-1) thymidine kinase (TK). *Org Lett* **1**, 16-19 (2012).
165. Alauddin, M.M., et al. Evaluation of 2'-deoxy-2'-fluoro-5-methyl-1-beta-D-arabinofuranosyluracil as a potential gene imaging agent for HSV-tk expression in vivo. *Mol Imaging* **1**, 74-81 (2002).
166. Alauddin, M.M., et al. Synthesis and evaluation of 2'-deoxy-2'-18F-fluoro-5-fluoro-1-beta-D-arabinofuranosyluracil as a potential PET imaging agent for suicide gene expression. *J Nucl Med* **45**, 2063-2069 (2004).

167. Buursma, A.R., et al. 18F-FEAU as a radiotracer for herpes simplex virus thymidine kinase gene expression: in-vitro comparison with other PET tracers. *Nucl Med Commun* **27**, 25-30 (2006).

168. Alauddin, M.M., et al. In vivo evaluation of 2'-deoxy-2'-[(18)F]fluoro-5-iodo-1-beta-D-arabinofuranosyluracil ([18F]FIAU) and 2'-deoxy-2'-[18F]fluoro-5-ethyl-1-beta-D-arabinofuranosyluracil ([18F]FEAU) as markers for suicide gene expression. *Eur J Nucl Med Mol Imaging* **34**, 822-829 (2007).

169. Chacko, A.M., et al. 5-[18F]Fluoroalkyl pyrimidine nucleosides: probes for positron emission tomography imaging of herpes simplex virus type 1 thymidine kinase gene expression. *Nucl Med Biol* **36**, 29-38 (2009).

170. Alauddin, M.M., Conti, P.S. & Fissekis, J.D. Synthesis of [18F]-labeled 2'-deoxy-2'-fluoro-5-methyl-1-β-D-arabinofuranosyluracil ([18F]-FMAU). *J Labelled Comp Rad* **45**, 583-590 (2002).

171. Kang, K.W., et al. Comparison of [14C]FMAU, [3H]FEAU, [14C]FIAU, and [3H]PCV for monitoring reporter gene expression of wild type and mutant herpes simplex virus type 1 thymidine kinase in cell culture. *Mol Imaging Biol* **7**, 296-303 (2005).

172. Serganova, I., et al. Molecular imaging of temporal dynamics and spatial heterogeneity of hypoxia-inducible factor-1 signal transduction activity in tumors in living mice. *Cancer Res* **64**, 6101-6108 (2004).

173. Borrelli, E., et al. Targeting of an inducible toxic phenotype in animal cells. *Proc Natl Acad Sci U S A* **85**, 7572-7576 (1988).

174. Ashton, W.T., et al. Activation by thymidine kinase and potent antiherpetic activity of 2'-nor-2'-deoxyguanosine (2'NDG). *Biochem Biophys Res Commun* **108**, 1716-1721 (1982).

175. Gambhir, S.S., et al. Imaging adenoviral-directed reporter gene expression in living animals with positron emission tomography. *Proc Natl Acad Sci U S A* **96**, 2333-2338 (1999).

176. Fatahzadeh, M. & Schwartz, R.A. Human herpes simplex virus infections: epidemiology, pathogenesis, symptomatology, diagnosis, and management. *J Am Acad Dermatol* **57**, 737-763; quiz 764-736 (2007).

177. Elion, G.B., et al. Selectivity of action of an antiherpetic agent, 9-(2-hydroxyethoxymethyl) guanine. *Proc Natl Acad Sci U S A* **74**, 5716-5720 (1977).

178. Furman, P.A., et al. Inhibition of herpes simplex virus-induced DNA polymerase activity and viral DNA replication by 9-(2-hydroxyethoxymethyl)guanine and its triphosphate. *J Virol* **32**, 72-77 (1979).

179. Field, A.K., et al. 9-([2-hydroxy-1-(hydroxymethyl)ethoxy]methyl)guanine: a selective inhibitor of herpes group virus replication. *Proc Natl Acad Sci U S A* **80**, 4139-4143 (1983).

180. Germershausen, J., et al. A comparison of the antiviral agents 2'-nor-2'-deoxyguanosine and acyclovir: uptake and phosphorylation in tissue culture and kinetics of in vitro inhibition of viral and cellular DNA polymerases by their respective triphosphates. *Biochem Biophys Res Commun* **116**, 360-367 (1983).

181. McGuirt, P.V. & Furman, P.A. Acyclovir inhibition of viral DNA chain elongation in herpes simplex virus-infected cells. *Am J Med* **73**, 67-71 (1982).

182. Nishiyama, Y. & Rapp, F. Anticellular effects of 9-(2-hydroxyethoxymethyl) guanine against herpes simplex virus-transformed cells. *J Gen Virol* **45**, 227-230 (1979).

183. Furman, P.A., et al. Inhibition by acyclovir of cell growth and DNA synthesis of cells biochemically transformed with herpesvirus genetic information. *Virology* **102**, 420-430 (1980).

184. Davidson, R.L., et al. Inhibition of herpes simplex virus transformed and nontransformed cells by acycloguanosine: mechanisms of uptake and toxicity. *Virology* **113**, 9-19 (1981).

185. Moolten, F.L. Tumor chemosensitivity conferred by inserted herpes thymidine kinase genes: paradigm for a prospective cancer control strategy. *Cancer Res* **46**, 5276-5281 (1986).

186. Culver, K.W., et al. In vivo gene transfer with retroviral vector-producer cells for treatment of experimental brain tumors. *Science* **256**, 1550-1552 (1992).

187. Brand, K., et al. Tumor cell-specific transgene expression prevents liver toxicity of the adeno-HSVtk/GCV approach. *Gene Ther* **5**, 1363-1371 (1998).

188. Shalev, M., et al. Suicide gene therapy toxicity after multiple and repeat injections in patients with localized prostate cancer. *J Urol* **163**, 1747-1750 (2000).

189. Herman, J.R., et al. In situ gene therapy for adenocarcinoma of the prostate: a phase I clinical trial. *Hum Gene Ther* **10**, 1239-1249 (1999).

190. Xu, F., et al. Phase I and biodistribution study of recombinant adenovirus vector-mediated herpes simplex virus thymidine kinase gene and ganciclovir administration in patients with head and neck cancer and other malignant tumors. *Cancer Gene Ther* **16**, 723-730 (2009).

191. Naldini, L. Viral vectors for gene therapy: the art of turning infectious agents into vehicles of therapeutics. *Nature Med* **7**, 33 (2001).

192. Thomas, C.E., Ehrhardt, A. & Kay, M.A. Progress and problems with the use of viral vectors for gene therapy. *Nat Rev Genet* **4**, 346-358 (2003).

193. Tjuvajev, J.G., et al. Imaging the expression of transfected genes in vivo. *Cancer Res* **55**, 6126-6132 (1995).

194. Tjuvajev, J.G., et al. Noninvasive imaging of herpes virus thymidine kinase gene transfer and expression: a potential method for monitoring clinical gene therapy. *Cancer Res* **56**, 4087-4095 (1996).

195. Jacobs, A., et al. Functional coexpression of HSV-1 thymidine kinase and green fluorescent protein: implications for noninvasive imaging of transgene expression. *Neoplasia* **1**, 154-161 (1999).

196. Black, M.E., et al. Creation of drug-specific herpes simplex virus type 1 thymidine kinase mutants for gene therapy. *Proc Natl Acad Sci U S A* **93**, 3525-3529 (1996).

197. Kokoris, M.S., et al. Enhancement of tumor ablation by a selected HSV-1 thymidine kinase mutant. *Gene Ther* **6**, 1415-1426 (1999).

198. Black, M.E., Kokoris, M.S. & Sabo, P. Herpes simplex virus-1 thymidine kinase mutants created by semi-random sequence mutagenesis improve prodrug-mediated tumor cell killing. *Cancer Res* **61**, 3022-3026 (2001).

199. Gambhir, S.S., et al. A mutant herpes simplex virus type 1 thymidine kinase reporter gene shows improved sensitivity for imaging reporter gene expression with positron emission tomography. *Proc Natl Acad Sci U S A* **97**, 2785-2790 (2000).

200. Luker, G.D., et al. Noninvasive imaging of protein-protein interactions in living animals. *Proc Natl Acad Sci U S A* **99**, 6961-6966 (2002).
201. Ponomarev, V., et al. Cytoplasmically retargeted HSV1-tk/GFP reporter gene mutants for optimization of noninvasive molecular-genetic imaging. *Neoplasia* **5**, 245-254 (2003).
202. Ray, P., et al. Imaging tri-fusion multimodality reporter gene expression in living subjects. *Cancer Res* **64**, 1323-1330 (2004).
203. Ponomarev, V., et al. A novel triple-modality reporter gene for whole-body fluorescent, bioluminescent, and nuclear noninvasive imaging. *Eur J Nucl Med Mol Imaging* **31**, 740-751 (2004).
204. Ray, P., Tsien, R. & Gambhir, S.S. Construction and validation of improved triple fusion reporter gene vectors for molecular imaging of living subjects. *Cancer Res* **67**, 3085-3093 (2007).
205. Likar, Y., et al. A new acycloguanosine-specific supermutant of herpes simplex virus type 1 thymidine kinase suitable for PET imaging and suicide gene therapy for potential use in patients treated with pyrimidine-based cytotoxic drugs. *J Nucl Med* **49**, 713-720 (2008).
206. Likar, Y., et al. PET imaging of HSV1-tk mutants with acquired specificity toward pyrimidine- and acycloguanosine-based radiotracers. *Eur J Nucl Med Mol Imaging* **36**, 1273-1282 (2009).
207. Najjar, A.M., et al. Molecular-genetic PET imaging using an HSV1-tk mutant reporter gene with enhanced specificity to acycloguanosine nucleoside analogs. *J Nucl Med* **50**, 409-416 (2009).
208. Ponomarev, V., et al. A human-derived reporter gene for noninvasive imaging in humans: mitochondrial thymidine kinase type 2. *J Nucl Med* **48**, 819-826 (2007).
209. Campbell, D.O., et al. Structure-guided engineering of human thymidine kinase 2 as a positron emission tomography reporter gene for enhanced phosphorylation of non-natural thymidine analog reporter probe. *J Biol Chem* **287**, 446-454 (2012).
210. Yu, Y., et al. Quantification of target gene expression by imaging reporter gene expression in living animals. *Nat Med* **6**, 933-937 (2000).
211. Yaghoubi, S.S., et al. Direct correlation between positron emission tomographic images of two reporter genes delivered by two distinct adenoviral vectors. *Gene Ther* **8**, 1072-1080 (2001).
212. Sun, X., et al. Quantitative imaging of gene induction in living animals. *Gene Ther* **8**, 1572-1579 (2001).
213. Jacobs, A., et al. Positron emission tomography-based imaging of transgene expression mediated by replication-conditional, oncolytic herpes simplex virus type 1 mutant vectors in vivo. *Cancer Res* **61**, 2983-2995 (2001).
214. De, A., Lewis, X.Z. & Gambhir, S.S. Noninvasive imaging of lentiviral-mediated reporter gene expression in living mice. *Mol Ther* **7**, 681-691 (2003).
215. Jacobs, A.H., et al. Improved herpes simplex virus type 1 amplicon vectors for proportional coexpression of positron emission tomography marker and therapeutic genes. *Hum Gene Ther* **14**, 277-297 (2003).
216. Ponomarev, V., et al. Imaging TCR-dependent NFAT-mediated T-cell activation with positron emission tomography in vivo. *Neoplasia* **3**, 480-488 (2001).
217. Koehne, G., et al. Serial in vivo imaging of the targeted migration of human HSV-TK-transduced antigen-specific lymphocytes. *Nat Biotechnol* **21**, 405-413 (2003).
218. Dubey, P., et al. Quantitative imaging of the T cell antitumor response by positron-emission tomography. *Proc Natl Acad Sci U S A* **100**, 1232-1237 (2003).
219. Su, H., et al. Quantitation of cell number by a positron emission tomography reporter gene strategy. *Mol Imaging Biol* **6**, 139-148 (2004).
220. Wu, J.C., et al. Positron emission tomography imaging of cardiac reporter gene expression in living rats. *Circulation* **106**, 180-183 (2002).
221. Shu, C.J., et al. Visualization of a primary anti-tumor immune response by positron emission tomography. *Proc Natl Acad Sci U S A* **102**, 17412-17417 (2005).
222. Cao, F., et al. In vivo visualization of embryonic stem cell survival, proliferation, and migration after cardiac delivery. *Circulation* **113**, 1005-1014 (2006).
223. Kim, S.J., et al. Quantitative micro positron emission tomography (PET) imaging for the in vivo determination of pancreatic islet graft survival. *Nat Med* **12**, 1423-1428 (2006).
224. Hasenbach, K., et al. Monitoring the glioma tropism of bone marrow-derived progenitor cells by 2-photon laser scanning microscopy and positron emission tomography. *Neuro Oncol* **14**, 471-481 (2012).
225. Sundaresan, G., et al. MicroPET imaging of Cre-loxP-mediated conditional activation of a herpes simplex virus type 1 thymidine kinase reporter gene. *Gene Ther* **11**, 609-618 (2004).
226. Chang, G.Y., et al. Positron emission tomography imaging of conditional gene activation in the heart. *J Mol Cell Cardiol* **43**, 18-26 (2007).
227. Tjuvajev, J.G., et al. Comparison of radiolabeled nucleoside probes (FIAU, FHBG, and FHPG) for PET imaging of HSV1-tk gene expression. *J Nucl Med* **43**, 1072-1083 (2002).
228. Miyagawa, T., et al. Imaging of HSV-tk reporter gene expression: comparison between [18F]FEAU, [18F]FFEAU, and other imaging probes. *J Nucl Med* **49**, 637-648 (2008).
229. Min, J.J., Iyer, M. & Gambhir, S.S. Comparison of [18F]FHBG and [14C]FIAU for imaging of HSV1-tk reporter gene expression: adenoviral infection vs stable transfection. *Eur J Nucl Med Mol Imaging* **30**, 1547-1560 (2003).
230. Yaghoubi, S., et al. Human pharmacokinetic and dosimetry studies of [(18)F]FHBG: a reporter probe for imaging herpes simplex virus type-1 thymidine kinase reporter gene expression. *J Nucl Med* **42**, 1225-1234 (2001).
231. Soghomonyan, S., et al. Molecular PET imaging of HSV1-tk reporter gene expression using [18F]FEAU. *Nat Protoc* **2**, 416-423 (2007).
232. de Vries, E.F., et al. [(11)C]FMAU and [(18)F]FHPG as PET tracers for herpes simplex virus thymidine kinase enzyme activity and human cytomegalovirus infections. *Nucl Med Biol* **27**, 113-119 (2000).

233. Miyagawa, M., et al. PET of cardiac transgene expression: comparison of 2 approaches based on herpesviral thymidine kinase reporter gene. *J Nucl Med* **45**, 1917-1923 (2004).
234. Buursma, A.R., et al. Monitoring HSVtk suicide gene therapy: the role of [(18)F]FHPG membrane transport. *Br J Cancer* **91**, 2079-2085 (2004).
235. Wu, J.C., et al. Molecular imaging of cardiac cell transplantation in living animals using optical bioluminescence and positron emission tomography. *Circulation* **108**, 1302-1305 (2003).
236. Hung, S.C., et al. Mesenchymal stem cell targeting of microscopic tumors and tumor stroma development monitored by noninvasive in vivo positron emission tomography imaging. *Clin Cancer Res* **11**, 7749-7756 (2005).
237. Lee, A.S., et al. Preclinical derivation and imaging of autologously transplanted canine induced pluripotent stem cells. *J Biol Chem* **286**, 32697-32704 (2011).
238. Johnson, M., et al. Titration of variant HSV1-tk gene expression to determine the sensitivity of 18F-FHBG PET imaging in a prostate tumor. *J Nucl Med* **50**, 757-764 (2009).
239. Jacobs, A., et al. Positron-emission tomography of vector-mediated gene expression in gene therapy for gliomas. *Lancet* **358**, 727-729 (2001).
240. Penuelas, I., et al. Positron emission tomography imaging of adenoviral-mediated transgene expression in liver cancer patients. *Gastroenterology* **128**, 1787-1795 (2005).
241. Yaghoubi, S.S., et al. Noninvasive detection of therapeutic cytolytic T cells with 18F-FHBG PET in a patient with glioma. *Nat Clin Pract Oncol* **6**, 53-58 (2009).
242. Yaghoubi, S.S., et al. Preclinical safety evaluation of 18F-FHBG: a PET reporter probe for imaging herpes simplex virus type 1 thymidine kinase (HSV1-tk) or mutant HSV1-sr39tk's expression. *J Nucl Med* **47**, 706-715 (2006).
243. Yong, J., et al. Multimodality imaging of beta-cells in mouse models of type 1 and 2 diabetes. *Diabetes* **60**, 1383-1392 (2011).
244. Tian, H., et al. Radio-deoxynucleoside analogs used for imaging tk expression in a transgenic mouse model of induced hepatocellular carcinoma. *Theranostics* **2**, 597-606 (2012).
245. Mergia, E., Koesling, D. & Friebe, A. Genetic mouse models of the NO receptor 'soluble' guanylyl cyclases. *Handb Exp Pharmacol* 33-46 (2009).
246. Kuhn, M. Function and dysfunction of mammalian membrane guanylyl cyclase receptors: lessons from genetic mouse models and implications for human diseases. *Handb Exp Pharmacol* 47-69 (2009).
247. Hofmann, F., et al. Function of cGMP-dependent protein kinases as revealed by gene deletion. *Physiol Rev* **86**, 1-23 (2006).
248. Bender, A.T. & Beavo, J.A. Cyclic nucleotide phosphodiesterases: molecular regulation to clinical use. *Pharmacol Rev* **58**, 488-520 (2006).
249. Kemp-Harper, B. & Feil, R. Meeting report: cGMP matters. *Sci Signal* **1**, pe12 (2008).
250. Kim, J.W., et al. Imaging cyclic AMP changes in pancreatic islets of transgenic reporter mice. *PLoS One* **3**, e2127 (2008).
251. Calebiro, D., et al. Persistent cAMP-signals triggered by internalized G-protein-coupled receptors. *PLoS Biol* **7**, e1000172 (2009).
252. Russwurm, M., et al. Design of fluorescence resonance energy transfer (FRET)-based cGMP indicators: a systematic approach. *Biochem J* **407**, 69-77 (2007).
253. Friebe, A. & Koesling, D. Regulation of nitric oxide-sensitive guanylyl cyclase. *Circ Res* **93**, 96-105 (2003).
254. Alderton, W.K., Cooper, C.E. & Knowles, R.G. Nitric oxide synthases: structure, function and inhibition. *Biochem J* **357**, 593-615 (2001).
255. Hess, D.T., et al. Protein S-nitrosylation: purview and parameters. *Nat Rev Mol Cell Biol* **6**, 150-166 (2005).
256. Hanafy, K.A., Krumenacker, J.S. & Murad, F. NO, nitrotyrosine, and cyclic GMP in signal transduction. *Med Sci Monit* **7**, 801-819 (2001).
257. Stone, J.R. & Marletta, M.A. Soluble guanylate cyclase from bovine lung: activation with nitric oxide and carbon monoxide and spectral characterization of the ferrous and ferric states. *Biochemistry* **33**, 5636-5640 (1994).
258. Derbyshire, E.R. & Marletta, M.A. Biochemistry of soluble guanylate cyclase. *Handb Exp Pharmacol* 17-31 (2009).
259. Cary, S.P., Winger, J.A. & Marletta, M.A. Tonic and acute nitric oxide signaling through soluble guanylate cyclase is mediated by nonheme nitric oxide, ATP, and GTP. *Proc Natl Acad Sci U S A* **102**, 13064-13069 (2005).
260. Ruiz-Stewart, I., et al. Guanylyl cyclase is an ATP sensor coupling nitric oxide signaling to cell metabolism. *Proc Natl Acad Sci U S A* **101**, 37-42 (2004).
261. Garthwaite, J. Concepts of neural nitric oxide-mediated transmission. *Eur J Neurosci* **27**, 2783-2802 (2008).
262. Zabel, U., et al. Calcium-dependent membrane association sensitizes soluble guanylyl cyclase to nitric oxide. *Nat Cell Biol* **4**, 307-311 (2002).
263. Agullo, L., et al. Membrane association of nitric oxide-sensitive guanylyl cyclase in cardiomyocytes. *Cardiovasc Res* **68**, 65-74 (2005).
264. Castro, L.R., et al. Cyclic guanosine monophosphate compartmentation in rat cardiac myocytes. *Circulation* **113**, 2221-2228 (2006).
265. Russwurm, M., Wittau, N. & Koesling, D. Guanylyl cyclase/PSD-95 interaction: targeting of the nitric oxide-sensitive alpha2beta1 guanylyl cyclase to synaptic membranes. *J Biol Chem* **276**, 44647-44652 (2001).
266. Kuhn, M. Molecular physiology of natriuretic peptide signalling. *Basic Res Cardiol* **99**, 76-82 (2004).
267. Garbers, D.L. Guanylyl cyclase receptors and their endocrine, paracrine, and autocrine ligands. *Cell* **71**, 1-4 (1992).
268. Matsukawa, N., et al. The natriuretic peptide clearance receptor locally modulates the physiological effects of the natriuretic peptide system. *Proc Natl Acad Sci U S A* **96**, 7403-7408 (1999).
269. Biel, M. & Michalakis, S. Cyclic nucleotide-gated channels. *Handb Exp Pharmacol* 111-136 (2009).
270. Kaupp, U.B. & Seifert, R. Cyclic nucleotide-gated ion channels. *Physiol Rev* **82**, 769-824 (2002).
271. Lohmann, S.M., et al. Distinct and specific functions of cGMP-dependent protein kinases. *Trends Biochem Sci* **22**, 307-312 (1997).
272. Pfeifer, A., et al. Structure and function of cGMP-dependent protein kinases. *Rev Physiol Biochem Pharmacol* **135**, 105-149 (1999).
273. Landgraf, W., et al. Effects of cyclic GMP on the secondary structure of cyclic GMP dependent protein kinase and analysis of the enzyme's amino-terminal domain by far-ultraviolet circular dichroism. *Biochemistry* **29**, 9921-9928 (1990).

274. Wall, M.E., et al. Mechanisms associated with cGMP binding and activation of cGMP-dependent protein kinase. *Proc Natl Acad Sci U S A* **100**, 2380-2385 (2003).
275. Lincoln, T.M., Thompson, M. & Cornwell, T.L. Purification and characterization of two forms of cyclic GMP-dependent protein kinase from bovine aorta. *J Biol Chem* **263**, 17632-17637 (1988).
276. Wernet, W., Flockerzi, V. & Hofmann, F. The cDNA of the two isoforms of bovine cGMP-dependent protein kinase. *FEBS Lett* **251**, 191-196 (1989).
277. Hofmann, F., et al. cGMP regulated protein kinases (cGK). *Handb Exp Pharmacol* 137-162 (2009).
278. Schlossmann, J. & Desch, M. cGK substrates. *Handb Exp Pharmacol* 163-193 (2009).
279. Weber, S., et al. Rescue of cGMP kinase I knockout mice by smooth muscle specific expression of either isozyme. *Circ Res* **101**, 1096-1103 (2007).
280. Surks, H.K. cGMP-dependent protein kinase I and smooth muscle relaxation: a tale of two isoforms. *Circ Res* **101**, 1078-1080 (2007).
281. Geiselhoringer, A., et al. Distribution of IRAG and cGKI-isoforms in murine tissues. *FEBS Lett* **575**, 19-22 (2004).
282. Feil, S., et al. Distribution of cGMP-dependent protein kinase type I and its isoforms in the mouse brain and retina. *Neuroscience* **135**, 863-868 (2005).
283. Vaandrager, A.B., et al. N-terminal myristoylation is required for membrane localization of cGMP-dependent protein kinase type II. *J Biol Chem* **271**, 7025-7029 (1996).
284. Conti, M. & Beavo, J. Biochemistry and physiology of cyclic nucleotide phosphodiesterases: essential components in cyclic nucleotide signaling. *Annu Rev Biochem* **76**, 481-511 (2007).
285. Francis, S.H., Corbin, J.D. & Bischoff, E. Cyclic GMP-hydrolyzing phosphodiesterases. *Handb Exp Pharmacol* 367-408 (2009).
286. Francis, S.H., Blount, M.A. & Corbin, J.D. Mammalian cyclic nucleotide phosphodiesterases: molecular mechanisms and physiological functions. *Physiol Rev* **91**, 651-690 (2011).
287. Kass, D.A., Champion, H.C. & Beavo, J.A. Phosphodiesterase type 5: expanding roles in cardiovascular regulation. *Circ Res* **101**, 1084-1095 (2007).
288. Kass, D.A., et al. Phosphodiesterase regulation of nitric oxide signaling. *Cardiovasc Res* **75**, 303-314 (2007).
289. Francis, S.H., et al. cGMP-dependent protein kinases and cGMP phosphodiesterases in nitric oxide and cGMP action. *Pharmacol Rev* **62**, 525-563 (2010).
290. Zaccolo, M. & Movsesian, M.A. cAMP and cGMP signaling cross-talk: role of phosphodiesterases and implications for cardiac pathophysiology. *Circ Res* **100**, 1569-1578 (2007).
291. Vandeput, F., et al. cGMP-hydrolytic activity and its inhibition by sildenafil in normal and failing human and mouse myocardium. *J Pharmacol Exp Ther* **330**, 884-891 (2009).
292. Gross-Langenhoff, M., et al. cAMP is a ligand for the tandem GAF domain of human phosphodiesterase 10 and cGMP for the tandem GAF domain of phosphodiesterase 11. *J Biol Chem* **281**, 2841-2846 (2006).
293. Schmidt, P.M. Biochemical detection of cGMP from past to present: an overview. *Handb Exp Pharmacol* 195-228 (2009).
294. Steinbusch, H.W., et al. Immunohistochemical localization of monoamines and cyclic nucleotides. Their application in quantitative immunofluorescence studies and tracing monoaminergic neuronal connections. *Acta Histochem Suppl* **35**, 86-106 (1988).
295. Tsien, R.Y. Intracellular measurements of ion activities. *Annu Rev Biophys Bioeng* **12**, 91-116 (1983).
296. Takahashi, A., et al. Measurement of intracellular calcium. *Physiol Rev* **79**, 1089-1125 (1999).
297. Paredes, R.M., et al. Chemical calcium indicators. *Methods* **46**, 143-151 (2008).
298. Grynkiewicz, G., Poenie, M. & Tsien, R.Y. A new generation of Ca2+ indicators with greatly improved fluorescence properties. *J Biol Chem* **260**, 3440-3450 (1985).
299. Gunther, T. Concentration, compartmentation and metabolic function of intracellular free Mg2+. *Magnes Res* **19**, 225-236 (2006).
300. Domaille, D.W., Que, E.L. & Chang, C.J. Synthetic fluorescent sensors for studying the cell biology of metals. *Nat Chem Biol* **4**, 168-175 (2008).
301. Han, J. & Burgess, K. Fluorescent indicators for intracellular pH. *Chem Rev* **110**, 2709-2728 (2010).
302. Minta, A. & Tsien, R.Y. Fluorescent indicators for cytosolic sodium. *J Biol Chem* **264**, 19449-19457 (1989).
303. Lippincott-Schwartz, J., Snapp, E. & Kenworthy, A. Studying protein dynamics in living cells. *Nat Rev Mol Cell Biol* **2**, 444-456 (2001).
304. Pozzan, T., Mongillo, M. & Rudolf, R. The Theodore Bucher lecture. Investigating signal transduction with genetically encoded fluorescent probes. *Eur J Biochem* **270**, 2343-2352 (2003).
305. Miyawaki, A. Visualization of the spatial and temporal dynamics of intracellular signaling. *Dev Cell* **4**, 295-305 (2003).
306. Tsien, R.Y. Constructing and exploiting the fluorescent protein paintbox (Nobel Lecture). *Angew Chem Int Ed Engl* **48**, 5612-5626 (2009).
307. Lemke, E.A. & Schultz, C. Principles for designing fluorescent sensors and reporters. *Nat Chem Biol* **7**, 480-483 (2011).
308. Shimomura, O., Johnson, F.H. & Saiga, Y. Microdetermination of calcium by aequorin luminescence. *Science* **140**, 1339-1340 (1963).
309. Adams, S.R., et al. Fluorescence ratio imaging of cyclic AMP in single cells. *Nature* **349**, 694-697 (1991).
310. Sammak, P.J., et al. Intracellular cyclic AMP not calcium, determines the direction of vesicle movement in melanophores: direct measurement by fluorescence ratio imaging. *J Cell Biol* **117**, 57-72 (1992).
311. Hempel, C.M., et al. Spatio-temporal dynamics of cyclic AMP signals in an intact neural circuitm. *Nature* **384**, 166-169 (1996).
312. Bacskai, B.J., et al. Spatially resolved dynamics of cAMP and protein kinase A subunits in Aplysia sensory neurons. *Science* **260**, 222-226 (1993).
313. Shimomura, O., Johnson, F.H. & Saiga, Y. Extraction, purification and properties of aequorin, a bioluminescent protein from the luminous hydromedusan, Aequorea. *J Cell Comp Physiol* **59**, 223-239 (1962).
314. Morin, J.G. & Hastings, J.W. Energy transfer in a bioluminescent system. *J Cell Physiol* **77**, 313-318 (1971).
315. Prasher, D.C., et al. Primary structure of the Aequorea victoria green-fluorescent protein. *Gene* **111**, 229-233 (1992).

316. Cody, C.W., et al. Chemical structure of the hexapeptide chromophore of the Aequorea green-fluorescent protein. *Biochemistry* **32**, 1212-1218 (1993).
317. Shimomura, O. Structure of the chromophore of Aequorea green fluorescent protein. *FEBS Letters* **104**, 220-222 (1979).
318. Chalfie, M., et al. Green fluorescent protein as a marker for gene expression. *Science* **263**, 802-805 (1994).
319. Heim, R., Prasher, D.C. & Tsien, R.Y. Wavelength mutations and posttranslational autoxidation of green fluorescent protein. *Proc Natl Acad Sci U S A* **91**, 12501-12504 (1994).
320. Heim, R., Cubitt, A.B. & Tsien, R.Y. Improved green fluorescence. *Nature* **373**, 663-664 (1995).
321. Cormack, B.P., Valdivia, R.H. & Falkow, S. FACS-optimized mutants of the green fluorescent protein (GFP). *Gene* **173**, 33-38 (1996).
322. Heim, R. & Tsien, R.Y. Engineering green fluorescent protein for improved brightness, longer wavelengths and fluorescence resonance energy transfer. *Curr Biol* **6**, 178-182 (1996).
323. Llopis, J., et al. Measurement of cytosolic, mitochondrial, and Golgi pH in single living cells with green fluorescent proteins. *Proc Natl Acad Sci U S A* **95**, 6803-6808 (1998).
324. Ormo, M., et al. Crystal structure of the Aequorea victoria green fluorescent protein. *Science* **273**, 1392-1395 (1996).
325. Förster, T. Energiewanderung und Fluoreszenz. *Die Naturwissenschaften* **33**, 166-175 (1946).
326. Miyawaki, A., et al. Fluorescent indicators for Ca2+ based on green fluorescent proteins and calmodulin. *Nature* **388**, 882-887 (1997).
327. Miyawaki, A., et al. Dynamic and quantitative Ca2+ measurements using improved cameleons. *Proc Natl Acad Sci U S A* **96**, 2135-2140 (1999).
328. Zaccolo, M., et al. A genetically encoded, fluorescent indicator for cyclic AMP in living cells. *Nat Cell Biol* **2**, 25-29 (2000).
329. Giepmans, B.N., et al. The fluorescent toolbox for assessing protein location and function. *Science* **312**, 217-224 (2006).
330. Lohse, M.J., et al. Monitoring receptor signaling by intramolecular FRET. *Curr Opin Pharmacol* **7**, 547-553 (2007).
331. Zhang, J., et al. Creating new fluorescent probes for cell biology. *Nat Rev Mol Cell Biol* **3**, 906-918 (2002).
332. Herbst, K.J., Ni, Q. & Zhang, J. Dynamic visualization of signal transduction in living cells: from second messengers to kinases. *IUBMB Life* **61**, 902-908 (2009).
333. Newman, R.H., Fosbrink, M.D. & Zhang, J. Genetically encodable fluorescent biosensors for tracking signaling dynamics in living cells. *Chem Rev* **111**, 3614-3666 (2011).
334. Gesellchen, F., et al. Measuring spatiotemporal dynamics of cyclic AMP signaling in real-time using FRET-based biosensors. *Methods Mol Biol* **746**, 297-316 (2011).
335. Carlson, H.J. & Campbell, R.E. Genetically encoded FRET-based biosensors for multiparameter fluorescence imaging. *Curr Opin Biotechnol* **20**, 19-27 (2009).
336. Nikolaev, V.O. & Lohse, M.J. Novel techniques for real-time monitoring of cGMP in living cells. *Handb Exp Pharmacol* 229-243 (2009).
337. Rich, T.C., et al. In vivo assessment of local phosphodiesterase activity using tailored cyclic nucleotide-gated channels as cAMP sensors. *J Gen Physiol* **118**, 63-78 (2001).
338. Rich, T.C., et al. Cyclic nucleotide-gated channels colocalize with adenylyl cyclase in regions of restricted cAMP diffusion. *J Gen Physiol* **116**, 147-161 (2000).
339. Wunder, F., et al. A cell-based nitric oxide reporter assay useful for the identification and characterization of modulators of the nitric oxide/guanosine 3',5'-cyclic monophosphate pathway. *Anal Biochem* **363**, 219-227 (2007).
340. Piggott, L.A., et al. Natriuretic peptides and nitric oxide stimulate cGMP synthesis in different cellular compartments. *J Gen Physiol* **128**, 3-14 (2006).
341. Sato, M., et al. Fluorescent indicators for cyclic GMP based on cyclic GMP-dependent protein kinase Ialpha and green fluorescent proteins. *Anal Chem* **72**, 5918-5924 (2000).
342. Honda, A., et al. Spatiotemporal dynamics of guanosine 3',5'-cyclic monophosphate revealed by a genetically encoded, fluorescent indicator. *Proc Natl Acad Sci U S A* **98**, 2437-2442 (2001).
343. Nausch, L.W., et al. Differential patterning of cGMP in vascular smooth muscle cells revealed by single GFP-linked biosensors. *Proc Natl Acad Sci U S A* **105**, 365-370 (2008).
344. Nikolaev, V.O., Gambaryan, S. & Lohse, M.J. Fluorescent sensors for rapid monitoring of intracellular cGMP. *Nat Methods* **3**, 23-25 (2006).
345. Biswas, K.H., Sopory, S. & Visweswariah, S.S. The GAF domain of the cGMP-binding, cGMP-specific phosphodiesterase (PDE5) is a sensor and a sink for cGMP. *Biochemistry* **47**, 3534-3543 (2008).
346. Niino, Y., Hotta, K. & Oka, K. Simultaneous live cell imaging using dual FRET sensors with a single excitation light. *PLoS One* **4**, e6036 (2009).
347. Niino, Y., Hotta, K. & Oka, K. Blue fluorescent cGMP sensor for multiparameter fluorescence imaging. *PLoS One* **5**, e9164 (2010).
348. Baird, G.S., Zacharias, D.A. & Tsien, R.Y. Circular permutation and receptor insertion within green fluorescent proteins. *Proc Natl Acad Sci U S A* **96**, 11241-11246 (1999).
349. Carvajal, J.A., et al. Molecular mechanism of cGMP-mediated smooth muscle relaxation. *J Cell Physiol* **184**, 409-420 (2000).
350. Sun, X., et al. RGS2 is a mediator of nitric oxide action on blood pressure and vasoconstrictor signaling. *Mol Pharmacol* **67**, 631-639 (2005).
351. Geiselhoringer, A., et al. IRAG is essential for relaxation of receptor-triggered smooth muscle contraction by cGMP kinase. *EMBO J* **23**, 4222-4231 (2004).
352. Pfeifer, A., et al. Defective smooth muscle regulation in cGMP kinase I-deficient mice. *EMBO J* **17**, 3045-3051 (1998).
353. Friebe, A., et al. Fatal gastrointestinal obstruction and hypertension in mice lacking nitric oxide-sensitive guanylyl cyclase. *Proc Natl Acad Sci U S A* **104**, 7699-7704 (2007).
354. Mergia, E., et al. Spare guanylyl cyclase NO receptors ensure high NO sensitivity in the vascular system. *J Clin Invest* **116**, 1731-1737 (2006).

355. Brandes, R.P., et al. An endothelium-derived hyperpolarizing factor distinct from NO and prostacyclin is a major endothelium-dependent vasodilator in resistance vessels of wild-type and endothelial NO synthase knockout mice. *Proc Natl Acad Sci U S A* **97**, 9747-9752 (2000).

356. Koeppen, M., et al. cGMP-dependent protein kinase mediates NO- but not acetylcholine-induced dilations in resistance vessels in vivo. *Hypertension* **44**, 952-955 (2004).

357. Schmidt, K., et al. Amplification of EDHF-type vasodilatations in TRPC1-deficient mice. *Br J Pharmacol* **161**, 1722-1733 (2010).

358. Holtwick, R., et al. Smooth muscle-selective deletion of guanylyl cyclase-A prevents the acute but not chronic effects of ANP on blood pressure. *Proc Natl Acad Sci U S A* **99**, 7142-7147 (2002).

359. Sabrane, K., et al. Vascular endothelium is critically involved in the hypotensive and hypovolemic actions of atrial natriuretic peptide. *J Clin Invest* **115**, 1666-1674 (2005).

360. Curry, F.R. Atrial natriuretic peptide: an essential physiological regulator of transvascular fluid, protein transport, and plasma volume. *J Clin Invest* **115**, 1458-1461 (2005).

361. Chen, W., et al. Atrial natriuretic peptide enhances microvascular albumin permeability by the caveolae-mediated transcellular pathway. *Cardiovasc Res* **93**, 141-151 (2012).

362. Baliga, R.S., et al. Synergy between natriuretic peptides and phosphodiesterase 5 inhibitors ameliorates pulmonary arterial hypertension. *Am J Respir Crit Care Med* **178**, 861-869 (2008).

363. Madhani, M., et al. Reciprocal regulation of human soluble and particulate guanylate cyclases in vivo. *Br J Pharmacol* **149**, 797-801 (2006).

364. Yamahara, K., et al. Significance and therapeutic potential of the natriuretic peptides/cGMP/cGMP-dependent protein kinase pathway in vascular regeneration. *Proc Natl Acad Sci U S A* **100**, 3404-3409 (2003).

365. Carmeliet, P. & Jain, R.K. Angiogenesis in cancer and other diseases. *Nature* **407**, 249-257 (2000).

366. Duda, D.G., Fukumura, D. & Jain, R.K. Role of eNOS in neovascularization: NO for endothelial progenitor cells. *Trends Mol Med* **10**, 143-145 (2004).

367. Aicher, A., et al. cGMP-dependent protein kinase I is crucial for angiogenesis and postnatal vasculogenesis. *PLoS One* **4**, e4879 (2009).

368. Feil, R., Feil, S. & Hofmann, F. A heretical view on the role of NO and cGMP in vascular proliferative diseases. *Trends Mol Med* **11**, 71-75 (2005).

369. Komatsu, Y., et al. Regulation of endothelial production of C-type natriuretic peptide in coculture with vascular smooth muscle cells. Role of the vascular natriuretic peptide system in vascular growth inhibition. *Circ Res* **78**, 606-614 (1996).

370. Kuhn, M. Endothelial actions of atrial and B-type natriuretic peptides. *Br J Pharmacol* **166**, 522-531 (2012).

371. Koika, V., et al. PKG-I inhibition attenuates vascular endothelial growth factor-stimulated angiogenesis. *Vascul Pharmacol* **53**, 215-222 (2010).

372. Eigenthaler, M., et al. Signal transduction by cGMP-dependent protein kinases and their emerging roles in the regulation of cell adhesion and gene expression. *Rev Physiol Biochem Pharmacol* **135**, 173-209 (1999).

373. Lincoln, T.M., Dey, N. & Sellak, H. Invited review: cGMP-dependent protein kinase signaling mechanisms in smooth muscle: from the regulation of tone to gene expression. *J Appl Physiol* **91**, 1421-1430 (2001).

374. Sarkar, R. & Webb, R.C. Does nitric oxide regulate smooth muscle cell proliferation? A critical appraisal. *J Vasc Res* **35**, 135-142 (1998).

375. Wegener, J.W., et al. cGMP-dependent protein kinase I mediates the negative inotropic effect of cGMP in the murine myocardium. *Circ Res* **90**, 18-20 (2002).

376. Wollert, K.C., et al. Increased effects of C-type natriuretic peptide on contractility and calcium regulation in murine hearts overexpressing cyclic GMP-dependent protein kinase I. *Br J Pharmacol* **140**, 1227-1236 (2003).

377. Fischmeister, R., et al. Compartmentation of cyclic nucleotide signaling in the heart: the role of cyclic nucleotide phosphodiesterases. *Circ Res* **99**, 816-828 (2006).

378. Castro, L.R., Schittl, J. & Fischmeister, R. Feedback control through cGMP-dependent protein kinase contributes to differential regulation and compartmentation of cGMP in rat cardiac myocytes. *Circ Res* **107**, 1232-1240 (2010).

379. Brenner, B.M., et al. Diverse biological actions of atrial natriuretic peptide. *Physiol Rev* **70**, 665-699 (1990).

380. Wagner, C., et al. Role of cGMP-kinase II in the control of renin secretion and renin expression. *J Clin Invest* **102**, 1576-1582 (1998).

381. Kurtz, A., et al. Stimulation of renin secretion by nitric oxide is mediated by phosphodiesterase 3. *Proc Natl Acad Sci U S A* **95**, 4743-4747 (1998).

382. MacFarland, R.T., Zelus, B.D. & Beavo, J.A. High concentrations of a cGMP-stimulated phosphodiesterase mediate ANP-induced decreases in cAMP and steroidogenesis in adrenal glomerulosa cells. *J Biol Chem* **266**, 136-142 (1991).

383. Gambaryan, S., et al. cGMP-dependent protein kinase type II regulates basal level of aldosterone production by zona glomerulosa cells without increasing expression of the steroidogenic acute regulatory protein gene. *J Biol Chem* **278**, 29640-29648 (2003).

384. Andersson, K.E. & Wagner, G. Physiology of penile erection. *Physiol Rev* **75**, 191-236 (1995).

385. Corbin, J.D. & Francis, S.H. Pharmacology of phosphodiesterase-5 inhibitors. *Int J Clin Pract* **56**, 453-459 (2002).

386. Persson, K., et al. Functional characteristics of urinary tract smooth muscles in mice lacking cGMP protein kinase type I. *Am J Physiol Regul Integr Comp Physiol* **279**, R1112-1120 (2000).

387. Norris, R.P., et al. Cyclic GMP from the surrounding somatic cells regulates cyclic AMP and meiosis in the mouse oocyte. *Development* **136**, 1869-1878 (2009).

388. Masciarelli, S., et al. Cyclic nucleotide phosphodiesterase 3A-deficient mice as a model of female infertility. *J Clin Invest* **114**, 196-205 (2004).

389. Pfeifer, A., et al. Intestinal secretory defects and dwarfism in mice lacking cGMP-dependent protein kinase II. *Science* **274**, 2082-2086 (1996).

390. Forte, L.R., Jr. Uroguanylin: physiological role as a natriuretic hormone. *J Am Soc Nephrol* **16**, 291-292 (2005).

391. Miyazawa, T., et al. Cyclic GMP-dependent protein kinase II plays a critical role in C-type natriuretic peptide-mediated endochondral ossification. *Endocrinology* **143**, 3604-3610 (2002).
392. Olney, R.C. C-type natriuretic peptide in growth: a new paradigm. *Growth Horm IGF Res* **16 Suppl A**, S6-14 (2006).
393. Massberg, S., et al. Increased adhesion and aggregation of platelets lacking cyclic guanosine 3',5'-monophosphate kinase I. *J Exp Med* **189**, 1255-1264 (1999).
394. Schinner, E., Salb, K. & Schlossmann, J. Signaling via IRAG is essential for NO/cGMP-dependent inhibition of platelet activation. *Platelets* **22**, 217-227 (2011).
395. Walter, U. & Gambaryan, S. cGMP and cGMP-dependent protein kinase in platelets and blood cells. *Handb Exp Pharmacol* 533-548 (2009).
396. Li, Z., et al. A predominant role for cAMP-dependent protein kinase in the cGMP-induced phosphorylation of vasodilator-stimulated phosphoprotein and platelet inhibition in humans. *Blood* **101**, 4423-4429 (2003).
397. Schwarz, U.R., Walter, U. & Eigenthaler, M. Taming platelets with cyclic nucleotides. *Biochem Pharmacol* **62**, 1153-1161 (2001).
398. Wilson, L.S., et al. Compartmentation and compartment-specific regulation of PDE5 by protein kinase G allows selective cGMP-mediated regulation of platelet functions. *Proc Natl Acad Sci U S A* **105**, 13650-13655 (2008).
399. Foller, M., et al. Anemia and splenomegaly in cGKI-deficient mice. *Proc Natl Acad Sci U S A* **105**, 6771-6776 (2008).
400. Kleppisch, T. & Feil, R. cGMP signalling in the mammalian brain: role in synaptic plasticity and behaviour. *Handb Exp Pharmacol* 549-579 (2009).
401. Reaume, C.J. & Sokolowski, M.B. cGMP-dependent protein kinase as a modifier of behaviour. *Handb Exp Pharmacol* 423-443 (2009).
402. Feil, R. & Kleppisch, T. NO/cGMP-dependent modulation of synaptic transmission. *Handb Exp Pharmacol* 529-560 (2008).
403. Imura, H., Nakao, K. & Itoh, H. The natriuretic peptide system in the brain: implications in the central control of cardiovascular and neuroendocrine functions. *Front Neuroendocrinol* **13**, 217-249 (1992).
404. Schmidt, H., et al. cGMP-mediated signaling via cGKIalpha is required for the guidance and connectivity of sensory axons. *J Cell Biol* **159**, 489-498 (2002).
405. Schmidtko, A., Tegeder, I. & Geisslinger, G. No NO, no pain? The role of nitric oxide and cGMP in spinal pain processing. *Trends Neurosci* **32**, 339-346 (2009).
406. Luo, C., et al. Presynaptically localized cyclic GMP-dependent protein kinase 1 is a key determinant of spinal synaptic potentiation and pain hypersensitivity. *PLoS Biol* **10**, e1001283 (2012).
407. Tedeschi, A., et al. The tumor suppressor p53 transcriptionally regulates cGKI expression during neuronal maturation and is required for cGMP-dependent growth cone collapse. *J Neurosci* **29**, 15155-15160 (2009).
408. Shelly, M., et al. Local and long-range reciprocal regulation of cAMP and cGMP in axon/dendrite formation. *Science* **327**, 547-552 (2010).
409. Ding, J.D., et al. Distribution of soluble guanylyl cyclase in the rat brain. *J Comp Neurol* **472**, 437-448 (2004).
410. Arancio, O., Kandel, E.R. & Hawkins, R.D. Activity-dependent long-term enhancement of transmitter release by presynaptic 3',5'-cyclic GMP in cultured hippocampal neurons. *Nature* **376**, 74-80 (1995).
411. Arancio, O., et al. Presynaptic role of cGMP-dependent protein kinase during long-lasting potentiation. *J Neurosci* **21**, 143-149 (2001).
412. Kleppisch, T., et al. Hippocampal cGMP-dependent protein kinase I supports an age- and protein synthesis-dependent component of long-term potentiation but is not essential for spatial reference and contextual memory. *J Neurosci* **23**, 6005-6012 (2003).
413. Paul, C., et al. Signaling through cGMP-dependent protein kinase I in the amygdala is critical for auditory-cued fear memory and long-term potentiation. *J Neurosci* **28**, 14202-14212 (2008).
414. Monfort, P., et al. Long-term potentiation in hippocampus involves sequential activation of soluble guanylate cyclase, cGMP-dependent protein kinase, and cGMP-degrading phosphodiesterase. *J Neurosci* **22**, 10116-10122 (2002).
415. Haghikia, A., et al. Long-term potentiation in the visual cortex requires both nitric oxide receptor guanylyl cyclases. *J Neurosci* **27**, 818-823 (2007).
416. West, A.R., Galloway, M.P. & Grace, A.A. Regulation of striatal dopamine neurotransmission by nitric oxide: effector pathways and signaling mechanisms. *Synapse* **44**, 227-245 (2002).
417. Feil, R., et al. Impairment of LTD and cerebellar learning by Purkinje cell-specific ablation of cGMP-dependent protein kinase I. *J Cell Biol* **163**, 295-302 (2003).
418. Lev-Ram, V., et al. Synergies and coincidence requirements between NO, cGMP, and Ca2+ in the induction of cerebellar long-term depression. *Neuron* **18**, 1025-1038 (1997).
419. Wang, H.G., et al. Presynaptic and postsynaptic roles of NO, cGK, and RhoA in long-lasting potentiation and aggregation of synaptic proteins. *Neuron* **45**, 389-403 (2005).
420. Pietrobon, M., et al. Interplay among cGMP, cAMP, and Ca2+ in living olfactory sensory neurons in vitro and in vivo. *J Neurosci* **31**, 8395-8405 (2011).
421. Langmesser, S., et al. cGMP-dependent protein kinase type I is implicated in the regulation of the timing and quality of sleep and wakefulness. *PLoS One* **4**, e4238 (2009).
422. Reneerkens, O.A., et al. Selective phosphodiesterase inhibitors: a promising target for cognition enhancement. *Psychopharmacology (Berl)* **202**, 419-443 (2009).
423. Boess, F.G., et al. Inhibition of phosphodiesterase 2 increases neuronal cGMP, synaptic plasticity and memory performance. *Neuropharmacology* **47**, 1081-1092 (2004).
424. Prickaerts, J., et al. Phosphodiesterase type 5 inhibition improves early memory consolidation of object information. *Neurochem Int* **45**, 915-928 (2004).
425. Wegener, G. & Volke, V. Nitric oxide synthase inhibitors as antidepressants. *Pharmaceuticals* **3**, 273-299 (2010).
426. Puzzo, D., et al. Amyloid-beta peptide inhibits activation of the nitric oxide/cGMP/cAMP-responsive element-binding protein pathway during hippocampal synaptic plasticity. *J Neurosci* **25**, 6887-6897 (2005).

427. Puzzo, D., et al. Phosphodiesterase 5 inhibition improves synaptic function, memory, and amyloid-beta load in an Alzheimer's disease mouse model. *J Neurosci* **29**, 8075-8086 (2009).

428. Jaumann, M., et al. cGMP-Prkg1 signaling and Pde5 inhibition shelter cochlear hair cells and hearing function. *Nat Med* **18**, 252-259 (2012).

429. Menniti, F.S., Faraci, W.S. & Schmidt, C.J. Phosphodiesterases in the CNS: targets for drug development. *Nat Rev Drug Discov* **5**, 660-670 (2006).

430. Kleiman, R.J., et al. Phosphodiesterase 9A regulates central cGMP and modulates responses to cholinergic and monoaminergic perturbation in vivo. *J Pharmacol Exp Ther* **341**, 396-409 (2012).

431. Sambrook, J. & Russell, D.W. Molecular cloning: a laboratory manual. Vol. 2. 2001, Woodbury, NY: CSHL Press.

432. Arber, W. & Linn, S. DNA modification and restriction. *Annu Rev Biochem* **38**, 467-500 (1969).

433. Dower, W.J., Miller, J.F. & Ragsdale, C.W. High efficiency transformation of E. coli by high voltage electroporation. *Nucleic Acids Res* **16**, 6127-6145 (1988).

434. Birnboim, H.C. & Doly, J. A rapid alkaline extraction procedure for screening recombinant plasmid DNA. *Nucleic Acids Res* **7**, 1513-1523 (1979).

435. McBride, L.J. & Caruthers, M.H. An investigation of several deoxynucleoside phosphoramidites useful for synthesizing deoxyoligonucleotides. *Tetrahedron Letters* **24**, 245-248 (1983).

436. Sanger, F. & Coulson, A.R. A rapid method for determining sequences in DNA by primed synthesis with DNA polymerase. *J Mol Biol* **94**, 441-448 (1975).

437. Huang, C., et al. Embryonic atrial function is essential for mouse embryogenesis, cardiac morphogenesis and angiogenesis. *Development* **130**, 6111-6119 (2003).

438. Dupe, V., et al. In vivo functional analysis of the Hoxa-1 3' retinoic acid response element (3'RARE). *Development* **124**, 399-410 (1997).

439. Tronche, F., et al. Disruption of the glucocorticoid receptor gene in the nervous system results in reduced anxiety. *Nat Genet* **23**, 99-103 (1999).

440. Herrera, P.L., Orci, L. & Vassalli, J.D. Two transgenic approaches to define the cell lineages in endocrine pancreas development. *Mol Cell Endocrinol* **140**, 45-50 (1998).

441. Herrera, P.L. Adult insulin- and glucagon-producing cells differentiate from two independent cell lineages. *Development* **127**, 2317-2322 (2000).

442. Eppig, J. The Jackson Laboratory. Committee on standardized genetic nomenclature for mice: guidelines for nomenclature of mouse and rat strains. 2011 [cited 2012/06/15]. Available from: http://www.informatics.jax.org/mgihome/nomen/strains.shtml.

443. Eppig, J. The Jackson Laboratory. International committee on standardized genetic nomenclature for mice: guidelines for nomenclature of genes, genetic markers, alleles, and mutations in mouse and rat. 2011 [cited 2012/06/15]. Available from: http://www.informatics.jax.org/mgihome/nomen/gene.shtml.

444. The Jackson Laboratory. Universal mouse numbering system (within entire colony). 2012 [cited 2012/06/01]. Available from: http://jaxmice.jax.org/support/husbandry/Universal_EarPunch_MouseNumberingSystem.pdf.

445. Saiki, R.K., et al. Primer-directed enzymatic amplification of DNA with a thermostable DNA polymerase. *Science* **239**, 487-491 (1988).

446. Townes, T.M., et al. Erythroid-specific expression of human beta-globin genes in transgenic mice. *EMBO J* **4**, 1715-1723 (1985).

447. Nagy, A., et al. Manipulating the Mouse Embryo: A Laboratory Manual. 2002, Woodbury, NY: Cold Spring Harbor Laboratory Press.

448. Williams, R.L., et al. Myeloid leukaemia inhibitory factor maintains the developmental potential of embryonic stem cells. *Nature* **336**, 684-687 (1988).

449. Nagy, A., et al. Derivation of completely cell culture-derived mice from early-passage embryonic stem cells. *Proc Natl Acad Sci U S A* **90**, 8424-8428 (1993).

450. Yagi, T., et al. A novel negative selection for homologous recombinants using diphtheria toxin A fragment gene. *Anal Biochem* **214**, 77-86 (1993).

451. Kuhbandner, S. Induzierbare Cre-vermittelte Rekombination im glatten Muskel der Maus [Inducible Cre-mediated recombination in smooth muscle of the mouse]. Dissertation. Fakultät Wissenschaftszentrum Weihenstephan, TU München, München (2001).

452. Southern, E.M. Detection of specific sequences among DNA fragments separated by gel electrophoresis. *J Mol Biol* **98**, 503-517 (1975).

453. Feinberg, A.P. & Vogelstein, B. A technique for radiolabeling DNA restriction endonuclease fragments to high specific activity. *Anal Biochem* **132**, 6-13 (1983).

454. Feinberg, A.P. & Vogelstein, B. "A technique for radiolabeling DNA restriction endonuclease fragments to high specific activity". Addendum. *Anal Biochem* **137**, 266-267 (1984).

455. Chomczynski, P. & Sacchi, N. Single-step method of RNA isolation by acid guanidinium thiocyanate-phenol-chloroform extraction. *Anal Biochem* **162**, 156-159 (1987).

456. Peterson, G.L. A simplification of the protein assay method of Lowry et al. which is more generally applicable. *Analytical Biochemistry* **83**, 346-356 (1977).

457. Lowry, O.H., et al. Protein measurement with the Folin phenol reagent. *J Biol Chem* **193**, 265-275 (1951).

458. Laemmli, U.K. Cleavage of structural proteins during the assembly of the head of bacteriophage T4. *Nature* **227**, 680-685 (1970).

459. Feil, S., Valtcheva, N. & Feil, R. Inducible Cre mice. *Methods Mol Biol* **530**, 343-363 (2009).

460. Bottenstein, J.E. & Sato, G.H. Growth of a rat neuroblastoma cell line in serum-free supplemented medium. *Proc Natl Acad Sci U S A* **76**, 514-517 (1979).

461. Kaech, S. & Banker, G. Culturing hippocampal neurons. *Nat Protoc* **1**, 2406-2415 (2006).

462. Suga, S., et al. Phenotype-related alteration in expression of natriuretic peptide receptors in aortic smooth muscle cells. *Circ Res* **71**, 34-39 (1992).

463. Chamley-Campbell, J., Campbell, G.R. & Ross, R. The smooth muscle cell in culture. *Physiol Rev* **59**, 1-61 (1979).

464. Chamley-Campbell, J.H., Campbell, G.R. & Ross, R. Phenotype-dependent response of cultured aortic smooth muscle to serum mitogens. *J Cell Biol* **89**, 379-383 (1981).
465. Siegl, D., et al. Myoendothelial coupling is not prominent in arterioles within the mouse cremaster microcirculation in vivo. *Circ Res* **97**, 781-788 (2005).
466. Constantinescu, C.C. & Mukherjee, J. Performance evaluation of an Inveon PET preclinical scanner. *Phys Med Biol* **54**, 2885-2899 (2009).
467. Vachaviolos, I.-A. Construction of targeting vectors for Cre/lox assisted genome modifications. Diploma. Department of Life Sciences, Faculty For Biochemistry And Biotechnology, University of Thessaly, Thessaly (2010).
468. Fomin, N. Characterization of the cGMP pathway in cells of the brain. Master of Science. Graduate School of Cellular & Molecular Neuroscience, Faculty of Science, Faculty of Medicine, Eberhard Karls Universität Tübingen, Tübingen (2011).
469. Li, L., et al. Expression of the SM22alpha promoter in transgenic mice provides evidence for distinct transcriptional regulatory programs in vascular and visceral smooth muscle cells. *J Cell Biol* **132**, 849-859 (1996).
470. Dobie, K., et al. Variegated gene expression in mice. *Trends Genet* **13**, 127-130 (1997).
471. Kozak, M. How do eucaryotic ribosomes select initiation regions in messenger RNA? *Cell* **15**, 1109-1123 (1978).
472. Hinnebusch, A.G. Molecular mechanism of scanning and start codon selection in eukaryotes. *Microbiol Mol Biol Rev* **75**, 434-467, first page of table of contents (2011).
473. Kozak, M. Effects of intercistronic length on the efficiency of reinitiation by eucaryotic ribosomes. *Mol Cell Biol* **7**, 3438-3445 (1987).
474. Kozak, M. Point mutations define a sequence flanking the AUG initiator codon that modulates translation by eukaryotic ribosomes. *Cell* **44**, 283-292 (1986).
475. Green, L.A., et al. A tracer kinetic model for 18F-FHBG for quantitating herpes simplex virus type 1 thymidine kinase reporter gene expression in living animals using PET. *J Nucl Med* **45**, 1560-1570 (2004).
476. Jacobs, A., et al. Quantitative kinetics of [124I]FIAU in cat and man. *J Nucl Med* **42**, 467-475 (2001).
477. Yamanaka, S. A fresh look at iPS cells. *Cell* **137**, 13-17 (2009).
478. Cohen, D.E. & Melton, D. Turning straw into gold: directing cell fate for regenerative medicine. *Nat Rev Genet* **12**, 243-252 (2011).
479. Wu, S.M. & Hochedlinger, K. Harnessing the potential of induced pluripotent stem cells for regenerative medicine. *Nat Cell Biol* **13**, 497-505 (2011).
480. Kiuru, M., et al. Genetic control of wayward pluripotent stem cells and their progeny after transplantation. *Cell stem cell* **4**, 289-300 (2009).
481. Lakso, M., et al. Efficient in vivo manipulation of mouse genomic sequences at the zygote stage. *Proc Natl Acad Sci U S A* **93**, 5860-5865 (1996).
482. Novelli, A., et al. Excitatory amino acid receptors coupled with guanylate cyclase in primary cultures of cerebellar granule cells. *J Neurosci* **7**, 40-47 (1987).
483. Lopez-Jimenez, M.E., et al. Functional cGMP-gated channels in cerebellar granule cells. *J Cell Physiol* **227**, 2252-2263 (2012).
484. Baltrons, M.A., et al. Regulation by calcium of the nitric oxide/cyclic GMP system in cerebellar granule cells and astroglia in culture. *J Neurosci Res* **49**, 333-341 (1997).
485. Brenman, J.E., et al. Interaction of nitric oxide synthase with the postsynaptic density protein PSD-95 and alpha1-syntrophin mediated by PDZ domains. *Cell* **84**, 757-767 (1996).
486. Jurado, S., Sanchez-Prieto, J. & Torres, M. Differential expression of NO-sensitive guanylyl cyclase subunits during the development of rat cerebellar granule cells: regulation via N-methyl-D-aspartate receptors. *J Cell Sci* **116**, 3165-3175 (2003).
487. Oh, S., Tokuyama, S. & McCaslin, P.P. Dual effects of NMDA-induced intracellular Ca2+ elevations on cGMP levels in cultured cerebellar granule neurons. *Gen Pharmacol* **28**, 153-157 (1997).
488. Poppe, H., et al. Cyclic nucleotide analogs as probes of signaling pathways. *Nat Methods* **5**, 277-278 (2008).
489. Held, K.F. & Dostmann, W.R. Sub-nanomolar sensitivity of nitric oxide mediated regulation of cGMP and vasomotor reactivity in vascular smooth muscle. *Front Pharmacol* **3**, 130 (2012).
490. Cawley, S.M., et al. Nitric oxide-evoked transient kinetics of cyclic GMP in vascular smooth muscle cells. *Cell Signal* **19**, 1023-1033 (2007).
491. Kotera, J., et al. cGMP-dependent protein kinase protects cGMP from hydrolysis by phosphodiesterase-5. *Biochem J* **372**, 419-426 (2003).
492. Bellamy, T.C. & Garthwaite, J. The receptor-like properties of nitric oxide-activated soluble guanylyl cyclase in intact cells. *Mol Cell Biochem* **230**, 165-176 (2002).
493. Garthwaite, J. New insight into the functioning of nitric oxide-receptive guanylyl cyclase: physiological and pharmacological implications. *Mol Cell Biochem* **334**, 221-232 (2010).
494. Batchelor, A.M., et al. Exquisite sensitivity to subsecond, picomolar nitric oxide transients conferred on cells by guanylyl cyclase-coupled receptors. *Proc Natl Acad Sci U S A* **107**, 22060-22065 (2010).
495. Griffiths, C., et al. A new and simple method for delivering clamped nitric oxide concentrations in the physiological range: application to activation of guanylyl cyclase-coupled nitric oxide receptors. *Mol Pharmacol* **64**, 1349-1356 (2003).
496. Furuya, M., et al. Novel natriuretic peptide, CNP, potently stimulates cyclic GMP production in rat cultured vascular smooth muscle cells. *Biochem Biophys Res Commun* **170**, 201-208 (1990).
497. Furuya, M., et al. Structural requirements of C-type natriuretic peptide for elevation of cyclic GMP in cultured vascular smooth muscle cells. *Biochem Biophys Res Commun* **183**, 964-969 (1992).
498. Aizawa, T., et al. Role of phosphodiesterase 3 in NO/cGMP-mediated antiinflammatory effects in vascular smooth muscle cells. *Circ Res* **93**, 406-413 (2003).
499. Itaba, S., et al. Presence of C-type natriuretic peptide (CNP) in guinea pig caecum: role and mechanisms of CNP in circular smooth muscle relaxation. *Neurogastroenterol Motil* **16**, 375-382 (2004).
500. Scott, R.B. & Maric, M. The effect of atrial natriuretic peptide on small intestinal contractility and transit. *Peptides* **12**, 799-803 (1991).

501. de Vente, J., Markerink-van Ittersum, M. & Gillespie, J.I. Natriuretic peptide responsive, cyclic guanosine monophosphate producing structures in the guinea pig bladder. *J Urol* **177**, 1191-1194 (2007).
502. Wheeler, M.A., et al. Age-dependent changes in particulate and soluble guanylyl cyclase activities in urinary tract smooth muscle. *Mol Cell Biochem* **169**, 115-124 (1997).
503. Mullershausen, F., et al. Direct activation of PDE5 by cGMP: long-term effects within NO/cGMP signaling. *J Cell Biol* **160**, 719-727 (2003).
504. Boolell, M., et al. Sildenafil: an orally active type 5 cyclic GMP-specific phosphodiesterase inhibitor for the treatment of penile erectile dysfunction. *Int J Impot Res* **8**, 47-52 (1996).
505. Lugnier, C., et al. Selective inhibition of cyclic nucleotide phosphodiesterases of human, bovine and rat aorta. *Biochem Pharmacol* **35**, 1743-1751 (1986).
506. Sonnenburg, W.K., Seger, D. & Beavo, J.A. Molecular cloning of a cDNA encoding the "61-kDa" calmodulin-stimulated cyclic nucleotide phosphodiesterase. Tissue-specific expression of structurally related isoforms. *J Biol Chem* **268**, 645-652 (1993).
507. Degerman, E., Belfrage, P. & Manganiello, V.C. Structure, localization, and regulation of cGMP-inhibited phosphodiesterase (PDE3). *J Biol Chem* **272**, 6823-6826 (1997).
508. Bellamy, T.C., Griffiths, C. & Garthwaite, J. Differential sensitivity of guanylyl cyclase and mitochondrial respiration to nitric oxide measured using clamped concentrations. *J Biol Chem* **277**, 31801-31807 (2002).
509. Coste, H. & Grondin, P. Characterization of a novel potent and specific inhibitor of type V phosphodiesterase. *Biochem Pharmacol* **50**, 1577-1585 (1995).
510. Mercapide, J., et al. Contribution of phosphodiesterase isoenzymes and cyclic nucleotide efflux to the regulation of cyclic GMP levels in aortic smooth muscle cells. *Biochem Pharmacol* **58**, 1675-1683 (1999).
511. Nagel, D.J., et al. Role of nuclear Ca2+/calmodulin-stimulated phosphodiesterase 1A in vascular smooth muscle cell growth and survival. *Circ Res* **98**, 777-784 (2006).
512. Polson, J.B. & Strada, S.J. Cyclic nucleotide phosphodiesterases and vascular smooth muscle. *Annu Rev Pharmacol Toxicol* **36**, 403-427 (1996).
513. Barnette, M.S., et al. Initial biochemical and functional characterization of cyclic nucleotide phosphodiesterase isozymes in canine colonic smooth muscle. *J Pharmacol Exp Ther* **264**, 801-812 (1993).
514. Tomkinson, A. & Raeburn, D. The effect of isoenzyme-selective PDE inhibitors on methacholine-induced contraction of guinea-pig and rat ileum. *Br J Pharmacol* **118**, 2131-2139 (1996).
515. Kaneda, T., et al. Effects of various selective phosphodiesterase inhibitors on carbachol-induced contraction and cyclic nucleotide contents in guinea pig taenia coli. *Journal of Veterinary Medical Science* **66**, 1047-1052 (2004).
516. Murthy, K.S. Activation of phosphodiesterase 5 and inhibition of guanylate cyclase by cGMP-dependent protein kinase in smooth muscle. *Biochem J* **360**, 199-208 (2001).
517. Qiu, Y., et al. Identification and functional study of phosphodiesterases in rat urinary bladder. *Urol Res* **29**, 388-392 (2001).
518. Longhurst, P.A., et al. The role of cyclic nucleotides in guinea-pig bladder contractility. *Br J Pharmacol* **121**, 1665-1672 (1997).
519. Mo, E., et al. Kinetics of a cellular nitric oxide/cGMP/phosphodiesterase-5 pathway. *J Biol Chem* **279**, 26149-26158 (2004).
520. Kim, D., et al. Upregulation of phosphodiesterase 1A1 expression is associated with the development of nitrate tolerance. *Circulation* **104**, 2338-2343 (2001).
521. Rybalkin, S.D., et al. Calmodulin-stimulated cyclic nucleotide phosphodiesterase (PDE1C) is induced in human arterial smooth muscle cells of the synthetic, proliferative phenotype. *J Clin Invest* **100**, 2611-2621 (1997).
522. Baez, S. An open cremaster muscle preparation for the study of blood vessels by in vivo microscopy. *Microvasc Res* **5**, 384-394 (1973).
523. Wolfle, S.E., et al. Prominent role of KCa3.1 in endothelium-derived hyperpolarizing factor-type dilations and conducted responses in the microcirculation in vivo. *Cardiovasc Res* **82**, 476-483 (2009).
524. Padilla-Parra, S. & Tramier, M. FRET microscopy in the living cell: different approaches, strengths and weaknesses. *Bioessays* **34**, 369-376 (2012).
525. Kamioka, Y., et al. Live imaging of protein kinase activities in transgenic mice expressing FRET biosensors. *Cell Struct Funct* **37**, 65-73 (2012).
526. Zipfel, W.R., Williams, R.M. & Webb, W.W. Nonlinear magic: multiphoton microscopy in the biosciences. *Nat Biotechnol* **21**, 1369-1377 (2003).
527. Greenberg, D.S., Houweling, A.R. & Kerr, J.N. Population imaging of ongoing neuronal activity in the visual cortex of awake rats. *Nat Neurosci* **11**, 749-751 (2008).
528. Dombeck, D.A., et al. Imaging large-scale neural activity with cellular resolution in awake, mobile mice. *Neuron* **56**, 43-57 (2007).
529. Heim, N., et al. Improved calcium imaging in transgenic mice expressing a troponin C-based biosensor. *Nat Methods* **4**, 127-129 (2007).
530. Jain, R.K., Munn, L.L. & Fukumura, D. Dissecting tumour pathophysiology using intravital microscopy. *Nat Rev Cancer* **2**, 266-276 (2002).
531. Pittet, M.J. & Weissleder, R. Intravital imaging. *Cell* **147**, 983-991 (2011).
532. Ensembl. Gene: Gt(ROSA)26Sor ENSMUSG00000086429. 2012 [cited 2012/06/26]. Available from: http://jul2012.archive.ensembl.org/Mus_musculus/Gene/Summary?g=ENSMUSG00000086429;r=6:113067428-113077333.

6 Appendix

6.1 ROSA26-lacZ Transcript Structure

Table 12. RT-PCR-based characterization of the ROSA26-lacZ reporter transgene.
The transcript structure was assembled from sequencing results of RT-PCR products (yellow highlight) and published sequences (in ref. 61, 532) of exon 1 of Gt(ROSA)26Sor-001 to -004 (abbreviated with 001-004 E1) and the lacZ CDS (amino acid sequence of the 5' part is shown in red). Fusion transcripts of Gt(ROSA)26Sor-003 and -004 and the ROSA26-lacZ transgene were not amplified as they do not bind BPZ1. '[' and ']' indicate exon borders, '*' and '#' indicate start and in-frame stop codons, '<' and '>' indicate primer 3' ends. RT-PCR product sizes were estimated from the sequencing results.

```
[003 E1


ggggcacgcg ggacacgccc cctcccgccg cgccattggc ctctccgccc accgccccac      003: Gt(ROSA26)Sor-003



acttattggc cggtgcgccg ccaatcagcg gaggctgccg gggccgccta aagaagaggc
                    [004 E1     003/004]
    [002 E1                           [001 E1                        004: Gt(ROSA26)Sor-004
                                                                     002: Gt(ROSA26)Sor-002
tgtgctttgg ggctccggct cctcagagag cctcggctag gtaggggatc gggactctgg      001: Gt(ROSA26)Sor-001
            ---- -BPZ1---- *-- >

cgggagggcg gcttggtgcg tttgcgggg ATG GGC GGC CGC GGC AGG CCC TCC

                001/002 E1] [ROSA26-lacZ transgene
                            #                                        BPZ1/RF127
GAG CGT GGT GGA GCC GTT CTG TGA gacagccgg ctcgcggttga ggacaaactc      96 bp
                                       <----- -RF127----


ttcgcggtct ttccagtggg gatcgacggt atcgataagc tggccgctct agaactagtg
-----
            •#• ••••••loxP• *•• •*• ••• ••• ••• ••• ••• #

gatccggaac ccttaataTA Acttcgtata ATG TAT GCT ATA CGA AGT TAT TAG

                                        #  *
                                        M   I   C   D   M
gtccctcgac ctgcagccca agctagctta tcgagcttg ATG ATC TGT GAC ATG

  A   D   P   V   V   L   Q   R   R   D   W   E   N   P   G   V
GCG GAT CCC GTC GTT TTA CAA CGT CGT GAC TGG GAA AAC CCT GGC GTT      lacZ


  T   Q   L   N   R   L   A   A   H   P   P   F   A   S   W   R      BPZ1/RF82
ACC CAA CTT AAT CGC CTT GCA GCA CAT CCC CCT TTC GCC AGC TGG CGT      370 bp
                                                         <--
  N   S   E   E   A   R   T   D   R   P   S   Q   Q   L   R   S      BPZ1/VI58
AAT AGC GAA GAG GCC CGC ACC GAT CGC CCT TCC CAA CAG TTG CGC AGC      413 bp
--- RF82--- --- ---                               < --- -VI58--
  L   N   G   E   W   R   F   A   W   F   P   A   P   E
CTG AAT GGC GAA TGG CGC TTT GCC TGG TTT CCG GCA CCA GAA
--- --- --- -
```

6.2   ROSA26-sr39tk Targeting Vector Construction

The adenoviral major late transcription unit SA site was amplified in a PCR reaction with DeepVent DNA polymerase from pROSA-ILD-P/F (provided by J. Deussing) using the primers MTH6 and MTH7. With these primers, a XbaI restriction site 5' to the SA site and a Kozak-ATG followed by a NheI restriction site 3' to the SA site are introduced into the PCR product, which was integrated into topoisomerase-activated pCR-Blunt-II-TOPO (Life Technologies), leading to pCR-Blunt-II-TOPO-SA. The PCR product was excised from pCR-Blunt-II-TOPO-SA with XbaI and ligated into XbaI-digested pUC19, leading to pSA. A loxP-flanked P_{PGK}-Neo^R-pA cassette (LNL) was excised with HindIII and XbaI from pCMV-LNL-lacZ (from R. Feil, 49), and was ligated into HindIII/NheI-digested pSA, resulting in pSA-LNL. NheI and XbaI have compatible cohesive ends, and upon ligation, both restriction sites are destroyed. The SA-LNL construct was excised with NdeI and HindIII and ligated into NdeI/HindIII-digested pCreER(GR)L (from R. Feil, 49), leading to pSA-LNL-ER-pA. pSA-LNL-ER-pA was digested with KpnI and NdeI, filled in and re-ligated to remove an unwanted EcoRI site 5' to the SA-LNL construct. The resulting plasmid was called pSA-LNL-ER-pA-EcoRI^0. To remove the remaining ER gene fragment and to generate a multiple cloning site (MCS) for reporter gene insertion, an oligonucleotide linker (MTH15/16) containing PacI and FseI restriction sites was ligated into EcoRI/HindIII-digested pSA-LNL-ER-pA-EcoRI^0, leading to pSA-LNL-Linker-pA. To flank the *HSV1*-sr39tk reporter CDS with PacI and FseI restriction sites for cloning into pSA-LNL-Linker-pA, oligonucleotides (MTH11/MTH12) carrying PacI, NheI, EcoRI, and FseI were ligated into EcoRI/HindIII-digested pUC19, leading to pLinker1. The *HSV1*-sr39tk reporter CDS was excised from pCMV-sr39tk (from S. Gambhir, 210) with NheI/EcoRI and ligated into NheI/EcoRI-digested pLinker1 leading to pPacI-sr39tk-FseI. The reporter gene was ligated into PacI/FseI-digested pSA-LNL-Linker-pA, leading to pSA-LNL-sr39tk-pA. The SA-LNL-sr39tk-pA construct was integrated into pROSA26.2 (from R. Kühn) using XbaI to generate the final targeting vector pROSA-SA-LNL-sr39tk-pA, containing an I-SceI restriction site for linearization prior to electroporation of ESCs.

6.3   ROSA26-mT/sr39tk Targeting Vector Construction

The mT/mG gene cassette (P_{CAG}-loxP-mT-pA-loxP-mG-pA-FRT-P_{PGK}-Neo^R-pA-FRT) was excised from the pROSA26-mT/mG targeting vector (Addgene 17787, ref. 79) by PacI and AscI, and was ligated into PacI/AscI-digested pLinker3, leading to pmT/mG. pLinker3 was created by inserting synthetic oligonucleotides (pLinker3_fwd/rev) carrying PacI/AscI restriction sites into EcoRI/HindIII-digested pUC19. To replace the mG gene in the mT/mG gene cassette by a MCS for the insertion of

alternative reporters, a fragment encompassing the second loxP site followed by mG-pA was isolated by EcoRI/HindIII digestion from pmT/mG, and subcloned into EcoRI/HindIII-digested pUC19, leading to ploxP-mG-pA. By digestion with Kpn2I and XhoI, the mG fragment was excised and exchanged by synthetic oligonucleotides (MCS_fwd/rev) containing FseI, XmaI, AsiSI and MluI restriction sites, resulting in ploxP-MCS-pA. The loxP-MCS-pA fragment was excised by EcoRI/HindIII and transferred back into the pmT/mG backbone, leading to pmT/MCS. Reporter genes which are to replace mG in the targeting constructs are introduced into pLinker5, which was generated by ligation of synthetic oligonucleotides (pLinker5_fwd/rev) carrying FseI, NcoI, HindIII, BamHI, EcoRI, MluI and AsiSI restriction sites into EcoRI/HindIII digested pUC19. The *HSV1*-sr39tk gene was isolated from pCMV-sr39tk via NcoI/BamHI and ligated into pLinker5, and then via FseI and AsiSI into pmT/MCS leading to pmT/sr39tk. To generate the ROSA26 targeting vector pROSA26-mT/sr39tk, the mT/sr39tk gene cassette (P_{CAG}-loxP-mT-pA-loxP-sr39tk-pA-FRT-P_{PGK}-Neo-pA-FRT) was introduced into the ROSA26-mT/mG targeting vector backbone via PacI and AscI.

6.4   cGi Constructs for Random Transgenesis

To generate the pCMV-cGi-6000 plasmid, pCMV-CreER[T] (obtained from R. Feil, 48) was digested with EcoRI, dephosphorylated, and ligated with a plasmid fragment carrying the cGi-6000 CDS isolated from cGi-6000 pCR-Blunt-II-TOPO (from M. Russwurm) with EcoRI. To generate the pSM445-cGi-500 plasmid, the CMV promoter was replaced in BamHI/EagI-digested pMGSV1 (from R. Feil, 48) by the SM445 promoter isolated from pBS-SM445 (from R. Feil) via BamHI/XhoI, leading to pMG-SM445. pBS-SM445 was generated by transferring the SM445 promoter fragment from pSM2736-lacZ obtained from R. Olson (469) via BamHI/SalI into pBluescript(+). The cGi-500 CDS was isolated with EcoRI from cGi-500 pCR-Blunt-II-TOPO (from M. Russwurm), and was ligated into EcoRI-digested pMG-SM445 leading to pSM445-cGi-500. Plasmids were tested for transgene integrity by sequencing and for successful expression by fluorescence microscopy after transient transfection into primary VSMCs. For oocyte injection, pCMV-cGi-6000 was digested with SalI/PvuI, and the 4.7 kb transgene-carrying fragment was isolated; pSM445-cGi-500 was digested with BsrBI, and the 4.9 kb transgene-carrying fragment was isolated. Final transgenes consist of either the CMV or the SM445 promoter followed by a rabbit β-globin intron, cGi-500 or cGi-6000 coding sequences, and two polyadenylation signals from rabbit β-globin gene and SV40 early region.

6.5 Screening of cGi Founder Animals

Table 13. Screening of cGi founder animals.
Founder animals that were obtained from oocyte injection of the respective transgene were tested for germ-line transmission (GLT). Progeny of founder animals was tested for cGi-type sensor expression ('yes', positive result; 'no', negative result; '?', result unsure; 'n.t.', not tested).

Founder			GLT	Screening				Status
Transgene, number	Sex	Date of birth		*In situ* fluorescence	Western blot	RT-PCR	Cell culture	
CMV-cGi-500-1	♂	02.01.2008 (01/08)	yes	?	no	no	no	discontinued
CMV-cGi-500-2	♂	02.01.2008 (01/08)	yes	?	no	no	no	discontinued
CMV-cGi-3000-1	♂	08.01.2008 (02/08)	yes	n.t.	no	n.t.	no	discontinued
CMV-cGi-3000-2	♀	08.01.2008 (02/08)	yes	n.t.	no	n.t.	n.t.	discontinued
CMV-cGi-6000-2	♂	08.06.2008 (23/08)	no	n.t.	n.t.	n.t.	n.t.	discontinued
CMV-cGi-6000-3	♂	08.06.2008 (23/08)	no	n.t.	n.t.	n.t.	n.t.	discontinued
CMV-cGi-6000-4	♂	14.07.2008 (29/08)	no	n.t.	n.t.	n.t.	n.t.	discontinued
CMV-cGi-6000-6	♂	**28.08.2008 (35/08)**	**yes**	**n.t.**	**yes**	**n.t.**	**yes**	discontinued
CMV-cGi-6000-8	♂	02.09.2008 (36/08)	yes	?	no	n.t.	n.t.	discontinued
CMV-cGi-6000-10	♂	**02.09.2008 (36/08)**	**yes**	**n.t.**	**yes**	**yes**	**yes**	**alive**
CMV-cGi-6000-11	♂	**02.09.2008 (36/08)**	**yes**	**?**	**yes**	**n.t.**	**n.t.**	discontinued
CMV-cGi-6000-13	♂	04.09.2008 (36/08)	no	n.t.	n.t.	n.t.	n.t.	discontinued
CMV-cGi-6000-14	♀	28.08.2008 (35/08)	yes	?	no	n.t.	n.t.	discontinued
CMV-cGi-6000-15	♀	28.08.2008 (35/08)	no	n.t.	n.t.	n.t.	n.t.	discontinued
CMV-cGi-6000-16	♀	02.09.2008 (36/08)	no	n.t.	n.t.	n.t.	n.t.	discontinued
CMV-cGi-6000-17	♀	02.09.2008 (36/08)	yes	n.t.	no	n.t.	n.t.	discontinued
CMV-cGi-6000-18	♀	02.09.2008 (36/08)	yes	n.t.	no	n.t.	n.t.	discontinued
CMV-cGi-6000-19	♀	04.09.2008 (36/08)	no	n.t.	n.t.	n.t.	n.t.	discontinued
SM445-cGi-500-1	♂	**03.10.2008 (40/08)**	**yes**	**?**	**yes**	**n.t.**	**yes**	discontinued
SM445-cGi-500-2	♀	07.10.2008 (41/08)	yes	?	no	n.t.	n.t.	discontinued
SM445-cGi-500-3	♀	07.10.2008 (41/08)	yes	?	n.t.	n.t.	n.t.	discontinued
SM445-cGi-500-4	♀	07.10.2008 (41/08)	yes	?	no	n.t.	n.t.	discontinued
SM445-cGi-500-5	♀	**07.10.2008 (41/08)**	**yes**	**yes**	**yes**	**yes**	**yes**	**alive**
SM445-cGi-500-6	♀	01.10.2008 (40/08)	no	?	n.t.	n.t.	n.t.	discontinued
SM445-cGi-500-7	♀	01.10.2008 (40/08)	yes	?	no	n.t.	n.t.	discontinued
SM445-cGi-500-8	♂	07.10.2008 (41/08)	yes	?	n.t.	n.t.	n.t.	discontinued
SM445-cGi-500-9	♂	01.10.2008 (40/08)	yes	?	no	n.t.	n.t.	discontinued
SM445-cGi-500-10	♂	08.10.2008 (41/08)	yes	?	no	n.t.	n.t.	discontinued
SM445-cGi-500-11	♂	08.10.2008 (41/08)	no	n.t.	n.t.	n.t.	n.t.	discontinued

6.6   Evaluation of cGMP Imaging in SMCs

Table 14. Parameter estimation for cGi-500 calibration with cGMP shown in Figure 27.

$(\Delta R/R)_{min}$ and $(\Delta R/R)_{max}$ define lower and upper limit of the fitted curve, EC_{50} the cGMP concentration in nM at half-maximal sensor activation, and h the Hill constant (values±SEM). A range is given for EC_{50}, as conversion of $\log(EC_{50})\pm SEM$ to $10^{(\log EC50\pm SEM)}$ results in different error ranges for +SEM and −SEM.

Parameter	Value±SEM
$(\Delta R/R)_{min}$	0.024±0.004
$(\Delta R/R)_{max}$	0.325±0.003
$\log (EC_{50})$	-6.24±0.02
EC_{50} [nM]	577 (553-602)
h	1.26±0.08
n	88
χ^2	0.0014
R^2	0.914

Table 15. Parameter estimation for DEA/NO dose-response curves shown in Figure 28B.

A_{min} and A_{max} define lower and upper limit of the fitted curve, EC_{50} the DEA/NO concentration at half-maximal peak area, and h the Hill constant (values±SEM). A range is given for EC_{50}, as conversion of $\log(EC_{50})\pm SEM$ to $10^{(\log EC50\pm SEM)}$ results in different error ranges for +SEM and −SEM.

Parameter	VSMCs	BSMCs	CSMCs
A_{min}	0.08±0.04	0.07±0.09	0.09±0.01
A_{max}	1.45±0.04	1.55±0.09	0.88±0.01
$\log (EC_{50})$	-6.97±0.02	-7.13±0.04	-6.835±0.004
EC_{50} [nM]	107.6 (102.4-113.1)	73.5 (66.4-81.3)	146.3 (145.0-147.7)
h	3.71±0.61	3.56±1.27	7.99±0.99
n	10	10	5
χ^2	0.004	0.014	0.0002
R^2	0.99	0.97	0.999

Table 16. Comparison of $\log(EC_{50})$ values from DEA/NO dose-response curves shown in Figure 28B.

The student's t-test was used for comparison of $\log(EC_{50})$ values.

Comparison	t	dF	P
VSMCs vs. CSMCs	6.102	8	0.0003
VSMCs vs. BSMCs	3.391	8	0.0095
BSMCs vs. CSMCs	6.789	6	0.0005

Table 17. Statistical analysis of PDE inhibitor studies shown in Figure 28D and E.

Comparison of measurements was performed with repeated measures analysis of variance on ranks (RM-ANOVA); single treatments are compared with Tukey's test.

Experiment	n	Treatment	Median	25%	75%	χ^2	P	Comparison of treatment	Diff. of Ranks	q	P<0.05
VSMC±SIL	12	1st peak	1.531	1.156	2.152	22.167	<0.001	2nd/3rd peak	23	6.640	Yes
		2nd peak	2.626	1.752	4.603			2nd/1st peak	13	3.753	Yes
		3rd peak	0.692	0.277	1.026			1st/3rd peak	10	2.887	No
VSMC±IBMX	10	1st peak	0.548	0.492	0.633	18.200	<0.001	2nd/3rd peak	19	6.008	Yes
		2nd peak	5.489	3.161	7.223			2nd/1st peak	11	3.479	Yes
		3rd peak	0.287	0.220	0.420			1st/3rd peak	8	2.530	No
BSMC±SIL	5	1st peak	0.705	0.661	0.941	10.000	<0.001	2nd/3rd peak	10	4.472	Yes
		2nd peak	2.069	1.655	2.437			2nd/1st peak	5	2.236	No
		3rd peak	0.433	0.397	0.605			1st/3rd peak	5	2.236	No
BSMC±IBMX	4	1st peak	0.687	0.527	0.830	8.000	0.005	2nd/3rd peak	8	4.000	Yes
		2nd peak	5.134	4.762	5.398			2nd/1st peak	4	2.000	No
		3rd peak	0.207	0.179	0.339			1st/3rd peak	4	2.000	No
CSMC±SIL	22	1st peak	0.614	0.410	1.029	30.545	<0.001	2nd/3rd peak	36	7.675	Yes
		2nd peak	1.610	1.292	2.150			2nd/1st peak	24	5.117	Yes
		3rd peak	0.265	0.166	0.407			1st/3rd peak	12	2.558	No
CSMC±IBMX	17	1st peak	1.968	1.581	2.126	34.000	<0.001	2nd/3rd peak	34	8.246	Yes
		2nd peak	8.655	7.834	10.480			2nd/1st peak	17	4.123	Yes
		3rd peak	0.553	0.279	0.715			1st/3rd peak	17	4.123	Yes

6.7   Supplementary Tables

Table 18. Restriction endonucleases.

Name	Recognition sequence	Supplier	Name	Recognition sequence	Supplier
AclI	AA|CGTT	NEB	KpnI	GGTAC|C	NEB
AscI	GG|CGCGCC	NEB	MluI	A|CGCGT	NEB
AsiSI	GCGAT|CGC	NEB	NcoI	C|CATGG	NEB
BamHI	G|GATCC	NEB	NdeI	CA|TATG	NEB
BsrBI	CCG|CTC	NEB	NheI	G|CTAGC	NEB
EagI	C|GGCGG	NEB	PacI	TTAAT|TAA	NEB
EcoRI	G|AATTC	NEB	PvuI	CGAT|CG	NEB
EcoRV	GAT|ATC	NEB	SalI	C|TCGAC	NEB
FseI	GGCCGG|CC	NEB	XbaI	T|CTAGA	NEB
HindIII	A|AGCTT	NEB	XhoI	C|TCGAG	NEB
I-SceI	TAGGG∧ATAA∨CAGGGTAAT	NEB	XmaI	C|CCGGG	NEB
Kpn2I	T|CCGGA	NEB			

Table 19. Oligonucleotides.

Name	Sequence (5' → 3')	Used for
MTH11	AATTAATTAACGGATCCATGCTAGCTAATGAGAATTCAGGCCGGCCT	Cloning pLinker1
MTH12	AGCTAGGCCGGCCTGAATTCTCATTAGCTAGCATGGATCCGTTAATT	Cloning pLinker1
pLinker3_fwd	AATTAATTAAGGCCGGCCGCGGCCGCATTTAAATGGCGCGCC	Cloning pLinker3
pLinker3_rev	AGCTGGCGCGCCATTTAAATGCGGCCGCGGCCGGCCTTAATT	Cloning pLinker3
pLinker5_fwd	AGCTGCGATCGCACGCGTGAATTCGGATCCAAGCTTCCATGGCTGGCCGGCC	Cloning pLinker5
pLinker5_rev	AATTGGCCGGCCAGCCATGGAAGCTTGGATCCGAATTCACGCGTGCGATCGC	Cloning pLinker5
MCS_fwd	CCGGAGGCCGGCCGGGTATCAGTGGCGATCGCACGCGTC	Cloning ploxP-MCS-pA
MCS_rev	TCGAGACGCGTGCGATCGCCACTGATACCCGGGCCGGCCT	Cloning ploxP-MCS-pA
MTH15	AGCTCCTTAATTAAGTTTAAACCAATGCATTGGCCGGCC	Cloning pSA-LNL-Linker-pA
MTH16	AATTGGCCGGCCAATGCATTGGTTTAAACTTAATTAAGG	Cloning pSA-LNL-Linker-pA
MTH6	TGTTCTAGAGTAGGGCGCAGTAGTCCAGGG	Cloning SA site
MTH7	ACTGCTAGCTCCATGGTGGCAAAGACCGCGAAGAGTTTGTC	Cloning SA site
MH8	CCCTTGCTCACCATATATG	Genotyping PCR cGi-3000 rev
MH12	TGCTCACCATATATTTTGCC	Genotyping PCR cGi-500 rev
MH5	GTCACTCGTGAAGACTCG	Genotyping PCR cGi-500/-3000/-6000 fwd
MH7	CCCTTGCTCACCATTAATC	Genotyping PCR cGi-6000 rev
Cre800	GCTGCCACGACCAAGTGACAGCAATG	Genotyping PCR Cre fwd
Cre1200	GTAGTTATTCGGATCATCAGCTACAC	Genotyping PCR Cre rev
ROSA10	CTCTGCTGCCTCCTGGCTTCT	Genotyping PCR ROSA26 common fwd
ROSA11	CGAGGCGGATCACAAGCAATA	Genotyping PCR ROSA26 wt rev
ROSA04	TCAATGGGCGGGGGTCGTT	Genotyping PCR ROSA26-mT/sr39tk rev
RF127	GCGAAGAGTTTGTCCTCAACC	Genotyping PCR ROSA26-sr39tk rev
SW8	AACTCCAGCTCCAGCTCG	Genotyping PCR SMr rev
SC135	GGCGATCCCTGAACATGTCC	Genotyping PCR SMKI rev
RF67	CTCAGAGTGGAAGGCCTGCTT	Genotyping PCR SMKI/SMr common fwd
SW16	CGCAAGGGTTACTCACCACA	Genotyping PCR SMKI/SMr wt rev
BPZ2	GCCGTTCTGTGAGACAGROSA	RT-PCR ROSA26 (263')
BPZ4	AAATGTTCTGGACAAACACTTC	RT-PCR ROSA26 (575–695R)
BPZ1	TGCGTTTGCGGGGATGG	RT-PCR ROSA26 (r265'f)
BPZ7	TAACTCCAGTTCTAGGGGG	RT-PCR ROSA26 (R26alt2)
BPZ6	CGCACTGCTCAAGCCTTTGTTC	RT-PCR ROSA26 (R26B)
RF82	GGCCTCTTCGCTATTACG	RT-PCR ROSA26 lacZ rev
VI58	CGCCATTCAGGCTGCGCAAC	RT-PCR ROSA26 lacZ rev
RR189	AAGCGCATGCTCCAGACTGC	RT-PCR ROSA26 P_{PGK}-Neo^R rev
M13rev	GGAAACAGCTATGACCATG	Sequencing
M13uni	AGGGTTTTCCCAGTCACGACGTT	Sequencing
pQEfor	GTATCACGAGGCCCTTTCGTCT	Sequencing
RF86	GTGGGGTGGGATTAGATAAATG	Sequencing

Table 20. Selected genetic properties of R1 ESCs and 'wild type' mouse strains.

Name	Type	Systematic name*	Appearance	Relevant genotypes#
R1	R1 ESCs‡ (XY karyotype)	129/Sv × 129/Sv-CP (129X1/SvJ × 129S1/Sv-Oca2+ Tyr+ Kitl^{Sl-J}/J)	white-bellied agouti	A^w/A^w $Oca2^p$ Tyr^{c-ch}/$Oca2^p$ Tyr^c × A^w/A^w $Oca2^+$ Tyr^+ $Kitl^{Sl-J}$
C57Bl/6 (B6)	Inbred strain	C57Bl/6NCrl	black	a/a $Tyrp1^b$
FVB/N	Inbred strain	FVB/NCrl	albino	A/A Tyr^c
B6D2	F1 Hybrid (♀C57Bl/6 × ♂DBA/2)	B6D2F1/Crl	black	a/a $Tyrp1^b$/+ $Myo5a^d$/+
CD1	Outbred strain	Crl:CD1(ICR)	albino	n.d.

*Substrain: Crl, Charles River Laboratories; J, Jackson Laboratories. #Alleles: *Agouti* (*A*, agouti; A^w, white-bellied agouti; *a*, non-agouti), *Tyrp1* (*B*, black; *b*, brown), *Tyr* (*C*, full color; *c-ch*, chinchilla; *c*, albino), *Myo5a* (*D*, dilute; *d*, non-dilute), *Oca2* (*P*, wild type; *p*, pink-eye dilution). ‡Strains used for ESC generation are noted; original nomenclature (449) and revised 129 strain nomenclature (in brackets).

Table 21. Conditions for genotyping PCRs.

Transgene	Primer	Cycles	T_d, time	T_a, time	T_e, time	Product sizes	
cGi-500	MH5 0.3 µL MH12 0.3 µL	35	94°C, 10 s	51°C, 30 s	72°C, 30s	tg wt	244 bp no product
cGi-3000	MH5 0.3 µL MH8 0.3 µL	35	94°C, 10 s	51°C, 30 s	72°C, 30s	tg wt	221 bp no product
cGi-6000	MH5 0.3 µL MH7 0.3 µL	35	94°C, 10 s	51°C, 30 s	72°C, 30s	tg wt	197 bp no product
Cre	Cre800 0.3 µL Cre1200 0.3 µL	35	95°C, 10 s	58°C, 30 s	72°C, 30 s	tg wt	402 bp no product
ROSA26-lacZ	ROSA10 0.3 µL ROSA11 0.3 µL RF127 0.2 µL	35	95°C, 10 s	65°C, 30 s	72°C, 30 s	wt (+) −	250 bp ~220 bp
ROSA26-sr39tk	ROSA10 0.3 µL ROSA11 0.3 µL RF127 0.2 µL	35	95°C, 10 s	65°C, 30 s	72°C, 30 s	wt (+) −	250 bp 195 bp
ROSA26-mT/sr39tk ROSA26-CAG-cGi500	ROSA10 0.3 µL ROSA11 0.3 µL ROSA04 0.2 µL	35	95°C, 10 s	61°C, 30 s	72°C, 30 s	wt (+) −	250 bp 195 bp
SMKI	RF67 0.3 µL SW16 0.3 µL SC135 0.3 µL	35	95°C, 10 s	65°C, 30 s	72°C, 30 s	wt (+) −	290 bp 275 bp
SMIβ rescue	RF67 0.3 µL SW16 0.3 µL SW8 0.3 µL	35	95°C, 10 s	61°C, 30 s	72°C, 30 s	wt (+) −	290 bp 195 bp

All PCR programs contain an initial denaturation (5 min at 94°C) and a final elongation step (5 min at 72°C). Primer sequences in **Table 19**, p. 141.

Table 22. Antisera and antibodies.

Name	Species (mono-/polyclonal)	Supplier (Order number)	Use	Dilution
βIII-Tubulin	Mouse (m)	Promega (G7121)	IF	1:1000
EGFP	Rabbit (p)	Abcam (ab290)	IF WB	1:500 to 1:2000 1:3000
EGFP	Mouse (m)	Santa Cruz (sc-81045)	IF WB	1:1000 1:2000
GLAST	Mouse (m)	Miltenyi (130-095-822)	IF	1:500
HSV1-tk	Rabbit (p)	W.C. Summers, Yale University	IF WB	1:500 1:2000
SM22	Rabbit (m)	Abcam (ab14106)	IF	1:500
Anti-mouse × Alexa 555	Goat (p)	Life Technologies	IF	1:500
Anti-rabbit × Alexa 488	Goat (p)	Life Technologies	IF	1:500
Anti-rabbit × Alexa 594	Goat (p)	Life Technologies	IF	1:500
Anti-rabbit × HRP	Goat (p)	Cell Signaling	WB	1:2000 to 1:5000

7   Own Publications

Articles

M. Föller, S. Feil, K. Ghoreschi, S. Koka, A. Gerling, M. Thunemann, F. Hofmann, B. Schuler, J. Vogel, B.J. Pichler, R.S. Kasinathan, J.P. Nicolay, S.M. Huber, F. Lang & R. Feil. Anemia and splenomegaly in cGKI-deficient mice. *Proc Natl Acad Sci U S A* **105**:6771-6 (2008).

K. Fischer, V. Sossi, A. Schmid, M. Thunemann, F.C. Maier, M.S. Judenhofer, J.G. Mannheim, G. Reischl, B.J. Pichler. Noninvasive nuclear imaging enables the in vivo quantification of striatal dopamine receptor expression and raclopride affinity in mice. *J Nucl Med* **52**:1133-41 (2011).

P.M. Müller, R. Gnügge, S. Dhayade, M. Thunemann, P. Krippeit-Drews, G. Drews & R. Feil. H_2O_2 lowers the cytosolic Ca^{2+} concentration via activation of cGMP-dependent protein kinase Iα. *Free Radic Biol Med.* **53**:1574-1583 (2012).

M. Thunemann, N. Fomin, C. Krawutschke, M. Russwurm & R. Feil. Visualization of cGMP with cGi biosensors. Methods Mol Biol. (In revision.)

M. Thunemann*, L. Wen*, M. Hillenbrand, A. Vachaviolos, S. Feil, T. Ott, M. Russwurm, C. de Wit & R. Feil. cGMP imaging in transgenic mice expressing cGi-500 biosensors. (In preparation, * = equal contribution.)

Conference proceedings

M. Thunemann, F. Cay, D. Bukala, M.S. Judenhofer, G. Reischl, M. Reimold, C.D. Claussen, H. Machulla, B.J. Pichler (2007). Influence of tracer mass and spatial resolution on the quantification of microPET experiments performed in mice. Joint Molecular Imaging Conference in Providence, RI, USA.

F. Cay, D. Bukala, M. Thunemann, M.S. Judenhofer, G. Reischl, H. Machulla, C.D. Claussen, B.J. Pichler (2007). Bolus / Infusion microPET imaging protocols for neuroimaging in mice and rats. Joint Molecular Imaging Conference in Providence, RI, USA.

M. Thunemann, S. Feil, B.J. Pichler & R. Feil (2010). In vivo Cell Tracking in krankheitsrelevanten Mausmodellen mittels Positronen-Emissions-Tomographie. 51. Jahrestagung der Deutschen Gesellschaft für Experimentelle und Klinische Pharmakologie und Toxikologie e. V. (DGPT) in Mainz.

M. Thunemann, N. Fomin, M. Hillenbrand, T. Ott, M. Russwurm & R. Feil (2012). Visualization of cGMP in living cells and tissues of transgenic mice. 78. Jahrestagung der Deutschen Gesellschaft für Experimentelle und Klinische Pharmakologie und Toxikologie e. V. (DGPT) in Dresden.

8   Curriculum Vitae

Martin Thunemann, Dipl.-Biochemiker

born 28.10.1982 in Bonn

10.10.2012	Disputation: "Generation and Characterization of Transgenic Mice for Noninvasive Cell Tracking with PET and for FRET-based cGMP Imaging."
since 2007	PhD student: "Generation and Characterization of Transgenic Mice for Noninvasive Cell Tracking with PET and for FRET-based cGMP Imaging." Signal Transduction - Transgenic Models, Interfaculty Institute for Biochemistry, Eberhard Karls Universität Tübingen. Supervisor: Prof. Dr. Robert Feil.
2007	Graduation in biochemistry (Dipl.-Biochemiker, final grade: 1.0).
2006-2007	Diploma thesis: „In vivo Quantifizierung von Rezeptor-Ligand-Wechselwirkungen mit microPET am Beispiel des dopaminergen Systems in Mäusen, Vergleich mit Autoradiographie und Immunfluoreszenz." Laboratory for Preclinical Imaging and Imaging Technology, Department of Radiology, Eberhard Karls Universität Tübingen. Supervisor: Prof. Dr. B.J. Pichler.
2006	Diploma exams in biochemistry, physical chemistry, neuropharmacology.
2001-2007	Student of biochemistry, Eberhard Karls Universität Tübingen.
2001-2006	Scholarship, Professor-Rhein-Stiftung, Königswinter.
2001	Abitur (final grade: 1.2).
1994-2001	Jugenddorf-Christophorusschule in Königswinter.

9 Acknowledgments